EXPERIMENTAL INVESTIGATION OF EMBANKMENT ON SOFT SOIL UNDER CYCLIC LOADING: EFFECT OF INPUT ACCELERATION

R. Hore*, S. Chakraborty[2], A. M. Shuvon[3], M. S. Mazhar[1] and M. A. Ansary[1]

[1]*Department of Civil Engineering, Bangladesh University of Engineering and Technology (BUET),Dhaka, Bangladesh.*
E-mail: riponhore@gmail.com
[2]*Department of Water Resources Engineering, Bangladesh University of Engineering and Technology (BUET)Dhaka, Bangladesh.*
E-mail: sudipta.ckr@gmail.com
[3]*Bangladesh Network office for Urban Safety (BNUS),Dhaka, Bangladesh.*
E-mail: amshuvon@gmail.com
**Corresponding Author*

ABSTRACT
This paper presents the results of shaking table tests on geotextile-reinforced embankment lying on soft clay. Construction of model embankment in a laminar box mounted on a shaking table, instrumentation, and results from the shaking table tests have been discussed in detail. The base motion parameters have been varied in different model tests. It has been observed that from these tests the response of the embankment with soft clay has been significantly affected by the base acceleration levels, frequency of shaking and magnitude of surcharge pressure on the crest. The effects of these different parameters on acceleration response at different elevations of the embankment, pore pressures and face deformations have been measured. The results obtained from this research are helpful in understanding the relative performance of reinforced soil-embankment under different test situations applied in the experiments.

Keywords: Laminar box, Soft soil, Amplification and acceleration

INTRODUCTION
The soil-foundation composed of clayey soil has become the focus of earthquake engineering in more cases. However, it is rather scarce to study the characteristic of pore water pressure in such soil-foundations with cohesive or clayey soil under earthquake action due to its clay content is thought of relatively high. Although such soil-foundations of higher clay content are not easily susceptible to liquidity, a rise of excess pore water pressure triggered by earthquakes and a drop of effective stress may lead to the soil softening. Also, soil-foundation softening may cause damage to the embankment. Today, there is no absolute conclusion on whether the softening effect of cohesive or clayey soils under earthquake excitation should be considered and under what shake condition the damage induced by excess pore water pressure may not be considered in analysis. Based on shaking table tests, this paper attempts to investigate the changing characteristics of the amplification, displacement and pore water pressure (due to input acceleration) in soft soil-foundations under harmonic wave. The soil-foundation in the test has been built with soft soils in Dhaka clay. The physical mechanism responsible for variation behavior of the pore water pressure in the repeated process has been studied. The results of experimental investigation have been expected to provide some research basis for softening problems of clayey embankment under earthquake actions.

METHODOLOGY

Previous Research

Developments of model testing in earthquake geotechnical engineering, two aspects of model testing have been given importance, namely rigid and laminar box. Design, development, calibration and performance of this equipment are very important (Prasad S. K. et al., 2004). Latha M. G. et al. (2006) has presented Shaking table studies which have been carried out on wrap-faced reinforced soil retaining walls to gain insight into their behaviour under dynamic loads. Soft soil with the larger void ratio, the higher water content and higher the saturation degree, the peak of excess pore water pressure during the repeated loading process will not be significantly higher than that of the previous cycle (Zhang, Z. et al., 2009). Moss, R. et al (2010) has proposed scale soil-structure models to mimic the coupled seismic response of underground structures and surrounding/supporting soil (termed soil-structural-interaction or SSI). Currently the seismic design of subways and other critical underground infrastructure rely on little to no empirical data for calibrating numerical simulations. Srilatha et al. (2014) has also been conducted series of laboratory shaking table tests for observing the performance of without reinforced and reinforced soil slopes through. Frequency of base acceleration has been varied from 1 Hz to 7 Hz in different tests. Acceleration of base shaking has been kept as 0.3 g in all the tests. A recent laboratory test has been conducted by Yazdandoust (2017) to assess the behavior and performance of steel-strip reinforced-soil retaining walls during seismic loading, a series of 1-g shaking table tests have been conducted on 0.9 m high reinforced-soil wall models with different strip lengths.

Current Investigation

Based on the aforementioned necessities the present research targets the seismic design of subway/ road way or railway embankment. A scale model testing platform has been developed for single degree of freedom shaking table tests that mimics the dynamic free-field conditions of Dhaka clayey soil where a sand retaining wall has been erected on clayey soil has been subjected to seismic loading. A total of 90 shaking table test have been carried out on this model embankment. The effect of frequency, amplitude, surcharge, pore water pressure and displacement along the different elevations (effect of input acceleration) has been observed.

Equipment and Materials

Shaking table: A computer-controlled servo-hydraulic single degree of freedom shaking table facility has been used to simulate the horizontal shaking action, associated with seismic and other vibration conditions. The testing platform is a square having 2×2 m^2 dimension and approximate payload capacity of 1000 kg, which has been made from steel plates. Shaking has been provided by a digitally controlled servo-hydraulic actuator with ±200 mm stroke and 30 kN force rating. The shaking table can be operated over an acceleration range of 0.05g to 2g and frequency range 0.05 to 50 Hz with a maximum amplitude of ±200 mm. Maximum velocities are 0.3 m/s.

Laminar box: In this study, embankment with soft clay soil models has been constructed in a laminar box to reduce boundary effects as far as practicable. The laminar shear box developed at BUET has composed of 24 hollow aluminum layers of frames. Each layer consists of an inner frame with inside dimensions of 915 mm × 1220 mm × 1220 mm. Laminar box mounted on the shake table has been presented in Fig. 1(a).

Backfill material & Reinforcement: Dry sand (Specific gravity=2.64) has been used as the backfill material. The sand has been classified as poorly graded sand (SP) according to the Unified Soil Classification System. Maximum dry density of the sand is 18 kN/m^3 and minimum dry density

observed in the loosest state is 15 kN/m3. A non woven polypropylene multifilament geotextile has been used for reinforcing the sand in the tests.

Model Construction and testing procedure

Re constitute clay soil sample: In this research work Dhaka soft clay soil has been used. The liquid limit of this soil has been found 40%. The water content of this soil sample has been found 23%. For preparing the soil sample used 50% of water content (1.25 times of liquid limit). From the direct shear test cohesion and friction have been found 14.8 KN/m2 and 10.03 respectively. After loading had been done, the water content of soil sample was 15% and unconfined compression strength (qu) was 20 kPa. The constitute clay layer thickness of the soil sample is 18 inch. Preparation of re constitute sample has been shown as Fig. 1(b). Two pore water pressure sensor: one is base level of sample and another is 18 inch above the base level have been used in this soil sample. Two acceleration sensors have been placed in the soil sample.

a)

b)

[Fig. 1]. Detail setting of Shake table test. (a) Laminar box mounted on shaking table (b) Placement of reconstitute soil sample

Testing Process: The model embankment has been constructed in a laminar box to a size of 915 mm x1220 mm in plan area and 1220 mm deep. Each geotextile layer has been wrapped at the facing for a length of 150 mm. To achieve uniform density, sand was placed in the laminar box using the pluviation (raining) technique (Hossain and Ansary, 2018). After the completion of all lifts up to full height of the wall (406 mm), surcharge in the form of three type concrete slabs (19/34/49 kg) have been applied to anchor the top wrapped geotextile. The facing formwork was removed carefully in sequential lifts from bottom to top after the backfill layers (2 inch) and surcharge have been completed. Fig. 2 shows the finished embankment for four-layer with 2 ft clay layer. A typical model configuration showing the instrumentation for the test wall with four layers of reinforcement has been shown in Fig. 3. Two pressure sensors; P1 and P2 have been placed inside the wall, in contact with the measure horizontal displacement, three displacement sensors (LVDTs), L1, L2 and L3, have been positioned at elevations 32, 42 and 56 inch, respectively, along the facing for the tests with four-layer configurations.

RESULTS AND DISCUSSIONS

Results obtained from sixteen different shaking table tests from ninety combinations on embankment with soft clay models have been discussed in this paper. The parameters varied in model tests are base acceleration, frequency and surcharge pressure on the crest. The base acceleration has been kept as 0.1g, 0.2g, 0.3g, 0.4 g and 0.5g in different tests. The frequency has been varied from 1 Hz to 15 Hz. The surcharge pressure on the embankment has been kept as 19, 34 and 49 kg. Soft clay layer has been used (24 in) which unconfined compression strength is 20 kPa. Model has been constructed using sand on the clay layer in equal lifts (Sv) of 4 and total wall height (H) is 16 in. The length (L) of the geotextile reinforcement at the interface of the sand layers has been kept the same in all tests as 15 in. Model wall

[Fig. 2].Setting of Setting of displacement sensor.

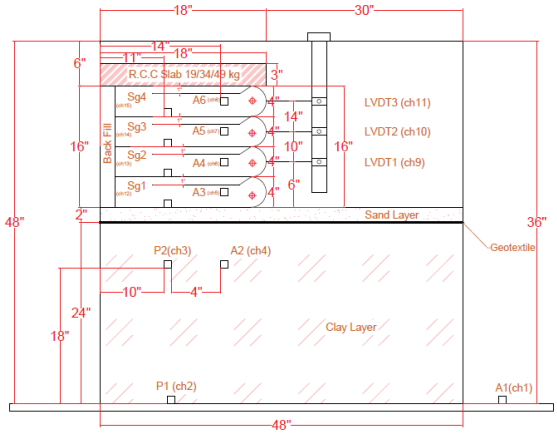

[Fig. 3]. Schematic diagram of typical test wall configuration and instrumentation

was subjected to 20 cycles of sinusoidal shaking. The average unit weight and relative density achieved were within the ranges 18 kN/m3 and 60% respectively for the same height of fall.

Acceleration response: Fig. 4(a) and Fig. 4(b) compare the acceleration amplification profile along the height of the wall for different configurations of wall and base motion after each test of 20 cycles of sinusoidal motion. Here the elevation (z) has been represented in non-dimensional form after normalizing by the full wall height (H). Maximum acceleration amplification has been observed at the top of the wall in all the tests. This observation is in concurrence with the results of physical tests reported by Telekes et al. (1994), El-Emam and Bathurst (2005) and Krishna et al (2007). Fig. 4(a) shows the acceleration amplifications along the height of the wall for different base accelerations of 0.1, 0.2, 0.3, 0.4 and 0.5g from ST2 (0.1g, 3 Hz and 19 kg) , ST8 (0.2g, 3Hz and 19 kg), ST14 (0.3g, 3Hz and 19 kg), ST20 (0.4g, 3 Hz and 19 kg) and ST26 (0.5g, 3Hz and 19 kg) model tests, respectively, which have been conducted at 3 Hz frequency, 19 Kg surcharge. However, within the range of tests conducted, acceleration amplifications at the top of the wall for 0.1,0.2, 0.3, 0.4 and 0.5g base accelerations are 1.06 to 1.22. Fig.4(b) shows the two sensor in clay soil sample layer for different base accelerations of 0.1, 0.2, 0.3, 0.4 and 0.5g from ST2, ST8, ST14, ST20 and ST26 model tests, respectively, which were conducted at 3 Hz frequency, 19 Kg surcharge.

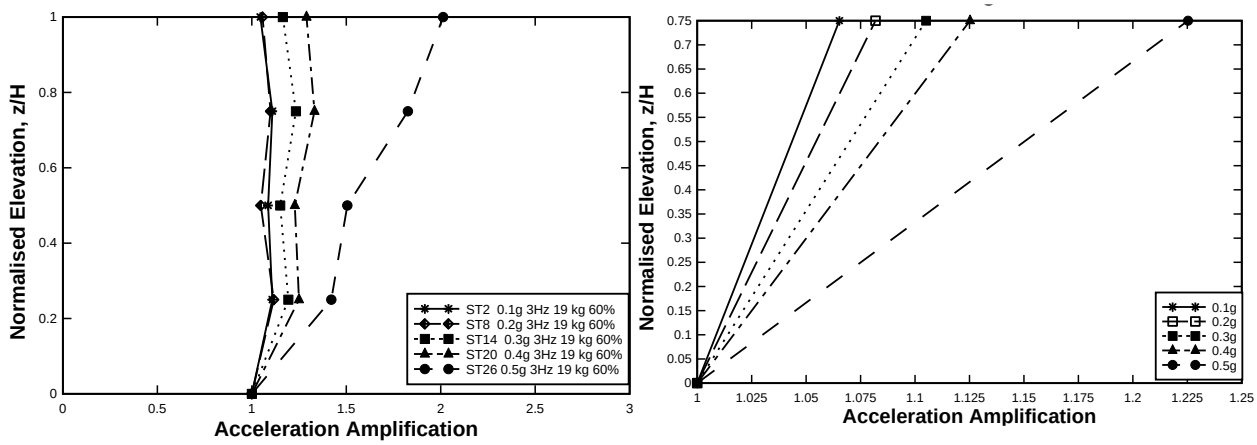

a) b)

[Fig. 4]: a) Effect of base acceleration on acceleration amplification b) Effect of base acceleration on acceleration amplification (Clay layer)

Face displacement response: Horizontal face displacements along the height of the wall have been monitored using three LVDTs positioned as shown in Fig. 3. Fig. 5 presents the displaced face profiles from various tests after 20 cycles of sinusoidal motion. Here elevation (z) and horizontal displacements (h) have been presented in non-dimensional form after normalizing them by the total height of the wall (H). Fig. 5 shows normalized displacement profiles of the facing after 20 cycles for different base accelerations of 0.1, 0.2, 0.3, 0.4 and 0.5g from tests ST1 (0.1g, 1Hz and 19 kg), ST7 (0.2g, 1Hz and 19 kg), ST13 (0.3g, 1Hz and 19 kg), ST19 (0.4g, 1Hz and 19 kg) and ST25 (0.5g, 1Hz and 19 kg) respectively. The normalized displacements are relatively high at the higher base accelerations. A maximum horizontal displacement of 2.02% of the total wall height, H, for 0.5g have been observed compared with 0.01% for 0.1g base acceleration. The displacements obtained in the present study are in close agreement with the results presented by Sakaguchi et al. (1992) and Krishna et al (2007) corresponding to the accelerations and frequency levels used in the present study.

Pore Pressure response: Fig. 6 presents typical pore pressure variations obtained from the model tests. Fig. 6 shows variations of the pore pressure from model tests ST66 (0.1g, 15Hz and 49 kg), ST72 (0.2g, 15Hz and 49 kg), ST78 (0.3g, 15Hz and 49 kg), ST84 (0.4g, 15Hz and 49 kg) and ST90 (0.5g, 15Hz and 49 kg) with of base acceleration 0.1, 0.2, 0.3, 0.4 and 0.5g respectively for 15Hz frequencies and surcharge load 49 kg. It is observed that pore water pressure has been increased with elevation. The highest pore water pressure is 0.38 kPa at base acceleration 0.5g. The highest pore water pressure for model tests ST66, ST72, ST78, ST84 and ST90 is 0.06, 0.09, 0.17, 0.26 and 0.38 kPa respectively.

CONCLUSIONS

The seismic response of geotextile-reinforced embankment on soft clayey soil has been investigated by conducting shaking table tests on model test. A model test with variations in acceleration and frequency of base motion, surcharge pressure on the crest and pore water pressure (effect of input acceleration) have been described along with the model preparation, testing methodology and results. It has been observed that the seismic response of the embankment has significantly been affected by the variations of the base motion, surcharge pressure on the crest and pore water pressure. In fact, accelerations have been amplified at higher elevations with low surcharge pressures. The acceleration amplification response with change in base shaking frequency clearly indicates the role of the fundamental frequency on the response of the system. In some case the face deformations are high with high base accelerations. Pore water pressure is high at higher elevations with low surcharge pressures and high base acceleration.

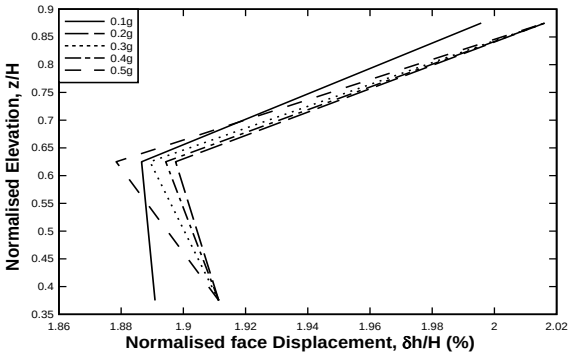

[Fig. 5]: Effect of Acceleration on displacement profile

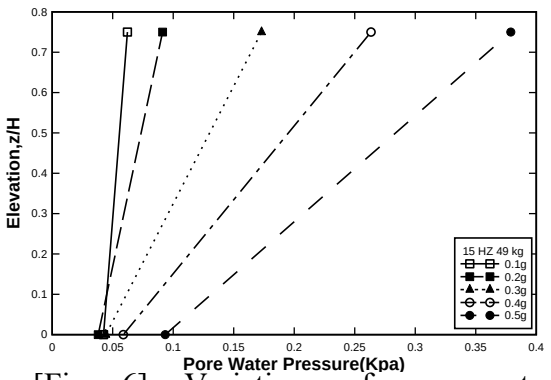

[Fig. 6]: Variations of pore water pressure with respect to Elevation (Effect of base acceleration)

ACKNOWLEDGMENTS

This research has been supported by Geotechnical and concrete Lab, BUET and this support is gratefully acknowledged.

REFERENCES

1. El-Emam, M. & Bathurst, R. J. (2005). Facing contribution to seismic response of reduced-scale reinforced soil walls. Geosynthetics International, 12, No. 5, 215–238.
2. Krishna, A. M. &Latha, G.M. (2007) Seismic response of wrap-faced reinforced soil retaining wall models using shaking table tests Geosynthetics International, 2007, 14, No. 6
3. Hossain, M. Z., &Ansary, M. A. (2018). Development of a portable traveling pluviator device and its performance to prepare uniform sand specimens. Innovative Infrastructure Solutions, 3(1), 53.
4. Moss R. E., Crosariol, V. &Kuo, S (2010) Shake Table Testing to Quantify Seismic Soil-Structure-Interaction of Underground Structures, Fifth International Conference on Recent Advances in Geotechnical Earthquake Engineering and Soil Dynamics, May 24th to 29th 2010.
5. Prasad, S. K., Towhata, I., Chandradhara, G. P. &Nanjundaswamy, P. (2004) Shaking table tests in earthquake geotechnical Engineering, SPECIAL SECTION:GEOTECHNICS AND EARTHQUAKE HAZARDS, CURRENT SCIENCE, VOL. 87, NO. 10, 25 NOVEMBER 2004.
6. Sakaguchi, M., Muramatsu, M. &Nagura, K. (1992). A discussion on reinforced embankment structures having high earthquake resistance. Proceedings of the International Symposium on Earth Reinforcement Practice, IS-Kyushu ’92, Fukuoka, Japan, Vol. 1, pp. 287–292.
7. Srilatha, N., Madhavi Latha, G. and Puttappa, C.G. (2014). Shaking Table Studies on Geotextile Reinforced Soil Slopes, Golden Jubilee Conference of the IGS Bangalore Chapter, Geo-Innovations, 30-31 October 2014, pp.1-8
8. Telekes, G., Sugimoto, M. &Agawa, S. (1994). Shaking table tests on reinforced embankment models. Proceedings of the 13th International Conference on Soil Mechanics and Foundation Engineering, New Delhi, India, Vol. 2, pp. 649–654.
9. Yazdandoust, M. (2017). Investigation on the seismic performance of steel-strip reinforced-soil retaining walls using shaking table test. Soil Dynamics and Earthquake Engineering, 97, Elsevier, pp.216-232.
10. Zhang, Z., Cho,C., Pan, Q. & Lu, X. (2009) Experimental Investigation on Excess Pore Water Pressure in Soft Soil-Foundations under Minor Shocks.World Academy of Science, Engineering and Technology International Journal of Civil and Environmental Engineering Vol:3, No:2, 2009.

DEVELOPMENT OF ZONATION FOR BANGLADESH BASED ON SOFT CLAY USING GIS

R. Hore[1]*, M. R. Arefin[2]& M. A. Ansary[1]

[1]Department of Civil Engineering, Bangladesh University of Engineering and Technology (BUET),Dhaka, Bangladesh.
E-mail: riponhore@gmail.com
[2]Department of Geology and Mining, Rajshahi University, Rajshahi, Bangladesh.
E-mail: riad.gmru@gmail.com

**Corresponding Author*

ABSTRACT
Zonation based on soft soil is very much important for selecting soft soil improvement techniques on the specific location of Bangladesh. In this research total 1000 boreholes have been conducted for SPT test around Bangladesh. From these boreholes 470 boreholes have been selected for soft clay soil layer formation. Three GIS maps have been created by Arc GIS 2010. One for soil parameters information and second is for SPT N value from 1 to 5. Another is for the soft clay layer thickness. The major part of Bangladesh is on the delta formed by the three major rivers brahmaputra, Jamuna and meghna. These rivers and many of the country's other minor rivers originate outside the national boundary of the country and make up the Jamuna-Brahmaputra-Meghna river system. For this reason, availability of soft clay is high in southern part of the country and in the riverside locations. This paper has proposed three GIS based map for which will be useful for selecting soft ground soil improvement techniques in the different regions of Bangladesh.

Keywords: Soft soil; SPT and Zonation

INTRODUCTION
Soft clay soil layer identification is very significant for selecting the different soil improvement techniques. So presenting the subsoil characteristics in one platform is major challenge. Basically soft clay soil is a finely-grained natural rock or soil material that combines one or more clay minerals with possible traces of quartz (SiO2), metal oxides (Al2O3, MgO etc.) and organic matter. Beside these soft clay deposits are mostly composed of phyllosilicate minerals containing variable amounts of water trapped in the mineral structure. Construction on soft clay soil may cause failure the structure. So before construction, implementation the soil improvement techniques has been necessary.

METHODOLOGY
Previous Research

Kamal and Midorikawa (2004) delineated the geomorphology of Dhaka city area, differentiating the ground of the city into seventeen geomorphic units using aerial photographs. These geomorphic units represent the soil conditions. They also classified the fill-sites into four classes based on the thickness of fills. Ansary, M.A. and Rashid,M.A.(2000) has conducted to analysis the mitigation of the disaster due to future shocks is an essential consideration for effective land use and proper town-planning. This is the first study initiated in Bangladesh as part of the micro-zonation investigations. Alam, J. and Islam, S. (2009) has described the understanding the geological setting of Bangladesh is important for

foundation design as well as to assess the Earthquake hazards. A brief description of the geology, stratification and subsoil investigation evidences of soil formations of Bangladesh has been presented in this paper. Hossain et. at. (2003) has evaluated sub-soil characteristics and liquefaction potential of Mirpur DOHS area. To characterize soil deposit eight bore holes were drilled at the project site. Moisture content, specific gravity, Atterberg limits, grain size distribution, unconfined compressive strength, density and shear strength parameters of the collected samples have been determined in the laboratory. Rahman (2004) updated the seismic micro-zonation maps for liquefaction as well as site amplification due to earthquake.

Current Investigation

All these research paper described the sub soil characteristic at specific location of Bangladesh. Basically seismic or liquefaction micro zonation map have been produced. In these research papers an attempt has been conducted to produce proposed zonation map base on soft clay soil using GIS Software 2010 which is effectively useful to selecting proper soil improvement techniques.

Geology of Bangladesh:

The Geology of Bangladesh has been affected by the country's location, as Bangladesh is mainly a riverine country. It is the eastern two-thirds of the Ganges and Brahmaputra river delta plain stretching to the north from the Bay of Bengal. There are two small areas of slightly higher land in the north-centre and north-west composed of old alluvium called the Madhupur Tract and the Barind Tract, and steep, folded, hill ranges of older (Tertiary) rocks along the eastern border. The down warping of the basement rocks under central and southern Bangladesh result from the pressure of sediments that have been accumulating since the Cretaceous period, mostly a large quantity of carbonate. In the Late Eocene epoch the conditions in the Bay of Bengal changed and these deposits ceased. In the late Cretaceous, the Indian Plate collided with the Eurasian Plate, after the Indian and African Plate split to form the Indian Ocean during the Triassic. The tectonic collision in the Cretaceous separated the Gulf of Assam and the Gulf of Burma, while narrow channels from the ocean fed water into the two gulfs. As ridges formed in the Tethys Ocean on the other side of the Shillong and Dinajpur Shields, small island arcs formed locally. The Tura sandstone, Sylhet limestone and Kopili shale were all deposited during an intermediate shall marine depositional environment in between these tectonic changes. A renewed period of collision and tectonic activity began with the Himalayan orogeny in the Eocene. As tectonic activity slowed somewhat, a river delta environment deposited of the other significant Cenozoic sedimentary units. Renewed tectonism in the Pliocene formed the Dinajpur Shield into a graben, relative to the horst of the Shillong Plateau and Mikir Hills. The Pliocene orogeny led into the Pleistocene ice age, resulting in regional extinction of many large mammals. A final period of uplift raised the red clay table lad 30 to 100 feet, along with St. Martin's Island in the Pleistocene. Surface rocks and stratigraphy in Bangladesh have been formed during the Cenozoic and rock units date to all epochs of the Cenozoic except for the Oligocene, which has been poorly preserved.

Sub Soil Condition

The sub-surface investigation work includes execution of 1000 borings, performance of the required field tests. Boreholes have been drilled vertically using wash boring technique. The density and stiffness characteristics of the subsoil layers in the boreholes have been measured by performing Standard Penetration Test (SPT). The bore logs along the alignment has been shown by Fig. 1. The sub soil investigation has been performed by Soil and Foundation Consultants. Thickness of soft clay layers varies from 1 to 20 m. The most common index properties for estimating liquefaction strength is the N-value obtained from the standard penetration test. The SPT consists of driving a thick-walled sampler into the granular soil deposit. The measured SPT N-value (blows per foot) is defined as the penetration resistance of the soil, which equals the sum of the number of bows required to drive the SPT sampler over the depth interval of 15 to 45 cm. Driving the standard split-barrel sampler of dimensions. a distance of 460 mm into the soil at the bottom of the boring and counting the number of blows to drive the sampler the last 305 mm to obtain the N number. Using a 63.5 kg driving mass (or hammer) falling "free" from a height of 760 mm.

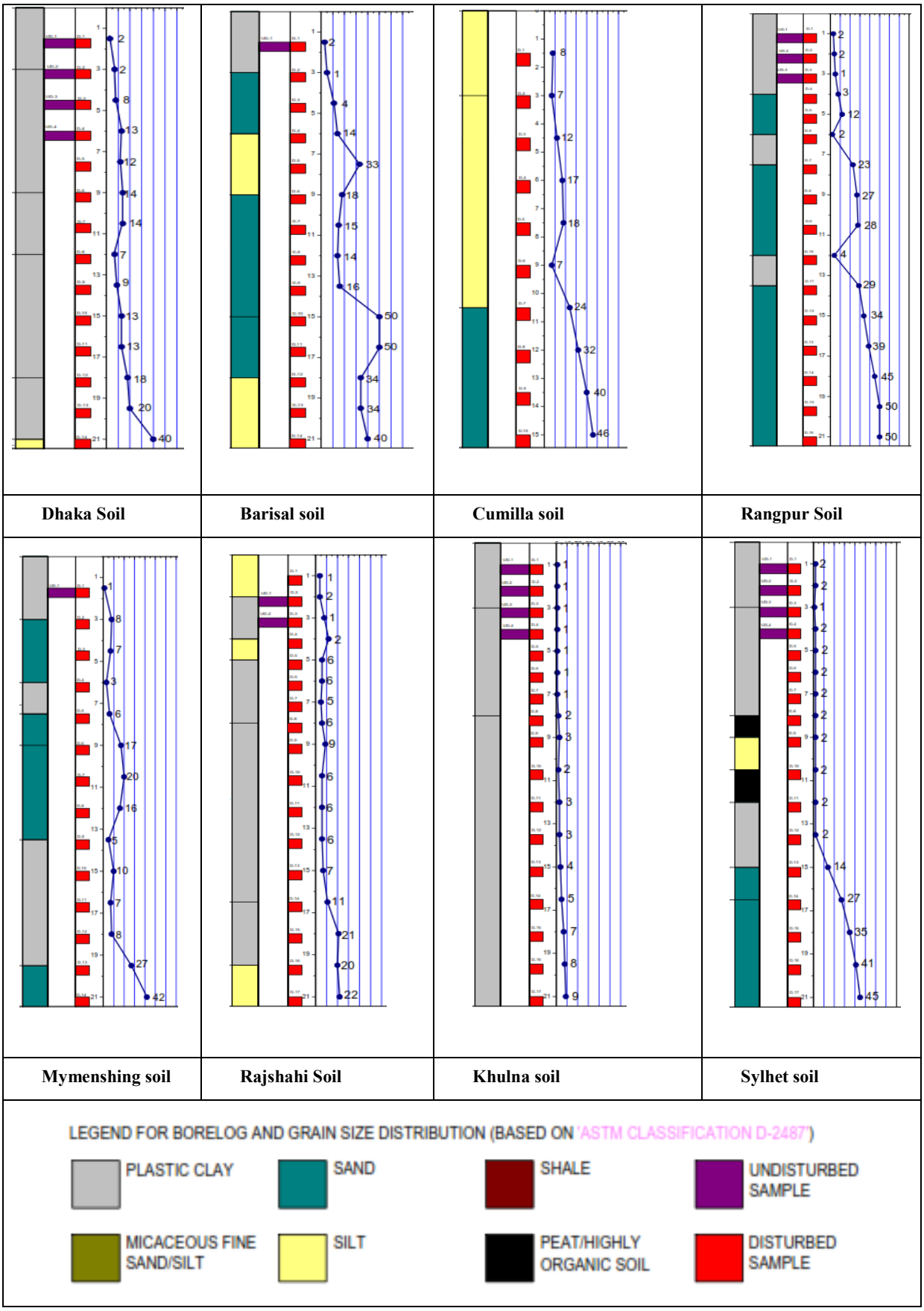

[Fig. 1].Sub Soil information

RESULTS AND DISCUSSIONS

Geographical information System (GIS)

GIS application in Geotechnical purpose and the spatial distribution is new dimension for data analysis for proper structural suitability study. First step for the GIS application is data processing for GIS input. Data processing belonging the modification of the location of the lithology and analysis the data. Classify the soft layer at particular interval depending on SPT (SPT value 1 to 5). Two map named SPT distribution and lithological thickness has been shown in Fig 2. After processing the data locations has been input into the GIS interface. Sub soil information has been shown in Table 1. Soft clay soil thickness layer, clay layer thickness, N value rang and soil type have been input in the table. Latitude, Longitude and location have also been shown in the table. This table has been imported to GIS interface.

Table 1: Sample Information of GIS input

LAT.	LONG.	Thickness Layer (m)	Thickness (m)	N value Range	N value (Max.)	N value (Min.)	Soil type	Location
92.00	24.83	0-18	18.00	1-5	5.00	1.00	Clay	Sylhet
92.15	24.89	0-7	7.00	1-4	4.00	1.00	Clay	Sylhet
91.89	24.91	0-4	4.00	1-5	5.00	1.00	Clay	Sylhet
91.98	24.91	2-5	3.00	1-5	5.00	1.00	Clay	Sylhet
92.10	25.16	4-6	2.00	3-5	5.00	3.00	Clay	Sylhet
91.80	24.98	0-6	6.00	3-5	5.00	3.00	Clay	Sylhet
91.93	24.95	2-7	5.00	1-5	5.00	1.00	Clay	Sylhet
91.75	24.85	0-3	3.00	1	1.00	1.00	Clay	Sylhet
91.72	24.88	0-4	4.00	1-4	4.00	1.00	Clay	Sylhet
92.15	24.88	0-4	4.00	1-4	4.00	1.00	Clay	Sylhet
91.85	24.91	2-4	2.00	4	4.00	4.00	Clay	Sylhet

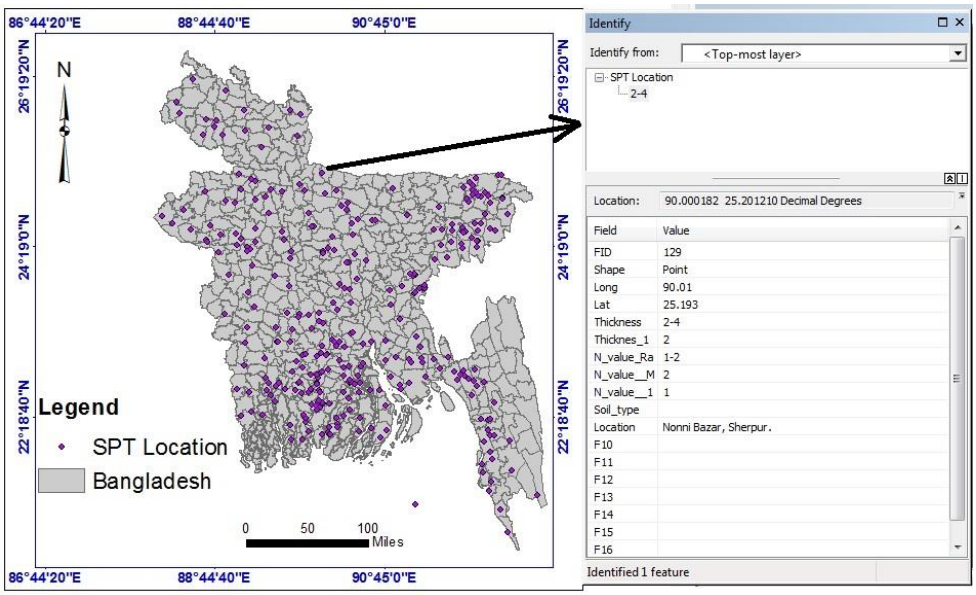

[Fig. 2]: SPT Location Map

In this research total 1000 boreholes have been conducted for SPT test around Bangladesh. From these boreholes 470 boreholes have been selected for soft clay soil layer formation. Three GIS maps

have been created by Arc GIS 2010. One for soil parameters information map and second is zonation map for SPT N value from 1 to 5. Another is zonation map for the soft clay layer thickness. Soil parameters information map has been shown in Fig. 3. From the map different sub soil parameters have been found by clicking the specific location of Bangladesh. Total 470 bore hole (soft clay soil layer) has been presented in the GIS interface map. On the other hand zonation map for SPT N value has been shown in Fig. 3. soft clay layer thickness has been shown in Fig. 4.

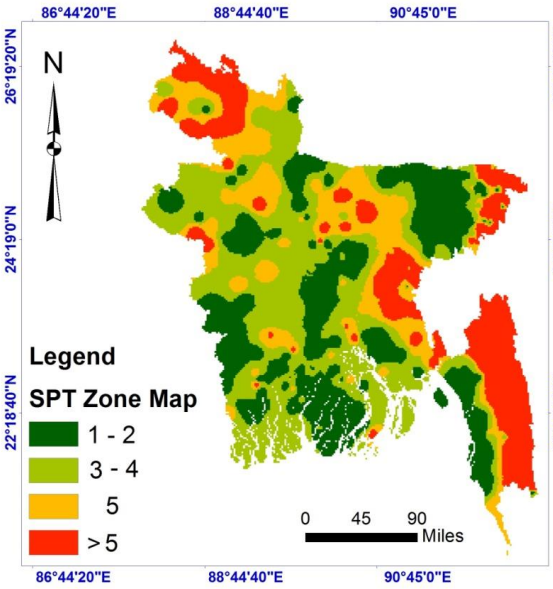

[Fig. 3]: Zonation map based on SPT value

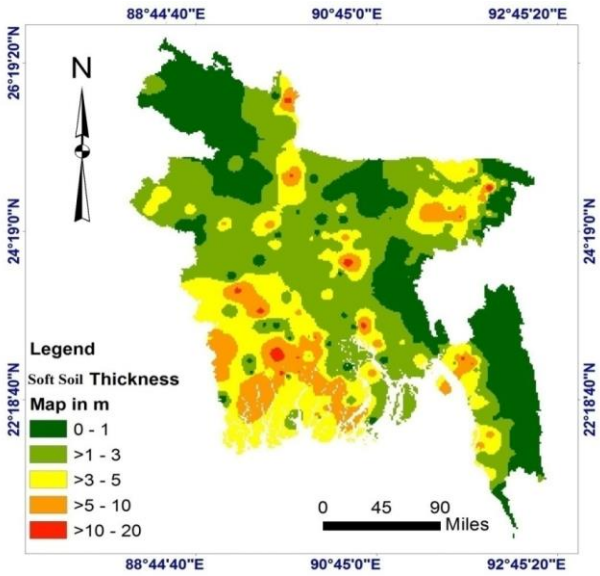

[Fig. 4]. Soft soil thickness map

CONCLUTION

Availability of soft clay is high in southern part of the country and in the riverside locations. The soft cay soil thickness is varying from 1 to 20 meters. This paper has proposed three GIS based map which will be useful for selecting soft ground soil improvement techniques in the different regions of the country.

REFERENCES

1. Alam, J.and Islam,S. (2009) "Geological Aspects of Soil Formation of Bangladesh" Bangladesh Geotechnical Conference 2009 (BGC-2009), Dhaka, Bangladesh.
2. Ansary, M.A. and Rashid,M.A.(2000), Generation of liquefaction potential map for Dhaka, Bangladesh, proceeding of 8th ASCE speciality conference on probabilistic Mechanics and Structural and Reliability, paper no.PMC 200-061.
3. Hossain, S.M.Z., Alam, M.S. and Islam, M.S., (2003). Geotechnical characterization and liquefaction potential of sub-soil of Mirpur DOHS, Undergraduate thesis, Department of Civil Engineering, Military Institute of Science and Technology, Dhaka,Bangladesh.
4. Jamiolkowski, M.(2003), "Soil Parameters Relevant to Bored PileDesign from Laboratory and In-Situ Tests," Deep Foundations on Bored and Auger Piles, Millpress, Rotterdam,The Netherlands, pp. 83–100.
5. Kamal and Midorikawa (2004) ,GIS-based geomorphological mapping using remote sensing data and supplementary geoinformation. A case study of the Dhaka city area, Bangladesh, December 2004International Journal of Applied Earth Observation and Geoinformation 6(2):111–125.
6. Rashid, A.(2000), "Seismic Microzonation of Dhaka City based on site amplification and liquefaction", M. Engg. Thesis, Department of Civil Engineering, BUET,Dhaka ,Bangladesh.

Rahman, M.G.(2004),"Seismic Damage Scenario for Dhaka City" , M.Sc. Engg. Thesis, Department of Civil Engineering, BUET, Dhaka, Bangladesh.

SOIL IMPROVEMENT USING LIME AND POLYPROPYLENE FIBERS

M. M. Hossain*, R. C.Malo &M. H. Safi
[1]*Department of Civil Engineering, Bangladesh University of Engineering & Technology, Dhaka, Bangladesh.*
E-mail:monirhshimul@gmail.com

**Corresponding Author*

ABSTRACT

Soil modification is the process which involves enhancing the anatomical substance of the soil apropos improve its strength, durability by mixing with additives. Foundation of a structure on the soft clay soil may be responsible for the excessive settlement of the structure. Soil modification helps to decreasing the foundation cost by increasing bearing capacity. In this study, lime and polypropylene fibres were used with soil to observe its effect on the bearing capacity. Different concentration of lime (0 to 15%) by weight of soil and 2% polypropylene fibres by weight of lime were mixed with different soil samples according to the soil categories like sandy and clay and silt soil. The necessary parameters of the soil were determined and unconfined compressive strength of the soil was also measured by laboratory testing machine with different curing days. The result revealed the optimum value of the unconfined compressive strength was obtained for the concentration of 10% lime for clay and silt soil on the other hand 7.5% for the sandy soil.

KEYWORD: Soil Improvement, Unconfined Compressive Strength, Lime, polypropylene fibres.

INTRODUCTION

Soil enhancement is the term of permanent solution by the originally and chemically improvement of soil properties. Implementation of earth increase the bearing capacity of the soil beside it's reduce the settlement of the foundation and control the shrink-swell of the soils. Stabilization of soil can be used to treat a wide range of sub-grade materials from expansive clays. There are various way to improve the subsoil which is very soft and expansive in the geotechnical field by using the different materials, like polypropylene fibres. The improvement of sub-structure, Pavement, roadways, building foundations, channel and reservoir linings, irrigation systems, water lines, and at sewer lines to avoid the damage due to the settlement of the soft soil or to the swelling action of the expansive soils. Requisite to develop by the chemical stabilization at the soft fine-grained soil. Chemical stabilization wind up mixing chemical additives with natural soils to remove moisture and increase strength of the soil especially in the sectors sub-grade. The stabilizing materials in the treatment process is either reinforcing of the bonds between the particles or filling of the pore spaces.

Chemically soil stabilization is achieved by the addition of proper percentages of cement, lime, fly ash, bitumen, or combinations of these materials to the soil. Alternative of the type and the determination of the concentration of the additive were used are dependent over the soil classification and the rate of improvement in soil quality desired. Mostly, little amounts of additives are required when it is simply desired to modify soil substance what gradation, workability, and plasticity. When it is term to improve the strength and durability respectively, bigger quantities of additive are used. After the additive has been mixed with soil, spreading and compaction are achieved by conventional means.It is a great chance to make settlement at foundation and basement with the changes of moisture content because moisture in the soil changes expansive soil will move. In the time of wetter clay grows, during dry seasons clay shrinks.

Santoni et al (2001), studied on six types of non-plastic cohesion less soils reinforced with monofilament polypropylene fiber the unconfined compressive strength of reinforced soil. They found optimum fiber

content is 0.8% and fiber content is less than 0.6% caused strain softening more than 0.85% causes strain hardening**.** *Kumar, Walia and Bajaj* (2007), have reinforced the black cotton soil with polyester synthetic. They investigated on unconfined compressive fly ash, lime and randomly oriented fibers on the characteristics of expansive soils. The results shows that unconfined compressive strength increases with increase of fiber content.*Chandra et la* (2008), have studied on three types of soil reinforced with polypropylene fiber of 0.3mm diameter the static triaxial test of unreinforced and reinforced soil shows that uniaxial compressive strength for lower value is 3.824 and optimum value is 9.712 MPa respectively. (1979), *Andersland and khattak* made a research on the kaolinite soil with the cellulose fiber fibers. The triaxial test was conducted the test results indicates the addition of fiber at 16% increase the maximum shear strength by 43% when the pure kaolinite is used. (1983),*Gray and Ohashi* were perform an extensive study on the shear strength of the soil reinforced with fibers and they concluded the inclusion of fibers in sands increases peak shear strength and limited post peak decrease in shear resistance. (1987), *Setty and Rao* have investigated on lateritic soil at optimum moisture content and reinforcement with polypropylene fiber. The triaxial test, CBR and tensile test are conducted the results indicated that the addition of fibers increases cohesion and slightly decreases Φ and also showed that CBR value has been improved by 2.2 times up to 2% fiber content and also improves dry strength.*Ranjan et al* (1996), studied on different types of soils likewise sand, medium sand, fine sand, silt sand and silt reinforced with polypropylene monofilament coir and bhabarthe result of triaxial test showed greater ductility, no loss of post peak strength and increase in stiffness. Due to tensile strength in fibers confining pressure is greater than critical confining pressure. *Charan* (1996), studied on silt, sand to coarse sand reinforced with polypropylene and natural fiber coir and bhabar the triaxial and CBR test were conducted the test results shows that the confining pressure is less than critical confining pressure and the CBR value is improved by two times at the fiber of 1.5%.

OBJECTIVE OF THIS STUDY

Bangladesh is full of resource because of its riverine. Bangladesh is country with pre-dominantly alluvial soil. Because of existence of high water table, in most cases, throughout the year the soil remains wet or saturated with water. In such a situation, engineers often have to go for costly foundation in constructing roads and buildings. Sub grade soil with a CBR value of less than 3 or SPT value of 2 or 3 often encountered in the field. When the SPT value is 2 or less, engineers are often forced to go for deep foundation even for low rise three to four story building. By improving the strength of sub grade soil, cost of road and building construction can be reduced effectively. Previous studies have revealed that lime and fiber added with soil can improve the bearing capacity of soil. This study is aimed at assessing the Improvement of bearing capacity of local soil by using lime and locally available polypropylene fiber in different proportions. If significant improvement is observed with the local soil then findings may be used by the practicing engineers for designing and ensuring economy in construction.

METHODOLOGY

The soil sample collected from different part of Dhaka city especially from the Aftab Nagor and Narayangonj area. These soil samples were classified according to Massachusetts Institute of Technology (MIT) classification. Atterberg limit test, sieve analysis as well as Hydrometer Analysis were conducted. The consistency limit test of soil by using the Casagrande apparatus. The ASTM standard procedure was followed for performing particle-size analysis of fine grinded soil that was based on the sedimentation of the particle, and was measured by flotation of hydrometer for 36 hours. Lime slurry can be used to exercise soils which is made by chemically change calcium carbonate (CaCO3) into calcium oxide beside hydrated lime is drawn up when quicklime chemically operate together with water. Locally available limestone was collected from the market. The limestone was converted into powder by drop a little bit of water.

Lime and polypropylene fiber has been added to test the improvement in stabilization of the soil samples. There curing periods: 0, 3, 7, 14, 21 and 28 days were used. Nine different percentages of lime: 0%, 2.5%, 5%, 7.5%, 10%, 12.5%, and 15% were used. It was mixed with a constant 2% nylon thread by weight of

lime. The compressive strengths of lime stabilized soil were evaluated for different curing period: 3, 7, 14, 21, and 28 days.

RESULT AND DISCUSSION

Soil Properties (Flat land soil Aftab Nagor, Dhaka) According to MIT soil classification, this soil is sandy silt and some clay.							
Parameters	Percentages (%)	Concentration of lime (%)	Compressive strength (psi)				
			3days	7days	14days	21days	28days
Sand	20	0	8	8	8	8	8
Silt	65	2.5	15	22	27	32	33
Clay	15	5	18	27	36	31	42
Liquid limit	27	7.5	18	30	37	46	50
Plastic limit	15	10	26	32	40	50	57
Plasticity index	12	12.5	22	35	38	48	54
Optimum Moisture content	19	15	20	24	21	36	37
Specific gravity	2.65						
Salinity	Nil						

***0 Control specimen**
Average value compressive strength
2% polypropylene fibres by weight of lime

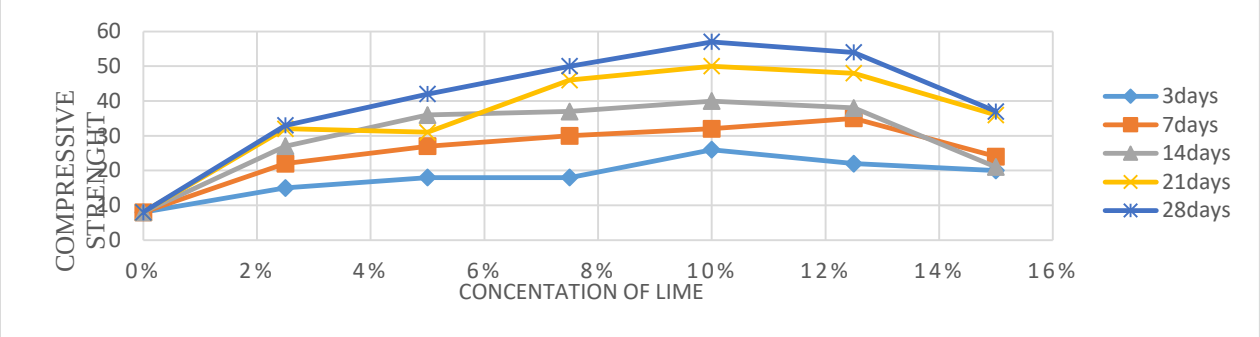

Unconfined compressive strength of flat soil with varying percentages of lime and various curing period.

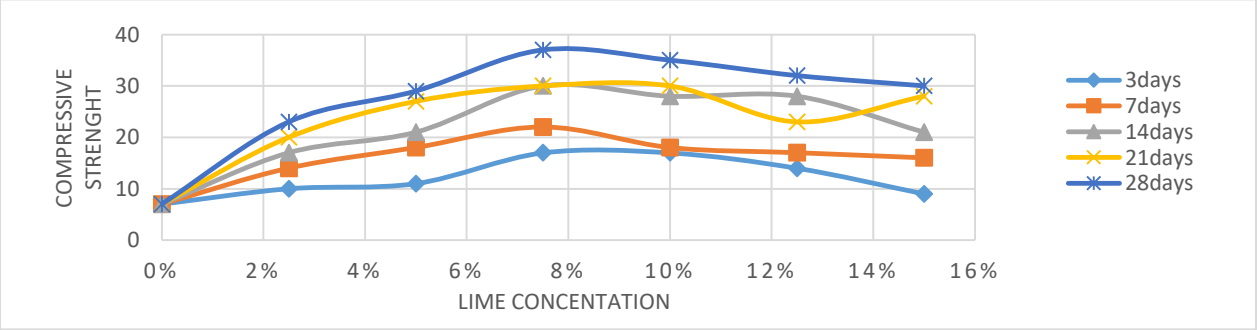

Unconfined compressive strength of field soil with varying percentages of lime and various curing period.

The result be associated with the classification of soil samples of soil sample are shown in the tabular form.

Soil Properties (fields soil from Narayanganj, Dhaka)

According to MIT soil classification, this soil is clayey, silt and some sand.							
Parameters	Percentages (%)	Concentration of lime (%)	Compressive strength (psi)				
			3days	7days	14days	21days	28days
Sand	15	0	7	7	7	7	7
Silt	25	2.5	10	14	17	20	23
Clay	60	5	11	18	21	27	29
Optimum moisture content	19	7.5	17	22	30	30	37
Specific gravity	2.6	10	17	18	28	30	35
Salinity	Nil	12.5	14	17	28	23	32
		15	9	16	21	28	30
***0 Control specimen** **Average value compressive strength** **2% polypropylene fibres by weight of lime**							

The concentration of limestone procedures are given as follows from the local market.

Lime properties		
No	Concentrations %	Parameters
1	70	Calcium oxid-CaO
2	30	Additive materials

CONCLUSION

The result stated which the optimum value of the unconfined compressive strength was obtained for the concentration of 10% lime with addition of 2% polypropylene fibers by the weight of lime for clay and silt soil on the other hand 7.5% with 2% polypropylene fibers by the weight of lime for the sandy soil. The increase is more than many times from the base strength of the normal soil. It is also noticeable that when the percentage of sand increase the strength decrease for the resion of the run-on of lime and polypropylene fibres in the earth. The bearing capacity increase with curing time.

ACKNOWLEDGEMENTS

The authors thankfully acknowledges the services given by the laboratory technicians of the Bangladesh university engineering and technology, (BUET) Geotechnical laboratory during the experiments. We also thankful to Eng. S.M.Tanjid Ahmed for his all kinds of support.

REFERENCES

A. Suat Akbulut, Seracettin Arasan, Ekrem Kalkan, "Modification of clayey soils using scrap tire rubber and synthetic fibers", Applied Clay Science 38, 2007, doi:10.1016/j.clay.2007.02.001.

A. S. Soganc, "The effect of polypropylene fiber in the stabilization of expansive soils", ISSRI, vol.9, 2015.

Amin Chegenizadeh, Hamid Nikraz, "Study on strength of fiber reinforced clayey sand", ICSE, 2011.

Arun Patidar, H. K. Mhiyar "An experimental study on stabilization of black cotton soil using HDPE wastage fibers, stone dust and lime", IJASTR, vol. 6, Issue 4, Dec 2014.

B. Soundara, K. P. Senthil Kumar"Effect of fibers on properties of clay", IJEAS, vol.2, Issue 5, May 2015.

Babak Amini Behbahani, Hadi Sedaghatnezhad, Foad Changizi, "Engineering properties of soils reinforced by recycled polyester fiber", IOSR-JMCE, vol. 13, Issue 2Mar-Apr. 2016, pp. 01-07, doi:10.9790/16841302030107.

K. Subash, "Stabilization of black cotton soil using glass and plastic granules", IJERT, vol 5, Issue 4, April 2016.

K. K. Ajmal, "An experimental study on partial replacement of soil with plastic granules", vol.7, IJSRT, Issue 4, April 2016

Yadav Parit, Meena Kuldeep Kumar, 2011; "A comparative study in soil plasticity of hall area and lecture complez area of NIT Rourkela. National Institute of Technology Rourkela, Rourkela-769008, India.

Eisazadeh et al. 2012; "Soil stabilization using lime. "Research Journal of Applied Sciences, Engineering and technology 8(4): 510-520, 2014.

M.R Thomson and B.J. Dempsuy, 1969, "Autogenous healing of lime soil mixtures." Highway Research Board, Issue Number: 263.

Endes and Grim, 1966, "A quick test for to determine requirements for lime stabilaization." Internet, Conf. on Soil Mech. and Found. Engg. , Paris Vol. 2 pp. 269-275, 1966.

Mr. Arpan Sen and Mr. Rishab Kashyap, 2012, "Soil stabilization using waste fiber material." National Institute of Technology Rourkela, Rourkela- 769008, India.

Paramreet Kaur and Gurdeep Sing, 2012, "Soil improvement with lime." IOSR Journal Of Mechanical and Civil Engineering(IOSRJMCE) ISSN : 2278-j684 Volume 1, Issue 1 (May-June 2012), PP 51-53, Sayed Mhadi Hejazi, Mohammad Sheikhzadeh, Sajed Mahdi Abtahi, Ali Zadhoush, 2011 : "A simple review of soil reinforcement by using natural and synthetic fibers." Constraction of building materials volume 3.

Swamson and Thomson, 1967; "Determination of fatigue life of a granular base material lightly stabilized with slag lime from indirect tensile testing." Journal of Transtportation Engineering Vol 136, Issue 8 ((August 2010).

Chaddock, B. C. J., (1996), "The Structural Performance of Stabilized Road Soil in Road Foundations,"

Lime stabilization.a.Thomas Telford.

Evans, P., (1998). "Lime Stabilization of Black Clay Soils in Queensland, Australia," Presentation to the

National Lime Association Convention, San Diego, California

Soil Mechanics and Foundation Engineering by *Arora.*

Geotechnical Engineering by *C.Venkataramiah.*

Soil Mechanics and Foundations by *B.C.Punmia, Ashok Kumar Jain and Arun Kumar Jain.*

Geotechnical Engineering by *S.K.Gulhati&ManojDatta.*

Foundation Engineering by *V.N.S.Murthy*.

4th International Conference on Advances in Civil Engineering 2018 (ICACE 2018)
19 –21 December 2018
CUET, Chittagong, Bangladesh
www.cuet.ac.bd

PERMEABILITY CHARACTERISTICS OF FLY ASH AND LIME TREATED SOILS

M. S. Islam, T. Islam* & N. Khatun

Department of Civil Engineering, Bangladesh University of Engineering &Technology, Dhaka, Bangladesh.

E-mail: ti.cebuet187@yahoo.com

**Corresponding Author*

ABSTRACT
Fly ash is used as soil stabilizer, which is technically viable, cost effective and environmentally beneficial alternative. This paper focuses on the evaluation of the effectiveness of fly ash on the coefficient of permeability of treated soils. Later, the efficacy of fly ash is compared with that of lime. Laboratory investigations were carried out on two soil samples which were collected from Porsha of Rajshahi (Soil Type-1) and from Mirpur of Dhaka (Soil Type-2). Soils were treated with lime and fly ash at different percentages of 1%, 3%, and 5% (by weight). The tests were performed on air-dry sample after allowing different reaction time. Soil Type-1 was clayey soil of low plasticity and its permeability was determined by using falling head method. Constant head test was performed for Soil Type-2 to determine its permeability characteristics as it was sandy soil. After mixing soil with additives at a definite proportion, a time varied from 3 to 14 days was allowed for the reaction of lime and fly ash to occur with water and soil particles. It was found that with the increase in additives, permeability and void ratio of both the soils decreased, where the decrease rate was more in case of fly ash treated soils than that of lime treated soils. Test results imply that fly ash treated soils can be used as lining for earth water reservoir, irrigation canal and pond.

Keywords: Fly ash; lime; permeability; stabilization

INTRODUCTION
Bangladesh is a land of rivers and canals. Its ground formation mainly consists of alluvial deposits. Due to lower water table in dry seasons, water flows from storage reservoir, ponds, etc. through the soil by percolation or seepage. This problem is severe in case of projects constructed on sandy and silty types of soils (Khatun, 2017). Proper use of fly ash can reduce the cost of stabilization with cement or lime, as fly ash is a waste material. Soil improvement in some locality is, therefore, essential particularly for water retention purpose in Bangladesh (especially, in Tangail, Manikganj, Thakurgaon, Sirajgong, Rangpur, Dinajpur, Cox's Bazar area). Fig. 1 shows the topography of pond in Porsha. It is situated in Naogaon district of Rajshahi division. At present, many parts of the Barind Tract suffer from problems of water scarcity (Uddin et al, 2017). Although a number of researches were carried out (Islam et al, 2005) to investigate the strength and deformation characteristics of stabilized soils, little attempt has been taken to assess the hydraulic characteristics of such treated soils in Bangladesh. The permeability of soil depends upon various factors, such as size and shape of the particle, particle orientation, temperature of liquid, soil compaction, etc. In addition to this, permeability of treated soil depends on additive types, additive content, procedure of mixing, curing time (reaction time) and procedure of curing, etc. (Arora, 2008). Indian Road Congress (IRC, 1973) and Haunsmann (1990) have described the basic mechanism of soil-lime interactions as: (1) Cat-ion exchange; (2) flocculation or

agglomeration; (3) carbonation; and (4) cementation. The objectives of this study are to investigate permeability characteristics of additives treated soils; and to evaluate the effect of additives content and curing age (reaction time) on the permeability of treated soils.

Depth of pond = 4 – 5 m, lower water table position due to scarcity of water

Fig. 1 Topography of a pond in Porsha, Naogaon

METHODOLOGY

Fly ash and lime were used as additives. A comprehensive laboratory investigation program was undertaken following ASTM standards in order to examine the physical, index, engineering characteristics of the base soils and chemical composition of additives.

Sampling and Collection of Soil Samples

Laboratory investigations (constant head permeability test and falling head permeability tests) on untreated and treated soil with three different lime and fly ash contents (1%, 3% and 5%) were carried out. The soil samples were collected from Porsha, Rajshahi (Soil Type-1, clay of low plasticity) and Mirpur, Dhaka (Soil Type-2, fine sand). The study area of Porsha is located in the Barind region, which lies within Naogaon district, lies in a part of North West region of Bangladesh (Uddin et al, 2017). Soil sampling was carried out according to the procedure outlined in ASTM 0420-87. For each location approximately 2m×2m area was excavated to a depth of 2m-3m using hand shovels. Proper care was taken to remove any loose material, debris, coarse aggregates and vegetation from the bottom of the excavated pit. Disturbed samples were collected from the bottom of the borrow pit through excavation by hand shovels. All samples were packed in large polythene bags covered by gunny bags so that the soils do not lose water content.

Experimental Setup

Constant head and falling head permeability were calculated using equations (1) and (2).

$$k_T = \frac{QL}{Ath} \qquad (1)$$

where, k_T= Coefficient of permeability at temperature T, cm/sec; L = Length of specimen in centimetres; t = Time for discharge in seconds; Q = Volume of discharge in cm^3; A = Cross-sectional area of permeameter; h = hydraulic head difference across length L, in cm of water.

$$k = \frac{aL}{At} \ln \frac{h_1}{h_2} \qquad (2)$$

where, a= Cross sectional area of the stand pipe; A= Cross sectional area of the soil sample; h_1= Hydraulic head across sample at beginning of the test; h_2= Hydraulic head across sample at end of the test; L= Length of the soil sample.

Void ratio of soil was calculated using equation (3), viscosity of water was also corrected.

$$e = \frac{G_s \gamma_w V_r}{W_s} - 1 \qquad (3)$$

where, W_s is the dry weight of the soil grain and V_r is the total volume of soil.

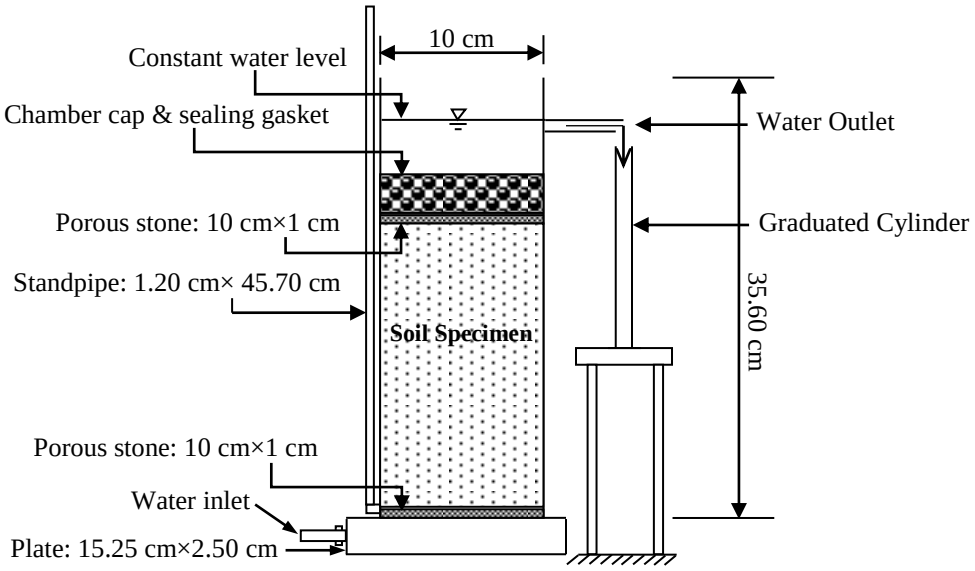

Fig. 2 Constant head experimental set-up used in this study

Sample Preparation

Disturbed samples collected from field were air-dried. The soil lumps were broken carefully with a wooden hammer so as to avoid breakage of soil particles. The required quantities of pulverized soil were sieved through sieve No. 40 (0.425 mm). The fly ash and lime treated soils were compacted following ASTM D558 method. The compacted samples were cured in moist environment for 7 days and air-dried.

Soil Properties

In Fig. 3, grain size distribution curves of the selected soil samples are presented. Their index properties are presented in Table 1. It is observed that, Soil Type-1 and Soil Type-2 are CL and SP, respectively.

Table 1 Index properties of the soil samples collected from study areas

Index Properties and Classification	Soil Type-1	Soil Type-2
Specific Gravity, G_s	2.65	2.72
Liquid Limit, LL (%)	35	-
Plastic Limit, PL (%)	19	-
Plastic Index, PI (%)	16	-
Sand % (0.06 mm~ 2 mm)	3	100
Silt % (0.002 mm~0.06 mm)	79	-
Clay % (< 0.002 mm)	18	-
Group Classification (ASTM D2487)	CL	SP

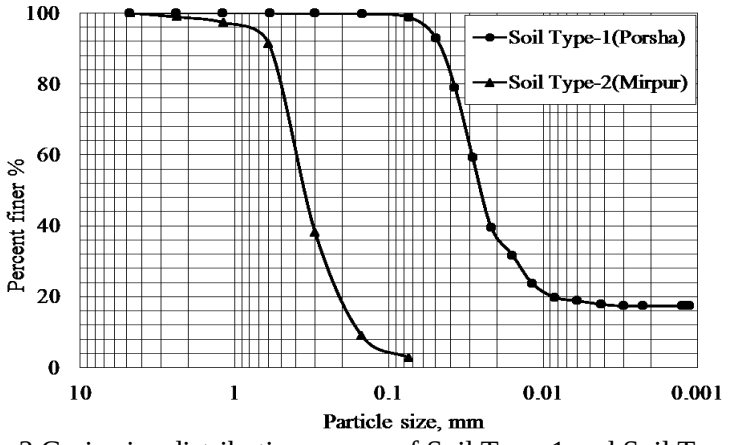

Fig. 3 Grain size distribution curves of Soil Type-1 and Soil Type-2

RESULTS AND DISCUSSIONS

Permeability of the two samples was tested in the laboratory to investigate the effect of lime and fly ash treatment. The tests were performed on the treated samples at 3 day, 7 day and 14 day (for Soil Type-1 and Soil Type-2) after mixing and subsequently cured for reaction to occur in air-dry state (the curing period was defined earlier as the reaction time).

Effect of Lime Content on Permeability and Void Ratio

To check the repeatability of test samples, two samples were prepared with similar conditions. From the tests, it was observed that both void ratio and permeability were varied significantly. Relationship between permeability and lime content for Soil Type-1 and Soil Type-2 is shown in Fig. 4. Permeability of sand is more than that of clay, as sand particles are larger. For this reason, sand (Soil Type-2) is more porous than clay (Soil Type-1) which can also be remarked from the figures. From Fig. 4, it is observed that permeability decreases with the increase of lime content. The decrease rate increases over the reaction time. Fig. 5 denotes the relationship between void ratio and lime content for Soil Type-1 and Soil Type-2. From the graphs, it is seen that the void ratio decreases with the increase of both the lime content and reaction time.

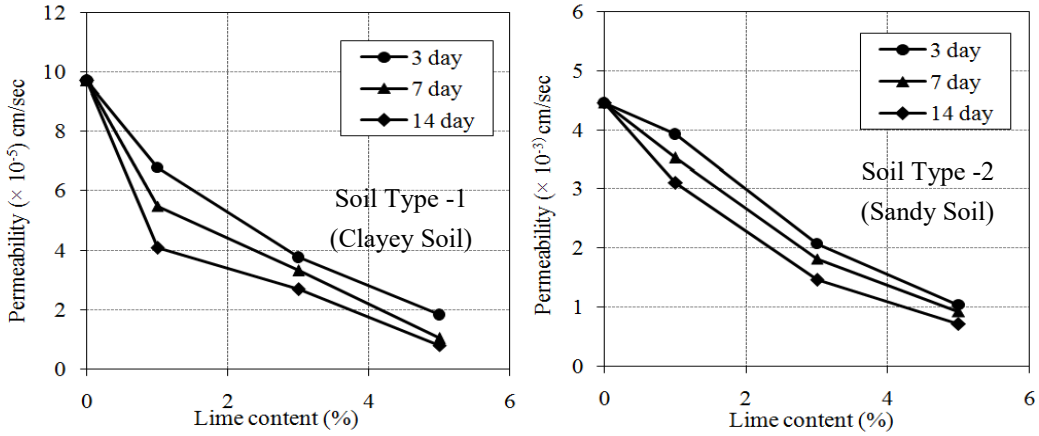

Fig. 4 Relationship between permeability and lime content of: (a) Soil Type-1; (b) Soil Type-2

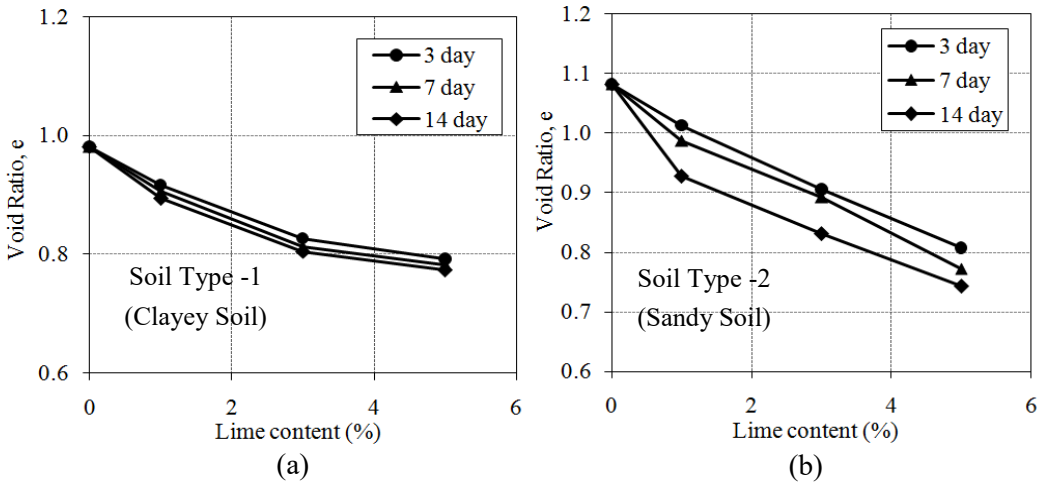

Fig. 5 Relationship between void ratio and lime content of: (a) Soil Type-1; (b) Soil Type-2

Effect of Fly Ash Content on Permeability and Void Ratio

Fig. 6 shows the relationship between permeability and fly ash content for Soil Type-1and Soil Type-2. Permeability decreases by the increase of fly ash content. Relationship between void ratio and fly ash content for both the types of soils are shown in Fig. 7. Permeability decreases by the addition of fly ash content. The decrease rate of permeability increases over the reaction time.

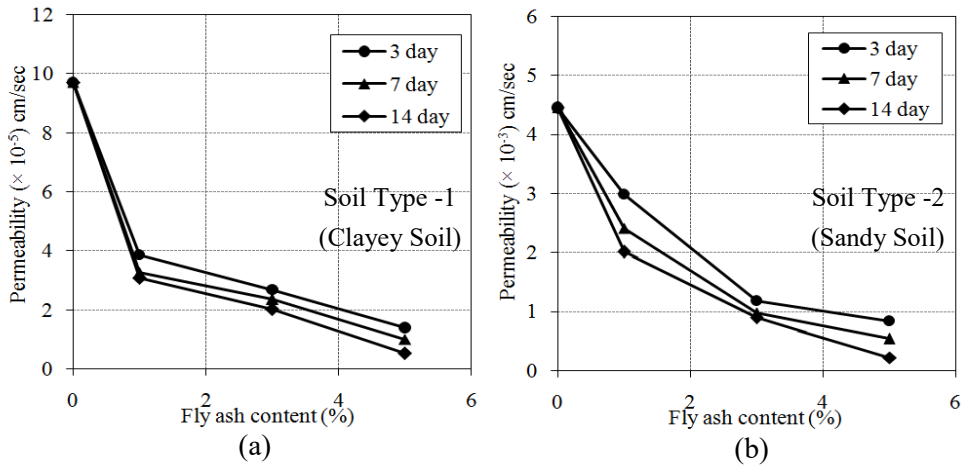

Fig. 6 Relationship between permeability and fly ash content of: (a) Soil Type-1; (b) Soil Type-2

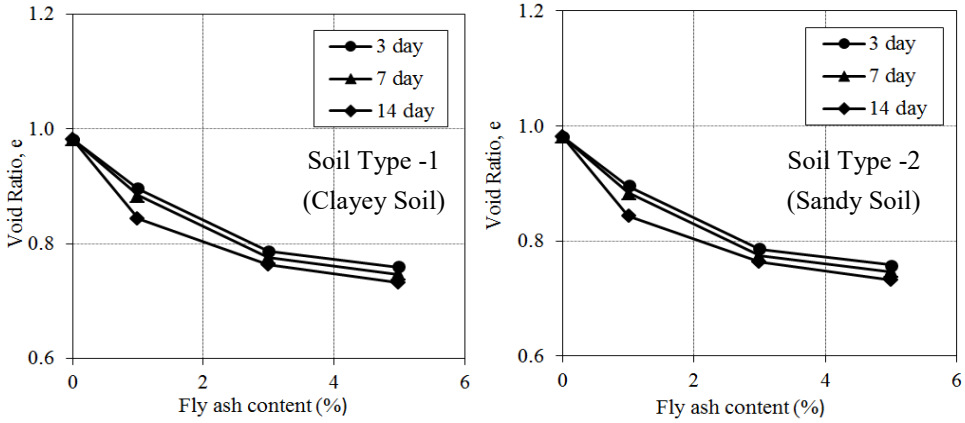

Fig. 7 Relationship between void ratio and fly ash content of: (a) Soil Type-1; (b) Soil Type-2

Comparison between Permeability and Void Ratio with Lime and Fly Ash content

Since permeability of treated soil is very sensitive to void ratio, soil fabric and structure, aging after reconstitution, stress level, etc., attention was given to maintain these controlling factors unchanged among the tests except the lime content, fly ash content and aging.

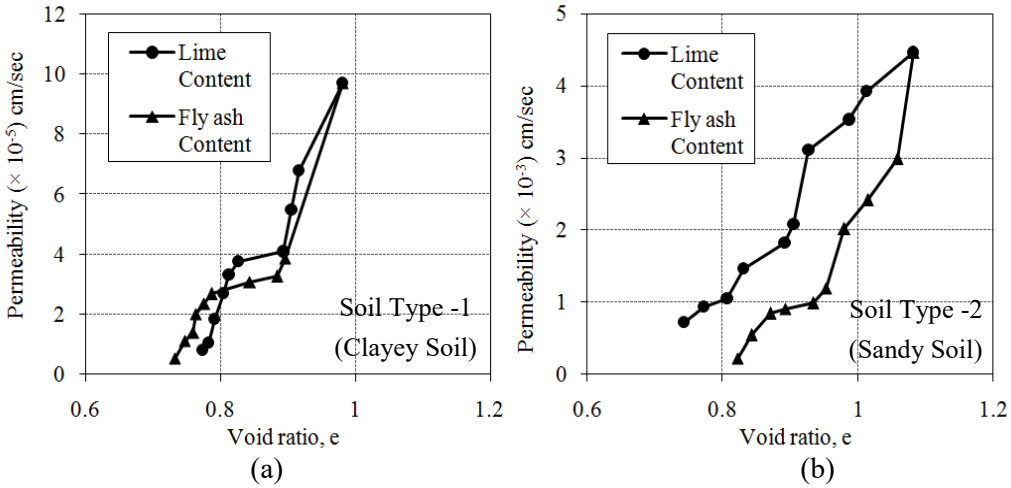

Fig. 8 Relationship between permeability and void ratio of: (a) Soil Type-1; (b) Soil Type-2

Fig. 8 denotes the relationship between permeability and void ratio of Soil Type-1 and Soil Type-2. For soil samples, the greater the void ratio, the higher the value of coefficient of permeability. The

coefficient of permeability varies with the void ratio as $\frac{e^3}{1+e}$ according to Kozeny-Carman equation (Lambe et al, 1969). From the figures, it is clearly visible that void ratio is proportional to permeability in both cases. From previous graphs of the relationship between void ratio and permeability with lime and fly ash, the similarity of the slopes in all cases showed the proportional correlation with void ratio and permeability. Addition of lime by 1%, 3%, and 5% decreased the rate of permeability gradually. It is observed from the comparison of the relationship between void ratio with lime and fly ash that the slope of change in case of lime content is steeper for sandy soil (Soil Type-2) than that of others. It means that the void ratio decreases more rapidly for sandy soil if lime is added. Fly ash also causes the decrease in void ratio but in lower rate. In case of clayey soil, lime and fly ash makes a similar role by decreasing the void ratio. From all figures, regarding to permeability characteristics, it is observed that the cohesive soil is more sensitive to additives than cohesionless soil. In case of Soil Type-1 which is clayey soil, permeability decreased 9-10 times, where in case of sandy soil (Soil Type-2) permeability decreased 4-5 times.

CONCLUSIONS

The following conclusions can be drawn based on the results obtained from the investigations:

1) Overall decrease in permeability of Soil Type-1 and Soil Type-2 were observed with the increase in additives (lime and fly ash content).
2) Permeability of treated soils was changed consistently with the void ratio pattern. That is, for increasing lime and fly ash content, void ratio decreased, and thus permeability of both of the soils also decreased. Void ratio of lime and fly ash treated soils were influenced by the presence of fines or small particles in soils. Soils (Soil Type-1 and Soil Type-2) with having substantial fines exhibited a decreasing tendency of void ratio with the increase of lime and fly ash content.
3) Fly ash is more effective to decrease the permeability of soil than lime.
4) Aging had no effect on the permeability and void ratio of untreated soils. But the void ratio and hence permeability of lime and fly ash treated soil were slightly changed with the reaction time.

ACKNOWLEDGMENTS

The authors acknowledge the infrastructural and financial support received from Bangladesh University of Engineering and Technology (BUET), Dhaka, Bangladesh for carrying out the research work.

REFERENCES

Arora, KR. 2008. *Soil Mechanics and Foundation Engineering*. Delhi: Standard Publishers Distributors.

Haunsmann, MR. 1990. *Engineering Principles of Ground Modification*. Singapore: McGrraw-Hill.

Indian Road Congress (IRC). 1973. *Recommended design criteria for the use of soil lime mixes in road construction*. IRC Highway Research Board: 51-1973. New Delhi.

Islam, MS.; Shah, A.; Haroon, RSk. and Salekin, S. 2005. Stabilization of Soft Organic Soils using Carbide Lime. *Proceedings of the 6th International Conference on Ground Improvement Techniques, Portugal, held on 18-19 July, 2005*: 325-332.

Khatun, N. 2017. *Coefficient of Permeability of Treated Soils. MSc.* Thesis (Civil & Geotechnical), Department of Civil Engineering, Bangladesh University of Engineering and Technology (BUET), Dhaka-1000, Bangladesh.

Lambe, TW. and Whitman RV. 1969. *Soil Mechanics*. Massachussets Institute of Technology NewYork: John Wiley & Sons: 287

Uddin, MN.; Pervin, R. and Alauddin, M. 2017. Analysis of Drought and Ground Water Depletion of Naogaon District in Bangladesh. *International Journal of Civil & Environmental Engineering (IJCEE)*, 17(01): 27-28.

4th International Conference on Advances in Civil Engineering 2018 (ICACE 2018)
19 –21 December 2018
CUET, Chittagong, Bangladesh
www.cuet.ac.bd

EFFECT OF PILE-GROUP CONFIGURATION ON THE LATERAL LOAD CARRYING CAPACITY OF PILE IN SANDY SOIL

M. M. Sazzad, M. Ashikuzzaman*, M. A. U. Roni&J. Islam

Department of Civil Engineering, RajshahiUniversity of Engineering &Technology, Rajshahi-6204, Bangladesh.
E-mail:ashik.amjr120116@gmail.com

**Corresponding Author*

ABSTRACT
Piles often withstand lateral loads from earthquakes, wind force, vehicle force, the wave impact, the ship impact and lateral earth pressure. Piles are usually construction in the field as groups. So to study the efficiency of the configuration (arrangement) of piles in groups to withstand lateral loads is significant. In this study, real small-scale model tests were performed with different configurations of pile groups. Steel pipes were used as model piles with outer diameter of 26.7 mm and wall thickness of 2 mm and penetrated into one cubic meter empty concrete cube filled with sandy soil. The concrete cube was filled with sand by dividing the total vertical length of cube in 10 layers with 150 blows per layer ensuring a relative density (D_r) of 72%. Several tests were performed on different configurations of pile groups. Two pile group and triangular pile group configurations were considered for the study. A single pile was also considered for comparison purpose. The embedment length (L) to diameter (d) ratio were kept 11 and 13 with a pile to pile spacing of 3d during the tests. Lateral loads were employed to the piles using a frictionless pulley. Lateral deformations were measured at each increment of load. From the experiment, it is observed that pile configuration has substantial effect on the stress-deformation behaviour of pile. Besides, the L/d ratio has significant effect on the lateral load carrying capacity of piles.

Keywords: Lateral Load; Pile-Group Configuration; Length to Diameter Ratio; Sand.

INTRODUCTION
Piles are being excessively used to bear structural load and transfer the loads to the bed rock or hard layer below the ground. Although piles are being used to carry vertical loads, they need to carry lateral loads during earthquake or wind. Several theoretical, experimental and analytical methods were developed and implemented to determine ultimate lateral load resistance, effect of soil parameters, effect of pile parameters, bending moment at different depth of the pile and so on. Structural foundations exposed to lateral and cyclic load due to different forces and natural calamities must satisfy two criteria for functioning these structures: (i) ultimate lateral resistance should be enough to support the structures and (ii) deflection of the piles should be in the permissible limit.
Meyerhof et al. (1972) carried out central inclined loads on single and group pile in sand having more similar properties in all of its particles which resulted in a partially empirical formulation to posit the deviation in ultimate resistance. This deviation was thought to be elliptical. The deviation was worked out on different ambiances like the axial loaded system which was modified later into a lateral loaded

system. Brown et al. (1988) conducted large scale pile tests on group pile and isolated single pile under two way cyclic lateral loading to determine shadowing effect. Franke (1988) conducted model tests on bored piles in the laboratory. The results revealed that the dislocation of pile group when spacing was less than 6d, was more than a single pile. The effect of soil layering on ultimate load bearing capacity of pile was determined by Laman et al. (2011) and Kam et al. (2018). Meyerhof et al. (1988) introduced an embedment length capable to take care of the piles instrumented as in non-fixed form but could be considered as fixed form. Thus, this test worked out the ultimate lateral load in loose soil. McVay et al. (1995) fingered different tests with several conditions. This test entails the centrifuge system for both single and 3x3 pile groups. In case of pile group, pile spacing was about 3 times and 5 times the diameter. They concluded from this test that, soil density has nothing to do with the efficiency of piles working as a group. Patra et al. (2001) presented the forthcomings of the test and emphasized on the texture of the pile to have more friction to counterbalance the applied force better than the others. Kim et al. (2001) suggested to change the usual tests along with various systems of binding the pile heads and set up the piles by proposing a factor. This modification factor introduced better results from the perspective of both quantity and quality of tests.

This paper represents the outcomes of several experiments carried out on group piles of different configurations for comparison with the experimental test of single pile. Tests of sand were conducted to find out the geotechnical properties. This paper emphasizes on the effect of pile-group configuration on the lateral load carrying capacity of the driven pile.

EXPERIMENTAL SETUP AND TESTING PROGRAM

Soil Properties

The properties of sand collected from the field was determined and presented in Table 1. The particle size distribution of the sand is depicted in Fig. 1.

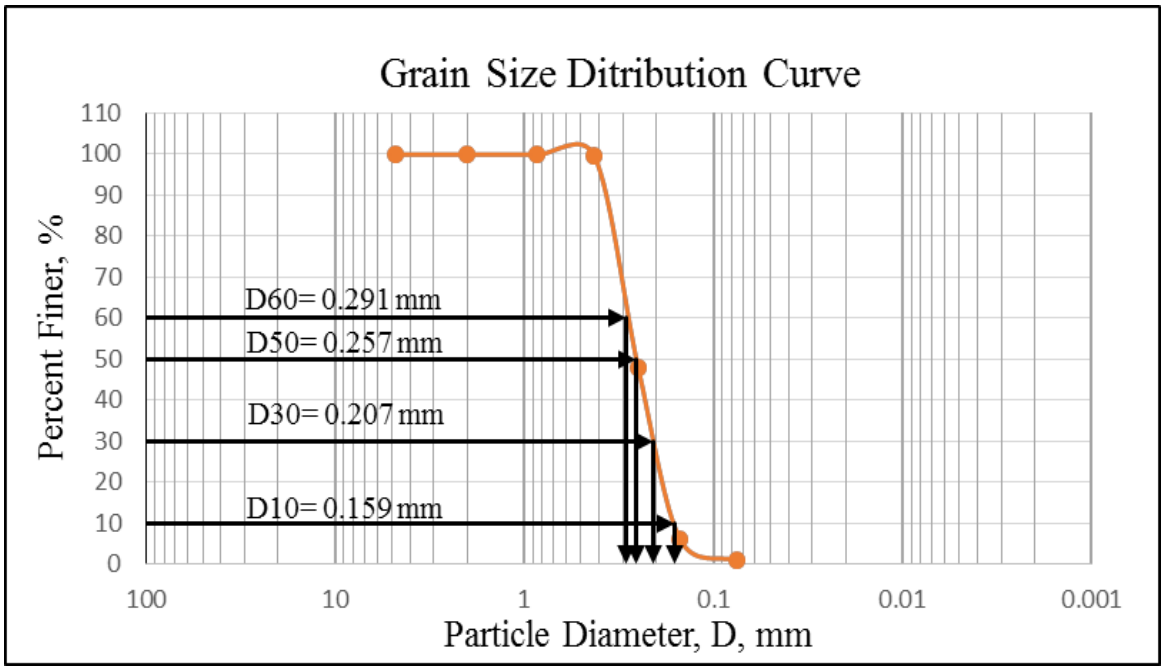

Fig. 1 Grain size distribution curve of sand

Table 1. Characteristics of sand used in the experimental study

Properties of sand	Values
Specific Gravity (G_s)	2.45

Fineness Modulus (FM)	1.20
Max. Unit Weight (γ_{max})	1.53 gm/cc
Min. Unit Weight (γ_{min})	1.20 gm/cc
Relative Density (D_r)	72 %
Uniformity Coefficient (C_u)	1.83
Coefficient of Curvature (C_c)	0.926
Friction Angle (Ø)	36.82°
D10, D30, D50, D60	0.159 mm, 0.207 mm, 0.257 mm, 0.291 mm

Pile and Pile Cap

Steel tubes were used as model pile for the experiment where the outer diameter of pile was 26.7 mm and the wall thickness of pile was 2 mm. Steel plate was taken as pile cap which was tighten by wire with the pile. The thickness of steel plate was 0.64 cm.

Test for Model Pile

Two different pile group configurations were used. One was two pile group and the other was triangular pile group. Apart from the group pile, a single pile was also considered. The spacing of piles was 3d where d is the diameter of pile. The configurations of different pile group and a single pile are depicted in Fig. 2.

Experimental Setup

A concrete model tank (Fig. 3) of size 1000 mm length, 1000 mm width, 1000 mm deep was used for this experiment. In the test, piles experienced only lateral load. An experimental setup was constructed to employ lateral load on the model pile of different configures and L/d ratios. To fill up the empty tank with sand, the tank height was divided into 10 layers by marker pen. Sand was poured into the tank up to the first layer and then it was compacted using the compactor with 150 blows. The procedure continued for the other layers till the tank was filled. After the tank was filled by sand, pile cap was placed on top of the sand in the tank and pile were installed with the help of a hammer. To apply the lateral load to the pile, a flexible wire was connected between the pile cap and load ram as shown in Fig. 3. The applied vertical load was transferred to lateral load by using a friction less pulley. Dial gage was fastened to the pile cap to obtain the lateral displacement. To diminish the effect of box boundaries, the soil thickness was kept below the pile tip at least 6 pile diameter.

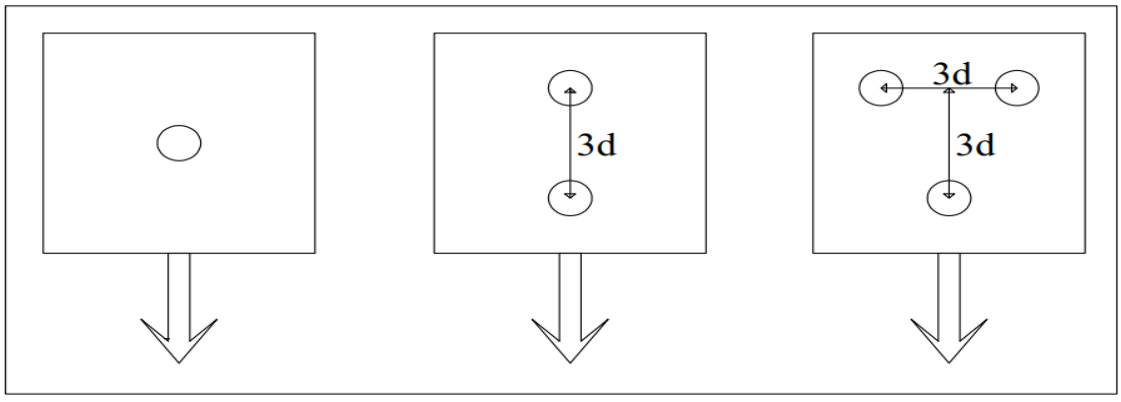

Fig. 2 Different pile group configurations (arrow indicates the direction of applied lateral load)

Experimental Procedure

The graphical diagram of the test setup is shown in Fig. 3. After driving the pile to the sand, lateral load was specified to the pile as the follow sequence: 0.0, 0.5, 1.0, 1.5, 2.0, 3.0, 4.0, 5.0, 6.0, 7.0, 8.0, 9.0, 10, 12, 14, 16 Kg and so on. Dial gage sensitive to 0.01 mm was used for determining the lateral displacement of piles. Deflections were recorded after each increment of applied load.

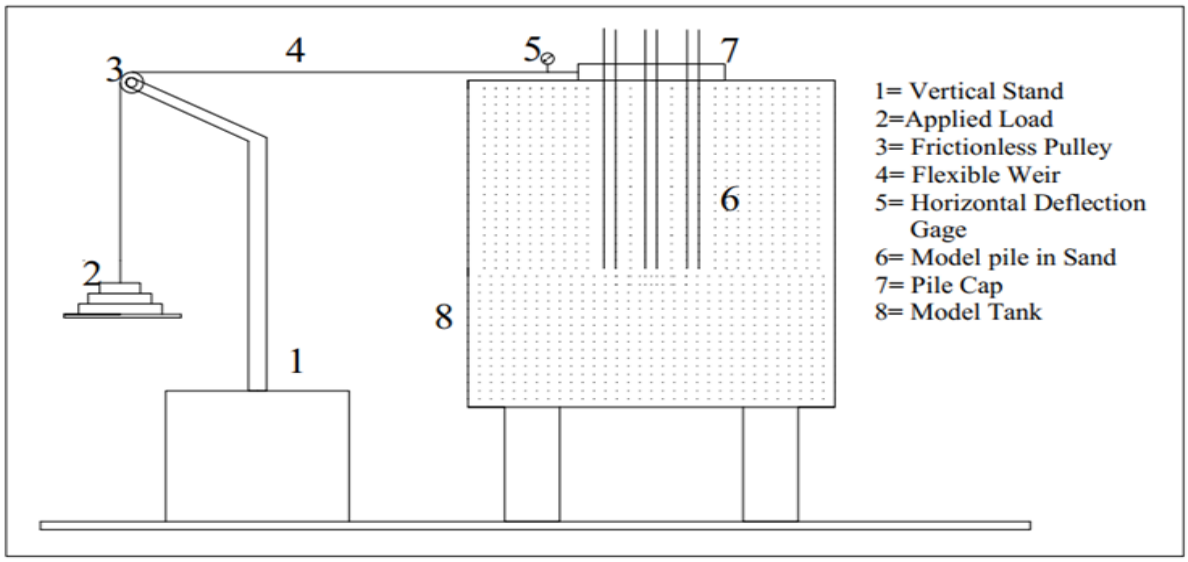

Fig. 3 Schematic diagram of experimental setup

EXPERIMENTAL RESULT AND DISCUSSION

The effect of pile configuration is studied by plotting the lateral pull exerted on the pile against the lateral deflection of pile head for both L/d=11 and 13, respectively and depicted in Figs. 4 and 5. The ultimate load carrying capacity of single pile and pile group is observed from the plot of lateral pull versus lateral deflection curves. It is perceived that the evolution of the lateral load carrying capacity of piles are non-linear in nature. In the next subsections, the effect of pile configuration on the load-deflection characteristics the single pile, two pile group and triangular pile group are presented.

Single Pile

The capacity of bearing lateral load of single pile for L/d=11 and 13, respectively are studied and the evolution of the lateral load carrying capacity of single pile is depicted in Figs. 4 and 5. From the Figs. 4 and 5, it is demonstrated that the capacity of bearing lateral pull of single pile is non-linear in nature. It is also illustrated that the ultimate capacity of bearing lateral pull of single pile increases with the increase of the length to diameter ratio (L/d).

Two Pile Group

The capacity of bearing lateral load of two pile group for L/d=11 and 13, respectively are studied and the capacity of bearing lateral load of two pile group is also depicted in Figs. 4 and 5. From the Figs. 4 and 5, it is observed that the capacity of bearing lateral load of two pile group is also non-linear in nature. It is also observed that the ultimate capacity of bearing lateral load of two pile group increases with the increase of the L/d ratio. Comparing to single pile, two pile group gives higher ultimate load carrying capacity. Also, the lateral displacement of pile decreases with the increase of the number of piles.

Triangular Pile Group

The capacity of bearing lateral load of triangular pile group for L/d=11 and 13, respectively are studied and the capacity of bearing lateral load of triangular pile group is also depicted in Figs. 4 and 5. From the Figs. 4 and 5, it is observed that the capacity of bearing lateral load of triangular pile group is also non-linear in nature. It is also observed that the ultimate capacity of bearing lateral load of triangular pile group increases with the increase of the L/d ratio. Comparing to single pile and two pile group, triangular pile group gives higher ultimate capacity of bearing lateral load. Note also that the stiffness of pile group system increases with the increase of the number of piles used in the test. It indicates that the load-deflection behavior is dependent on the pile configuration.

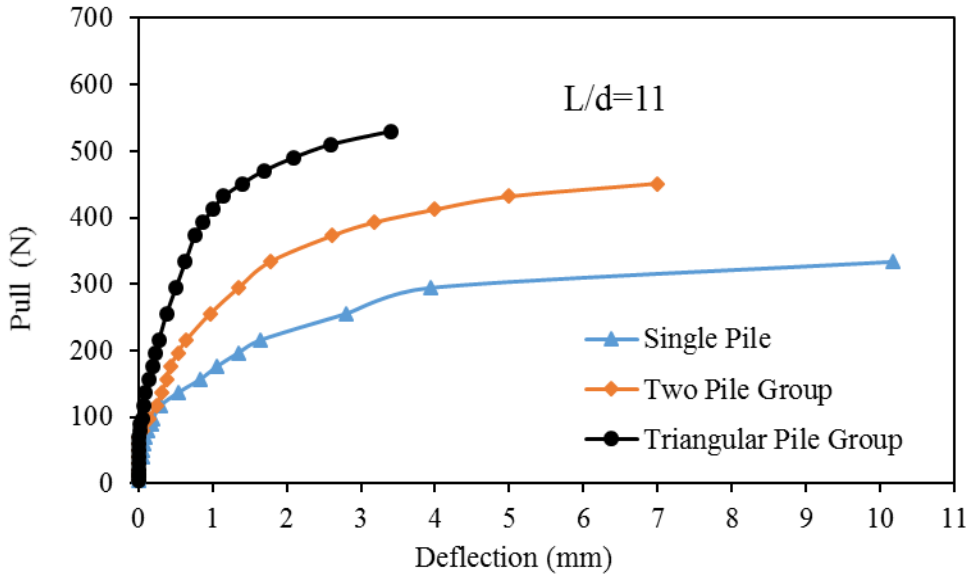

Fig. 4 Lateral load-deflection curve for different pile configurations for L/d=11

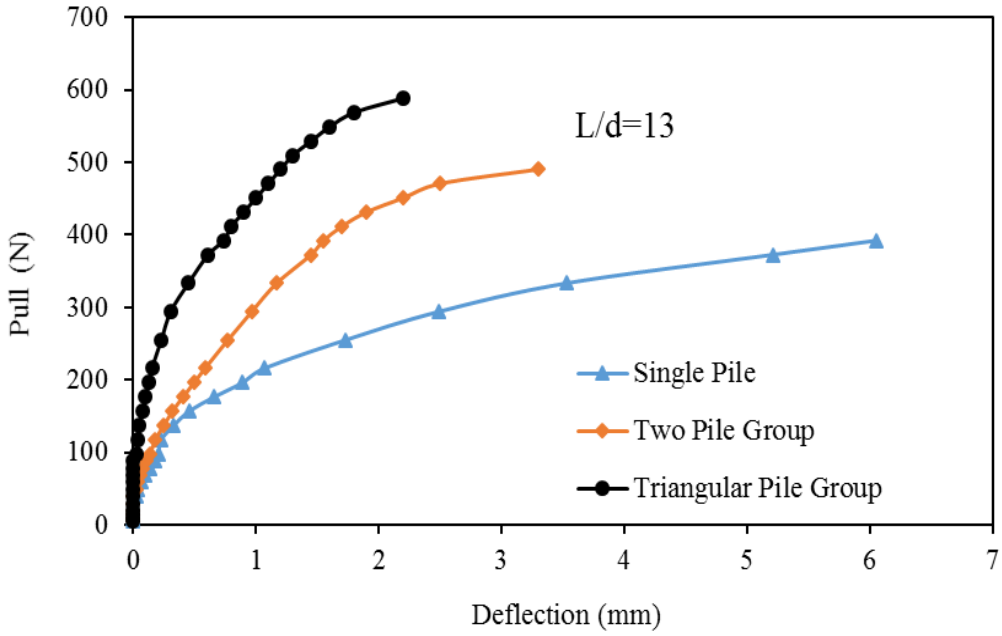

Fig. 5 Lateral load-deflection curve for different pile configurations for L=13

CONCLUSIONS

In the present study, laboratory based small scale model tests were performed to investigate the capacity of bearing lateral load of piles of dissimilar configurations for two different L/d ratios. The load-deflection characteristics were also studied. In this study, laboratory based small scale model tests were performed with different configurations of pile groups. Steel pipes with outer diameter of 26.7 mm and wall thickness of 2 mm were used as model pile and penetrated into one cubic meter empty concrete cube filled with sandy soil. The lateral load was exerted on the pile and corresponding lateral displacement was measured. From the experimental study, it is noted that the load-deflection characteristics are dependent on the configuration of the pile used. The evolution of the load-deflection curve is non-linear in nature. The initial stiffness of the pile group system is dependent on the configuration of the pile. It is also noted that the ultimate load bearing capacity of pile is a function of both the pile configuration and L/d ratio.

REFERENCES

Brown, DA, Morrison, C and Reese, LC. 1988. Lateral load behavior of pile group in sand. J. *Geotech. Engrg*., 114: 261-1276.

Erdal, U and Laman, M. 2011. Lateral resistance of a short rigid pile in a two layer cohesionless soil. *Acta Geotechnica Slovenia*, 2: 19-43.

Franke, E. 1988. Group action between vertical piles under horizontal loads, in Deep Foundations on Bored and Augur Piles. *W. F. V. Impe, Ed*., Balkema, Rotterdam, Netherlands.

Kam, N and Ksaibati, R. 2018. Effect of soil layering on shorter-term pile setup. J. *Geotech. Geoenviron. Eng*., 144(5): 04018020.

Kim, BT, Kim, NK, Lee, WJ and Lim, YS. 2001. Experimental load-transfer curves of laterally loaded piles in Nak-Dong river sand. *J. Geotech. Geoenviron. Eng.*, 130: 416-425.

Meyerhof, GG and Ranjan, G. 1972. The bearing capacity of rigid piles under inclined loads in sand, III: pile groups. *Can. Geotech. J.*, 10: 428-438.

Meyerhof, GG, Sastry, VVRN and Yalcin, AS. 1988. Lateral resistance and deflection of flexible piles. *Can. Geotech. J*., 25: 511-522.

McVay, M, Casper, R and Shang, T. 1995. Lateral response of three row groups in loose and dense sands at 3D and 5D pile spacing. *J. Geotech. Engrg.*, 121(5): 436-441.

Patra, NR and Pise, PJ. 2001. Ultimate lateral resistance of pile groups in sand. *J. Geotech. Geoenviron. Eng.*, 127: 481-487.

4th International Conference on Advances in Civil Engineering 2018 (ICACE 2018)
19 –21 December 2018
CUET, Chittagong, Bangladesh
www.cuet.ac.bd

DEVELOPMENT OF A MICROCONTROLLER BASED SOIL CRACK DETECTOR WITH TOMOGRAPHIC TECHNOLOGY

M. S. Rahman, M. A. Nahid*& A. Mushtaq

Department of Civil and Environmental Engineering, Shahjalal University of Science and Technology, Sylhet, Bangladesh.
Email:nahidraju28@gmail.com
**Corresponding Author*

ABSTRACT
Every year many valuable structures are damaged due to uneven crack formation in foundation soil. Therefore, in many cases, it is necessary to detect crack generation and propagation at an early stage for taking preventive measure. This paper describes the design, fabrication and experimental approach of a newly build cost effective soil crack detector based on electro-resistivity and microcontroller technology at laboratory scale. The device was designed and fabricated with local accessories, materials and electronics tools available in our country. The performance of the instrument has been checked with repeatability test and relative standard deviation for a set of observations has been found very small as only 1.31%. The device has been calibrated with a standard multi meter for achieving accurate result. The machine error was only 5.04%. In this paper, 2D electrical resistivity tomography method was adopted to investigate soil crack of centimetric scale in crop land and river bank soil. The electrical resistivity measurements were carried out using soil crack detector at laboratory scale using Wenner array. The measurement at 2cm and 1.5cm electrode spacing were taken to detect the soil crack. A specific stainless steel electrode was designed for resistivity measurement. The apparent measured resistivity of the soil specimen was processed using the OriginPro software for generating 2D electrical resistivity tomograph. The range of interpreted electrical resistivity associated with cracking is considerable from 106 to 225.5 Ω-m. The study revealed that the soil cracks show higher resistivity than surrounding intact soil.

Keywords: Arduino; Electrical resistivity tomography; Microcontroller; OriginPro; Soil crack; Wenner four-pin method.

INTRODUCTION

Tomography is the process for generating a two dimensional image of a slice or section through a three-dimensional object. During the 1970s, tomographic reconstruction of cross-sectional data was first applied in medical diagnostics (Villa and Lynnerup, 2012). Electrical resistivity tomography is a method which is versatile, quick and non-destructive for soil sample. The application of electrical resistivity tomography is measuring bed rock and water table depth, detecting sink holes and hidden void, profiling the land sleep geometry, leachate contamination and soil crack detection. Electricity has significant influence on soil. Electrical properties have strong relation to physical and chemical properties of soil such as texture, salinity, water content and cracks. Cracks in soils are naturally occurring phenomena resulting from the seasonal variations in the weather (Hossain and Sakai, 2008). Cracks may increase soil compressibility at consolidation rate and reduce soil strength (Morris et al.1992). They can cause heavy disaster to the civil engineering structures in many ways (Tiwari, 2015). Crack reduces strength and may lead to seepage and percolation problems. Cracks induced by environmental agents also reduce the bearing capacity of the soil and increase its propensity to erosion. Erosion is common mode of failure of embankment. Dam failure creates devastating disasters

with tremendous loss of life and property, especially in densely populated country like Bangladesh. Most of the dams in the world are earthen dam. Belci dam is one of the largest earthen dams which was built in 1962 on Tazlaur River, near Slobozia in Romania. On 28 July 1991, Belci dam was damaged. The failure process of Belci dam was erosion of downstream prism face, simultaneously with its saturation. In short time the sliding of downstream occurred followed by a rapid and profound erosion (Asman and Bratianu, 2013). Twenty-five people were killed by the flood wave and 119 houses were destructed. Suvi dam is another example of dam failure. The upstream side of the dam had multiple longitudinal cracks indicating to movement towards the reservoir. Due to large longitudinal crack Suvi dam was damaged. Similarly, Rudama Tadam dam was also damaged due to cracks. Crack can cause slope instability and can contributes to the land slides in hilly areas. In 1979 a large landslide occurred in the Dunedin, South Island, New Zealand. After the investigation it was found that landslide was accelerated due to crack (Hancox, 2008). Moreover, In case of water canals, cracking increases the water loss through cracked surface area. Thus increases the cost of irrigation.
There are a number of commercial soil crack detectors available in the international market having different features and functions. Most of them are very costly and complicated. There are many problems such as long waiting time and non-availability of repairing the instrument quickly if they are directly imported from another country. The purpose of the research is to make cost effective soil crack detector device for detecting soil crack. The main objectives of this study are given below-

- To design and fabricate a cost effective soil crack detector.
- To detect the position and specification of the crack with tomographic technology.

METHODOLOGY

There are five major parts of the current study which is identified as hardware implementation approach, program development approach, model design of the product, fabrication of the product and application of the product.

Hardware implementation approach

After some rigorous researches, components and equipment suitable and available for the system had been selected to ensure the system performance and to please the major objective of the research. The main components of the device were Arduino mega 2560 microcontroller, various kind of displays, potentiometers, 550w power supply and sensors.

Program development approach

A program was developed for the soil crack detector. The program was written in C++ programming language by ARDUINO IDE compiler. All kind of equations and calculations were written in the program so there is no need any manual calculations.

Model design and fabrication

Before starting design and fabrication of the soil crack detector, computer aided 3D design was done for better understanding and for practical use of the device. Final device was built after the analysis and validation test. Locally available materials were used to fabricate the device. The body was made

[Fig. 01] Isometric view of the device

[Fig. 02] Displays of the device

[Fig. 03] Back view of the device

[Fig. 04] Electrode connecting cable

in 20 grade stainless steel. The cutting, drilling, welding and painting process was done in a local steel workshop. The device has a height of 260mm, width of 200mm and depth of 250mm. It has four LCD displays with backlight offers easy to read main result of resistivity at a specific nodal point as well as

electrode depth, electrode spacing, resistivity value in linear bar graph, sensor reading from voltage and current sensor.

Arduino Mega 2560

Arduino mega is easily available microcontroller in the market. It consumes low power and it can operate any kind of complicated task easily. It has a 16Mhz microprocessor, 8KB of RAM and 256KB of memory. The displays, sensors and power supply are connected to the microcontroller. [Fig. 05] shows Arduino mega 2560 microcontroller.

[Fig. 05]

Performance test

To test the performance of the device two different types of test samples were collected from cropland and river bank for artificially making soil cracks. Single type of crack and multi cracks were made for both the soil sample.

2D resistivity imaging technique

For the experiment Wenner four pin method was selected which was developed by Dr. Frank Wenner, US Bureau of Standards in 1915. The Wenner array consists four collinear, equally spaced electrodes. The two outer electrodes are current electrode and two inner electrodes to measure voltage drop due to resistance of soil path when current passed between the outer electrodes. Electrode A and B refer to current electrode and electrode M and N refer to potential electrode. In the Wenner array, distance AM = MN = NB = a = spacing. The main advantage of using Wenner array is apparent resistivity can easily calculable and the instrument sensitivity is not as crucial as other array. [Fig. 06] shows Wenner method to determine resistivity of soil. Eq. (1) shows the apparent soil resistivity by the Wenner method.

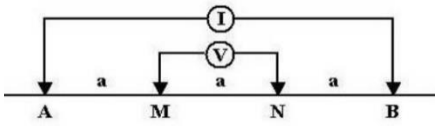

[Fig. 06]

$$\rho_E = \frac{4\pi a R_W}{1+\frac{2a}{\sqrt{a^2+4b^2}}-\frac{a}{\sqrt{a^2+b^2}}} \quad (1)$$

where,

ρ_E = measured apparent soil resistivity (Ω-m)

a = electrode spacing (m)

b = depth of the electrodes (m)

R_W = Wenner resistance measured as "V/I"

For measuring resistivity at each nodal point of a soil sample sufficient number of electrodes along a straight line are attached to a multi-core cable and penetrate to ground at a small depth which is shown in the [Fig. 07]. For the first reading electrode number 1, 2, 3 and 4 are used. Electrode 1 and 4 are used as current electrode which is denoted as C1 and C4 on the other hand electrode 2 and 3 are used as potential electrode which is denoted as P1 and p2. Then electrode 2,3,4 and 5 are used to measure resistivity of another nodal point. This is repeated down the line of electrodes until electrode 16, 17, 18 and 19 are used for the last measurement. The resistivity data will be then acquired from data level a = 1. If the electrode spacing is considered as ‘d’ then the total spacing between electrode 1 and 4 will be ‘3d’. The resistivity will be then acquired from the middle point of them at ‘3d/2’ depth. In the conventional way for measuring resistivity at different depth of soil sample the spacing between the electrodes are increased instead of penetrating them into the soil profile. In that way spacing between electrodes are increased as ‘2d’ for measuring resistivity at data level a = 2 and increased as ‘3d’ for measuring resistivity at data level a = 3. The process is continued for each data level. As the electrodes are not directly penetrated at soil profile in conventional way so the resistivity values are not appropriate. For the true resistivity data, the values are need to process in a software which is known as data inversion process. The software programs

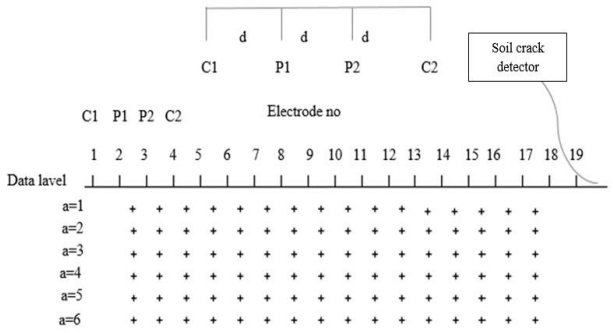

[Fig. 07]

are highly expensive and needs device compatibility for data acquisition. For the filed measurement the conventional way is very necessary. The research was only lab based and inexpensive way to detect soil cracks so that for avoiding data inversion process electrode was directly penetrated through the soil profile for data acquisition at each data level. “OriginPro” software was used for creating tomography of each cross sectional area of the soil specimen from the resistivity data of each nodal point.

Laboratory soil box

A soil box was used with soil crack detector in the laboratory for a quick and accurate measurement. The soil was compacted in the box. Then the electrodes were placed in the box in straight line. For measuring purpose three scales were attached with the soil box [Fig. 08]. Scale 1 was placed perpendicular to the soil box to measure electrode depth, scale 2 was placed parallel to the length of the soil box to measure spacing between electrodes and the scale 3 was placed parallel to the width of the box to measure distance between cross sections of soil specimen. [Fig. 09] shows cross sections of the soil specimen. All the measurements were conducted on the soil sample under controlled conditions (room temperature 22°C).

[Fig. 08]

[Fig. 09]

Experimental setup

[Fig. 10] shows experimental setup for soil crack detection.

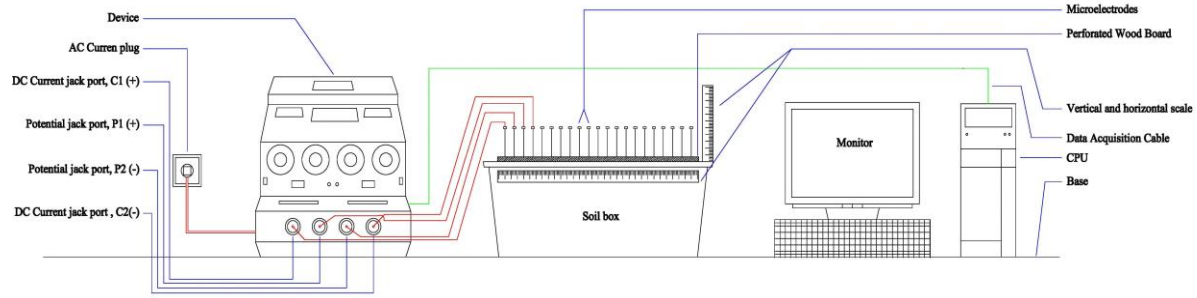

[Fig. 10]

RESULT AND DISCUSSIONS

Single crack in crop land soil

Crack has higher resistivity than soil. An artificial single crack was made by polystyrene for this experiment which was placed at cross section-03 at a distance of 15 cm from the origin point of the soil box and placed 3 cm under from the surface of the soil. The depth of the crack was 4.5 cm, thickness was 1.5cm. The width of the crack was 4cm which is not visible here because of 2D imaging. [Fig. 11] shows resistivity data of cross section-01 of the soil profile. The apparent resistivity was almost same in every nodal point at this section because of no crack. The highest value of resistivity was 39.63 Ω-m in this section. [Fig. 12] shows the tomography of this cross section.

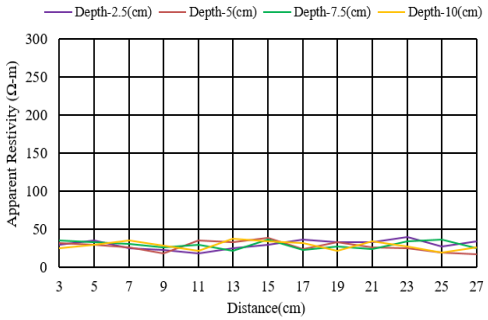

[Fig. 11]

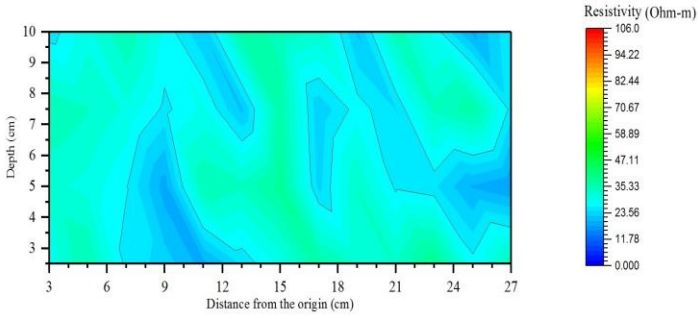

[Fig. 12]

There is small variation of colour in this profile which means small variation of resistivity here. So no crack was found in this section. The moisture content was 17% during the experiment.

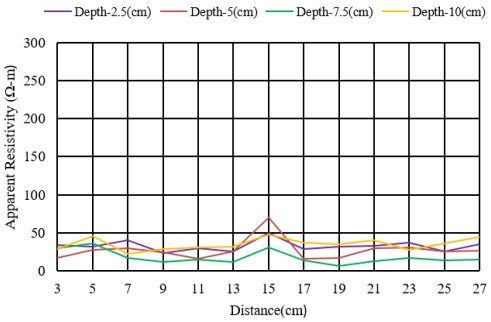

[Fig. 13]

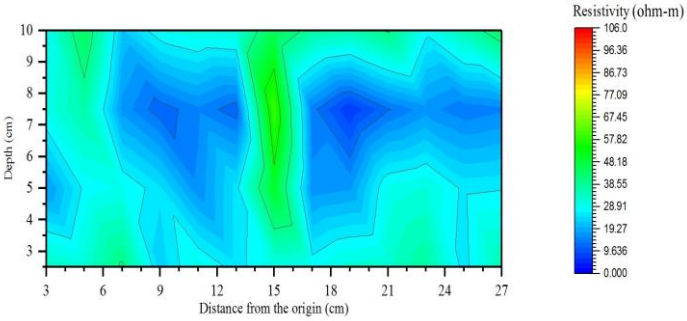

[Fig. 14]

[Fig. 13] Shows resistivity data of cross section-02 of the soil profile. The apparent resistivity was increased marginally at 15cm distance due to partial soil crack effect. Due to placing the crack at cross section-03 it had an effect on cross section-02. The highest value of resistivity was 70 Ω-m in this section. [Fig. 14] shows the tomography of this cross section which represents the partial soil crack effect.

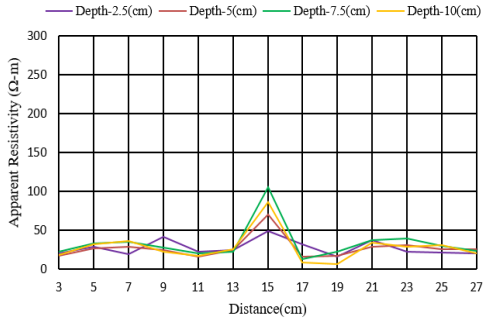

[Fig. 15]

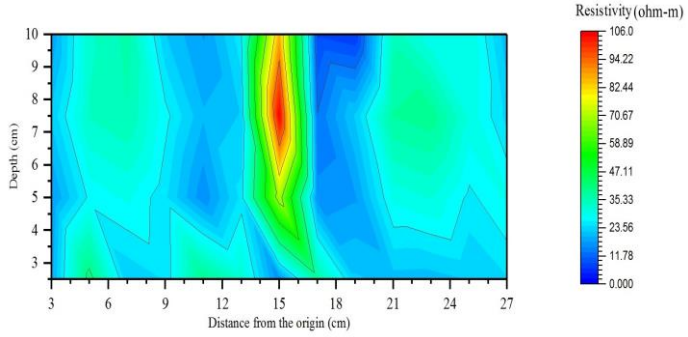

[Fig. 16]

[Fig. 15] Shows resistivity data of cross section-03 of soil profile. The apparent resistivity was increased dramatically at 15cm distance due to soil crack. The soil crack was directly placed in this section so the resistivity was increased very high in comparison with section-01. The highest value of resistivity was 106 Ω-m in this section. The apparent resistivity was decreased at the position 13 and 17cm where the electrical current path tends to concentrate which (low voltage drop) decreased the resistivity. The resistivity of those places were 22.32 Ω-m and 13.47 Ω-m. [Fig. 16] shows the tomography of this cross section which represents the soil crack. The colour variation is high in this section. The red colour represents the soil crack and beside the crack the blue colour represents sudden decreased resistivity due to voltage drop.

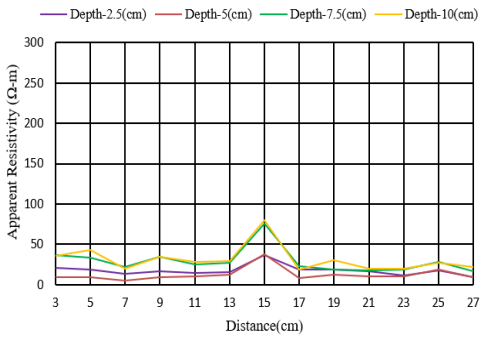

[Fig. 17]

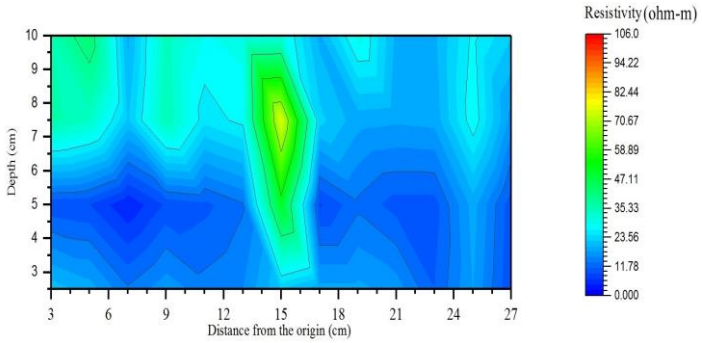

[Fig. 18]

Similarly, [Fig. 17] and [Fig. 18] shows partial soil crack effect at cross section-04 where the highest value of resistivity was 80.28 Ω-m.

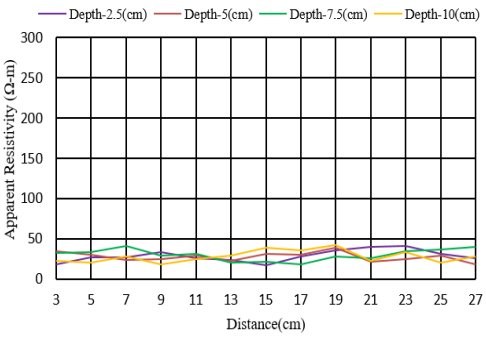

[Fig. 19]

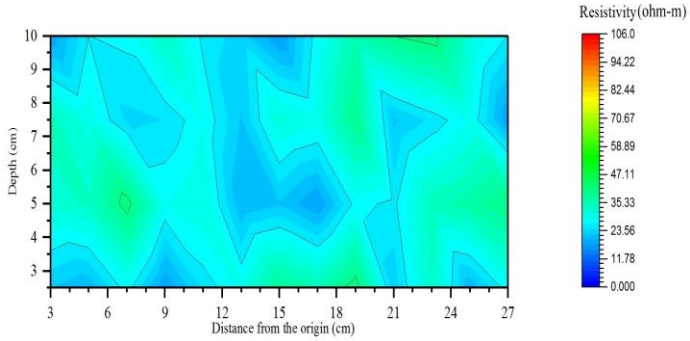

[Fig. 20]

On the other hand, [Fig. 19] and [Fig. 20] shows no soil crack effect at cross section-05 where the highest value of resistivity was 41.88 Ω-m.

CONCLUSIONS

Soil crack detection is very important challenge for the engineers. The soil crack detector can offer laboratory test using very simple and low cost technique which can be used in geotechnical engineering. This study proposed a unique idea to design cost-effective soil crack detector in the laboratory from locally available material which could allow researchers to detect the crack from soil sample. However, the capacity of power supply was limited to 550W and only Wenner array was used for data collection.

REFERENCES

Asman, I. and Bratianu, G. 2013. Project for rehabilitation of Belci Dam after the 1991 failure. *9th European Club Symposium*, 10–12 April, 2013, Venice, Italy.

Hancox and Graham, T. 2008. The 1979 Abbotsford landslide, Dunedin, New Zealand: a retrospective look at its nature and causes. *Landslides*, 5(2): 177-188.

Hossain MZ. and Sakai, T. 2008. Severity of flood embankments in Bangladesh and its remedial approach. *Agricultural Engineering International: CIGR Journal*, Manuscript LW 08 004. Vol. X. May, 2008.

Morris; Graham, PH.; Williams, J. and David, J. (1992). Cracking in drying soils. *Canadian Geotechnical Journal*, 29(2): 263-277.

Tiwari, A. 2015. *Quantification of cracks and shrinkage using image analysis*. MTech Thesis, NIT, Rourkela, Odisha, India.

Villa, C and Lynnerup, N. 2012. Hounsfield units range in CT-scans of bog bodies and mummies. *Anthropol Anz.*, 69(2):127-45.

A QUALITATIVE ANALYSIS ON THE CAUSES AND CONSEQUENCES OF INDOOR AIR POLLUTION IN THE SLUM AREAS OF CHITTAGONG

S. Nuzhat*, N. Islam & S. Arefeen

Department of Environmental Science, Asian University for Women, Chittagong, Bangladesh.
E-mail: samiha.nuzhat@auw.edu.bd; nafisa.islam@auw.edu.bd; sinthia.arefeen@auw.edu.bd

**Corresponding Author*

ABSTRACT
While air pollution has been a matter of scrupulous concern because of its irreparable drawbacks, indoor air pollution is often disregarded as harmful as outdoor air pollution. As a result of the detrimental impacts of indoor air pollution, people, especially residents of poorer households, staying at home for a substantial amount of time are exposed to toxic reagents (for example- carbon dioxide and carbon monoxide) that exacerbates their health problems. The idea of this research is to assess Indoor Air Quality (IAQ) in the slum areas of Chittagong, Bangladesh, and highlight distinct problems faced by the residents of those residences, relating to indoor air pollution. The field research is conducted in the households of four slums areas of Chittagong which are socially and culturally diverse in background and have various practices of household maintenance such as cooking practices with solid fuels, biomass, electricity, LPG, charcoal etc. Other practices include use of insect repellent, improper waste management and ventilation system. Findings of this study provoked emergence of several health issues and degraded standard of living, pertinent to the sources and consequences of indoor air pollution there. Interviews of the members of those households in the slums based on survey questionnaire have included the quotidian issues that they combat pertaining to indoor air pollution.

Keywords: Indoor Air Quality (IAQ), Indoor Air Pollution, LPG (Liquefied Petroleum Gas), Survey Questionnaire

INTRODUCTION

Air pollution has found its way inside the houses of people via different means. According to World Bank (2014), nearly 3 billion of the world's poorest still rely on solid fuels (wood, animal dung, charcoal, crop wastes and coal) burned in inefficient and highly polluting stoves for cooking and heating. This is likely to be the largest origin of indoor air pollution. Incessant exposure to the smokes released while cooking or using smoke-releasing materials (mosquito coil and cigarettes) give rise to indoor air pollution. The term indoor air pollution (IAP) focuses specifically on the pollution initiated in domestic household. OECD (2015) refers indoor air pollution to chemical, biological and physical contamination of indoor air. The incidence of IAP is high in poverty-stricken area, particularly slums. This issue is inextricably linked to poverty (Bruce et al., 2006). The poor have to utilize fossil fuels and inefficient stoves. The health and economic condition of the households attribute in keeping the people in poverty thus acting as an impediment in having a fruitful transition. Households generally ascend the energy ladder once their socioeconomic conditions improve (Bruce et al., 2006). They use fuels and appliances that are more efficient, clean, and convenient but more expensive as well (Bruce et al., 2006). Women and children in the slums are primarily affected as they stay longer in the house. In houses with restricted ventilation (conventional in developing countries), exposures experienced by household members, particularly women and young children who spend a large proportion of their time indoors, have been

measured to be many times higher than World Health Organization (WHO) guidelines and national standards (Bruce et al., 2006).

According to Smith (1987), smoke released from coal and biomass emit various health-impairing pollutants including particulate matter (PM), carbon monoxide (CO), sulfur oxides, nitrogen oxides, aldehydes, benzene, and polyaromatic compounds . These pollutants mainly affect the lungs by causing inflammation, reduced ciliary clearance, and impaired immune response (Bruce et al., 2000). Vrijheid et al. (2012) confirms that air pollution may impair neurodevelopment. The presence of a gas cooker at home during pregnancy is associated with slower mental development (Vrijheid et al., 2012). A smaller number of studies have found that indoor air pollution from biomass fuels (IAP) and passive smoking are also risk factors for TB and its sequelae (Lin et al., 2007). There is consistent evidence that the susceptibility of chronic obstructive pulmonary disease and acute respiratory infections in childhood elevates due to indoor air pollution (Bruce et al. 2000). Bruce et al. (2000) states that due to modernization, there has been as a switch from biomass fuels to petroleum products and electricity. As a result, the ubiquity of all the above mentioned risk factors of indoor air pollution, has made it a common phenomenon in the slum households.

METHODOLOGY

Our first step during this research was to identify the reasons and consequences of indoor air pollution from previous researches. We accumulated all the information and narrowed down to the main reasons why indoor air pollution is so prevalent, especially in slums. Subsequently, we configured a questionnaire which included all the necessary questions required to understand the situation of the households in terms of indoor air pollution. The questionnaire included personal information about the interviewee like jobs, salary, age, period of stay in the area, physical problems and daily habits. It also included questions about the structure and condition of the house and the materials used to build walls, roof and floor. Choosing the sample area was our next step. Since this was a qualitative research, we used a sample size of four slums and interviewed five households from each of them. The four slums, we chose for our survey are Chittagong Railway Slum, Khejurtola Slum, Taktar Pole Slum and Lalkhan Bazar Slum. The slums varied highly in terms of geographical location, diversity of people, and facilities received by the slum dwellers. With the permission of the interviewees, we took records of their personal information including the financial condition of the families and health-related problems they have been facing. Later on, we sorted the data from the survey and did a qualitative analysis of the information found from the survey in the above mentioned four slums.

RESULTS

Major findings from the survey have been added below to illustrate the common scenario of Indoor Air Pollution in the slums of Chittagong and to find out linkages between the exposure and consequences of Indoor Air Pollution in the slum households of Chittagong.

According to previous discussions, exposure of Indoor Air Pollution is influenced by cooking practices, ventilation system, usage of insect repellents and some other practices and are thought to be reliable for several health problems, lower standard of living and some other problems. So, the necessary data derived from each of the slums we visited for interviewing people has been mentioned in the table separately and discussed thoroughly.

Table 1: Information Collected from Railway Slum

Parameters	**Household 1**	**Household 2**	**Household 3**	**Household 4**	**Household 5**
Number of Members	4	5	2	4	3
Cooking Practice	Gas Stove (Natural Gas)	Gas Stove (Natural Gas)	Gas Stove (Natural Gas)	Gas Stove (Natural Gas)	Gas Stove (Natural Gas)
Ventilation	Bad	Very Bad	Not Good Not Bad	Bad	Very Bad
Insect Repellents	Mosquito	Aerosol	Mosquito	Mosquito	Mosquito

	Coil/Net		Net	Coil	Net
Number of Smokers	0	0	1	0	0
Major Health Issues	Skin Disease	Diabetes, Pneumonia	Coughs	High Blood Pressure	Allergy
Living Standard Measure	Extremely Poor	Poor	Middle-Class	Poor	Poor

Table 2: Information Collected from Khejurtola Slum

Parameters	**Household 1**	**Household 2**	**Household 3**	**Household 4**	**Household 5**
Number of Members	3	1	2	4	4
Cooking Practice	Gas Stove (with LPG)	Gas Stove (with LPG)	Mud Stove (with Straw)	Mud Stove (with Straw)	Mud Stove (with Straw)
Ventilation	Not Good Not Bad	Bad	Not Good Not Bad	Very Bad	Not Good Not Bad
Insect Repellents	Mosquito Net	Mosquito Net	Mosquito Coil	Mosquito Coil	Mosquito Coil
Number of Smokers	0	1	0	1	1
Major Health Issues	Skin Disease	Skin Disease	Ear Problem	Respiratory Diseases	Coughs, Continuous Fever
Living Standard Measure	Extremely Poor	Poor	Poor	Extremely Poor	Extremely Poor

Table 3: Information Collected from Taktar Pole Slum

Parameters	**Household 1**	**Household 2**	**Household 3**	**Household 4**	**Household 5**
Number of Members	6	4	2	3	4
Cooking Practice	Mud Stove (with Straw and Wood)	Gas Stove (with Natural Gas)	Gas Stove (Natural Gas)	Gas Stove (with Natural Gas)	Mud Stove (with Straw and Wood)
Ventilation	Not Good Not Bad	Bad	Very Bad	Bad	Bad
Insect Repellents	Mosquito Net	Mosquito Net	Mosquito Coil	Mosquito Net, Mosquito Coil	Mosquito Coil, Mosquito Net
Number of Smokers	1	0	1	0	0
Major Health Issues	Body Pain, Coughs	Anemia, Skin Disease	Hormonal Problem & Skin Disease	Body Pain	Asthma, High Blood Pressure
Living Standard Measure	Extremely Poor	Poor	Poor	Poor	Extremely Poor

Table 4: Information Collected from Lalkhan Bazar Slum

Parameters	**Household 1**	**Household 2**	**Household 3**	**Household 4**	**Household 5**
Number of Members	3	4	4	4	4
Cooking Practice	Mud Stove (with Straw)	Mud Stove (with Straw)	Gas Stove (Natural Gas)	Gas Stove (Natural Gas)	Gas Stove (with Natural Gas)
Ventilation	Bad	Very Bad	Not Good Not Bad	Not Good Not Bad	Bad
Insect Repellents	Mosquito Coil, Mosquito Net	Mosquito Net, Mosquito Coil	Mosquito Net	Mosquito Net	Mosquito Coil
Number of Smokers	1	1	2	1	1
Major Health Issues	N/A	Eye Problem, Skin Disease	High Blood Pressure	High Blood Pressure,	Respiratory Diseases

				Diabetes	
Living Standard Measure	Poor	Poor	Middle-Class	Poor	Poor

DISCUSSIONS

It is found from our survey that Indoor Air Quality (IAQ) varies a lot in households of different income and different areas. Some other practices such as cooking practice, tobacco smoke exposure, ventilation system, use of insect repellents and so on also keep an impact in this issue.

Firstly, cooking practice of a household often plays a vital role in maintaining Indoor Air Quality (IAQ) of the households. Traynor et al. (1987) found out that wood burning stoves are responsible for increasing concentration of Carbon Monoxide, Nitrogen Oxides, Formaldehyde, Total Suspended Particles, Submicron Suspended Particles and so many other toxic chemicals. On the other hand, gas stoves are one of the major sources of nitrogen di oxide (NO_2), Organic Carbon Compounds and some other hazardous gases as it burns carbon compounds and nitrogen compounds (Gauderman et al., 2000). Therefore, judging several evidence of experts' researches, it is quite clear that using fuel based stoves is responsible for indoor air pollution and when the certain household is situated in a congested and crowded area just like the slums of Chittagong it is quite tough to maintain good air quality in the households, as the pollutants released from the stoves directly enter into the household. So, connecting with our field research, cooking practice is responsible for indoor air pollution in the slums of Chittagong.

Secondly, tobacco smoke exposure is another inhibitor of Indoor Air Pollution. Mueller et al. (2011) pointed out that tobacco smoke releases some particles that degrades indoor air quality, if they aren't ventilated properly and initiate the production of cancer cells gradually. It can also be proved right from our field research. We found out that in the slums, the smokers are discouraged by their family members to smoke inside the households, as it seems physically problematic for the family members. To explain it in the language of academicians, this type of discouragement is happening to keep themselves away from 'Passive Smoking'. As the hazardous gases released from tobacco affect the people staying around, keeping the indoor air free from such chemicals is quite important and so we have seen no smokers to smoke inside the households.

Then, scarcity of good ventilation system in the households of the slums of Chittagong is another reason that promotes indoor air pollution in the slum households. Researchers prioritized a household's ventilation rate for maintaining the household's IAQ. For a well-ventilated household,

$C_{in} = C_{out}$ (1)

Here,

C_{in} = Indoor Concentration

C_{out} = Outdoor Concentration

Q = Outdoor Air Ventilation Rate

S = Indoor Contaminant Source Strength

R = Rate of Removing Contaminant by Filtration, Air Cleaning and Other Mechanism (Persily & Levin, 2011)

In a badly ventilated household, $S > R$ or, $S - R > 0$

As a result, $C_{in} - C_{out} > 0$

or, $C_{in} > C_{out}$ (2)

From Eq. (2), it is quite clear that if a household is not well-ventilated (when $S >> R$), the concentration of the contaminants inside the household is higher than outside. And from our visit to the slums, we were surprised seeing that most of the slum household has no window, as the rooms are too small to make enough space for keeping one window. As a result, Indoor Air Quality has a more chance of degrading faster than Outdoor Air Quality due to lack of air flow and due to not being well ventilated.

A final way of initiating indoor air pollution is frequent use of Insect Repellent and it is a common phenomenon in the slum dwellers which might cause huge degradation in the Indoor Air Quality (IAQ) of the slum households. Exposure of hazardous chemicals through mosquito repellents gradually affects the eyes, skin and other parts of the body (Khan & Saxena, 2012). And from our survey, we have also noticed that the white section of the eyes of the people who have more tendency to use chemical insect repellent

is little yellow and some of them had to face many other respiratory or skin diseases. The slum dwellers who stay at home for more time duration have more possibilities to be affected by the detrimental effects of insect repellents.

For the consequences of indoor air pollution, our survey mainly focused on the impacts of indoor air pollution in the living standard of the slum dwellers and on their health.

To measure the living standard in the result section, we have followed World Bank's update on measuring poverty line (World Bank Group, 2014). According to the World Bank, international poverty line denotes a maximum income of 1.90$ per day per person, where in lower middle income class poverty line is 3.20$ per day per person and in upper middle income class poverty line is 5.50$ per day per person (2014). So, this measurement was used to decide the living standard of the interviewed households. Here, in Table 1-4, the living standard of the members of the household were decided from the income of the family. If the average income per person is under 1.90$ per day the household was treated as extremely poor; otherwise poor or rich. And such hierarchy based on income is a result of indoor air pollution in some cases, as an indoor air pollution affected household hardly has enough money to ensure a better lifestyle. Even if they have financial capacity, they have lack of environmental supports from surroundings. This is why, lower living standard is an indirect but dominant effect of indoor air pollution.

Apart from the effects of Indoor Air Pollution in the living standard of the family, another major effect of this is the health effects. As discussed in the introduction with brief literature review that health problems such as coughs, bronchitis, respiratory diseases, skin diseases etc. are often found due to prevalence of indoor air pollution. A case study from Kenya found higher prevelance of respiratory diseases in the congested households with low IAQ (Ezzati and Kammen, 2001). In fact, households of developing countries with lower income are more exposed to contaminants and such contaminants cause higher frequency of respiratory diseases mixed with the air (Smith and Mehta, 2003; Pandey, Boleij, Smith and Wafula, 1989). Our survey in the four slums also proved that contaminated indoor air is weakening the immune system of the slum dwellers which gradually causes the exposure of several diseases. Besides, from our interviewees, we came to know that the patients of diabetics and higher or lower blood pressure feel truly suffocating to stay home for a long time and they often need to go outside to breathe from comparatively fresher air. So, even though without considering a control or comparison, connecting the literatures with our findings in terms of higher frequency of respiratory diseases and worsened immune system, we can say that health hazards are a serious consequence brought by indoor air pollution.

CONCLUSIONS

Indoor air pollution is a matter of huge concern for the slum dwellers of Chittagong because the slums are excessively populated and life standard of people is degrading very fast there. Degradation of Indoor Air Quality is initiated by several ways, as we have discussed and it is causing severe detrimental health effects lowering life standard. So, it is quite urgent to bring technological and scientific changes in the lives of the slum dwellers to fight successfully against indoor air pollution.

ACKNOWLEDGMENTS

This project was funded by Asian University for Women and so we want to express our cordial gratefulness to the University authority. We also want to thank Professor Mukesh Gupta who has supervised us throughout the project providing us with his valuable guidance and suggestions.

REFERENCES

Apte, M; Grimsrud, DT and Gundel, LA. 1987. Indoor air pollution from burning stoves. *Environ. Sci. Technol.* 21(7): 691-697.

Bruce N. G., Perez-Padilla R., Albalak R. 2000. Indoor Air Pollution in Developing Countries: A Major Environmental and Public Health Challenge. Bulletin of the World Health Organization. 78(9): 1078–92.

Bruce, N; Rehfuess, E; Mehta, S; Hutton, G and Smith, K. 2006. Indoor air pollution.

Ezzati, M & Kammen, DM. 2001. Indoor air pollution from biomass combustion and acute respiratory infections in Kenya: an exposure-response study. *The Lancet*, 358(9282): 619-624.

Gauderman, WJ; McConnell, R and Gilliland, F. 2000. Association between Air Pollution and Lung Function Growth in Southern California Children. *American Journal of Respiratory & Critical Care Medicine*. 162: 1383-90.
Khan, MY and Saxena, A. 2012. Mosquito repellents: Cause of indoor air pollution.
Lin H-H; Ezzati, M and Murray M. 2007. Tobacco smoke, indoor air pollution and tuberculosis: A systematic review and meta-analysis. *PLoS Med*, 4(1).
Mueller, D; Uibel, S and Braun, M. 2011. Tobacco smoke particles and indoor air quality (ToPIQ) – the protocol of a new study. *J Occup Med Toxicol*. 6: 35.
OECD. 2015. The economic consequences of indoor and outdoor air pollution.
Pandey, MR; Boleij, JSM; Smith, KR and Wafula, EM. 1989. Indoor air pollution in developing countries and acute respiratory infection in children. *Lancet*, 427-429.
Persily, A and Levin, H. 2011. Ventilation measurements in IAQ studies: problems and opportunities. In *Proceedings of Indoor Air 2011, 12th International Conference on Indoor Air Quality and Climate*.
Salthammer T. 2014. Release of organic compounds and particulate matter from products, materials, and electrical devices in the indoor environment. *The Handbook of Chemistry*, 12(1).
Smith, KR. 1987. *Biofuels, Air Pollution, and Health: A Global Review*. New York: Plenum Press.
Smith, KR & Mehta, S. 2003. The burden of disease from indoor air pollution in developing countries: comparison of estimates. *International Journal of Hygiene and Environmental Health*, 206(4-5): 279-289.
Traynor, GW; Apte, MG; Carruthers, AR; Dillworth, JF; Grimsrud, DT and Gundel, LA. 1987. Indoor air pollution due to emissions from wood-burning stoves. *Environmental Science & Technology*, 21(7): 691-697.
Vrijheid, M; Martinez, D; Aguilera, I; Bustamante, M; Ballester, F; Estarlich, M; and Tardon, A. 2012. INMA Project. Indoor Air Pollution from Gas Cooking and Infant Neurodevelopment. *Epidemiology*, 23(1): 23-32.
World Bank Group. 2014. *World Development Indicators 2014*. World Bank Publications.

4th International Conference on Advances in Civil Engineering 2018 (ICACE 2018)
19 –21 December 2018
CUET, Chittagong, Bangladesh
www.cuet.ac.bd

SPATIO-TEMPORAL CHANGE ANALYSIS OF WETLAND IN CHITTAGONG CITY CORPORATION BY REMOTE SENSING AND GIS TECHNIQUE

M. S. N. Hredoy*, M. N. H. Naim, M. S. Sikdar& M. K. Islam

*Department of Urban and Regional Planning, Chittagong University of Engineering &Technology, Raozan, Chittagong, Bangladesh.

E-mail:hridhowlader@gmail.com

**Corresponding Author*

ABSTRACT
Recurrent change in the water body due to rapid urbanization is a very common phenomenon now-a-days. Chittagong, the commercial capital of Bangladesh facing unplanned urbanization in recent couple of decades. Changing of land use has become common phenomenon and changing of water body into other is one of its examples. In this study the change of wetland of Chittagong city corporation area has been identified. Remote sensing and GIS based technique is applied between the years 1980 to 2018 to identify the change. Remote sensing datasets and GIS have been used to analyze the trend change with Normalized Difference Water Index (NDWI) and Post-classification change detection methods. The potential causes of wetland loss were analyzed after the classification. It has been found that around 28.92% wetland and river, canal & pond decrease significantly over the last 38 years. This change makes the city vulnerable for water logging and drainage system as its consequence. Increase temperature is also a consequence of this change which is affecting the environment and climate change. The main cause of reducing wetland is indiscriminate land filling and encroachment to the wetland for constricting high rise building for various purposes. So, it is necessary to revive these wetland and water body to make the drainage system functional.

Keywords: Wetland, Land use/Land cover changes, Satellite images, NDWI

INTRODUCTION
Due to anthropogenic activity of human across the earth surface, sea-level rise, climate change, increasing temperature and other unknown potential effect of global environment have been arising (Coomes et al., 2001; Hassan & Nazem, 2015). Which are mostly driven by the human and the resultant modification of landscape configuration at global, regional and local level (Weng, 2014). And these change is happening by diminishing forest area agricultural land and filling water body for the expansion of impervious surface alongside human settlement (Yin, Stewart, Bullard, & MacLachlan, 2005). These changes have so many negative impacts on water quality, ecosystem, aquatic life etc. In recent decades, accelerated population growth coupled with rapid urban growth triggered these phenomena (Hassan & Nazem, 2015).
In recent practice, remote sensing in conjunction with GIS technology help to monitor these change and its advance tool aid in better understanding and analyzing these change because of having multiple characteristics of satellite image like temporal resolution, spectral resolution, spatial resolution etc. The use of Landsat satellite to monitor these change has become a common approach in recent years (Hassan & Nazem, 2015; Turner ll, Lambin, & Reenberg, 2010; NASA, 2016)
Bangladesh is a developing country and one of the most populated in the world and the study area Chittagong is the second largest metropolitan city in Bangladesh sharing 19.7% GDP of the country

(BBS, 2011; Hassan & Nazem, 2015). Due to huge population pressure the area is being urbanized haphazardly day by day and the result is altering land use which is decreasing the number of hill, forest or vegetated area, water body etc. and subsequently increasing impervious urban area. Especially water body of this city decrease drastically due to urbanization. In this study the definition of water body is lake, ponds, lagoon, river, aqua fishing, and vast sea water. These change also putting negative impact on the environment and function of the city like water logging (Hassan & Nazem, 2015; Rana, 2011). Therefore, the aim of this study is to monitor the wet land or water body change of Chittagong City Corporation (CCC) area and make a comparison & analyze these change.

METHODOLOGY

Chittagong is the second largest city and prime sea port and the heart of commercial and business activities in Bangladesh (Ahmed et al., 2014). It is lies within 22°14' and 22°24' N Latitude and between 91°46' and 91°53' E Longitude (Chittagong city-Banglapedia, 2018). Chittagong city corporation area (CCC) has an area of 160.99 sq. km and it is divided into 41 wards for administrative purpose. Chittagong city is located towards south-east of the capital city of Dhaka on the bank of Karnaphuli River and surrounded by rich natural resources like green hilly terrain, sea etc. (Ahmed et al., 2014).

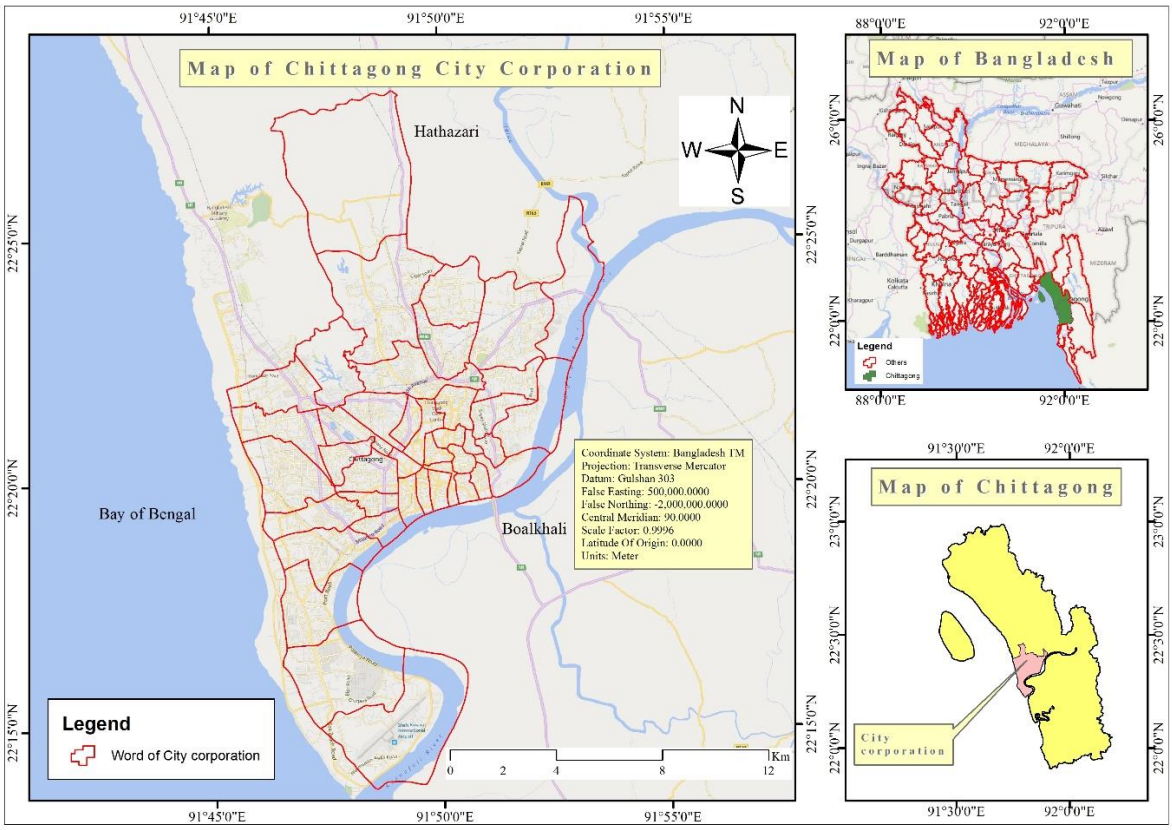

Fig. 1: Location Map of Chittagong City Corporation area

To find out the amplitude of the water bodies of Chittagong City Corporation area, Landsat images of 1990 (TM), 2005 (TM), 2018 (OLI-TRS) were used. Spatial resolution of these images was 30m and these images were captured within June-August (during rainy season). Band 2 & 4 for TM and Band 3 & 5 for OLI-TRS were used to calculate NDWI. The study was conducted under the framework of Geographic Information System (GIS) and Remote Sensing. The satellite images were processed by (Earth Resource Data Analysis System) ERDAS IMAGINE 14 and the wetland change was detected by ArcGIS 10.5 software. The wetlands were identified by unsupervised classification which was conducted by NDWI. The equation used for calculating NDWI given by Mcfeeters (2007) as follows

$$\text{NDWI} = \frac{Green - NIR}{Green + NIR} \qquad (1)$$

Justification of the classified images was performed by calculating accuracy assessment with 60 Ground Control Points which are dispersed throughout Chittagong City Corporation area. Finally, the images

for wetland of Chittagong City Corporation of different years were used to detect the change by contingency matrix analysis in ArcGIS.

RESULT AND DISCUSSION

This research aims at deriving the change of waterbody of Chittagong city of a duration of 28 years. As because of different physical change waterbody is decreasing and the rate is alarming. [Fig. 2] is representing the land use of Chittagong City Corporation Area using Water index NDWI for 1990, 2005 and 2018 respectively using remote sensing data. The land use of the area is divided into water body and other land use. from the map. It can be said that there is a decrease in waterbody in 2018 than 1990 & 2005.

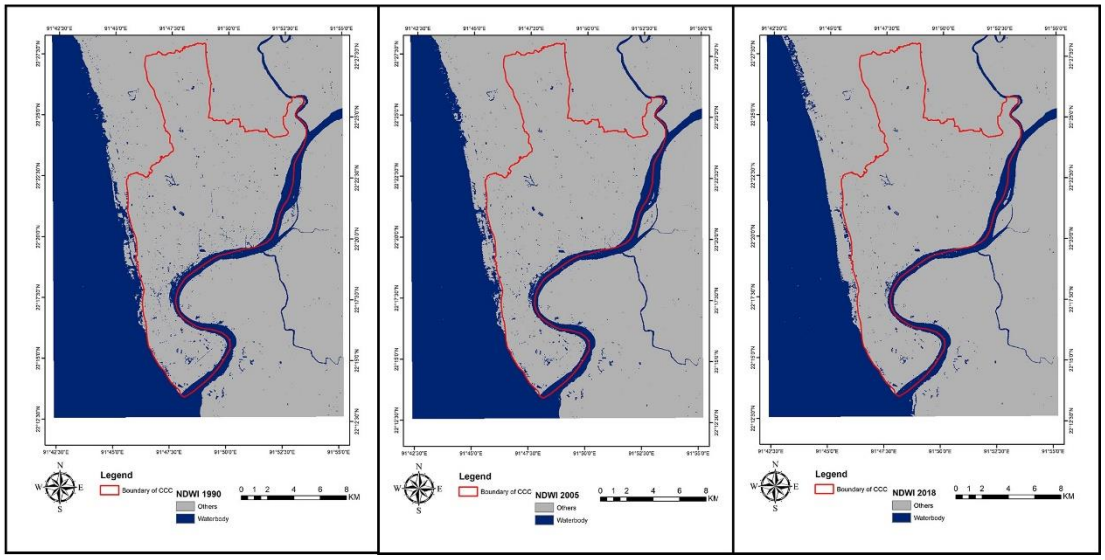

Fig 2: Land use of Chittagong City Corporation Area using NDWI

In 1990 area covered with water is higher than other year. The reason of waterbody reduction is waterbody is replaced by other land use in this time period. [Fig. 3] showing the change in waterbody for the time period of 1990-2005 & 2005-2018 respectively. From the map it can be said that the change of waterbody is higher for time period 2005-2018 than 1990-2005.

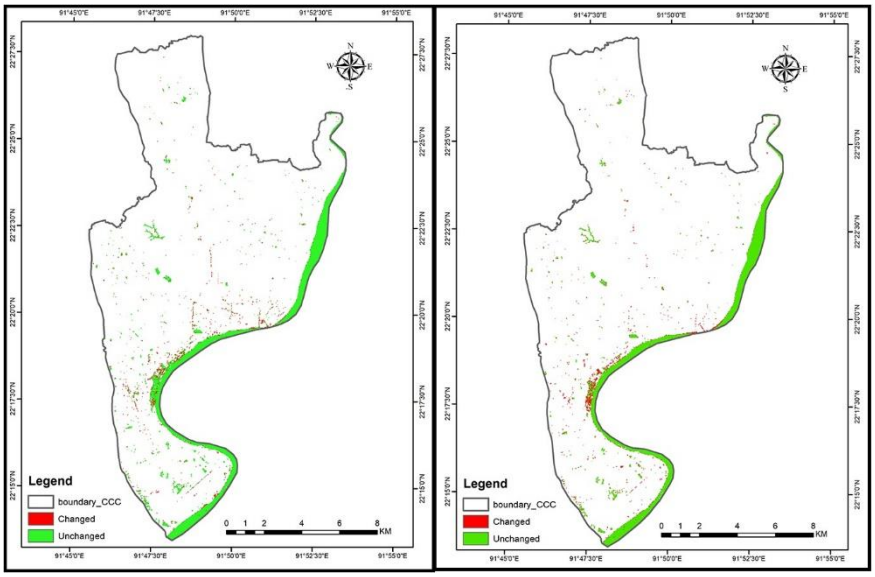

Fig. 3: Waterbody Change Map of Chittagong city for 1990-2005 & 2005-2018 respectively

Table 1 is representing the change of the area of waterbody in Chittagong City Corporation Area in the year 1990,2005 & 2018. In the year 1990 the waterbody of city corporation was 39.81 sq.km. which was 23.15% of the total city corporation area. In 2005 it was reduced to 34.98-acre area which was

20.33% of the total area and in 2018 it is further reduced to 28.31-acre area which was 16.46% of the total area. From 2005 to 2018-time period percentage of change of water body is -28.92% which is higher than 1990-2005-time period where percentage of change is -12.15% and all the value of percentage of change is indicating reduction of waterbody. From 1990 to 2005 waterbody is reduced to around 12% whereas the reduction increased to around 16% from 2005 to 2018. It is due to the rapid urbanization and population growth as waterbody of CCC area is replaced by other land use. There is huge impact of land use change in the reduction of waterbody in the study area. Waterbody of the Chittagong City Corporation area is converted forcefully into other land use like residential, commercial, industrial area etc.

Table 1: Change of the Area of Waterbody in CCC for Different Year

Year	Waterbody area(in acre)	Percentage of Total Area	Percentage of Change
1990	39.81	23.15	-
2005	34.98	20.33	-20.15%
2018	28.31	16.46	-28.92%

Conversion of waterbody to other land use affect greatly the environment. With the reduction of waterbody, temperature is increasing day by day at a higher rate (Hassan & Nazem, 2015).

Table 2: Summary of accuracy assessment

Year	User Accuracy		Producer Accuracy		Overall Accuracy
	Water	Other	Water	Other	
1990	65.63	76.25	72.58	79.25	70.58
2005	74.82	82.76	76.58	81.23	76.01
2018	80.87	87.85	75.00	83.33	79.21

Accuracy assessment of the overall classification of is described in table 2. In this table overall accuracy, producer accuracy and user accuracy is shown. Minimum overall accuracy for the classification of remote sensing data is 60%. From the analysis it can be seen that accuracy assessment for different year's classification is greater than 70% which justify the overall analysis.

CONCLUSION

Land use and land cover change affects a wide range of socioeconomic, biological, climatic, and hydrologic systems. Besides understanding land use and land cover changes is essential not only for biodiversity monitoring but also for land planning, food security, economic policy, and climate change. This study reveals the change of wetland during 1990-2018 (28 years) in Chittagong City Corporation area concluding with a decrease of wetland during this time period. Due to uncontrolled land use and land cover change the Chittagong City is losing its' wetlands mostly along with other land uses like open space, vegetation etc. So proper measures should be taken to preserve the existing waterbodies and also to restore the declined wetlands to its' original condition.

REFERENCES

Ahmed, B., Rahman, M. S., Rahman, S., Huq, F. F., & Ara, S. (2014). *Landslide Inventory Report of Chittagong Metropolitan Aea, Bangladesh.* Dhaka-1000.

BBS. (2011). *No Title*. Dhaka: GOVERNMENT OF THE PEOPLE'S REPUBLIC OF BANGLADESH.

Coomes, O. T., Lambin, E. F., Turner, B. L., Geist, H. J., Agbola, S. B., Angelsen, A., … Xu, J. (2001). The causes of land-use and land-cover change : Moving beyond the myths The causes of land-use and land-cover change : moving beyond the myths Helle Sk a. *Global Environmental Change 11*,

11(December 2001), 261–269. https://doi.org/https://doi.org/10.1016/S0959-3780(01)00007-3
Chittagong city-Banglapedia. (2018, 09 02). Retrieved from http://en.banglapedia.org/index.php?title=Chittagong_city
Hassan, M. M., & Nazem, M. N. I. (2015). Examination of land use/land cover changes, urban growth dynamics, and environmental sustainability in Chittagong city, Bangladesh. *Environment, Development and Sustainability*, *18*(3), 697–716. https://doi.org/10.1007/s10668-015-9672-8
Mcfeeters, S. K. (2007). The use of the Normalized Difference Water Index (NDWI) in the delineation of open water features. *International Journal of Remote Sensing*, *1161*, 1425–1432. https://doi.org/10.1080/01431169608948714
NASA. (2016). *Landsat 8 (L8) Data Users Handbook*. Department of the Interior U.S. Geological Survey.
Rana, M. M. P. (2011). Urbanization and sustainability: Challenges and strategies for sustainable urban development in Bangladesh. *Environment, Development and Sustainability*, *13*(1), 237–256. https://doi.org/10.1007/s10668-010-9258-4
Turner ll, B. L., Lambin, E. F., & Reenberg, A. (2010). The emergence ofland change science for global environmental change and sustainability. *Proc. Natl. Acad. Sci. USAce*, *104*(2007), 20666–20671. Retrieved from http://www.pubmedcentral.nih.gov/articlerender.fcgi?artid=3001449&tool=pmcentrez&rendertype=abstract
Weng, Q. (2014). A remote sensing – GIS evaluation of urban expansion and its impact on surface temperature in the Zhujiang Delta , China. *International Journal of Remote Sensing*, *22*(10), 1999–2014. https://doi.org/10.1080/713860788
Yin, Z. Y., Stewart, D. J., Bullard, S., & MacLachlan, J. T. (2005). Changes in urban built-up surface and population distribution patterns during 1986-1999: A case study of Cairo, Egypt. *Computers, Environment and Urban Systems*, *29*(5 SPEC. ISS.), 595–616. https://doi.org/10.1016/j.compenvurbsys.2005.01.008

4th International Conference on Advances in Civil Engineering 2018 (ICACE 2018)
19 –21 December 2018
CUET, Chittagong, Bangladesh
www.cuet.ac.bd

STABILITY ANALYSIS OF HILL SLOPE AT CHITTAGONG IN BANGLADESH: A CASE STUDY AT FOY'S LAKE RESIDENTIAL AREA HILL

A. Hossain*& M. A. Alim

Department of Civil Engineering, RajshahiUniversity of Engineering &Technology, Rajshahi-6204, Bangladesh.
E-mail:ahmedhossain090001@gmail.com

**Corresponding Author*

ABSTRACT:
Bangladesh is renowned as one of the most susceptible countries to natural disaster. The common disaster in this country are flood, cyclone induced storm surges, droughts, earthquakes and river bank erosion. Moreover, slope failures in hilly area have become newly added burning issue. It caused the death of an enormous number of people in Chittagong city and its adjacent urban centers specially 127 people in 2007 and 152 people in 2017. Slope failures incorporate all categories of gravity or saturation related failures in earth materials. In this study, soil sample was collected from Foy's lake residential area hill and using field and lab experiments, soil parameters such as soil type, soil cohesion (c), moisture content (w), degree of saturation and unit weight of soil (γ) have been determined. Considering a slope model, slope stability analyses are carried out by the slope stability program of GEO5 software (2018 version). Finally, to know the occurrence of slope failures, effect of varying slope angle, surcharge load distance from crest of the slope, different degree of saturation has also been studied here.

KEYWORDS: Slope failures, Degree of Saturation, Slope angle, Surcharge.

INTRODUCTION

A World Bank report (Dilley et al., 2005) represents a profile of world-wide exposure to landslide hazard issues. Land area of the globe exposed to landslide is 3.7 million Km^2. The population exposed to landslide is 300 million, which is 5 percent of the total world's population. Petly (2008) reports that, in terms of the occurrence of landslide fatalities in the year 2007, by nation, most seriously affected country was China with 695 landslide induced death, followed by Indonesia (465), India (352), Nepal (168), Bangladesh (150) and Vietnam (130). In Bangladesh, population density on steep slopes is mounting due to scarcity of land. According to Network for Information, Response and Preparedness Activities on Disaster (NIRAPAD), around 50,000 people living on the slopes of hills in Chittagong are in great jeopardy of landslide during the rainy season. Of them, around 15,000 people are living on the slopes or bottom of 12 hills that were identified as Red Zones by a government formed technical committee in 2008. One of these red zone is Foy's lake residential area hill ($22^0 22' 20'' N$, $91^0 47' 35'' E$). This zone is also considered as moderate risk area according to GPS survey incorporated by Mahmood & Khan (2010). The hill management committee was formed following a landslide of Chittagong hills on June 11, 2007 that left 127 people killed. It also saw another landslide on August 18, 2008 that killed eleven (11) people. On 16th June 2017, at least 152 people, including several officers and members of the army have been killed in landslides triggered by torrential rain in Rangamati, Bandarban, Chittagong, Khagrachhari and Cox's Bazar districts. Since the year of 2000, overall deaths due to landslide in different zones of Bangladesh are shown in the table below.

Table 1: (Deaths in Land Slide since 2000)

Year	Chittagong	Cox's Bazar	Bandarban	Rangmati
2000	13	--	--	--
2007	127	--	--	--
2008	11	17	--	--
2010	--	54	--	--
2011	17	--	--	--
2012	28	29	27	--
2015	--	5	9	--
2017	32	--	6	110

In this analysis, soil sample of a slope from different points was collected from Foy's lake residential hill area. By laboratory experiment, property of the soil samples was found out and further used in the slope model to carry out stability analyses. Process of slope instability is triggered mainly due to an excessive degree of saturation. Moreover, people build their houses on the terrain of slope. Load and location of these houses may also cause failure of the slope. Since, there are a lot of other hills in the same area, assuming to have varying slope angle, different degree of saturation and varying surcharge distance from the crest of the slope, the effect of this factors leading to slope instability are discussed and analyzed in this study. Figure 1 shows the location from where the soil sample was collected.

Fig. 1: Foy's Lake Residential Area Hill at Chittagong in Bangladesh

MATERIALS AND SLOPE GEOMETRY

Soil sample obtained from different field location is considered homogeneous by physical observations and laboratory experiments. On the field, bulk density of soil sample was determined by core cutter method. The cylindrical core cutter was pressed into the ground by steel rammer. After driving the core fully into the ground, it was removed from the ground without disturbing the core contents. Then, bulk unit weight of soil sample was measured and it was found to be 16.87 kN/m^3. By measuring moisture content (18.16%), dry unit weight of the soil sample was found to be 14.28 kN/m^3.

Grain size distribution and soil type

Soil sample was collected from different location of the hill. According to sand, silt and clay fractions, determined from the grain size distribution curve of soil samples, all the soil sample was found to be clay type (using USDA classification chart). The specific gravity of the soil sample was measured by pycnometer method and it was found to be 2.65. Using the value of specific gravity and dry unit weight, void ratio and degree of saturation of soil sample were measured by formula. The soil sample had a void ratio of 82% with 59% degree of saturation.

Unconfined compression test

In this test, at first, the soil sample was compacted to its field density. Prepared sample was placed on the loading device after measuring its initial length and diameter. Undrained cohesion of soil sample was found to be 50 kN/m^2 for 59% saturation (field). To obtain the value of undrained cohesion for 70%, 80% and 90% saturated soil sample, specific amount of soil was mixed with 21.66%, 24.75% and 27.85% water respectively. The value of undrained cohesion obtained from unconfined compression test have been found to be 40 kN/m^2, 31 kN/m^2 and 22 kN/m^2 for 70%, 80% and 90% saturated soil sample respectively (figure 2). It means that, water content is contributing to the cohesion property of soil. When water percolates into the soil masses, then pore water pressure develops inside the soil masses and the water tries to move the soil grains away from each other. As a result, cohesion value of soil masses decreases.

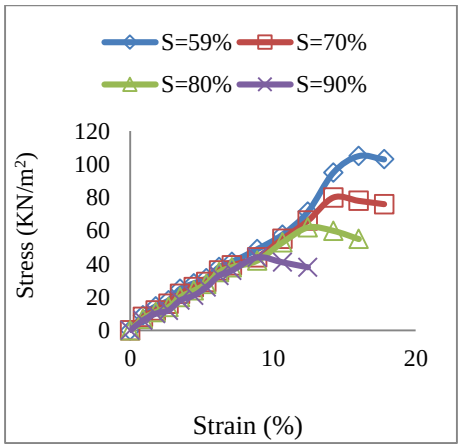

Fig. 2: Unconfined Compression test result

Slope geometry

Based on field observations, slope model used in this analysis is shown below.

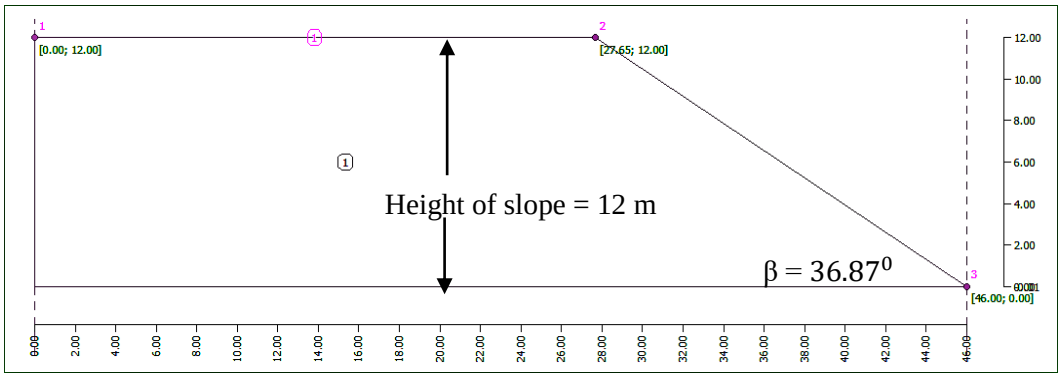

Fig. 3: Slope geometry model

SLOPE STABILITY ANALYSIS

In this study, slope stability analysis has been carried out by slope stability program of GEO5 software (2018 version). It should be noted that, slope stability program is based on **Limit Equilibrium Method** (LEM). The slip surface is considered as circular (Bishop, Fellenius/Petterson, Janbu, Morgenstern-Price or Spencer methods) and polygonal (Sarma, Janbu, Morgenstern-Price or Spencer methods).

Slope stability analysis by GEO5 software

For slope stability analysis, following parameters are considered which are given in table 2.

Table 2: Parameters used for slope stability analyses

Parameters	Description
Stress state	Total stress (Undrained Condition)

Bulk Unit weight	16.87
Cohesion of soil	50 kN/m^2

Stability analysis considering circular and polygonal slip surface are shown in figure 4 and figure 5

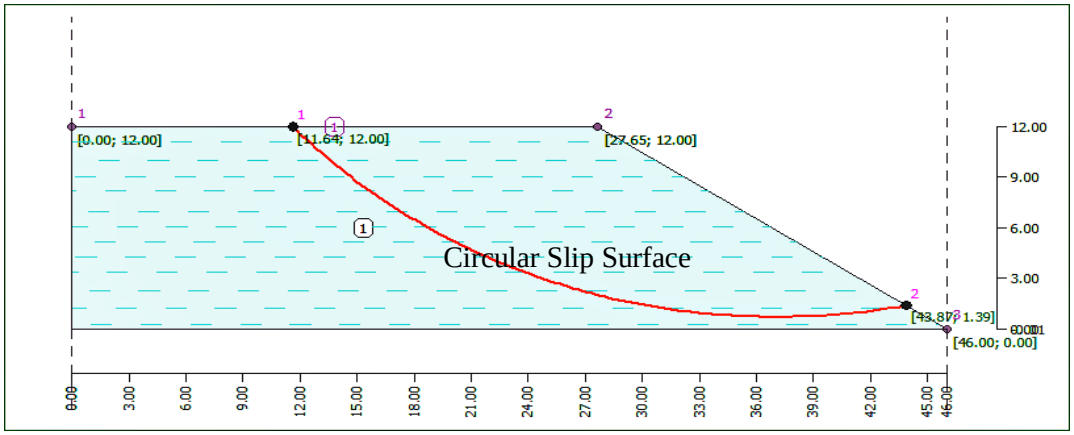

Fig. 4: Slope stability analysis (Circular Slip Surface)

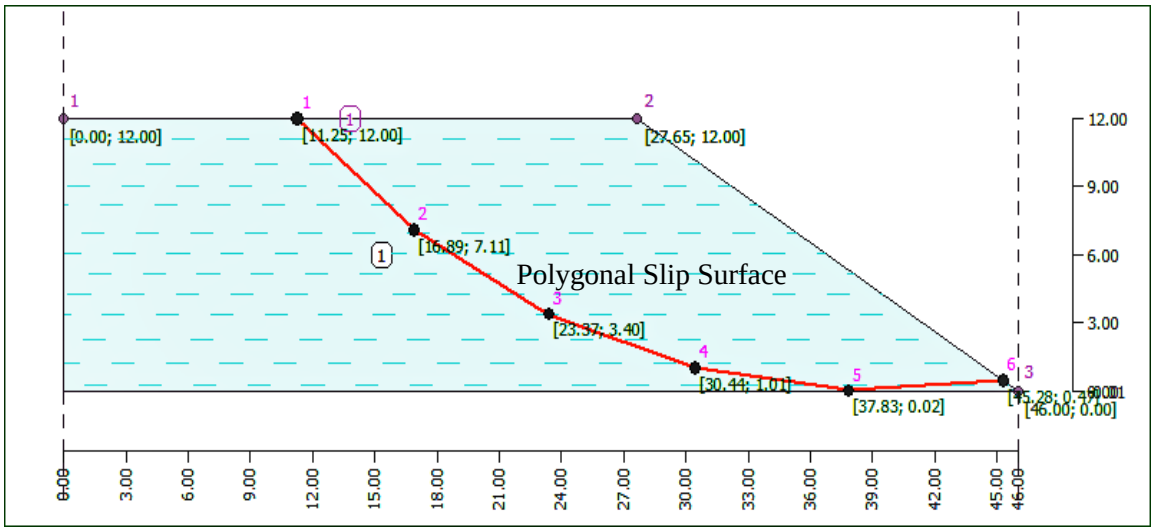

Fig. 5: Slope stability analysis (Polygonal Slip Surface)

Slope stability results

Following table shows factor of safety by different slope stability methods considering circular and polygonal slip surface. Circular slip surface was converted to polygon by considering ten segments. Analysis settings was considered standard and optimized type.

Table 3: Analysis result by GEO5 Software

Method	**Circular Slip Surface**		**Polygonal Slip Surface (No of Segments = 10)**	
	Standard	**Optimized**	**Standard**	**Optimized**
Bishop :	1.95	1.58	N/A	N/A
Fellenius / Petterson :	1.95	1.58	N/A	N/A
Spencer :	1.95	1.58	Not found.	1.38
Janbu :	1.95	1.58	1.63	Not found
Morgenstern-Price :	1.95	1.58	1.63	1.25
Sarma :	N/A	N/A	2.47	1.78

Effect of degree of saturation, slope angle and surcharge distance

During monsoon, degree of saturation of soil sample increases with the increase of rainfall, which is the main reason for failure of the slope. Also with the increase of slope angle and surcharge load, the slope becomes unstable. Now, further analyses were performed considering 59% (field), 70%, 80% and 90% degree of saturation with 30^0, 36.87^0 , 40^0, 50^0 ,60^0 ,70^0 and 80^0 slope angle for without surcharge and with surcharge condition. Value of surcharge is taken as 200 kN/m^2 for this study. The obtained results are given below.

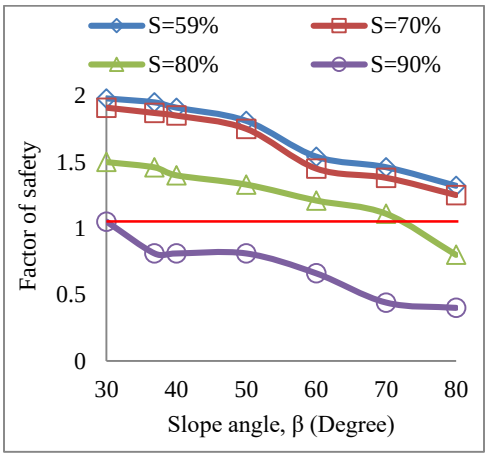

Fig. 6: Without surcharge

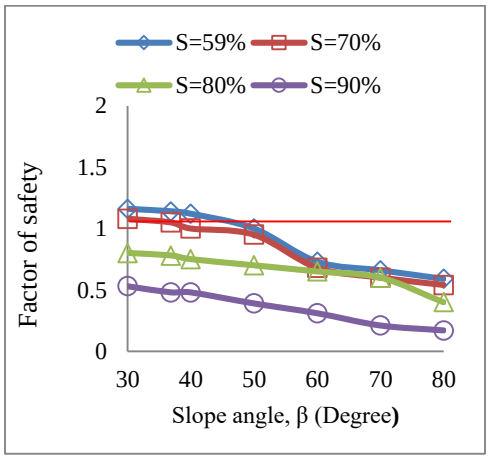

Fig. 7: Surcharge at crest

Figure 6 represents variation of factor of safety with different slope angle without application of surcharge. It is evident that, for 90% degree of saturation, factor of safety remained below unity for slope angles ranging from 30^0 to 80^0. For 80% degree of saturation, initially factor of safety remained at 1.5, but it showed a downward trend with the increase of slope angle and finally fall below unity for slope angle greater than 70^0. For soils having 59% and 70% degree of saturation, both lines showed similar behavior with increase of slope angle starting at a factor of safety value of approximately 2 and ending at just below 1.5. Figure 7 shows relationship between factors of safety with different slope angle for varying degree of saturation with application of surcharge at the crest of the slope. In this case, factor of safety remains below unity for 90% and 80% degree of saturation for all slope angles. On the other hand, initially factor of safety remained above one for 59% and 70% degree of saturation at 30^0 slope angle, but went below unity at 40^0 slope angle.

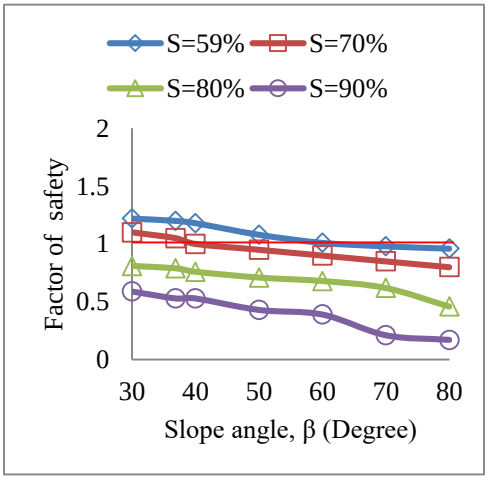

Fig. 8: Surcharge at 3m from crest

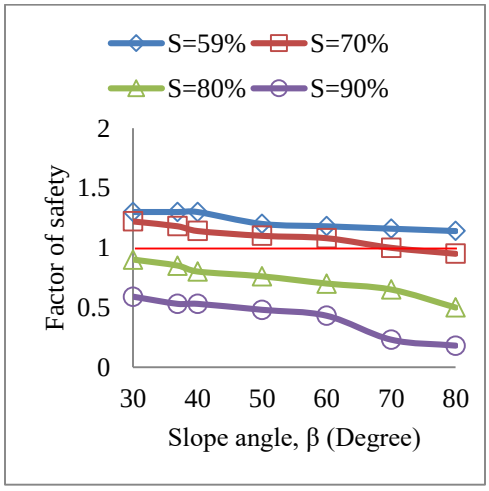

Fig. 9: Surcharge at 6m from the crest

Figure 8 and 9 represents application of surcharge condition at a distance of 3 meter and 6 meter respectively from the crest of the slope. Comparing these two diagrams, it is evident that, factor of safety increases with the increase of distance of surcharge load from the crest of the slope. In figure 8, 59% saturated soil sample lies above red line upto to 60^0 slope angle and lies over red line from 60^0 to 80^0 slope angle. Whereas in figure 9, both 70% and 59% saturated soil sample lies critically above red line (factor of safety =1), but 80% and 90% saturated soil sample never reached unit factor of safety which is quite similar behavior when surcharge is placed at 3m from crest.

CONCLUSIONS

In this study, the effect of degree of saturation with varying slope angle is studied using the slope stability program of GEO5 software (2018 version). The effect of varying surcharge distance from the crest of the slope for distinct slope angle and degree of saturation has also been incorporated here. It is observed that the factor of safety decreases as the slope angle increases and this criteria is also governed by the degree of saturation of soil sample. With the increase of degree of saturation, cohesive property of soil sample decreases (decrease of cohesion value C) which finally attributes to the failure of slope. Since CHT (Chittagong Hill Tracts) is a landslide prone area and mainly due to slope related failure, following points can be summarized here:

- Rainfall intensity must be monitored frequently specially in monsoon. Excessive rainfall will eventually increase degree of saturation of soil sample and these would lead to slope failure.
- Human is responsible for hill cutting without proper guidelines. These activities must be monitored with the measurement of slope angle. Since, high slope angle induces slope failure.
- Often people build their houses on the terrain of a slope. Distance from the crest of the slope must be taken into consideration since it could lead to slope failure.

REFERENCES

Anvil Chakma, Sanjoy Kumar Barua (2017, June 14). Horror strikes hills, *The Daily Star*, Retrieved from http://www.thedailystar.net

Das, B. M., & Sivakugan, N. (2016). Fundamentals of Geotechnical engineering. Cengage Learning.

Disaster Risk Management Series No. 5, Natural Disaster Hotspots: A Global Risk Analysis (Maxx Dilley et al., 2005)

Greenbaum, D., Tutton, M., Bowker, M. R., Browne, T. J., Buleka, J., Greally, K. B., & O'Connor, E. A. (1995). Rapid methods of landslide hazard mapping: Papua New Guinea case study (p. 1)

Hansen, A, 1984 Landslide Hazard Analysis. In slope instability, (D. Brunsen and D.B Prior eds.), Johan Wiley & Sons, New York,pp. 523-602.

Kjekstad, O., & Highland, L. (2009). Economic and Social Impacts of Landslides 30.

Kyoji Sassa, Paolo Canuti (2008). Landslides -Disaster Risk Reduction, Retrieved from http://books.google.com

Mahmood & Khan (2010), Landslide Risk Management in South Asia.

Network for Information, Response and Preparedness Activities on Disaster (NIRAPAD)

Petley, D. N. (2008). The global occurrence of fatal landslides in 2007. In Geophysical research abstracts (Vol. 10, p. 3).

Sassa, K. (2009). Report of the 2008 First World Landslide Forum in 18–21 November 2008 at UNU, Tokyo.

Sassa, K., & Canuti, P. (Eds.). (2008). Landslides-disaster risk reduction. Springer Science & Business Media.

Schuster & Highland (2001), Economic and Social Impacts of Landslides (p. 575)

4th International Conference on Advances in Civil Engineering 2018 (ICACE 2018)
19 –21 December 2018
CUET, Chittagong, Bangladesh
www.cuet.ac.bd

STABILITY ANALYSIS OF SELECTED HILL SLOPES OF RANGAMATI

T. E. Elahi, M. A. Islam*& M. S. Islam

Department of Civil Engineering, Bangladesh University of Engineering & Technology, Dhaka, Bangladesh.
Email: azijul@ce.buet.ac.bd
**Corresponding Author*

ABSTRACT
Landslide is a very common natural disaster in Bangladesh. Excessive rainfall, cutting of hill slopes, deforestation, steep slope and erosion are mainly responsible for landslides. To determine the soil types, failure pattern and reasons behind the landslide that occurred in 2017, both disturbed and undisturbed soil samples were collected from five locations of affected areas of Rangamati. Laboratory tests were performed to determine index and shear strength parameters of hill soil. Among five soil samples, three have been identified as sand with fine fractions ranging from 21.7 to 42.6%. The remaining two soil samples have been classified as sandy lean clay (CL) and sandy silty clay (CL-ML). For all the soils, angle of internal friction varies from 27^o to 40^o with very low cohesive strength. The two clay samples are soft clays and have cohesion of 17.5 and 9.4 kPa respectively. From field observation of the affected areas, slope angles have been found to be ranging from 50^o to 70^o and height of the slopes varies from 10m to 20m. For evaluating the stability of slopes of the affected areas, Finite Element Model (FEM) analysis have been performed using PLAXIS 2D. The soil and slope properties obtained from the test results and field observations were used during the FEM analysis. For all cases, Factor of Safety has been found less than 1.5 which indicates that the slopes were susceptible to landslides. Furthermore, the failure pattern of slopes obtained from FEM analysis have been found similar to the actual failure patterns.

Keywords: Landslide; Stability analysis; PLAXIS 2D; Factor of safety.

INTRODUCTION

Landslide has become a regular hazard in the hill tracts of Bangladesh which occurs almost every year. Bangladesh is a very densely populated developing country and hilly or mountainous terrain occupies almost 12% of the total area of the whole country. Scarcity of land force people to live in the foot of hills specially the poor people. Every year a lot of people living there die because of landslide.

Any observable downward and outward movement of slope-forming soil, rock and vegetation under the influence of gravity is defined as landslide. It is one of the most significant natural damaging disaster in hilly areas, which includes wide ground movements such as fall of rocks, deep failure of slopes and flow of shallow debris (Chisty 2014; Rahman 2012). Human activities like deforestation, cultivation on hills and cutting of hill toes have made the slopes unstable. In addition, excessive rainfall during monsoon cause rain cut erosion which results to landslides. Expanding population in the landslide prone area due to migration are the primary means by which humans are contributing to the landslide. The new settlements create disturbing to the natural drainage system and destabilizing slopes. Speedy urbanization, building and road construction through deforestation and excavation of hill slopes are causing landslide in densely populated cities located in hilly areas (Galli and Guzzetti 2007).

Laboratory and field tests have indicated that a homogeneous slope under rainfall conditions is prone to suffer from surface erosion or shallow landslides whereas deep seated failures are often induced by

rainfall in slopes with weak layers (Maula and Zhang 2011; Islam et al. 2017). High rainfall saturates the soil which increases the weight of soil mass thereby resulting in slope failure (Islam 2017). Egeli and Pulat (2011) found that shallow landslides in nearly saturated non cohesive or slightly cohesive soil is caused by high intensity, short duration rainfall which infiltrates into soil and changes inter granular friction and effective stresses. Precipitation and run-off are closely related to the sudden inundation of hill slope and landslide. According to Moriwaki et al. (2004) for a slope of loose sand with high water content, pore water pressure can increase remarkably during failure and can decrease strength of soil. Steep hill slopes are generally more vulnerable to this disaster. Susceptibility of a hill is moderate and high at a slope of 20^o to 30^o and 40^o to 60^o respectively, whereas hills of Chittagong are cut at 70^o or greater slope. Islam et al. (2014) found that in Chittagong, most of the slopes were steeper than 75^o and was the cause of landslide. Erosion is another factor which is responsible not only for water clogging in urban areas, but also for shallow landslides in CHT (Islam and Islam 2018).

Physical process of landslide is directly related to the stability of soil. Generally slope stability is evaluated based on factor of safety and is defined as the ratio of average shear strength of the soil to the average shear stress developed along the failure surface. If average shear stress developed exceeds the shear strength of soil a slope is considered unstable. Numerical analysis of slope stability is commonly performed by Limit Equilibrium Method (LEM) and Finite Element Method (FEM). Hammouri et.al (2008) analyzed the stability of soil by FEM and LEM and found that both method gave almost same shape and location of critical slip surfaces. According to study by Kupka et.al (2009), FEM produces same result as LEM for simple geometry and ground condition.

Strength Reduction Method (SRM) is usually used to analyze the stability of existing hill slopes in FEM. In this method strength parameter will be reduced until the failure of slope and ratio of the actual parameter to critical parameter is considered as Factor of Safety (FS). Main benefits of using SRM is that critical surface failure is developed automatically from the shear strain resulting from application of gravity loads and shear strength reduction and also does not require any assumption of inter slice force distribution. It can also be applied to many complex conditions and can give information about stress, pore water pressure which is not possible by LEM. In this study, FEM analysis will be performed for slope stability analysis.

During last five decades, Chittagong were hit by 12 major landslides (Sarker and Rashid, 2013). During the last three decades the death toll is approximately 200 because of landslides and CHT suffered massive economic and property loss. Heavy monsoon rain over 343 millimeters triggered a number of landslides and floods in Rangamati, Chittagong and Bandarban - three hilly districts of Bangladesh and killed about 152 people on June 12, 2017. A lot of homes have been masked in mud and rubble which includes over 5,000 homes in the Kawkhali upazilla of Rangamati district. So CHT needs special focus for landslide because of the huge damage caused by such disaster. And stability analysis of existing slopes is required to determine which slope is vulnerable to failure. This study is aimed to determine the characteristics of soil and different index and engineering properties will be found out which will be used for FEM analysis. Finally, stability of existing hill slopes will be analysed numerically using software PLAXIS 2D.

METHODOLOGY

For this study soil samples have been collected from five different locations of Rangamati district. The sample collection locations and properties of hill slopes are observed which is presented in Table 1. Undisturbed samples were collected using shelby tube from a depth of 1 m from each locations. Then both the top and bottom of the Shelby tube was waxed in order to maintain the moisture content as same as the field condition. Before testing, the undisturbed samples were extruded using a mechanical extruder. A number of laboratory tests were conducted in order to determine different physical, index and engineering properties of collected soil samples as per ASTM standards which will be used for numerical analysis. Modulus of elasticity of soil has been assumed from literature (Bowels 1996) and poisson's ratio is assumed as 0.3. Site condition and existing slopes of the locations are presented in Fig. 1.

Table 1. Location and properties of existing hill slopes

Sample ID	Location	Latitude	Longitude	Slope height	Slope angle
S-1	Manikchari Army Camp	$22^0$38' 55.8492" N	$92^0$8' 15.7956" E	15m	70º
S-2	Manikchari (South)	22^0 38' 41.7948' N	92^0 8' 18.5316" E	10m	50º
S-3	Shapchari Shalbagan	22^0 38' 49.1352" N	92^0 7' 50.3904" E	10m	65º
S-4	Deppoyachari JatriChauni	22^0 38' 38.9184" N	92^0 8' 35.9544" E	15m	70º
S-5	Kaching	22^0 41' 32.2008" N	92^0 6' 20.7684" E	10m	50º

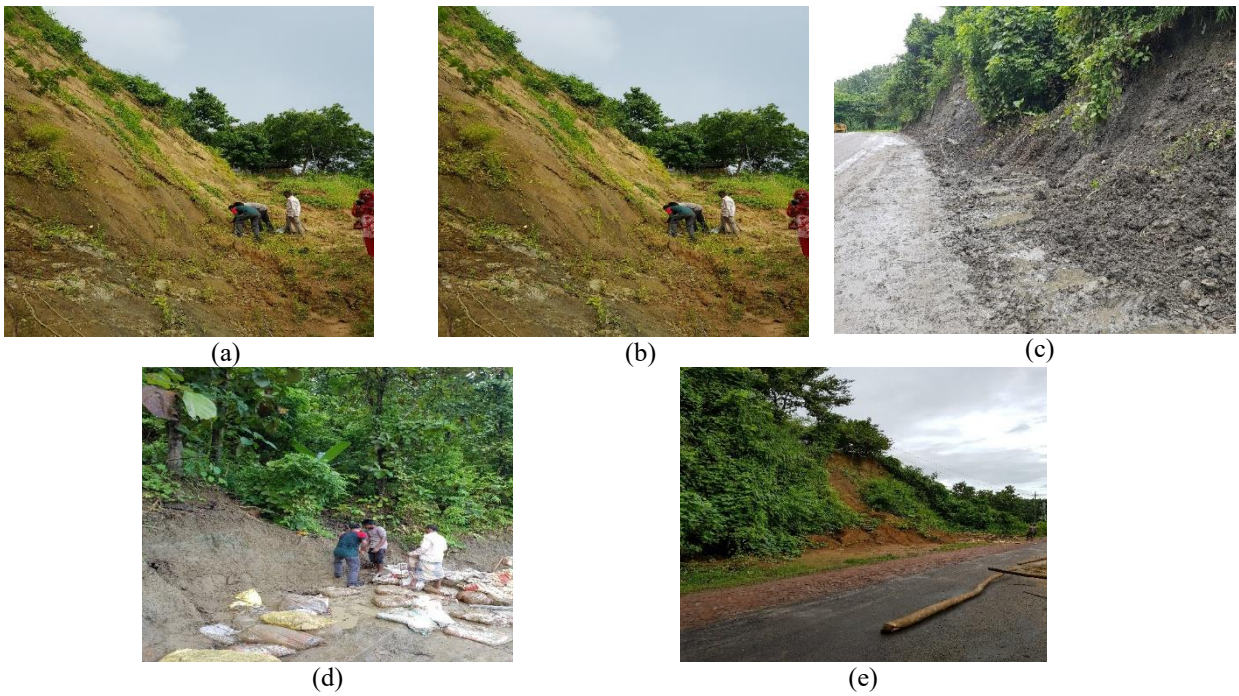

Fig. 1: Field observation and physical condtion of the different slope locations at Rangamati: (a) Manikchari Army Camp; (b) Manikchari south; (c) Shapchari Shalbagan; (d) Deppoyachari Jatri Chauni; (e) Kaching

A scheme of 2D slope has been developed based on existing slope geometry and soil properties for stability analysis. Plain strain model is selected for analysing slope stability. It assumes infinite length perpendicular to plane section and out of the plane displacement is zero. 15-node elements are used for modelling by which failure load and safety factors are correctly predicted. The soil was modelled according to Mohr-Coulomb (MC) model. The linear elastic perfectly plastic Mohr-Coulomb model involves five input parameters, i.e. E and ν for soil elasticity; φ and c for soil plasticity and y as an angle of dilatancy. In general, effective stress states at failure are quite well described using the Mohr-Coulomb failure criterion with effective strength parameters φ' and c'. As hill slope is modelled so for all practical purpose phreatic surface has been considered at the bottom of slope. Standard fixities has been used for modelling which sets boundary conditions, prescribed displacements in x and y direction $u_x=u_y=0$. When geometry model is fully defined and materials properties are assigned to all clusters and structural objects, geometry has to be divided into finite elements in order to perform finite element calculation. In this study medium mesh is used.

A safety analysis in PLAXIS can be executed by reducing the strength parameters of soil. This process is called Phi-c reduction. In this approach, the strength parameters tan φ and c of the soil are successively reduced until the collapse of the slope occurs. The total multiplier ΣMsf is defined as the ratio of the strength parameters entered as input values over the reduced ones.

$$\Sigma\text{Msf} = \frac{tan\phi_{input}}{tan\phi_{output}} = \frac{c_{input}}{c_{output}} \qquad (1)$$

The strength parameters of soil are thereby reduced automatically step by step with an increment Msf equal to 0.1 until failure. The factor of safety (FS) is given by the ratio of the available strength over the strength at failure. It is equal to the value of ΣMsf at failure. ΣMsf is set to 1.0 at the start of a calculation to set all material strength to their input values. A safety calculation is performed using the Load advancement number of steps procedure. The incremental multiplier Msf is used to specify the

increment of the strength reduction of the first calculation step. The increment is by default set to 0.1, which is generally found to be a good starting value. The final step is resulted in a fully developed failure mechanism. If that is the case, the factor of safety is given by:

$$FS = \frac{available\ strength}{strength\ at\ failure} = \text{value of } \Sigma\text{Msf at failure} \qquad (2)$$

Table 2. Index properties of Soil samples

Sample ID	Natural Moisture Content (%)	Specific Gravity	In-Situ Density (kN/m^3)	Dry Density (kN/m^3)	Atterberg Limits			% Finer No. 200 sieve	Soil Classification
					Liquid Limit (%)	Plastic Limit (%)	Plasticity Index (%)		
S-1	13.3	2.66	18.5	16.4	28	24	4	21.7	SM
S-2	13.9	2.69	19.0	16.7	35	25	10	47.4	SC
S-3	25.6	2.69	18.9	15.1	33	20	13	72.0	CL
S-4	18.4	2.65	19.0	16.1	24	18	6	66.5	CL-ML
S-5	15.5	2.75	16.8	14.5	24	17	7	42.6	SM-SC

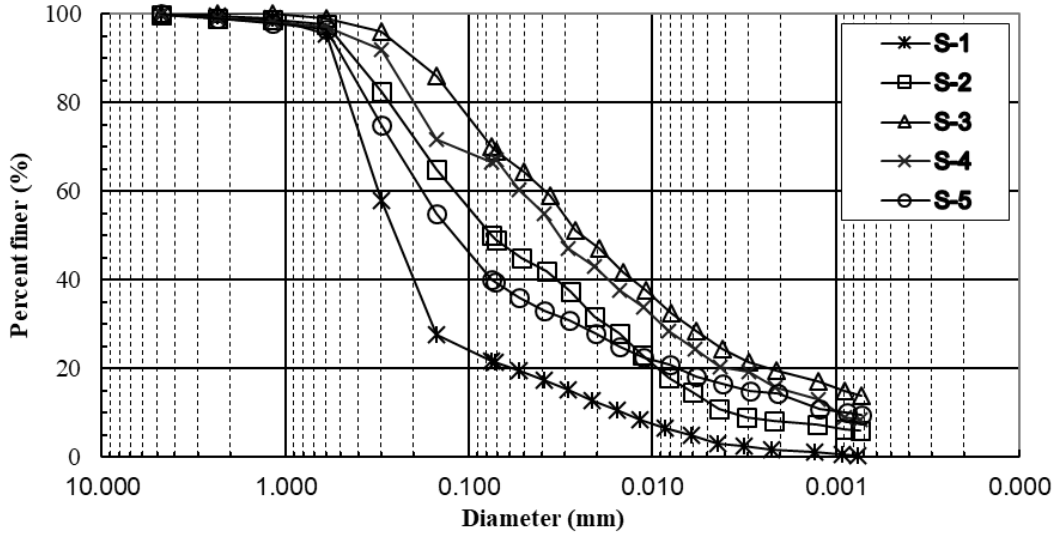

Fig. 2: Grain size distribution for all samples.

Table 3. Engineering properties of the soil samples

Sample ID	Shear Strength Parameters		Permeability, k (m/s)	Void ratio, e	Modulus of Elasticity, E (kN/m^2)
	Cohesion, c (kN/m^2)	Friction angle, ϕ			
S-1	0	39.7	1.9×10^{-07}	0.595	3.0×10^{4}
S-2	8.6	37.3	5.4×10^{-08}	0.580	2.0×10^{4}
S-3	18.0	0	3.0×10^{-10}	0.746	1.0×10^{4}
S-4	9.4	27.4	3.1×10^{-08}	0.620	1.5×10^{4}
S-5	1.8	30.2	5.3×10^{-08}	0.854	2.5×10^{4}

RESULTS AND DISCUSSIONS

The index properties and engineering properties of soil samples are presented in Table 2 and 3 respectively. Grain size distribution of soil samples are shown in Fig. 2. On the basis of these soil properties and grain size distribution, soil samples have been classified as per Unified Soil Classification System (USCS). Sample S-1, S-2 and S-6 identified as silty sand (SM), clayey sand (SC) and silty clayey sand (SC-SM) respectively and fine percent of these soil varies from 21.7% to 47.4%. Sample S-3 and S-4 have been identified as sandy lean clay (CL) and sandy silty clay (CL-ML) which contains fine fractions 72% and 66.5% respectively. From laboratory tests it is seen that in situ unit weight of soil samples are found to vary from 16.8 kN/m^3 to 19.02 kN/m^3. Internal angle of friction and cohesion were measured from direct shear tests. Angle of friction, φ varies from 27^o to 40^o. Cohesive strength of all soil samples are quite low and for two samples CL and CL-ML value is 18 kPa and 9.4 kPa respectively. Using the soil properties obtained from laboratory tests, numerical analysis of existing

hill slopes has been performed in PLAXIS 2D by phi-c reduction method. For the analysis, the slopes were assumed as homogenous soil and the dimensions of the slopes were assumed as uniform. Factor of safety (FS) obtained from numerical analysis is presented in Table 4.

Table 4. FS of selected existing hill slopes of Rangamati

Sample ID	Location	Slope height	Slope angle	FS
S-1	Manikchari Army Camp	15m	70º	0.896
S-2	Manikchari (South)	10m	50º	1.304
S-3	Shapchari Shalbagan	10m	65º	0.542
S-4	Deppoyachari JatriChauni	15m	70º	0.855
S-5	Kaching, Rangamati-Khagrachari Road	10m	50º	0.819

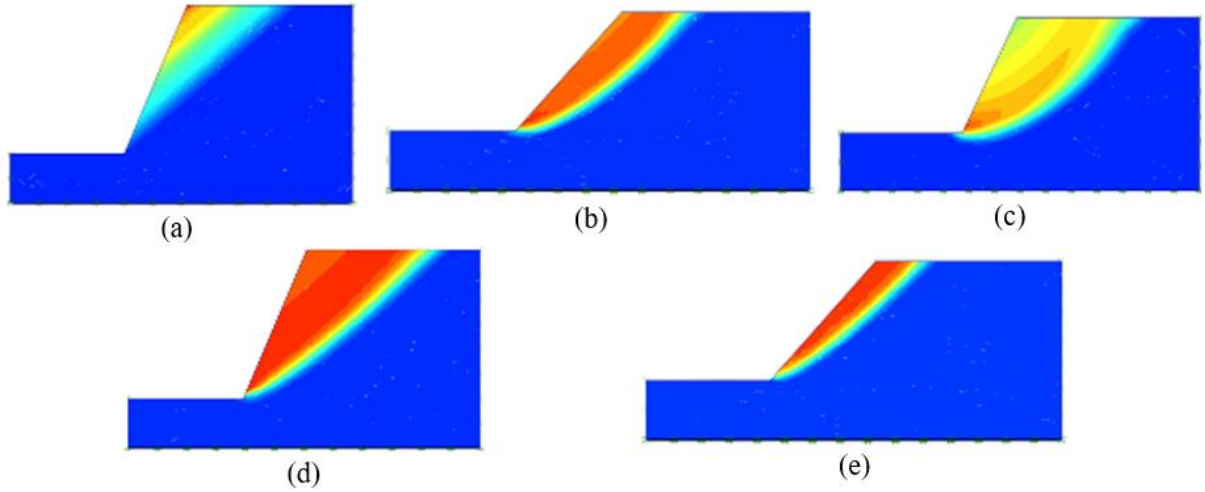

Fig. 3: Failure surface from numerical analysis: (a) shallow slope wedge failure and local failure for S-1; (b) slope toe general slope failure for S-2; (c) base failure for S-3; (d) slope toe general slope failure for S-4; (e) slope toe; surficial failure for S-5

From the analysis it is found that for all the five slopes FS is less than 1.5 which clearly shows that slopes are susceptible to failure. Since the slopes had already failed, the incident validates the present study. FS is minimum for slope with soil S-3, because the slope consists of soft clay with low cohesive strength. Since the soil is clay, friction angle is almost zero. So shear strength is provided only from cohesion parameter not from friction angle. Furthermore, with the increase of depth, shear strength does not increase for pure cohesive soil. Natural moisture content is very high, 25.6% almost close to saturation limit (27.73%). In addition, excessive rainfall infiltrates into soil and make clay very soft. Thus shear strength reduces with precipitation and eventually slope fails. On the other hand FS is maximum for slope with soil S-2 since friction angle is quite high (φ=37.34º) and shear strength comes from both cohesion parameter and friction as well. Moreover FS is high because of less slope angle and moisture content is 13.86%, less than saturation water content (21.56%). From the numerical analysis failure pattern is also observed for each case and those are presented in Fig. 3.

Analysing the failure patterns of slopes it is observed that for slopes with soil S-2, S-4 and S-6 failure surface intersect at the toe of slope and failure is called toe failure. This failure is usually seen in sandy soils with moderate to high friction angle and steep slopes. From laboratory tests it is found that all these soils have higher angle of internal frictions which is in agreement with. On the other hand, for slope with soil S-1 shallow wedge type failure is observed which means failure surface intersects the hill slope above its toe forming a wedge. From the literature (Islam et al. 2014), it is found that for hills with slope angle greater than internal angle of friction is prone to failure. In this study all slope angles are greater than φ of existing slopes. So obtained results in good agreement with literature. For soil S-3 (CL) failure is deep seated base failure and this type of failure is generally found in cohesive soil. The obtained failure surface can also be explained from the field observation of the site. The toe failure pattern at south of Manikchari (S-2) which is shown in Figure 1(b) is quite similar from the FEM analysis shown in Figure 3(b).

CONCLUSIONS

Following conclusions can be made from this study-

a) All the existing hill slopes have slope angles greater than 50^{o} and from numerical analysis it is found that they are prone to failure. So slope angles must be reduced or earth retaining measures should be adopted for increasing the safety of slopes.
b) For clayey type of soil deep seated base failure occurs and for sandy type of soils slope failure or toe failure occurs.
c) Field observation of the landslide damaged locations are similar to the FEM model analysis. Depending on the soil type and slope angle, different types of failure occurs.
d) Proper measures should be taken considering the failure mechanism and field soil investigation in order to prevent landslides.

ACKNOWLEDGMENTS
The authors acknowledge the infrastructural and financial support received from Bangladesh University of Engineering and Technology, Dhaka, Bangladesh for carrying out the research work. Technical cooperation regarding PLAXIS 2D software was provided by BUET-Japan Institute of Disaster Prevention and Urban Safety (BUET-JIDPUS).

REFERENCES
Bowles, J.E. 1996. *Foundation Analysis and Design*, McGraw-Hill, New York.
Chisty, K.U., 2014. Landslide in Chittagong City : A Perspective on Hill Cutting. Journal of *Bangladesh Institute of Planners*, 7(December), pp.1–17.
Egeli, I. & Pulat, H.F., 2011. Mechanism and modelling of shallow soil slope stability during high intensity and short duration rainfall. *Scientia Iranica*, 18(6), pp.1179–1187.
Galli, M. & Guzzetti, F., 2007. Landslide vulnerability criteria: A case study from Umbria, central Italy. *Environmental Management*, 40(4), pp.649–664.
Hammouri, N.A.; Malkawi, A.I.H. & Yamin, M.M.A. 2008. Stability analysis of slopes using the finite element method and limiting equilibrium approach. *Bulletin of Engineering Geology and the Environment*, 67(4), pp.471–478.
Islam, MS; Hussain, MA; Khan YA; Chowdhury, MAI and Haque MB. 2014. Slope Stability Problem in the Chittagong City, Bangladesh. *Journal of Geotechnical Engineering*, 2394-1987, 1, pp.13–25.
Islam, MA. 2018. *Measures for landslide prevention in Chittagong Hill Tracts of Bangladesh. M.Sc.* Thesis, Department of Civil Engineering, Bangladesh University of Engineering and Technology, Dhaka-1000, Bangladesh
Islam, MS and Islam MA. 2018. Reduction of Landslide Risk and Water-logging Using Vegetation. International Conference on Civil and Environmental Engineering, ICCEE, Kuala Lumpur, Malaysia.
Islam, MS; Hussain, MA; Khan YA; Chowdhury MAI and Haque MB. 2014. Slope Stability Problem in the Chittagong City, Bangladesh. Journal of Geotechnical Engineering, 1(3), pp. 13-25.
Kupka, M.; Herle, I. & Arnold, M. 2009. Advanced calculations of safety factors for slope stability. *International Journal of Geotechnical Engineering*, 3(4), pp.509–515.
Islam, MA; Islam, MS and Islam, T. 2017. Landslides in the Chittagong Hill Tracts and Possible Measures. International Conference on Disaster Risk Mitigation, ICDRM, Dhaka, Bangladesh.
Maula, BH. & Zhang, L. 2011. Assessment of embankment factor safety using two commercially available programs in slope stability analysis. *Procedia Engineering*, 14, pp.559–566.
Moriwaki, H.; Inokuchi, T.; Hattanji, T.; Sassa, K.; Ochiai, H. and Wang, G. 2004. Failure processes in a full-scale landslide experiment using a rainfall simulator. *Landslides*, 1(4), pp.277–288.
Rahman, MZ. 2012. *Slope stability analysis and road safety evaluation*. MS Thesis, Lulea University of Technology, Sweden.
Sarker, A. and Rashid, A. (2013). "Landslide and flashflood in Bangladesh," in R. Shaw, F. Mallik and A. Islam, (eds.). *Disaster Risk Reduction Approaches in Bangladesh*, Springer Japan, pp. 165-189.
Mia, MT.; Sultana, T. and Paul, A. 2015. Studies on the Causes, Impacts and Mitigation Strategies of Landslide in Chittagong city, Bangladesh. *Journal of Environmental Science & Natural Resources*, 8(2), pp.1–5.

4th International Conference on Advances in Civil Engineering 2018 (ICACE 2018)
19 –21 December 2018
CUET, Chittagong, Bangladesh
www.cuet.ac.bd

LIQUEFACTION POTENTIAL ASSESSMENT OF SELECTED ZONES AT RAJSHAHI DISTRICT IN BANGLADESH

A. Hossain*, M. Ashikuzzaman& S. Hasnaeen

Department of Civil Engineering, RajshahiUniversity of Engineering & Technology, Rajshahi-6204, Bangladesh,
E-mail:ahmedhossain090001@gmail.com

**Corresponding Author*

ABSTRACT
In recent years, earthquake has become the most catastrophic occurrence all over the world. Bangladesh is in highly risk of earthquake as it sits in juncture of several active tectonic plates named Indian plate, the Eurasian plate and the Burmese plate. The massive amounts of sand and sediment present in the soil that makes up much of Bangladesh presents another danger, in addition to hiding the potentially devastating mega thrust fault. In an earthquake, the shaking will cause the sandy ground to behave like a liquid in a process known as liquefaction. In this paper, liquefaction potential index (LPI) is evaluated by SPT data collected from different bore log of selected zones of Rajshahi district using Seed's method, Tokimatsu & Yoshimi (T-Y) method considering design magnitude of earthquake of 6.5 based on previous earthquake history and peak ground acceleration of 0.12g. Study area selected for this analysis are Bagha, Bagmara, Charghat, Paba, Godagari, Puthia, Tanore and Rajshahi City. This assessment may possibly be helpful to the designers, city planners, architects and developers to achieve knowledge about liquefaction susceptibility of Rajshahi District (RD).

Keywords: Liquefaction; SPT-N Value; Seed's Method; Tokimatsu & Yoshimi Method; Liquefaction Potential Index.

INTRODUCTION
Rajshahi district is located on the north western part of Bangladesh beside Padma River. Though Earthquake is not a common hazard in this area, its intensity, magnitude and number has been increased now days. The earthquake record suggests that since 1900 more than 100 moderate to large earthquakes occurred in Bangladesh, out of which more than 65 events occurred after 1960. This brings to light an increased frequency of earthquakes in the last 30 years. Earthquake based liquefaction is one of the newly added burning issue these days. Following table shows database of earthquake occurred near Rajshahi District during the last 100 years.

Table 1. Earthquake scenario near Rajshahi District

Earthquake Magnitude, Mw	Years Ago	Focus Depth (km)	Location
6.9	7	50	Mangan, Sikkim, India
6.1	37	17	Gantok, Sikkim, India
8.7	88	15	Lakhipur, Assam, India
7.2	100	15	Kishorganj, Dhaka, Bangladesh
6.8	95	15	Netrokona, Dhaka, Bangladesh

STUDY AREA

Study area selected for this study are: Bagha, Bagmara, Charghat, Paba, Godagari, Puthia, Tanore and Rajshahi City which are shown in fig. 1.

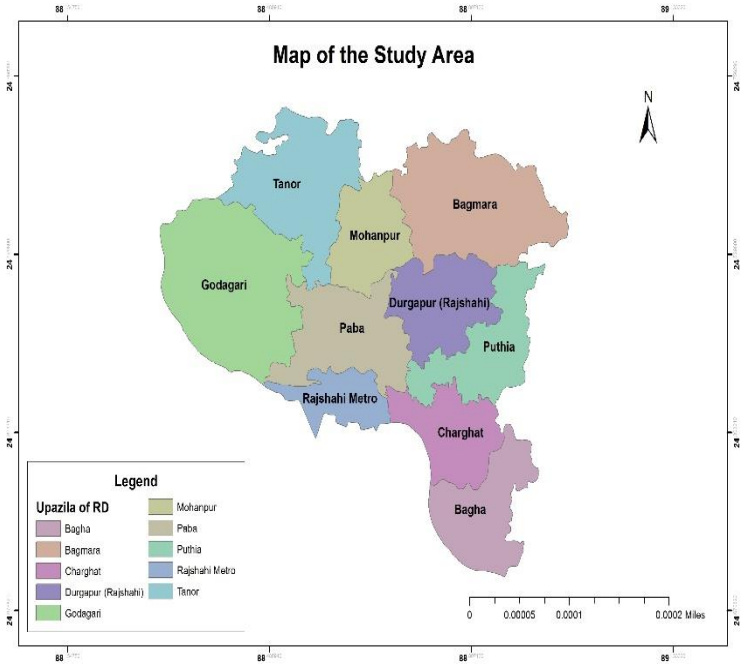

Fig. 1 Study Area

METHODOLOGY

According to Bangladesh National Building Code (BNBC, 2010 draft version), Bangladesh is divided into four seismic zones. Each zone has a seismic zone coefficient (Z) which represents the maximum considered peak ground acceleration (PGA). Among the four zones, Rajshahi District is located in zone-1 with zone coefficient of 0.12 which is used in this analysis. Magnitude of earthquake considered is 6.5 depending on the previous earthquake history of this area. In this study, Seed's Method and Tokimatsu & Yoshimi (T-Y) Method has been used for analysis of liquefaction which are shown with help of flow chart (Fig. 2 and Fig. 3). Both the methods involve determination of cyclic resistance ratio (CRR) and cyclic stress ratio (CSR). The ratio of CRR to CSR is defined as factor safety. Factor of safety value of greater than unity indicates the soil layer is non-liquefiable while factor of safety value less than unity indicates soil layer to be liquefiable.

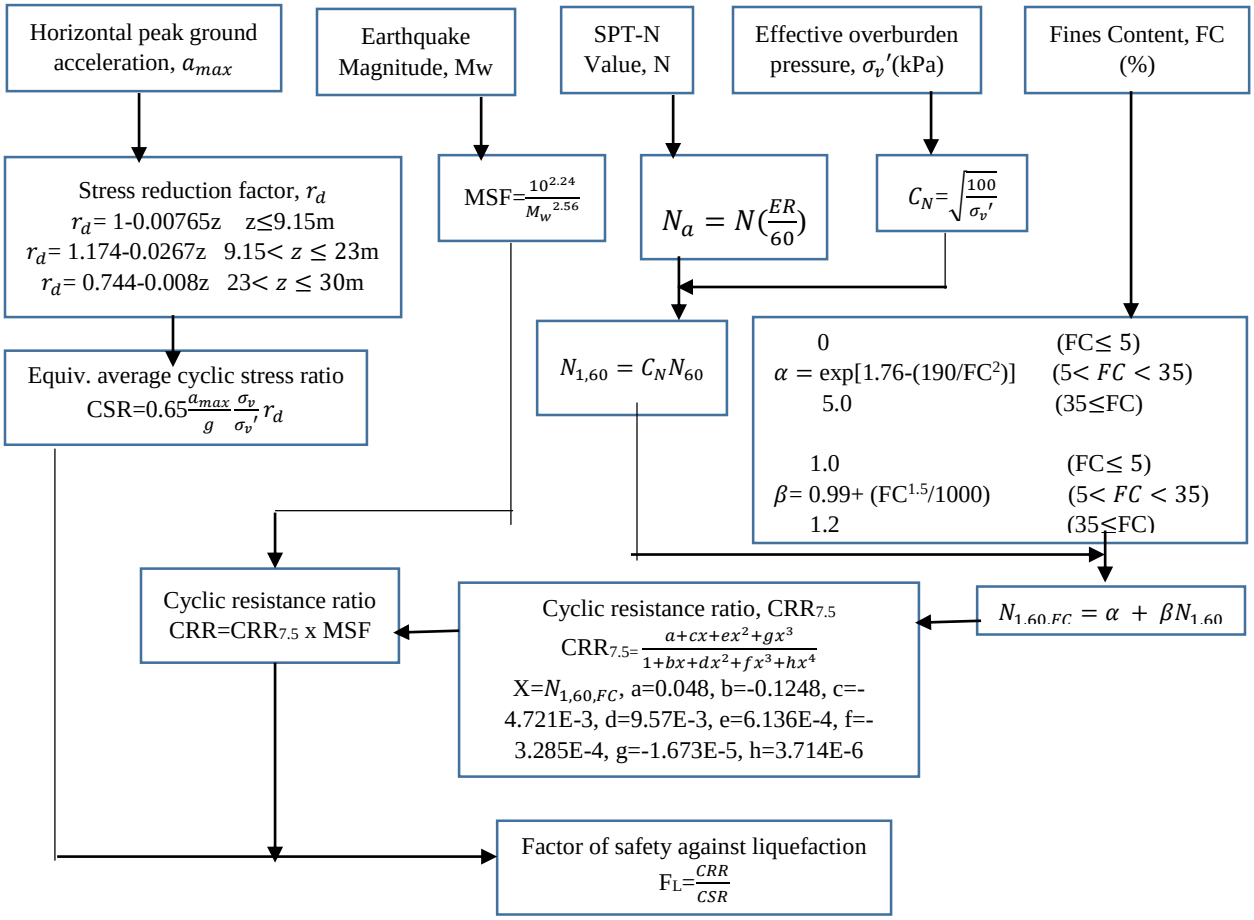

Fig. 2 Flowchart of Seed's method

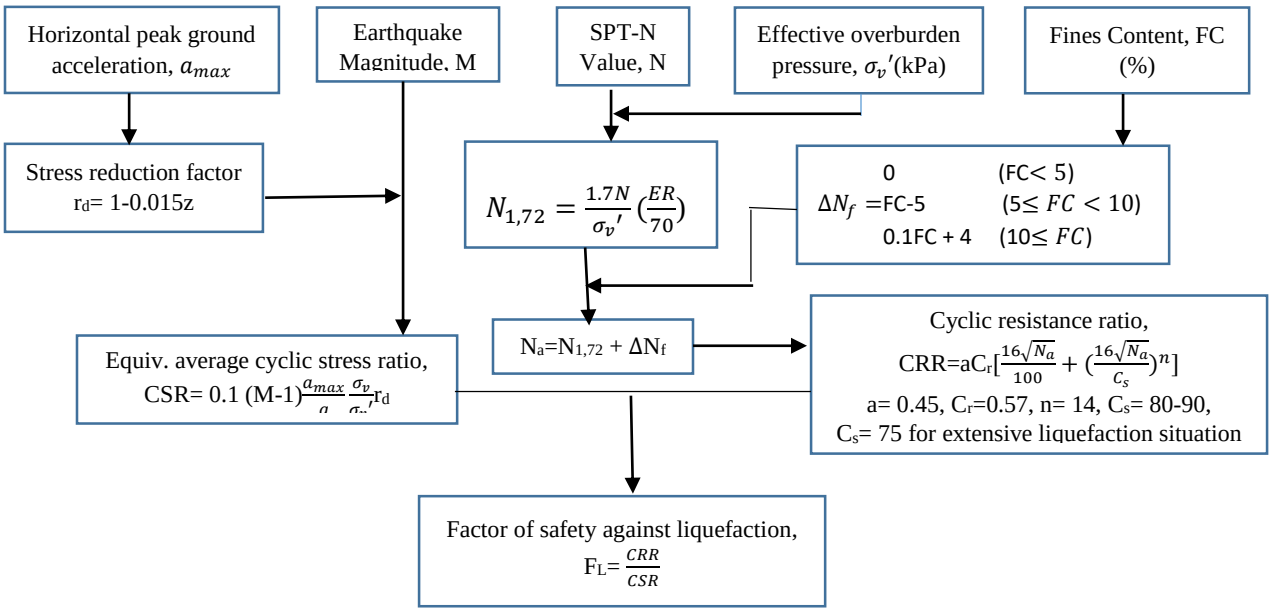

Fig. 3 Flowchart of T-Y method

Liquefaction potential index

Liquefaction potential index (LPI) is a single-valued parameter to evaluate regional liquefaction potential. For the soil profiles with the depth less than 20 m. LPI is calculated using the following expression (Luna and Frost, 1998):

$$LPI = \sum_{i=1}^{n} w_i F_i H_i \quad (1)$$

Here, $F_i = 0$ for $FS_i \geq 1.0$

Where H_i is thickness of the discretized soil layers; n is number of layers; F_i is liquefaction severity for i -th layer; FS_i is the factor of safety for i -th layer; w_i is the weighting factor (= 10–0.5 z_i); and z_i is the depth of i -th layer (m). LAZxevel of liquefaction severity depends mostly on the value of LPI which is illustrated in table 2.

Table 2. Level of liquefaction severity

LPI	Iwasaki et al. (1982)	Luna and Frost (1998)	Merm (2003)
LPI = 0	Very low	Little to none	None
0 < LPI < 5	Low	Minor	Low
5 < LPI < 15	High	Moderate	Medium
15 < LPI	Very high	Major	High

RESULTS AND DISCUSSION

Following table shows calculations for factor of safety along with liquefaction potential index and level of liquefaction severity according to Iwasaki et al., (1982) for BH 27.

Table 3. Calculation of Factor of safety and Liquefaction Potential Index (Seed's method)

Depth (ft)	Depth (m)	Unit weight, kN/m3	rd	CSR	N1,60, FC	Mw	MSF	CRR	FS	LPI	Total LPI	Comment (Iwasaki et al.,1982)
3	0.91	13.03	0.993	0.07	6	6.5	1.441	0.10	1.34	0		
6	1.82	14.18	0.986	0.07	8	6.5	1.441	0.12	1.66	0		
10	3.04	14.91	0.976	0.07	9	6.5	1.441	0.14	1.86	0		
15	4.57	15.44	0.965	0.09	11	6.5	1.441	0.17	1.77	0	0	Very Low
20	6.09	16.39	0.953	0.11	17	6.5	1.441	0.26	2.39	0		
30	9.14	16.68	0.930	0.12	16	6.5	1.441	0.24	1.99	0		
40	12.19	17.49	0.848	0.12	21	6.5	1.441	0.32	2.69	0		

Similarly, table 4 shows calculations for factor of safety along with liquefaction potential index and level of liquefaction severity according to Iwasaki et al., 1982 for BH 25.

T

able 4. Calculation of Factor of safety and Liquefaction Potential Index (T-Y method)

Depth (ft)	Depth (m)	Unit weight, kN/m3	rd	CSR	Mw	Round Na	CRR	FS	LPI	Total LPI	Comment (Iwasaki et al.,1982)
3	0.91	11.96	0.986	0.06	6.5	2	0.05	0.89	0.96		
6	1.82	11.96	0.972	0.06	6.5	2	0.05	0.90	0.81		
10	3.04	15.19	0.954	0.06	6.5	11	0.13	2.19	0		
15	4.57	16.23	0.931	0.07	6.5	17	0.21	2.65	0	1.78	Low
20	6.09	16.39	0.908	0.08	6.5	17	0.21	2.36	0		
30	9.14	17.18	0.862	0.09	6.5	21	0.37	3.82	0		
40	12.19	17.85	0.817	0.09	6.5	25	0.83	8.46	0		

Overall analysis results considering the flowchart of the figs. 2 and 3 and eqn. no. 1 are shown in table 5.

Table 5. Representation of LPI for different boreholes and methods

Location	Borehole No.	Liquefaction Potential Index for Mw = 6.5 and a_{max}=0.12g			
		Seed' Method		Tokimatsu &Yoshimi Method	
		LPI	Liquefaction Severity	LPI	Liquefaction Severity
Bagha	BH 1	0	Very Low	0	Very Low
	BH 2	0	Very Low	0	Very Low
	BH 3	0	Very Low	0	Very Low
	BH 4	0	Very Low	0	Very Low
Bagmara	BH 5	0	Very Low	0	Very Low
	BH 6	0	Very Low	0	Very Low
	BH 7	0	Very Low	0	Very Low
	BH 8	0	Very Low	0	Very Low
Charghat	BH 9	0	Very Low	0	Very Low
	BH 10	0	Very Low	0	Very Low
	BH 11	0	Very Low	0	Very Low
	BH 12	0	Very Low	0	Very Low
Godagari	BH 13	0	Very Low	0	Very Low
	BH 14	0	Very Low	0	Very Low
	BH 15	0	Very Low	0	Very Low
	BH 16	0	Very Low	0	Very Low
Paba	BH 17	0	Very Low	0	Very Low
	BH 18	0	Very Low	0	Very Low
	BH 19	0	Very Low	0	Very Low
	BH 20	0	Very Low	0	Very Low
Puthia	BH 21	0	Very Low	0	Very Low
	BH 22	0	Very Low	0	Very Low
	BH 23	0	Very Low	0	Very Low
	BH 24	0	Very Low	0	Very Low
Rajshahi City	BH 25	0.213	Low	1.784	Low
	BH 26	0	Very Low	0.969	Low
	BH 27	0	Very Low	0	Very Low
	BH 28	0	Very Low	0.969	Low
Tanore	BH 29	0	Very Low	0	Very Low
	BH 30	0	Very Low	0	Very Low
	BH 31	0	Very Low	0	Very Low
	BH 32	0	Very Low	0	Very Low

CONCLUSIONS

In this study, factor of safety along with liquefaction potential index determined using Seeds method and T-Y method. Level of liquefaction severity according to different LPI value has been studied here and borehole are classified as “Very low”, “low”, “high”, “very high” category. Also comparative study has been done in tabular format to show the variation of obtained results according to the methods used in this study. Analysis results are consistent for all the collected borehole database except for BH 26 and BH 28.

ACKNOWLEDGEMENTS

The authors would like to give thanks **Md. Shakil Ar Salan**, Department of Urban & Regional Planning, Rajshahi University of Engineering & Technology (RUET) for his great support for the completion of the paper.

REFERENCES

Bangladesh National Building Code (BNBC), 2010. Housing and Building Research Institute and Bangladesh Standards and Testing Institution, Dhaka, Bangladesh.

Chang, M; Kuo, CP; Shau, SH and Hsu, RE. 2011. Comparison of SPT-N based analysis methods in evaluation of liquefaction potential during the 1999 Chi-Chi earthquake in Taiwan. Com. Geotech., 38:393-406.

Iwasaki, T; Tokida, K; Tatsuoka, F; Wantanable, S; Yasuda, S and Sato, H. 1982. Microzonation for soil liquefaction potential using simplified methods. Proc of 3rd International Earthquake Microzonation Conference, Seattle, pp. 1319-1330.

Luna, R and Frost, J. D. 1998. Spatial Liquefaction Analysis System. Journal of computing in Civil Engineering, 12:1(48).

4th International Conference on Advances in Civil Engineering 2018 (ICACE 2018)
19 –21 December 2018
CUET, Chittagong, Bangladesh
www.cuet.ac.bd

NUMERICAL INVESTIGATION OF PULLOUT CAPACITY OF HORIZONTALLY LOADED VERTICAL ANCHOR PLATE EMBEDDED IN COHESIONLESS SOIL

S. Sakib*& M. S. Islam

Department of Civil Engineering, Bangladesh University of Engineering and Technology, Dhaka, Bangladesh.
E-mail: shadmansakib.1353@gmail.com

**Corresponding Author*

ABSTRACT
Horizontally loaded vertical anchors play a significant role in the stabilization of geotechnical structures. Owing to the variation in different soil parameters, achieving accuracy in design has become more intricate. Through the past few decades researches have been carried out to determine the pullout capacity of anchor plates, which has led to the development of many analytical relations. Subsequently, this paper focuses on the numerical investigation of horizontally loaded vertical anchor plate with embedment depth, H to anchor height ratio, $B \leq 7$ in cohesionless soil. The credibility of the numerical model has been verified by replicating load-displacement curves and failure mechanisms from existing experimental database. Compared to the previous data, the finite element analysis showed a 10-20% decrease of capacity in case of surface anchors ($H/B = 1$) and also an increase in pullout capacity (up to 40%) as the depth of embedment of anchor plate increases. The failure mechanisms, as anticipated by the earth pressure theories, were also observed in the analysis. At lower embedment ratios, shear failure of the soil passive region and subsequent ground heaving similar to isolated footings were observed. The failure becomes local as the embedment increases and plate dimension decreases.

Keywords: Vertical anchor plate; embedment depth ratio; pullout capacity; finite element

INTRODUCTION

For the civil engineering structures that requires foundation systems to withstand the horizontal pullout forces, an efficient and economic design solution can be obtained through the use of earth anchors. These earth anchors are typically attached with the retaining structures and embedded in the soil to sufficient depth so that they resist pullout forces with safety. The ultimate pullout capacity of an earth anchor such as vertical anchor plate depends on several factors. The pullout capacity of an anchor is primarily derived from the passive force imposed by the soil in front of the anchor plate. If the embedment depth (H) to anchor height (B) ratio or embedment depth ratio (H/B) (Fig. 1) of the anchor plate is relatively small, at ultimate pullout load the passive failure surface developed in soil in front of the anchor will intersect the ground surface. This is referred to as shallow anchor condition. At greater embedment depth ratios, local shear failure in soil will take place at ultimate load, and these anchors are called deep anchors (Das, 1990). Other important governing factors are anchor length (L) to height (B) ratio or aspect ratio, (L/B), shear strength parameters of the soil (soil friction angle, φ and cohesion, c) and angle of friction at the anchor-soil interface, δ. Literature reveals that many researches have been conducted on the capacity of vertical anchors especially for anchor plate including that by Hueckel (1957), Ovesen and Stromann (1972), Neely et al. (1973), Das (1975), Akinmusuru (1978) and, Ghaly (1997) etc. Again, Bowles (1997), Naser (2006), Jadid et al. (2018) and Shahriar (2018) were found to be strictly applicable to block anchors.

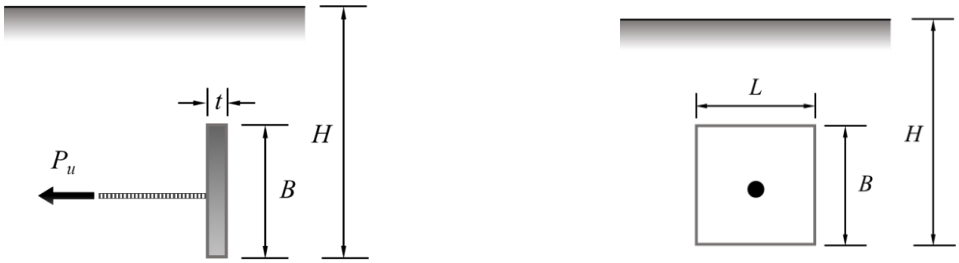

(a) (b)

Fig. 1: Definition of terms related to vertical anchor plates; (a) side view, (b) front view [*B* - height, *L* - length, *t* - thickness of the anchor, *H* - depth of embedment, P_u - pullout load]

Majority of past researches has been experimentally based and, as a result, current design practices are largely based on empiricism. Since the cost of performing laboratory tests on each and every field problem combination is prohibitive, it is necessary to be able to model soil pullout resistance numerically for the purposes of design. The most complete numerical study first appears to be that by Rowe and Davis (1982). They described a theoretical assessment of anchor plates in sand which considered the effect of anchor plate embedment, friction angle, dilatancy, and initial stress state and anchor plate roughness for vertical anchor plates. The sand was assumed to have a Mohr-Coulomb failure criterion. Tagaya et al. (1983, 1988) conducted two dimensional plane strain and axisymmetric finite element analyses by the constitutive law of Lade and Duncan (1975). Scale effects for circular anchor plates in dense sand were investigated by Sakai and Tanaka (1998) by a constitutive model for a non-associated strain hardening-softening elasto-plastic material. Koutsabeloulis and Griffiths (1989) investigated the trap door problem by the initial stress finite element method. Both plane strain and axisymmetric works were conducted. Upper and lower bound limit analysis techniques have been used by Murray and Geddes (1987, 1989) and Basudhar and Singh (1994) to estimate the capacity of vertical strip anchor plates. Merifield et al. (2006) presented the results of a rigorous numerical work to estimate the ultimate capacity load for vertical anchor plate in cohesionless material. Rigorous bounds have been obtained using two numerical procedures that are based on finite element method of the upper and lower bound of limit analysis. For comparison purposes, numerical and theoretical results of the break-out factor have also been obtained by the more conventional displacement finite element method. In the current research a numerical model of horizontally loaded vertical plate anchor was prepared to observe the effect of different governing factors on the pullout load. Such a model can be employed for testing and designing vertical anchors. As vertical anchors can reduce the moments induced in a retaining structure, their economic design and use can ensure the stability of wide range of structures.

METHODOLOGY

The current numerical analysis was conducted with PLAXIS 3D, a finite element program for geotechnical applications. To ensure the credibility of the finite element analysis, at first the experimental results obtained from Choudhary and Dash (2016) were replicated. For further analysis a 20 m × 20 m × 10 m cohesionless soil bed was modelled (Fig. 2). The cohesionless soil was assumed to have a Mohr-Coulomb failure criterion and modelled with 10 node wedge element. This type of element provides a second order interpretation of displacements. The dimensions of the model have been carefully chosen in a way that the stress and displacement gradients would decrease and become zero near the boundaries. A square anchor plate with dimensions 500 mm × 500 mm and thickness 50 mm was modelled using 6 node plate element. The plate elements have only 5 degrees of freedom per node in the rotated coordinate system. These elements are directly integrated over their cross section and numerically integrated using 3 - point Gaussian integration. Material properties given in Table 1 were assigned to the different elements and the whole model was meshed. Merifield and Sloan (2006) suggested using greater concentration of elements in areas with high stress gradient. For soil - anchor system such regions exist surrounding the anchor edges. Thus, for efficient modeling, both highly concentrated elements and small elements were ensured near the anchor.

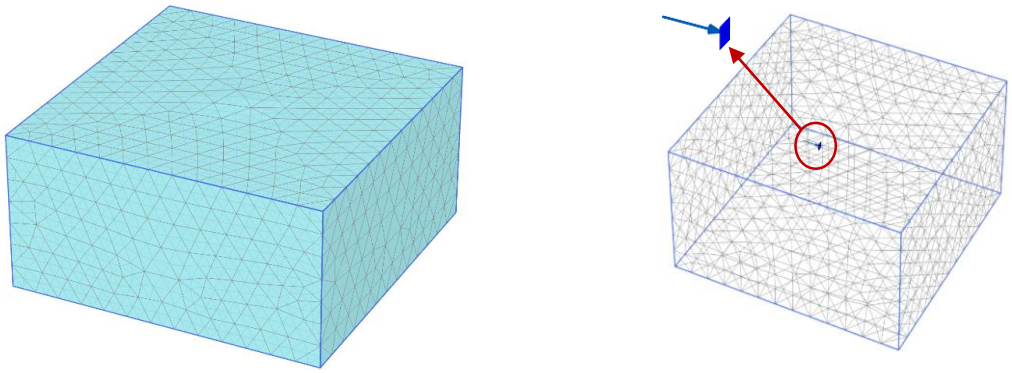

(a) (b)

Fig. 2: Finite element model; (a) soil bed after meshing, (b) applied point load and distribution of elements around anchor plate (inside the circle)

Table 1 Geometric and mechanical properties used for finite element modelling

Anchor Plate	
Length (*L*)	500 mm
Height (*B*)	500 mm
Thickness (*t*)	50 mm
Poisson's ratio	0. 3
Unit weight	78.5 kN/m^3

Cohesionless Soil	
Maximum dry density	17.0 kN/m^3
Minimum dry density	14.0 kN/m^3
Relative Density (RD)	30%, 50%, 75%
Poisson's ratio	0.3
Interface reduction factor (R_{inter})	0.5

A horizontal point load was applied at the centre of passive side of the anchor plate to simulate the pullout load from the earth retaining structure. The finite element analysis was carried out in three stages. In the initial stage the whole soil mass was activated. Then the construction of the plate anchor was modelled by activating it. And finally the point load was applied at the centroid of the plate anchor. The pullout load vs. horizontal displacement of anchor plate was obtained for every case and the passive failure surface was also observed. The pullout load was determined using the method described by Neely et al. (1973).

RESULTS AND DISCUSSIONS

Failure mechanism of anchor plate

Observation of the numerical model shows that with the increment of embedment depth, mode of failure of the anchor plate changes. The failure mechanisms of anchor plate for different embedment depths and relative densities of backfill soil are shown in the Fig. 3. A section of the soil bed through the centre line of the anchor plate was observed. For small embedment depths (*H/B* = 3 and 5), the soil in front the anchor plate moves forward and upwards (Fig. 4). The failure surface propagates to the surface and bulging of the surface soil is observed. In this case general shear failure occurs which is similar to failure of an isolated footing at shallow depth. As the anchor plate is displaced the soil behind the plate collapses to fill the void. The different colored surfaces indicate the movement of the soil mass around the anchor. The movement of soil mass closest to the anchor is the highest and it reduces as the distance from the anchor increases. For deeper anchors (*H/B* = 7), the observed failure pattern is a bit different. Here the movement of the soil mass in contact with the anchor plate is large and it propagates upward. Unlike the shallow anchors the failure surface does not reach the ground surface. Rather local failure occurs, which is similar to the failure of deep isolated footing. In such cases heaving of the ground surface may not be observed at all.

Effect of embedment depth ratio

If the anchor plate was placed just below the ground surface (*H/B* = 1), the pullout capacity was found to be insufficient. So the practice is to place the anchor plate at a certain depth below the ground surface. To demonstrate the effect of embedment depth ratio (*H/B*) on the anchor plate, it was placed at different

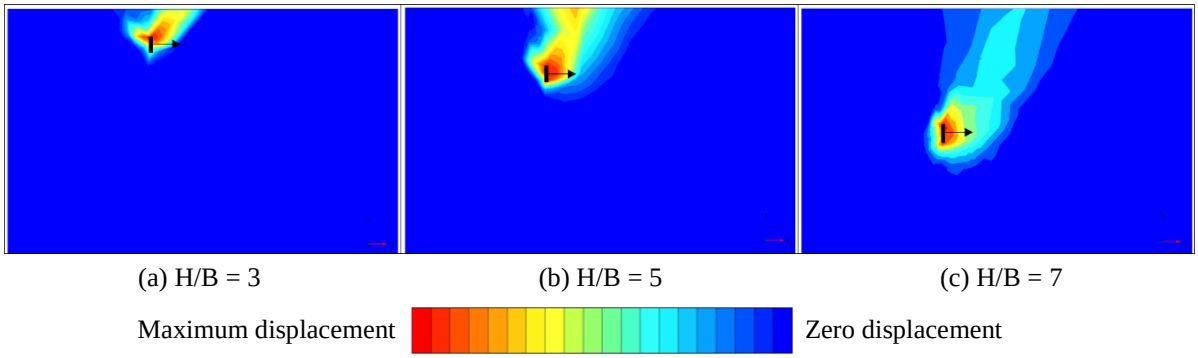

Fig. 3: Displacement of cohesionless soil in front of anchor plate (black rectangle) as predicted by PLAXIS 3D for different embedment depth ratio (H/B) [arrows indicate the direction of pullout load]

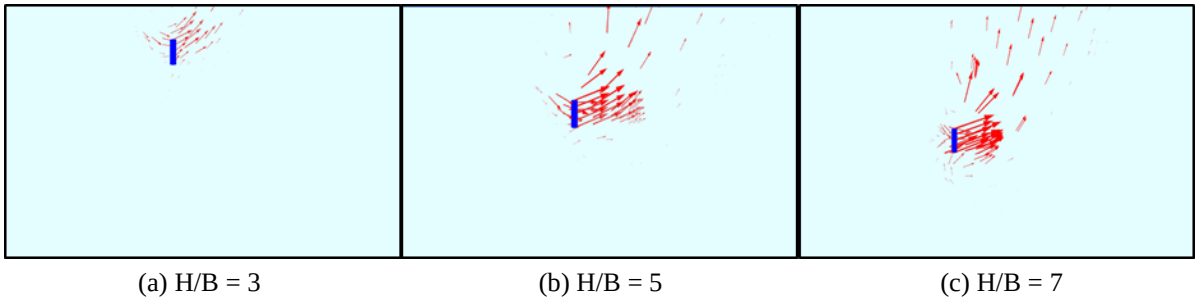

Fig. 4: Velocity plot for soil movement (red arrows) in front of plate anchor (blue rectangles)

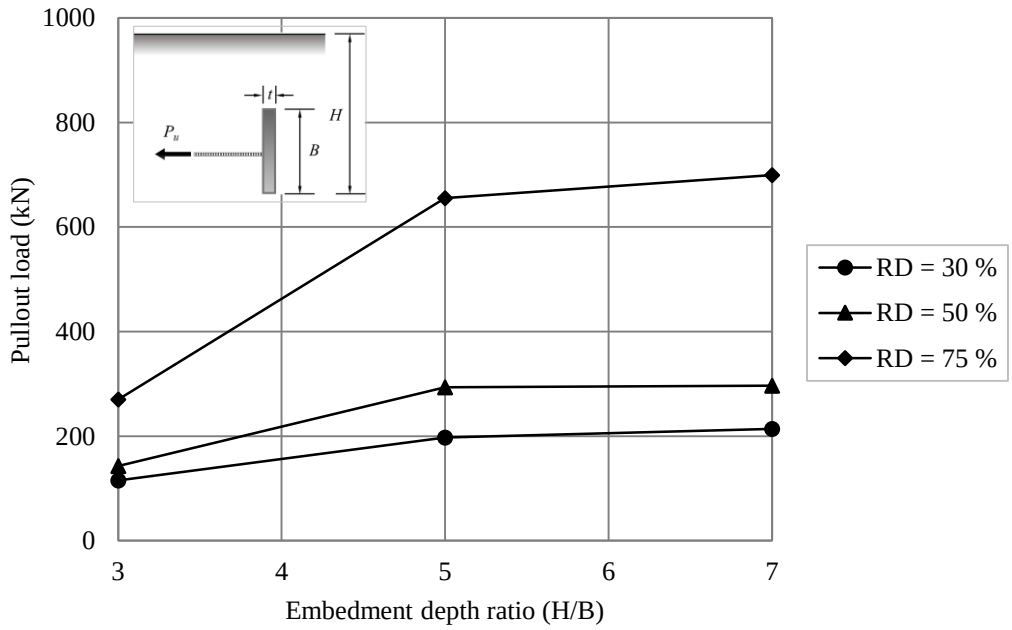

Fig. 5: Increase of pullout capacity with the increase of embedment depth ratio

depths (*H/B* = 3, 5, 7) and the corresponding pullout loads were observed. Fig. 5 shows the results obtained from the numerical investigation. As the volume of the soil above the anchor plate increases, the increase of the pullout capacity is expected. In the figure it can be seen that, with the increase of the embedment depth ratio for H/B = 3 to 5, the pullout capacity of the anchor plate increases slightly for lower relative densities and significantly for higher relative densities. The previous analytical approaches also show the increase of pullout capacity with increasing embedment depth (Fig. 6) but their predictions were noticeably lower than the value obtained from the numerical analysis.

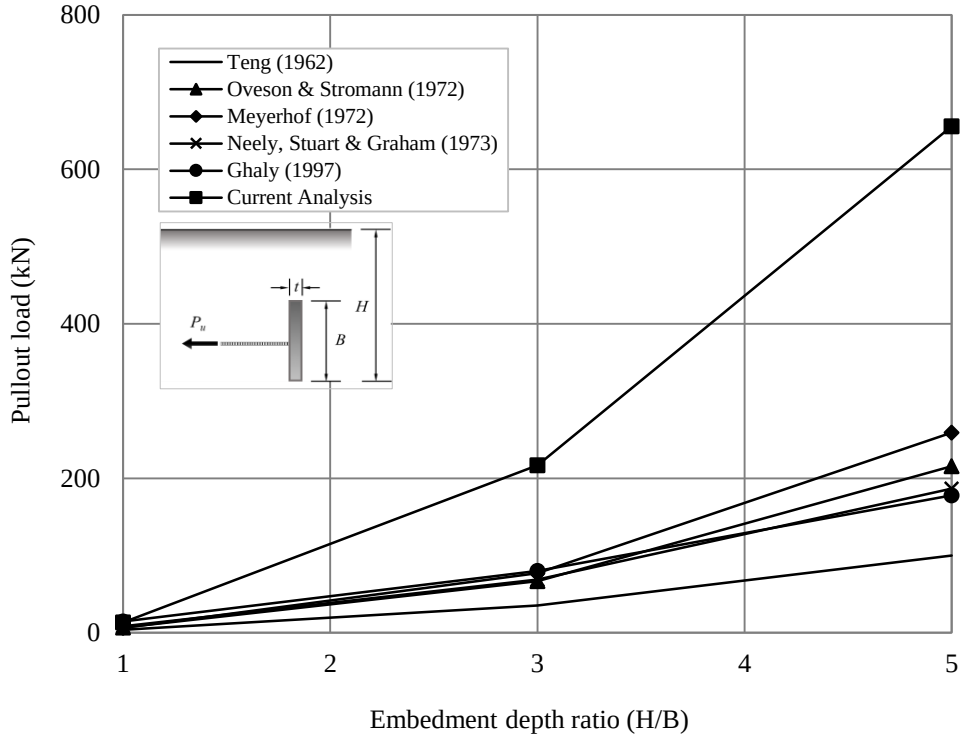

Fig. 6: Comparison of numerical model with previous analytical models

For H/B = 5 to H/B = 7 it was observed that there was no significant increase of the pullout capacity of plate anchors. But the failure mechanism of the anchor at greater depth is different from the anchor at shallower depth, as was discussed in the previous section. Compared to the previous data, the finite element analysis showed a 10-20% decrease of capacity in case of surface anchors (H/B = 1) and also an increase in pullout capacity (up to 40%) as the depth of embedment increases. During the derivation of the analytical models a failure surface was assumed and then the analysis was carried out. All the governing parameters were not given equal importance. In the numerical investigations all the parameters were taken into consideration at a time. This is likely to be the reason for the discrepancies observed in Fig. 6. Although with the increase of embedment depth the pullout capacity increases, in some cases it may not be economical to excavate deep, place the anchor plate and backfill the soil. In that case other anchoring mechanisms can be used or the spacing between the anchors may be reduced.

CONCLUSIONS

In the study research pullout behavior of horizontally loaded vertical plate anchor was investigated numerically. The data obtained from the analysis bear much resemblance with the previous experimental, theoretical and numerical models. The discrepancies found can be attributed to omission of a few factors by the previous researchers and assumed failure mechanisms. At lower embedment depth ratio ($H/B \leq 5$) general shear failure was observed and failure surface reached ground surface. For higher embedment depth ratio ($H/B > 5$) local shear failure was observed and failure surface did not reach the ground surface. This failure mechanism was in agreement with the experimental model. The pullout capacity increased with the increase of relative density of the soil mass surrounding the anchor. Also at higher relative density the collapse of the soil mass behind the anchor plate, triggered by the anchor movement was reduced. The findings of this study can be utilized for efficient and economic design of earth retaining structures.

ACKNOWLEDGMENTS

The authors acknowledge the infrastructural and financial support received from Department of Civil Engineering of Bangladesh University of Engineering and Technology (BUET), Dhaka, Bangladesh for carrying out the research work. Authors are also thankful to the BUET - Japan Institute of Disaster

Prevention and Urban Safety (BUET-JIDPUS) for providing access to their Computational and Simulation Laboratory and use PLAXIS 3D for this research.

REFERENCES

Akinmusuru, JO. 1978. Horizontally loaded vertical plate anchors in sand. *Journal of the Geotechnical Engineering Division,* ASCE, 104(2): 283-286.

Basudhar, PK. and Singh, DN. 1994. A generalized procedure for predicting optimal lower bound break-out factors of strip anchors. *Géotechnique*, 44(2): 307-318.

Bowles, JE. 1997. *Foundation Analysis and Design.* Singapore: The McGraw-Hill Companies, Inc. pp. 778-780.

Choudhary, AK and Dash, SK. 2016. Load-carrying mechanism of vertical plate anchors in sand. *Int. J. Geomech.,* 10.1061/(ASCE) GM. 1943-5622.0000813, 04016116.

Choudhary, AK and Dash, SK. 2014. Pullout behaviour of vertical plate anchor embedded in sand. Proceedings, *Indian Geotechnical Conference IGC-2014,* pp. 1506-1509

Das, BM. 1990. *Earth Anchors*. Amsterdam, Netherlands: Elsevier.

Das, BM. and Seeley, GR. 1975. Load-displacement relationships for vertical anchor plates. *Journal of the Geotechnical Engineering Division*, ASCE, 101(GT7): 711-715.

Dickin, EA. and King, JW. 1997. Numerical modeling of the load-displacement behavior of anchor walls. *Computers and Structures,* 63(4): 849-858.

Ghaly, AM. 1997. Load-displacement prediction for horizontally loaded vertical plates. *J. Geotech. Geoenviron. Engrg*., 10.1061/(ASCE)1090-0241(1997)123:1(74): 74-76.

Hanna, A; Rahman, F and Ayadat, T. 2011. Passive earth pressure on embedded vertical plate anchors in sand. *Acta Geotechnica,* 6: 21-29.

Hansen, JB. 1966. Resistance of rectangular anchor slab. *Danish Geotechnical Institute,* 21: 12-13.

Koutsabeloulis, NC and Griffiths, DV. 1989. Numerical modelling of the trap door problem. *Géotechnique*, 39(1): 77-89.

Jadid, R; Abedin, MZ, Shahriar, AR. and Arif, MZU. 2018. Analytical model for pullout capacity of a vertical concrete anchor block embedded at shallow depth in cohesionless soil. *International Journal of Geomechanics, ASCE,* 10.1061/(ASCE) GM.1943-5622.0001212.

Merifield, RS and Sloan, SW. 2006. The ultimate pullout capacity of anchors in frictional soils. *Can. Geotech. J.,* 43: 852-868.

Murray, EJ and Geddes, JD. 1987. Uplift of anchor plates in sand. *Journal of Geotechnical Engineering*, ASCE, 113(3): 202-215.

Murray, EJ and Geddes, JD. 1989. Resistance of passive inclined anchors in cohesionless medium. *Géotechnique*, 39(3): 417-431.

Naser, AS. 2006. Pullout capacity of block anchor in unsaturated sand. Unsaturated Soils 2006 (GSP 147), Proceedings, *Fourth International Conference on Unsaturated Soils, ASCE.* (pp. 403-414). Arizona.

NAVFAC DM 7.02 1986. *Foundations and earth structures*, Naval Facilities Engineering Command, Alexandria.

Neely, WJ; Stuart, JG and Graham, J. 1973. Failure loads of vertical anchor plates in sand. *Journal of the Geotechnical Engineering Division*, ASCE, 99(9): 669-685.

Ovesen, NK. 1964. Anchor slabs, calculation methods, and model tests. *Danish Geotechnical Institute*, Copenhagen, 16: 5-39.

Ovesen, NK and Stromann, H. 1972. Design methods of vertical anchor slabs in sand. Proceedings, *Specialty Conference on Performance of Earth and Earth-Supported Structures*, ASCE. 2.1: 1481-1500.

Rowe, RK and Davis, H. 1982. The behaviour of anchor plates in sand. *Géotechnique*, 32(1): 25-41.

Shahriar, AR. 2018. *Development of an analytical model for the analysis of pullout capacity of anchors embedded in frictional soils. MSc* Thesis, Department of Civil Engineering, Bangladesh University of Engineering and Technology, Bangladesh

Tagaya, K; Tanaka, A and Aboshi, H. 1983. Application of finite element method to pullout resistance of buried anchor. *Soils and Foundations*, 23(3): 91-104.

Tagaya, K; Scott, RF and Aboshi, H. 1988. Pullout resistance of buried anchor in sand, *Soils and Foundations*, 28(3): 114-130

4th International Conference on Advances in Civil Engineering 2018 (ICACE 2018)
19 –21 December 2018
CUET, Chittagong, Bangladesh
www.cuet.ac.bd

EXPERIMENTAL STUDIES ON THE CHARACTERISTIC BEHAVIOUR OF DISPERSIVE SOIL AND STABILIZATION WITH FLY ASH

M. Ashraf *& M.S. Islam

Department of Civil Engineering, Bangladesh University of Engineering and Technology, Dhaka, Bangladesh.

Email: marziashorno@gmail.com

**Corresponding Author*

ABSTRACT:
Dispersive soil is exceptional clayey soil which exhibits highly erosive behavior in presence of water. Soil dispersion is mainly due to the presence of exchangeable Sodium present in the structure. The attractive forces between the molecules are less than the repulsive forces under saturated conditions. Once a dispersive soil is exposed to water, clay particles detach away from each other and remain as suspended particles in water. This research presents experimental studies and tests for identifying the degree of dispersion and approaches for minimizing this dispersive phenomena. Dispersive soil was collected from Bhanga Upazilla at Faridpur, Bangladesh. Crumb Test, Double Hydrometer Test, Pinhole Test were performed in order to identify dispersive behaviour. Collected soil was found as moderate or highly dispersive. Then the focus was to find out the influence of fly ash (3%, 6% and 9% by weight) for the stabilization of dispersive soil. It was observed that reduction of dispersion of the soil due to addition of fly ash was remarkable. Along with diminishing dispersive phenomena, fly ash also increased the overall strength of the sample in unconfined compressive strength (UCS) tests. Especially use of 9% of fly ash both in reduction of dispersion and increasing of strength gave best results. The improvement of the soil property is due to increased cementatious bond and flocculation among the soil particles.

Keywords: Dispersive soil; Fly Ash; Pinhole Test; Crumb Test; Double Hydrometer Test .

INTRODUCTION:

Dispersion is the property of soil by virtue of which soil break down into their component particles when wet. Once a dispersive soil is exposed to water, clay particles may disperse and remain as suspended particles in water. In appearance, dispersive clays are like normal clays that are stable and somewhat resistant to erosion, but in reality they can be highly erosive and subject to severe damage or failure. The common soil classification index tests do not distinguish between dispersive and non dispersive clay soils. The recommended tests for the identification of dispersive clay soils are Pinhole test, Crumb test and Double Hydrometer test and Chemical test (Pore water extraction test).
Recently, in our country embankment has been collapsed due to presence of dispersive soil in Faridpur Bhanga Upazilla. Recent researches have reveal that much of erosion is associated with presence of sodic soil. For stabilization of dispersive soil is the use of chemical additives have been used from the past few decades. The most common treatments applied are fly ash, lime, cement etc. In our country fly ash is recognized one of the common residues produced from combustion of coal. In past, fly ash was unconditionally released into the atmosphere. Again if fly ash can be used as soil stabilizer, no extra cost will required for producing soil stabilizer. For all those reasons, utilization of

fly ash is anticipated to be very advantageous in stabilization of dispersive soil, both economically and environmentally.

METHODOLOGY:

First, Index properties (ASTM D4318) and specific Gravity (ASTM D854) of the soil samples collected from Faridpur, bhanga Upazilla was determined. Standard proctor test (ASTM D1557) was performed for both untreated sample and treated sample with varying percentage of (3%, 6% and 9%) fly ash. To determine the degree of dispersion, physical tests such as Pinhole test (ASTM D 4647-93), Crumb test (ASTM D6572), Double Hydrometer test (ASTM D 4221-99) were also performed. The same tests were performed for sample mixed with 3%, 6%, and 9% fly ash in order to check that whether the characteristic behavior would have been improved. The unconfined compression (ASTM D2166) test was conducted on both cured (7, 14 and 21 days) and uncured soil.

RESULTS & DISCUSSIONS:

A summary of index properties, the optimum moisture content and the maximum dry density of the used clay materials is given in Table 1.

Table 1: Properties of dispersive clay sample

Parameters	Value
Optimum Moisture Content (%)	19.88
Maximum Dry Density (kN/m^3)	15.5
Liquid Limit, w_L (%)	43
Plastic Limit, w_p (%)	26
Shrinkage limit, w_s (%)	18
Specific Gravity	2.73

According to the standards, a series of laboratory tests including compaction, unconfined compressive strength, and Pinhole Test, Crumb Test, Double Hydrometer Test were conducted on both treated and untreated soil to evaluate the potential of a stabilizer to reduce the dispersion. The Standard Test procedure followed in determining the properties of the soil is given in Table 2. The tests for identifying depersive soil like Crumb, Double Hydrometer test and pinhole test is described briefly. The same tests were performed for sample mixed with 3%, 6%, and 9% fly ash for stabilization.

Table 2: laboratory test performed on dispersive soil with different Fly ash content

Type of Test	Sample	No of Test	Test Method
Standard Compaction Test	Untreated soil	1	ASTM D698
	soil- fly ash mixture	3	
Pinhole Test	Untreated soil	2	ASTM D 4647- 93
	soil- fly ash mixture	3	
Double Hydrometer Test	Untreated soil	1	ASTM D422
	soil- fly ash mixture	3	
Crumb Test	Untreated soil	2	ASTM D6572
	soil- fly ash mixture	3	
	soil- fly ash mixture	3	
Unconfined Compression Test	Untreated soil	4	ASTM D2166
	soil- fly ash mixture	12	

Crumb Test: This test consists of preparing a cubical specimen of about 15 mm size at natural moisture content and placing in 250 ml of distilled water. With the passage of time the tendency of colloidal size particles to deflocculates and going into the suspension was observed. Results are interpreted after 1 hour and there are four grades of possible reaction: non dispersive, slightly dispersive, moderately dispersive and high dispersive soil according to ASTM D6572. From this test

results, the selected soil sample instantly crumbled, slaked and formed colloidal suspension highly turbid water had been seen at 1 hour observation (Grade 4).

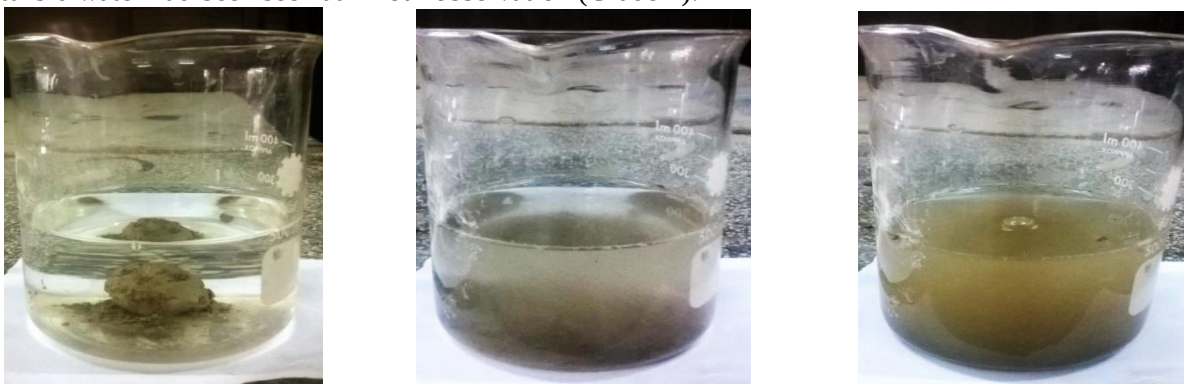

(a) (b) (c)

Fig.1:Observation from crumb test: (a) Observation at instant. (b) At 15 minutes. (c) At 1hour

Pinhole Test: Pinhole test measures dispersion by causing water flow through a 1mm hole punched in soil specimen. This method relates the turbidity of suspended clay colloid, flow rates and final diameter after water flow as indicators of the clay dispersion. In our tests we have followed ASTM D4647 Method A in order to classify soil sample. (D-1, D-2, ND-4,ND-3, ND-2 and ND-1).
From the test, it was observed that water collected from sample has moderate turbidity. It also showed increase in the pinhole diameter about 4 times of initial diameter. at 180 mm head. According to ASTM D 4647- 93 this soil sample corresponds to ND4 which signifies that this soil is moderately dispersive.

Fig.2: Observation from Pinhole Test

Double Hydrometer Test: In this method basically two hydrometer tests are performed: 1. Standard Hydrometer test, 2. Hydrometer test performed with no mechanical agitation nor chemical dispersing agent. Dispersion result is expressed as the ratio given below.

$$\text{Dispersion} = \frac{\%\ \text{clay}\ (0.005)\ \text{without dispersing agent}}{\%\ \text{clay}\ (0.005)\ \text{with dispersing agent}} \times 100$$

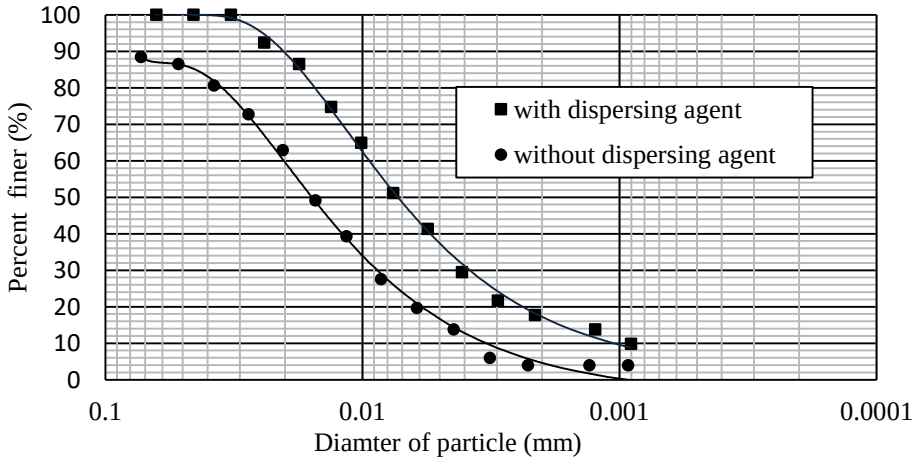

Fig. 3: Double Hydrometer Test for Soil + 0% fly ash

From the gradation curves it is shown that percentage of clay without dispersing agent is 16 and with dispersing agent it has been found 36. The results indicate that soil has percent dispersion 16/36=44.44. According to ASTM D422 this result falls in the range between 30% to 50% which indicates the soil is moderately dispersive.

Stabilization with Fly Ash:

Crumb Test with Fly ash: The soil crumb with 3% fly ash slaked into the water. No reaction at instant and slight slaking and but no cloudiness with the addition of 6% fly ash which is assigned with dispersion "grade 1".No cloud is formed for the soil mixed with 9% fly ash and assigned with dispersion 'Grade 1' where soil sample was transformed into fully non dispersive.

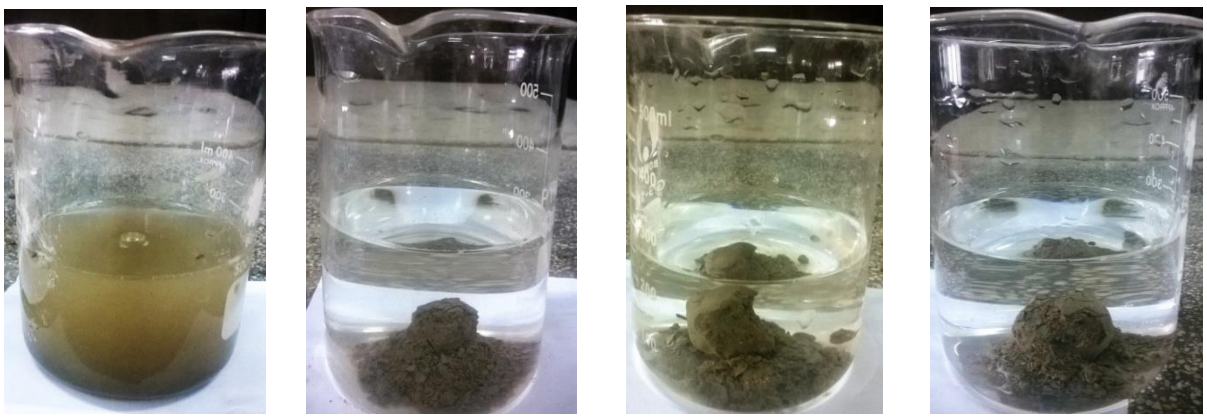

No Fly Ash 3% Fly Ash 6% Fly Ash 9% Fly Ash

Fig. 4: Observation of Crumb Test; Crumb with 0%, 3%, 6% and 9% fly ash respectively

Double Hydrometer Test with Fly Ash: Double hydrometer test was performed and the percent dispersion calculated for 3%, 6%, and 9% fly ash were about 20%, 15 % and 11% respectively.

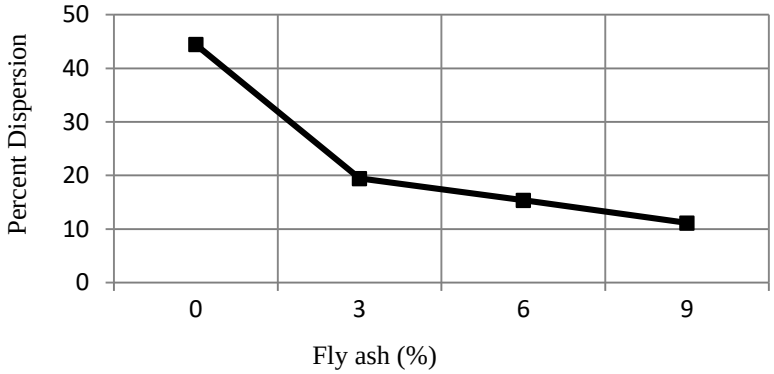

Fig. 5: Reduction of dispersion for fly ash mixed sample from Double Hydrometer test

Pinhole Test with Fly Ash: pinhole test was carried out for selected samples which were compacted to optimum moisture content corresponding to 3%, 6% and 9% fly ash respectively

Table 3: Observation from Pinhole Test of soil mixed with Fly Ash

% of Fly Ash mixed with soil sample	Final flow rate (ml/s)	Corresponding head(mm)	Final diameter of the hole	Condition of water flowing through the hole	Dispersion
3%	3 (on average)	1020	2.5 mm	Barely dark	ND2(slightly dispersion)
6%	3 (on average)	1020	1.2 mm	Clear	ND1 (No dispersion)

9%	2.5(on average)	1020	Exactly 1 mm	Clear	ND1 (No dispersion)

Fig. 6: Observation from Pinhole Test of soil mixed with 3%,6% and 9%Fly Ash respectively

Compaction Test: Figure 7 shows that maximum dry density while the optimum moisture content decreases with the increase of percentage of fly ash

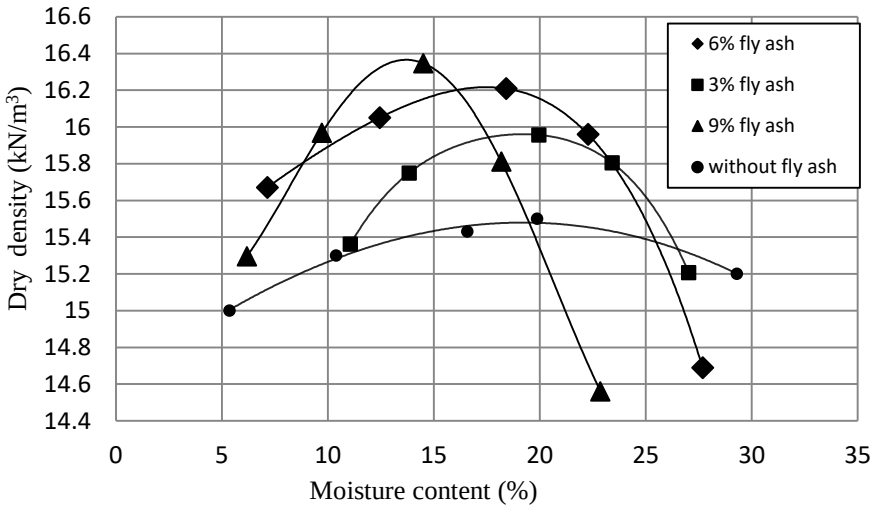

Fig. 7: Moisture content – Dry density relationship for untreated and treated soil samples

Observation from Unconfined Compression Test: This test was conducted on both cured and uncured specimens and the curing was done for 7 days, 14 days and 21 days. The UCS test results of the selected soil – coal fly ash mixtures reveals that the compressive strength increases with the increase in fly ash content. Strength also increases with curing time. Figure 8 shows increase of fly ash causes decrease of ductility as the curve for 9% fly ash mixed soil shifts to the left.

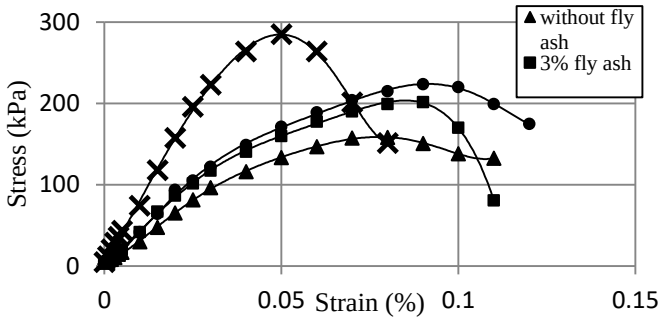

Fig. 8: UCS test result for 7 days of curing

Figure 9 shows the increase the unconfined compressive strength with the increase of the curing time. With 21 days of curing maximum compressive strength has been obtained which signifies that with curing time the cementatious bond between the molecules became stronger.

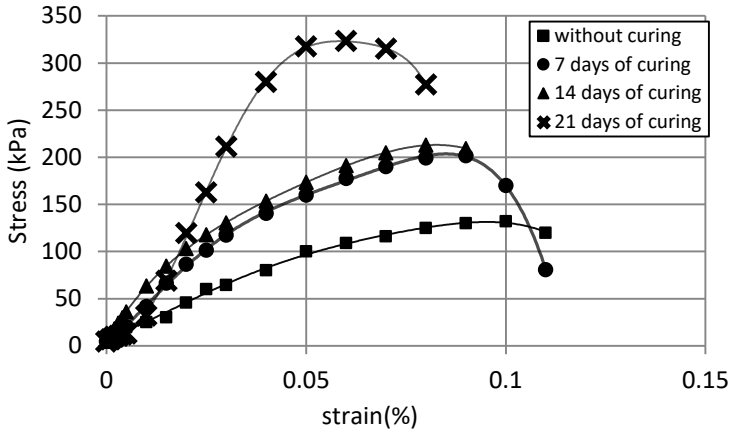

Fig. 9: UCS Test result for various curing time

CONCLUSION:

The degree of dispersion was identified though various tests, it has come for sure that the soil contains moderate or high dispersion and so it needed to be stabilized. Influence of varying percentage of (3%, 6% and 9%) fly ash content on dispersion phenomena was also checked out, and it reveals that using 9% fly ash by weight gives the best result in diminishing the dispersion to a negligible amount and also enhancing the compressive strength of soil.

ACKNOWLEDGEMENT:

The author would like to express sincere gratitude to Bangladesh University of Engineering and Technology for providing laboratory facilities for conducting this study.

REFERENCES:

Abbaslou, H., Hadifard, H. and Poorgohardi, A.(2016) "Characterization of Dispersive Problematic Soils and Engineering Improvements: A Review", Computations and Materials in Civil Engineering in Spiral Publishing, Vol. 1, No.2, pp. 65-83.

Indraratna,B., Nutalaya,P. and Kuganenthira,N.(2015), "Stabilization of a dispersive soil by blending with fly ash", Quarterly Journal of Engineering Geology Vol.24,pp.275-290.

Karthik,S. ,Ashok kumar,E., Gowtham,P., Elango,G., Gokul,D., and Thangaraj, S. (2014), "Soil Stabilization By Using Fly Ash", IOSR Journal of Mechanical and Civil Engineering (IOSR-JMCE), Vol. 10, pp. 20-26.

Premkumar,S., Piratheepan, J., Rajeev, P. and Arulrajah, A. (2016), "Stabilizing Dispersive Soil Using Brown Coal Fly Ash and Hydrated Lime", Journal of Geotechnical Engineering Division, ASCE.

Vakili,A.H., Selamat,M.R., Moayedi,H. and Amani,H. (2013), "Stabilization of Dispersive Soils by Pozzolan" , Forsenic Engineering ASCE, pp. 726-735.

4th International Conference on Advances in Civil Engineering 2018 (ICACE 2018)
19 –21 December 2018
CUET, Chittagong, Bangladesh
www.cuet.ac.bd

EFFECT OF GROUNDWATER TABLE ON PULLOUT CAPACITY OF ANCHOR IN FRICTIONAL SOIL

M. R. Rahman* & M. S. Islam
Department of Civil Engineering, Bangladesh University of Engineering & Technology, Dhaka, Bangladesh.
E-mail: rahi.rj.rr@gmail.com
**Corresponding Author*

ABSTRACT
Vertical anchors are one of the most important design structures in the geotechnical engineering field. Many researchers have proposed different types of methods to estimate horizontal pullout force of anchor based on experimental, analytical and numerical approach. However, ground water table, which might pose a significant threat to the stability of a structure, is hardly considered by the researchers. Subsequently, this paper focuses numerically on how the pullout capacity of anchor is affected by the submergence of anchor. In doing so, finite element program PLAXIS-2D was adopted in the current investigation. The developed finite element model was validated using established data of anchor pullout force. The pullout force was observed varying depth of groundwater table. Results indicate that a maximum of about 40 percent of pullout capacity may be reduced due to the effect of groundwater table, in contrast to 50 percent reduction of bearing capacity in case of conventional shallow footing due to the effect of the same.

Keywords: Anchor plate; Pullout resistance; Groundwater effect; Finite element method

INTRODUCTION

Soil anchoring is one of the most effective internally stabilized foundation systems to resist the horizontal pullout force or overturning moment coming on to the retaining structure. This anchor system is used to stabilize retaining structures through a complex soil-structure interaction. Anchors are used to transmit forces in specified direction from retaining structure to the ground. Review of pertinent literature reveals that numerous experiments were conducted to determine the capacity of the vertical anchor plate since the inception of the concept of anchoring. Plenty of researchers were observed to study vertical plate anchors, including Das and Seeley (1975), Ovesen (1981), Dickin and Leung (1983, 1985), Murray and Geddes (1989), Dickin and King (1997), Duncan and Mokwa (2001). Most of these studies were found to adapt laboratory model test or full-scale field test. On the other hand, block anchor behavior is studied by very few investigators. To the authors' knowledge, only few researchers like Bowles (1997), Duncan and Mokwa (2001), Naser (2006), and Khan et al. (2017) studied the behavior of block anchors. In addition to these experimental studies, some researchers were observed to investigate theoretical formulation of such geotechnical problems. The theoretical investigations can be found in the works of Meyerhof (1973), Rowe and Davis (1982), Murray and Geddes (1989), Basudhar and Singh (1994), Bowles (1997), Merifield and Sloan (2006), Jadid (2016), Jadid et al. (2018) and Shahriar (2018).

Although the varieties in experimental and theoretical results in the literature are immense, very few rigorous numerical analyses have been performed to determine the pullout capacity of anchors in cohesionless soil (Merifield and Sloan 2006). Some rigorous numerical studies include Rowe and Davis (1982), Basudhar and Singh (1994), Merifield and Sloan (2006). Most of the above-mentioned investigators focused on rough anchors. Very few studies were found on smooth anchors. It is worth

mentioning that although all the studies are based on limit equilibrium and limit analysis (upper-lower bound) neither of these studies included the effect of groundwater table.
Subsequently, the purpose of this study is to find out the amount of correction needed for the pullout capacity of vertical anchors due to the effect of groundwater table. This study has adapted numerical methods for the observation of groundwater table effect. Finally, a correction factor is suggested to use to minimize this effect.

PROBLEM DEFINITION

A rigid vertical strip anchor was considered for the study. The height between the top of the soil to the bottom of the anchor was denoted by H. The anchor has a width of B and its thickness is considered negligible compared to its width. The horizontal pullout force (P_u) was assumed to be acted on the center of gravity of the anchor. The groundwater table was 'z' distance below from the top of the soil. The soil mass was assumed to be perfectly plastic and it obeys Mohr-Coulomb failure criterion and an associated flow rule. A schematic view of the problem considered is presented in figure 1.

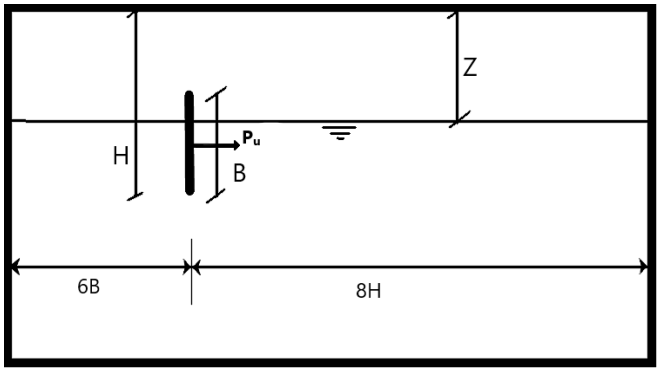

Figure 1: Problem definition [H= Anchor Depth; Z= GWT depth; B= Width of the anchor; P_u= Pullout Capacity]

FINITE ELEMENT MESH AND BOUNDARY CONDITION

A rectangular domain was chosen with suitable boundary condition. The finite element mesh was produced in PLAXIS-2D. The boundary was located at a distance L_f from the front face of anchor and L_b from the backface of the anchor. The distance L_f was equal to 8H while the distance L_b was equal to 6B (refer to figure 1). These distances are selected to ensure the velocity of the soil element remains zero at each boundary. These distances are later verified using the total displacement plot. Fifteen nodded element was used in the model. Distributions of the elements are shown in figure 2. Owing to computational efficiency, *very fine* mesh type was selected from the default menu of PLAXIS-2D. The elements near the anchor were kept denser than the elements at the boundary.

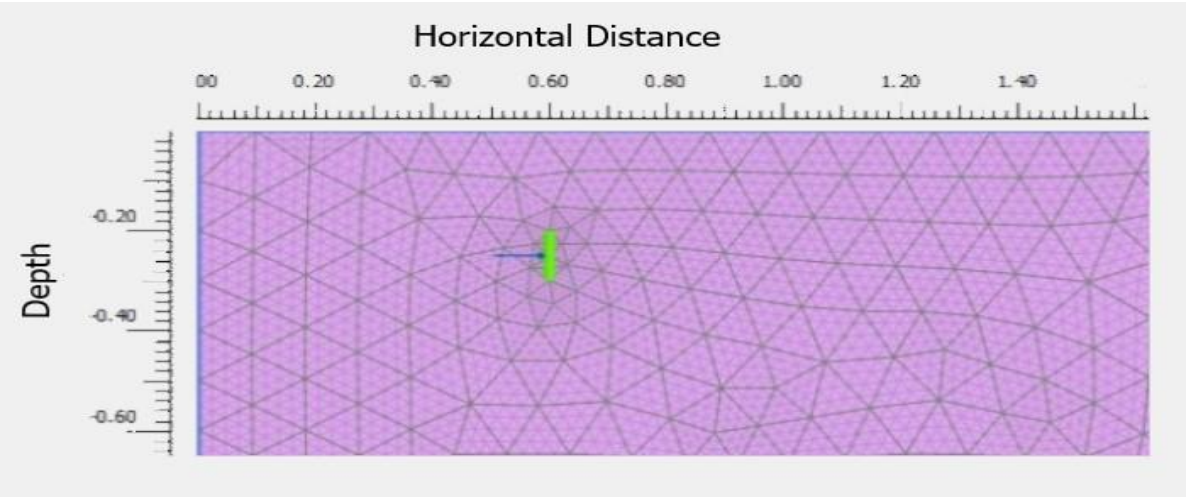

Figure 2: Finite element mesh of PLAXIS-2D for H/B=3 [Nodes: 714; Elements: 5881]

VERIFICATION OF THE MODEL

The finite element model of PLAXIS-2D was verified with the results of Merifield and Sloan (2006) as well as Kumar and Sahoo (2012). The pullout capacity of anchor with different embedment ratio was compared using a dimensionless breakout factor $N_\gamma = Pu/\gamma BH$. The results were obtained for $\varphi = 20^o$ using the three methods mentioned. These results are plotted in figure 3. The result of the current study is in close agreement with both of the published result of Merifield and Sloan (2006) and Kumar and Sahoo (2012).

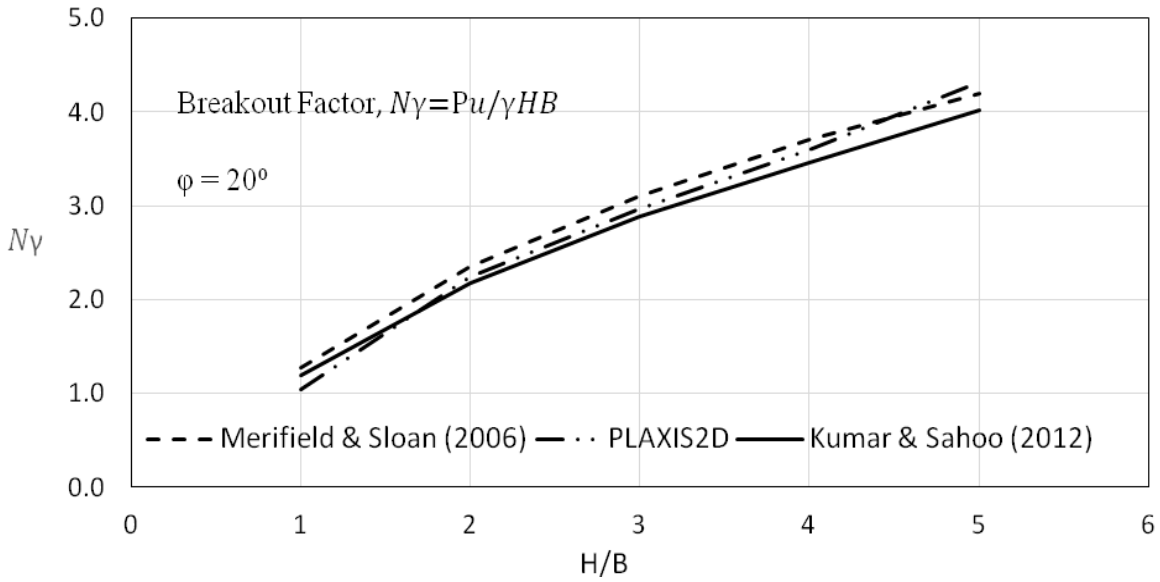

Figure 3: Comparison with the results of Merifield & Sloan (2006) and Kumar & Sahoo (2012)

Furthermore, the boundary condition was also verified using the total displacement diagram shown in figure 4 which clearly shows that the soil situated in the boundary are unaffected by the anchor and thus have no displacements.

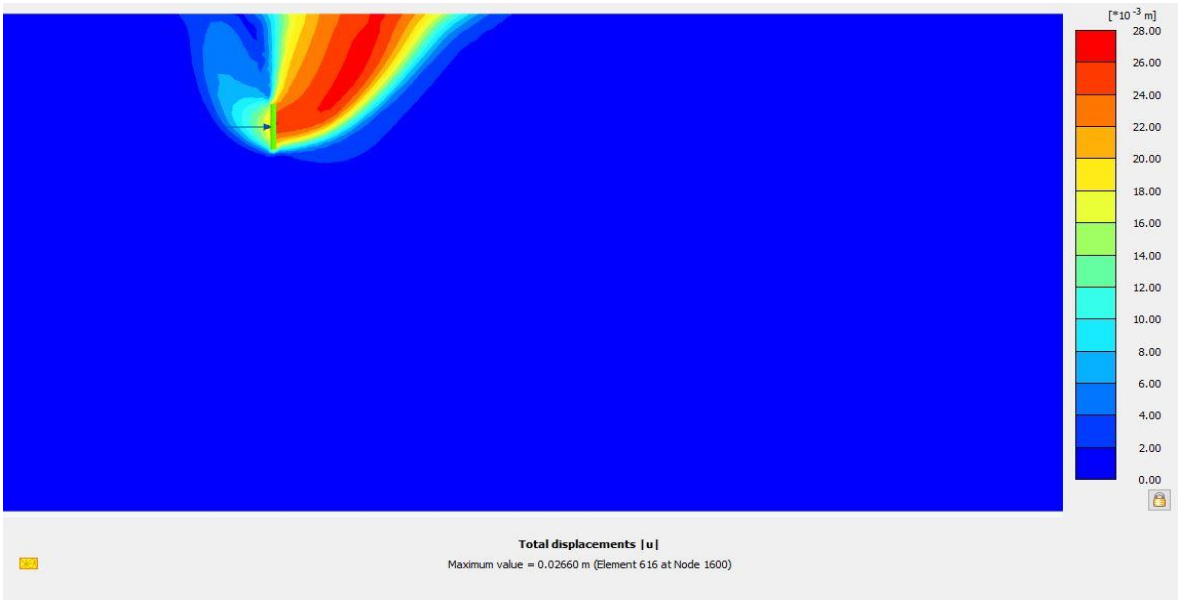

Figure 4: Total displacement plot for H/B=3

ANALYSIS

The ultimate pullout capacity of the anchor was recorded keeping different levels of groundwater table. The ratio of z/H was taken from 0 to 1.5 at an increment of 0.1. This analysis has been done for two separate embedment ratios. i.e. H/B=3 & H/B=5. The ultimate pullout capacity was determined from the load-displacement curve. The properties of soil and anchor are stated in Table. 1. Related literature for estimating parameters can be found in the studies of Rowe and Davis (1982), Bowles (1997), and CFEM (2006).

Table 1: Properties of soil and anchor used in FE modeling using PLAXIS-2D

	Name	Value
Soil Properties	Unit Weight (unsaturated), γ_{unsat}	17 kN/m^3
	Unit Weight (saturated), γ_{sat}	20 kN/m^3
	Modulus of Elasticity, E	1000 kN/m^2
	Poisson's Ratio, υ	0.3
	Cohesion, c	0.1 kN/m^2
	Angle of friction, φ	20º; 30º; 40º
	Dilatancy angle, ψ	20º; 30º; 40º
	Interface roughness, R_{inter}	1
Anchor Properties	Material	Steel
	EA	200 kN/m
	EI	1.667 x 10^{-3} kN-m^2/m
	Thickness, d	0.01 m
	Unit weight, w	0.4 kN/m/m
	Poisson's Ratio, υ	0.3

RESULTS AND DISCUSSION

The following results are obtained from the study:

The ultimate pullout capacity was observed keeping different levels of groundwater table for H/B=3 and H/B=5. The pullout capacity decreases in both cases with increasing level of groundwater table. As shown in figure 5 the pullout capacity of H/B=5 was higher than the pullout capacity of H/B=3, and the previous has a greater decrease than the later one. Thus, it can be said that the decrease amount increases with embedment ratio.

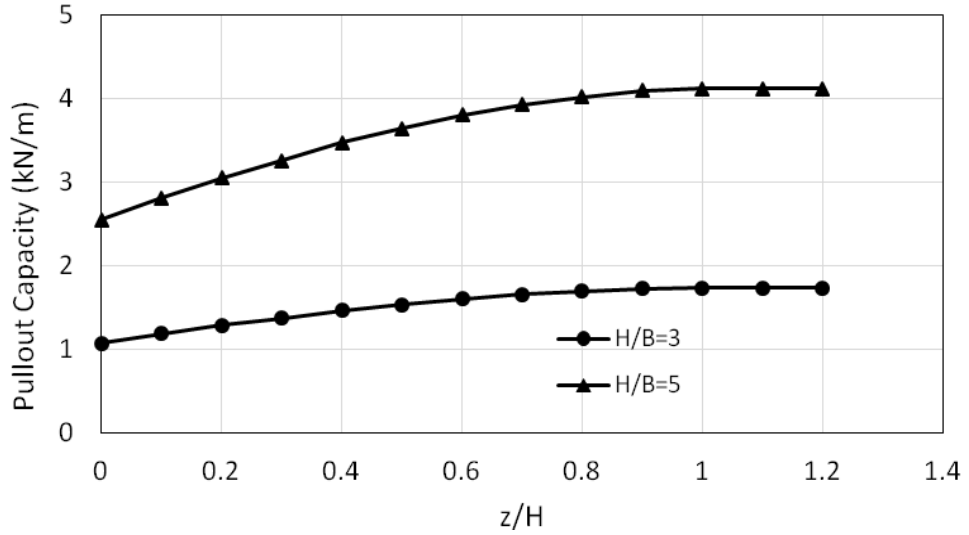

Figure 5: Comparison of decrease in pullout capacity due to GWT effect for different embedment ratio

The ultimate pullout capacity was observed with soils having different internal frictional angle, i.e. φ=20º; 30º; 40º. The pullout capacity increases with the increase of φ and the amount of decrease increases with the increase of φ. The comparison was shown in figure 6.

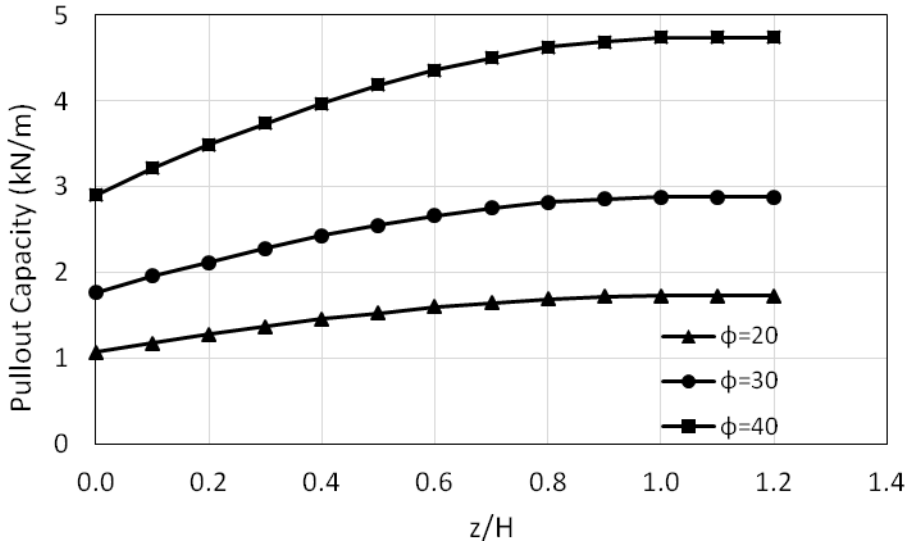

Figure 6: Comparison of decrease in pullout capacity due to GWT effect for different φ angle

Groundwater table doesn't have an effect on pullout capacity of anchor when it is located below the bottom of the anchor. Thus the pullout capacity remains constant when z/H is greater than or equal to 1.

A correction factor, $\rho = P_{submerged}/P_{dry}$ was introduced generalize the effect of groundwater table on pullout capacity of anchor. Where, $P_{submerged}$ denotes to the pullout capacity when the groundwater table is above the anchor level and P_{dry} denotes to the pullout capacity when the groundwater table is below the anchor level. A ρ vs. z/H plot was shown in figure 7 to observe the general pattern of decrease for the given soil. All the results mentioned previously can be generalized in this format.

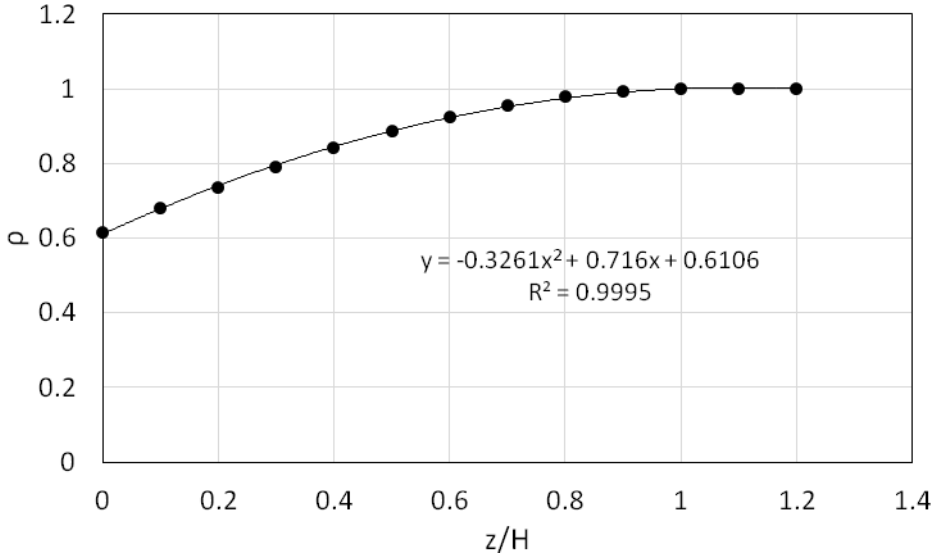

Figure 7: Generalized pattern of decreasing of pullout capacity due to GWT effect

As shown in figure 7, the decrease pattern is not linear. The rate of decrease of pullout capacity increases as lower z/H ratio approaches.

$$\rho = P_{submergered}/P_{dry} = -0.3261(z/H)^2 + 0.716(z/H) + 0.6106; \text{ when } 0<z/H<1 \quad (1)$$

$$\rho = P_{submergered}/P_{dry} = 1; \text{ when } z/H>1 \quad (2)$$

The above equations can be used to find out the submerged pullout capacity if the dry pullout capacity is known.

CONCLUSION

The groundwater table has a significant effect on pullout capacity of anchor as it decreases almost 40% of its capacity in contrast to 50% reduction of bearing capacity in case of conventional shallow footing due to the effect of the same. Moreover, it seems quite clear that the decrease rate is independent of the internal friction angle and embedment ratio of anchor. Further studies are needed to identify the factors responsible for the pattern of the decrease rate of the pullout capacity.

ACKNOWLEDGMENT

The authors acknowledge the infrastructural and financial support received from Bangladesh University of Engineering and Technology (BUET), Dhaka, Bangladesh for carrying out the research work. The "Computational and Simulation Laboratory" of BUET-JIDPUS was used for accessing the original version of PLAXIS-2D.

REFERENCES

Basudhar, PK and Singh, DN. 1994. A generalized procedure for predicting optimal lower bound break-out factors of strip anchors. *Géotechnique,* 44(2): 307-318.

Bowles, JE. 1997. *Foundation Analysis and Design (5th ed.),* The McGraw-Hill Companies. Singapore.

Das, BM and Seeley, GR. 1975. Load-displacement relationships for vertical anchor plates. *Journal of the Geotechnical Engineering Division,* 101(7):711-715.

Dickin, EA and King, JW. 1997. Numerical modeling of the load-displacement behavior of anchor walls. *Computers & Structures,* 63(4):849-858.

Dickin, EA and Leung, CF. 1983. Centrifuge model tests on vertical anchor plates. *Journal of Geotechnical Engineering,* 109(12):1503-1525.

Dickin, EA and Leung, CF. 1985. Evaluation of design methods for vertical anchor plates. *Journal of Geotechnical Engineering,* 111(4):500-520.

Duncan, M. and Mokwa, R. 2001. Passive earth pressures: theories and test. *Journal of Geotechnical and Geoenvironmental Engineering,*127(4):248-257

Jadid, R.; Abedin, MZ; Shahriar, AR and Arif, MZU. 2018. Analytical model for pullout capacity of a vertical concrete anchor block embedded at shallow depth in cohesionless soil. *International Journal of Geomechanics*, 18(7):1-8.

Jadid, R. 2016. *Modeling of pullout resistance of concrete anchor block embedded in cohesionless soil.* MSc Thesis, Bangladesh University of Engineering and Technology, Dhaka, Bangladesh.

Khan, AJ; Mostofa, G. and Jadid, R. 2017. Pullout resistance of concrete anchor block embedded in cohesionless soil. *Geomechanics and Engineering, An International Journal*, 12(4):675-688.

Kumar, J., and Sahoo, JP. 2012. Upper bound solution for pullout capacity of vertical anchors in sand using finite elements and limit analysis. *International Journal of Geomechanics,* 12(3):333-337.

Merifield, RS and Sloan, SW. 2006. The ultimate pullout capacity of anchors in frictional soils. *Canadian Geotechnical Journal,* 43:852-868.

Meyerhof, GG. 1973. Uplift resistance of inclined anchors and piles. *Proceedings of the 8th International Conference on Soil Mechanics and Foundation Engineering*, 3:167–172.

Murray, EJ and Geddes, JD. 1989. Resistance of Passive Inclined Anchors in Cohesionless Medium. *Géotechnique,* 39(3):417-431

Naser, AS. 2006. Pullout capacity of block anchor in unsaturated sand. *Proceedings of the Fourth International Conference on Unsaturated Soils,* 403-414.

Rowe, RK and Davis, H. 1982. The behavior of anchor plates in sand. *Géotechnique,* 32(1):25-41.

Shahriar, AR. 2018. *Development of an analytical model for the analysis of pullout capacity of anchors embedded in frictional soils,* MSc Thesis, Bangladesh University of Engineering and Technology, Dhaka, Bangladesh.

4th International Conference on Advances in Civil Engineering 2018 (ICACE 2018)
19 –21 December 2018
CUET, Chittagong, Bangladesh
www.cuet.ac.bd

MICROMECHANICAL RESPONSES OF GRANULAR MATERIALS SUBJECTED TO LOAD REVERSAL

M. M. Sazzad*

Department of Civil Engineering, Rajshahi University of Engineering & Technology, Rajshahi, Bangladesh.
E-mail: mmsruet@gmail.com

**Corresponding Author*

ABSTRACT
The objective of this paper is to investigate the micromechanical responses of granular materials such as sand subjected to load reversal using the two dimensional oval shape particles by the discrete element method (DEM). Sample consisting of 8450 ovals was isotropically compressed to 100 kPa in different stages using the periodic boundaries. The isotropically compressed numerical sample was subjected to load reversal repeatedly during shear. The numerical data were recorded at regular interval to perform the post analysis of the micromechanical parameters such as the average coordination number, slip coordination number, effective coordination number, fabric, etc. The results depict that load reversal during shear has significant effect on the micromechanical responses of granular materials. The micromechanical parameters exhibit massive change in the contact characteristics at the onset of load reversal. The fabric quantified by fabric tensor is measured and its evolution is monitored and reported as well.

Keywords: Load reversal; Micromechanical response; Granular materials; Discrete element method; Fabric tensor.

INTRODUCTION
Granular materials such as sand often subject to the cyclic loading or reaped loading or load reversal. The responses of granular materials under load reversal is interesting and important to the geotechnical engineers. Consequently, a number of studies were reported in the literature considering the cyclic loading or reaped loading or load reversal. The complex behaviours during load reversal arises due to the particulate nature of granular materials. However, the study of these particulate responses at the grain scale is limited due to the restricted facilities available at present in laboratory based studies. The laboratory based experimental studies on the other hand considered and reported the overall behaviour of granular materials at the boundary. Although the measurement of responses at the boundary scale often referred to as macro scale response contributes to the understanding and modelling of granular materials under reaped loading or load reversal, the complexities arise at the macro scale responses due to the grain scale responses and their inter-relationship are not fully understood.

Discrete element method (DEM) (Cundal and Strack, 1979) is a numerical tool that can help understand the fundamental aspects of soil mechanics by exploring the micro-structure and fabric of particulate system. Using the DEM, it is possible to study the micro-mechanics of granular materials by conducting the numerical experiments or element tests at different loading conditions and stress paths. With the increase of the computer processing speed, it is now possible to handle large number of particles and thus DEM is gaining increasing popularity to researchers in different disciplines. The application of DEM in geo-mechanics is also gaining inordinate popularity in recent years in different aspects such as anisotropy (Sazzad and Suziki, 2010; Sazzad and Rahat, 2017), cyclic responses (O'Sullivan et al.,

2008; Sazzad, 2014; Nguyen et al. 2014), stress paths (Sazzad and Suzuki, 2013; Lui et al., 2017), fabric evolution (Kuhn, 1999; Kuhn 2014), etc. Even if it used in the simulation of different aspects of granular materials in geo-mechanics, it has been used in a very limited number of studies to examine and extract the micromechanical responses considering the load reversal. For example, O'Sullivan and Cui (2009) validated the DEM simulation with the experiments and explored the micromechanics of granular materials during load reversal using circumferential periodic boundaries in quasi-static triaxial tests. During the load reversal, the sudden change of principal stress direction during unloading and also during loading causes huge changes in the fabric orientations. The changes of the stresses measured at the boundaries are directly linked to the change of such fabrics. The quantification and measurement of the fabric change at micro-scale is not possible using the conventional experiments. The use of DEM can explore the understanding of these micro-structural and fabric change during load reversal. Accordingly, DEM has been used in the present study to enhance our understanding of the evolution of micromechanics during load reversal.

To carry out the numerical experiments, a numerical sample consisting of 8450 ovals was generated in a rectangular box. The generated numerical sample was compressed in different stages to make an isotropic sample using the periodic boundaries. . The isotropically compressed numerical sample was subjected to load reversal several times during shear for biaxial loading conditions. The numerical data were recorded at regular time interval. Later, the recorded data were processed to extract the micromechanical parameters where necessary.

METHODOLOGY

In the present study, Discrete element method briefly DEM is used which has become a very popular numerical method for particulate approach. It is pioneered by Cundall and Strack (1979) and widely used in different branches of science and engineering to model and simulate the discrete nature of granular materials. The method is computationally intensive. As a result it limits the number of particles to be considered in a model. However, with the advances in computer's processing power and advanced numerical algorithms for sorting the nearest neighbor particles in a model, it is increasing used now a days to numerically simulate the behavior of granular materials by considering millions of particles even on a single computer processor.

The basic concepts of DEM is very simple. Each particle in DEM is treated individually and it can move and rotate through the interactions of the interparticle contacts. The kinematics of each particle are monitored. The translational and rotational accelerations of a 2D particle in DEM are computed using the Newton's second law of motion as follows:

$$m\ddot{x}_i = \sum F_i \qquad i = 1-2 \qquad (1)$$

$$I\ddot{\theta} = \sum M \qquad (2)$$

where F_i are the force components, M is the moment, m is the mass, I is the moment of inertia, $\ddot{x}_i$ are the translation acceleration components and $\ddot{\theta}$ is the rotational acceleration of the particle. Velocities and displacements of particles are obtained by integrating the accelerations over time successively. For details of DEM, readers are referred to Cundall and Strack (1979). Computer program OVAL (Kuhn, 2003), written in FORTRAN language, is used to analyze the particulate assemblies using DEM. It has already been used for many DEM studies so far and its usefulness has been recognized (Sazzad and Suzuki, 20111; Sazzad, 2016; Kuhn, 2017; Sazzad and Habib, 2017). Simple linear contact model consisting of two springs and a friction slider is used.

SAMPLE PREPARATION

To prepare a numerical sample, 8450 ovals were randomly generated in a rectangular frame with a height to width ratio of two. The height to width ratio of each oval is 0.6. Eleven different sizes (i.e., width of oval) of ovals ranging from 1 to 2 mm were used to generate the sample. The initial sample was generated in such a way that the particles have no initial contact. The sample, generated in this way, was

very loose and thus it was subjected to isotropic compression in different stages with a given interparticle friction coefficient using the periodic boundary, a boundary condition in which the periodic cells are surrounded by the identical cells. The compression was continued till the continuum stresses reached 100 kPa. After the end of isotropic compression, an interparticle friction coefficient of 0.50 is used during the simulation. The void ratio of the numerical samples at the end of isotropic compression became 0.194. The isotropically compressed numerical is depicted in Fig. 1.

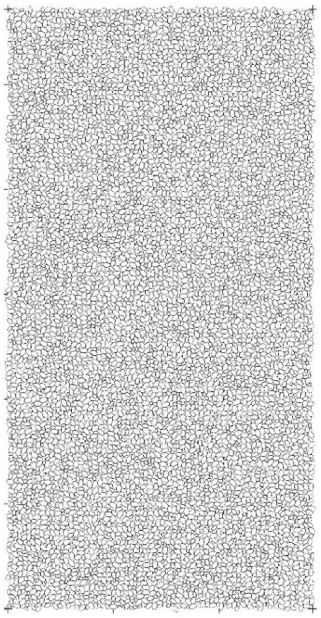

Fig. 1 Isotropically compressed samples composed of oval shaped particles.

NUMERICAL SIMULATION

Simulations of biaxial tests were carried out by considering dry granular assemblies under the strain control condition. During the test, the sample height decreased vertically during loading with a very small strain increment of 0.00002% in each step by keeping the stress in lateral direction constant (i.e., 100 kPa) while the sample height increased vertically with a very small strain increment of 0.00002% in each step during unloading by keeping the stress in lateral direction constant. The parameters used in the simulations are presented in Table 1. Note that the coefficients of global viscous damping used in the current study (Table 1) have been taken sufficiently small to keep the effect of numerical damping minimum and to obtain more stable solutions during the simulation. When the biaxial shear up to 2% axial strain was completed, the first unloading started for an axial strain of 1%. Immediately after the completion of unloading, reloading began and continued for the next 2% axial strain. The process (unloading and loading) continued several times to observe the change in the evolution of micro-parameters and fabric during load reversal.

Table 1 DEM Parameters used in the simulations

DEM parameters	Value
Normal contact stiffness (N/m)	1×10^8
Shear contact stiffness (N/m)	1×10^8
Mass density (kg/m^3)	2650
Increment of time step (s)	1×10^{-6}
Interparticle friction coefficient	0.50
Damping coefficients	0.05

RESULTS AND DISCUSSIONS

The evolution of the stress ratio, q/p, with axial strain, ε_1, during load reversal is depicted in Fig. 2. Here, the deviatoric stress, q is defined as $q=(\sigma_1-\sigma_2)/2$ (a) and the mean stress p is defined as $p=(\sigma_1+\sigma_2)/2$, where σ_1 and σ_2 are the stresses in vertical and lateral directions. Stress ratio sharply increases at the small strain level and becomes steady with further increase in strain. When the first load reversal i.e. unloading begins the stress ratio sharply decreases. This behavior is similar to that reported in the experimental studies (e.g., O'Sullivan and Cui, 2009). The stress ratio starts increasing again when the second load reversal i.e. the loading begins for the second time. It should be noted that during reloading some permanent deformation (plastic deformation) has taken place. The unloading and loading are continued for several times and it is interesting to note that the peak values of stress ratio graduating increase at the end of successive loading and at the same time, the peak values of stress ratio graduating at the end of successive unloading. This is clearly attributed to the changes in the fabric and micro-structural orientations during the successive loading and unloading. The evolution of void ratio with axial strain is depicted in Fig. 2(b). It is observed that the void ratio gradually decreases as the sample is subjected to successive load reversal. This reveals that the sample is getting denser gradually as the sample undergoes successive loadings and unloadings.

The evolution of the micro-mechanical parameters such as the coordination number and slip coordination number with axial strain are depicted in Fig. 3. Coordination number and slip coordination number are defined here as (Sazzad, 2016):

$$Z=\frac{2N_c}{N_p} \qquad (3)$$

$$Z_{sl}=\frac{2N_c^{sl}}{N_p} \qquad (4)$$

Fig. 3(a) depicts that coordination number sharply decreases with strain during the first loading. The change in the coordination number further intensifies when the first unloading begins. The coordination number starts accumulating against when the second loading or reloading begins. The continuous decrease in coordination number is the consequence of the rapid change in the ordination of the fabric or the micro-structures in the granular system. The increase in the coordination is due to the increase in the contacts in the major principal stress direction during reloading.

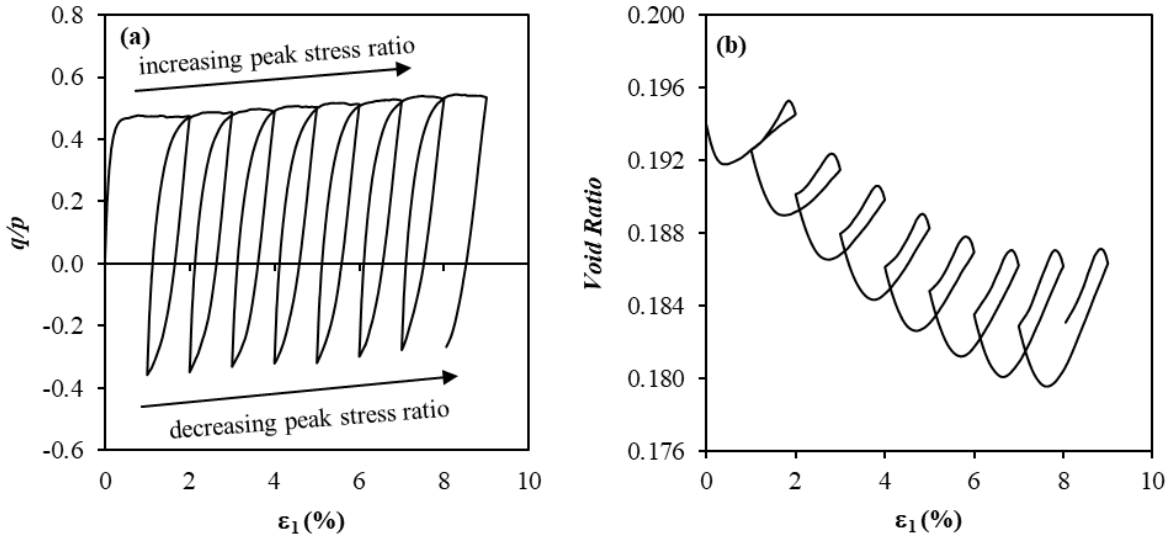

Fig. 2 Evolution of (a) the stress ratio and (b) void ratio with axial strain during load reversal

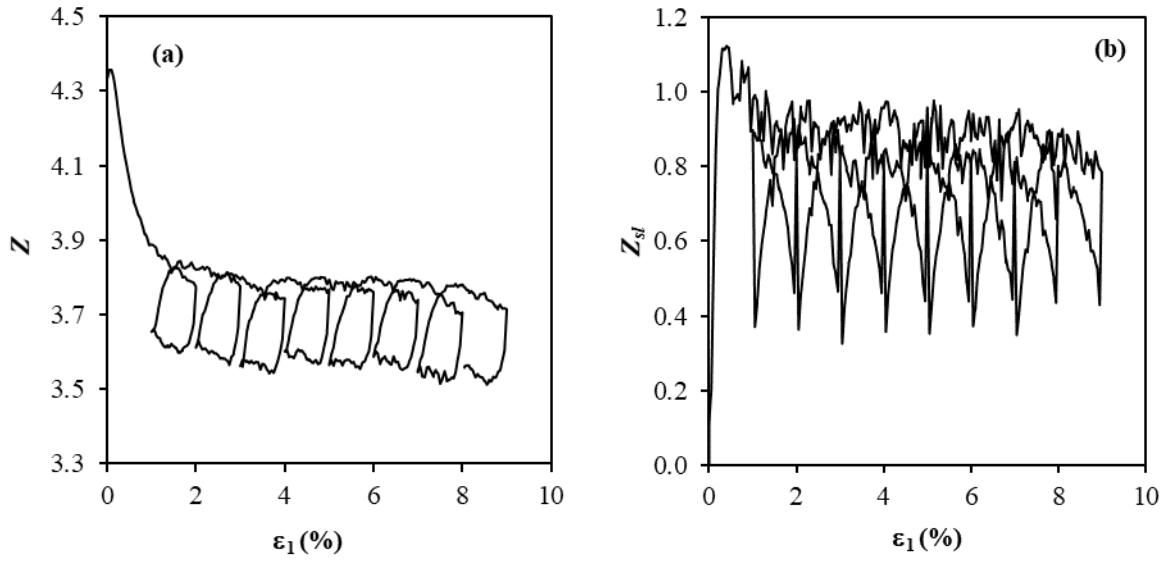

Fig. 3 Evolution of (a) coordination number and (b) slip coordination number with axial strain during load reversal

Slip coordination number on the other hand sharply increases as the loading starts. It is noted in Fig. 3(b) that the sharp decrease in the slip coordination takes place at the moment of unloading. The evolution of the fabric is quantified using the fabric tensor. The fabric considering all the contacts is quantified using the following tensor (Sazzad, 2014; Sazzad and Habib, 2017):

$$H_{ij} = \frac{1}{N_c} \sum_{\alpha=1}^{N_c} n_i^{\alpha} n_j^{\alpha} \qquad (5)$$

Here, n_i^{α} is the unit contact normal vector of the $\alpha-$th contact and N_c is the number of contacts. The evolution of the strong contact fabric is quantified using the tensor (Sazzad, 2014):

$$H_{ij}^{s} = \frac{1}{N_c} \sum_{s=1}^{N_c^s} n_i^{s} n_j^{s} \qquad (6)$$

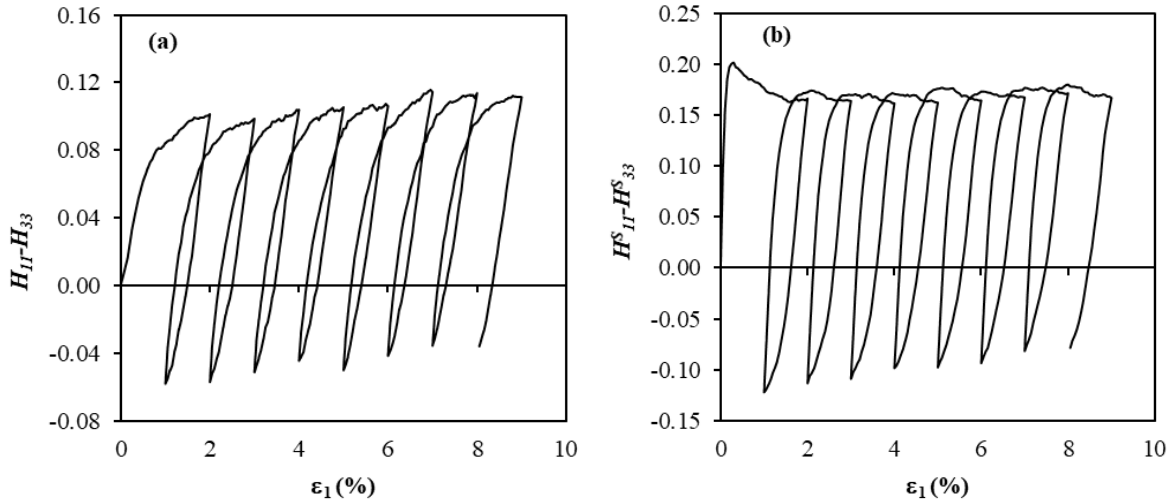

Fig. 4 Evolution of deviatoric fabric (a) considering all contacts and (b) considering strong contacts with axial strain during load reversal

Here, n_i^s is the unit contact normal vector of the $s-$th contact and N_c^s is the number of strong contacts. A contact is defined as strong contact if it carries a contact force greater than the average contact force. It is very interesting to note that the evolution of fabric with axial strain has an excellent similarity with the evolution of stress ratio. The similarity is closer when the fabric for strong contact is considered.

CONCLUSIONS

This study presents the micromechanical behavior of a particulate system during load reversal. For this purpose, DEM is used to model the discrete behaviors of granular. A rectangular sample consisting of 8450 ovals were generated in a rectangular frame and a virtual sample was prepared which was subjected to load reversal. The macro as well as the micro-mechanical responses of the granular system was explored. It is observed that plastic deformation takes place within each unloading loading cycle. It is noted that the peak values of stress ratio gradually increase at the end of successive loadings while the peak values of stress ratio gradually decrease at the end of successive unloading. This clearly attributes to the changes in the fabric and micro-structural orientations during the successive loadings and unloadings. The micro-mechanical parameters such the coordination and the slip coordination number are significantly influenced by the load reversal. The coordination number and the slip coordination number decrease progressively during the successive loadings and unloadings.

REFERENCES

Cundall, PA and Strack, ODL. 1979. A discrete numerical model for granular assemblies. *Geotechnique*, 29(1):47-65

Kuhn, MR. 2003 Smooth convex three-dimensional particle for the discrete element method. *J Engrg Mech*, 129:539-547

Kuhn, MR. 1999. Structured deformation in granular materials. *Mech Mater*, 31:407-429

Kuhn, MR. 2014. Dense granular flow as a topologically disordered process. *Granular Matter*, 16(4): 499-508.

Kuhn, MR. 2017. Contact transience during slow loading of dense granular materials. *Journal of Engineering Mechanics*, 143 (1):C4015003(9)

Liu, Y; Liu, H and Mao, H. 2017. DEM investigation of the effect of intermediate principle stress on particle breakage of granular materials. *Computers and Geotechnics*, 84:58-67.

Nguyen, N-S, François, S and Degrande, G. 2014. Discrete modeling of strain accumulation in granular soils under low amplitude cyclic loading. *Computers and Geotechnics*, 62:232-243

O'Sullivan, C and Cui, L. 2009. Micromechanics of granular material response during load reversals: Combined DEM and experimental study. *Powder Technology*, 193(3):289-302

O'Sullivan, C; Cui, L and O'Neill, SC. 2008. Discrete element analysis of the response of granular materials during cyclic loading. *Soils Found*, 48:511-530

Sazzad, MM (2014) Micro-scale behavior of granular materials during cyclic loading. *Particuology* 16:132–141

Sazzad, MM and Suzuki K. 2013. Density dependent macro-micro behavior of granular materials in general triaxial loading for varying intermediate principal stress using DEM. *Granular Matter* 15:583–593

Sazzad, MM and Suzuki, K. 2010. Micromechanical behavior of granular materials with inherent anisotropy under cyclic loading using 2D DEM. *Granular Matter*, 12:597–605

Sazzad, MM and Habib, MA. 2017. Simulation of the behavior of granular materials for varying void ratios using DEM. *International Journal of Advanced Structures and Geotechnical Engineering*, 6(3):96-102.

Sazzad, MM and Rahat, T. 2017. Influence of aspect ratio of granular materials on the mechanical behavior during cyclic loading by DEM. *International Conference on Mechanical, Industrial and Materials Engineering*, pp.1-6.

Sazzad, MM and Suzuki, K. 2011. Effect of interparticle friction on the cyclic behavior of granular materials using 2D DEM. *J Geotech Geoenviron Eng*, 137:545-549

Sazzad, MM. 2016. Micro-scale responses of granular materials at different confining pressures using DEM. *Acta Geotech. Slovenica*, 13:26-36

4th International Conference on Advances in Civil Engineering 2018 (ICACE 2018)
19 –21 December 2018
CUET, Chittagong, Bangladesh
www.cuet.ac.bd

PRESSURE DEPENDENT BEHAVIOR OF GRANULAR MATERIALS AT VARYING INTERMEDIATE PRINCIPAL STRESS BY DEM

M. M. Sazzad*& A. Hossain

Department of Civil Engineering, Rajshahi University of Engineering & Technology, Rajshahi Bangladesh
E-mail:mmsruet@gmail.com

**Corresponding Author*

ABSTRACT
The goal of the present paper is to simulate the granular material behaviors like sand for varying intermediate principal stress under different mean stresses using the widely used particulate approach namely the discrete element method (DEM). Spheres were considered to model the round shape sand particles. The consideration of spheres as sand particles lessens the computational cost while simulating the behavior using the DEM. Spheres were randomly generated in a cube shaped box without any initial contacts at the beginning stage of sample preparation. The randomly generated samples were consolidated isotropically to different target mean stresses (25 kPa, 50 kPa and 100 kPa) in several stages using the periodic boundaries. The numerically prepared samples were sheared under the strain control condition by varying the intermediate principal stress. The numerical data were recorded at regular intervals and they were processed to get the macro-mechanical responses such as the stresses, strains, etc. The results from the numerical study depict that they agree well with the experimental behaviors for sand. The development of stress components and strain components are sturdily dependent on the variation of the intermediate principal stress. The stress and strain components are affected by the variation of mean stress. The evolution of the dilatancy index is dependent on the variation of mean stress. The dependence of grain-scale parameters on the variation of mean stress is also measured and reported.

Keywords: Intermediate principal stress; Pressure dependent behavior; Granular materials; Discrete element method.

INTRODUCTION

Granular material behavior is decidedly dependent on the mean stress applied during the laboratory tests. Experimental studies such as Fukushima and Tatsuoka (1984) depicted that the angle of shearing resistance is highly dependent on the confining pressure of moderate to high level. The effects become more significant when the stress paths applied during the laboratory tests are different. The effect of stress paths can be studied more generally by controlling the intermediate principal stress using a non-dimensional parameter known as b and defined as follows: $b = (\sigma_2' - \sigma_3')/(\sigma_1' - \sigma_3')$, where σ_1' is the major principal effective stress, σ_2' is the intermediate principal effective stress and σ_3' is the minor principal effective stresses. In the literature, numerous experimental studies were reported to examine the effect of b (Lam and Tatsuoka, 1988; Lade, 2006, Sun et al., 2008; Kandasami and Murthy, 2015; among others). These studies indicated that the angle of shearing resistance increases from b =0 to certain value b and beyond that value, the angle of shearing resistance decreases or increases or even remains almost constant. These uncertainties in the experimental studies may arise due to the differences in soil types, experimental conditions, stress paths and even from the changes in

the initial fabric of the samples to be tested. The limitations in the experimental studies regarding the controlling of the same initial fabric can be evaded by using the numerical technique such as the discrete element method, briefly DEM pioneered by Cundall and Strack (1979). Numerically, the effect of intermediate principal stress or in other word, b value was studied by several researchers using DEM (Ng, 2004; Sazzad et al., 2012; Sazzad and Suzuki, 2013). However, the effect of mean stress was not considered in the earlier studies. Consequently, this study has used DEM as numerical tool to model the discrete behavior of granular materials at different mean stresses under varying intermediate principal stress. Thus, the objective of the present study is firstly to simulate the experimental behavior of granular materials for varying intermediate principal stress or in other word, for varying b values under different mean stresses and secondly to explore the stress-strain-dilative behavior and grain-scale parameters using the DEM. For this purpose, a cube sample consisting of spheres was prepared numerically and this numerically prepared virtual sample was subjected to shear under varying b values and mean stresses. The data were collected at regular interval during shear and post-analysis was carried out.

DEM AND OVAL

Discrete element method (DEM), a very popular numerical method for particulate approach, is used in this study. It is introduced by Cundall and Strack (1979) and applied in different branches of science and engineering to simulate the discrete behavior of granular materials. The method is computationally rigorous. As a result, it limits the consideration of the maximum number of particles to be used in a model. However, with the advances in computer's processing power, it is increasingly used now a days to simulate the characteristics of granular materials by considering millions of particles even on a single computer processor.

The basic concepts of DEM are simple. Each particle in DEM is treated individually and it can move and rotate by the interactions of the interparticle contacts. The translational accelerations as well as the rotational accelerations of a 3D particle in DEM are calculated using the Newton's second law of motion and can be expressed as follows:

$$m\ddot{x}_i = 1-3 \qquad (1)$$

$$I\ddot{\theta} = \sum M \qquad (2)$$

where F_i are the components of force, M is the moment, m is the mass of particle, I is the moment of inertia of particle, $\ddot{x}_i$ are the components of translation acceleration and $\ddot{\theta}$ is the rotational acceleration of particle. Velocities and displacements of particles are obtained by integrating the accelerations over time successively. Interested readers are referred to Cundall and Strack (1979) for the detailed explanation of DEM. Computer program OVAL (Kuhn, 2003), written in FORTRAN language, is used to analyze the particulate assemblies using DEM. In OVAL, both 2D and 3D particles can be considered. Spheres have been used in the present study to model the round shape sand. OVAL has already been used for many DEM studies so far and its usefulness has already been recognized (Sazzad and Suzuki, 2010; Sazzad, 2014; Kuhn, 2017; Sazzad and Habib, 2017). Simple linear contact model consisting of two springs and a friction slider is used.

PREPARATION OF NUMERICAL SAMPLE

A virtual sample comprising of 8000 spheres was randomly generated in a cubic frame. The diameters of particles varied from 3 to 4.5 mm. The initial sample was generated without any initial contact between particles. The sample, generated in this way, was very loose and thus, it was subjected to isotropic compression in different stages to 25, 50 and 100 kPa with given interparticle friction coefficients using the periodic boundaries. Later, the interparticle friction coefficient was changed and a value of 0.50 was used during the simulation. The void ratios of the numerical samples after the completion of isotropic compression to 25, 50 and 100 kPa became 0.600, 0.571 and 0.570, respectively. The small difference of the observed void ratio of the samples for mean stresses of 25, 50 and 100 kPa is believed to have an insignificant effect on the total behavior of the numerical study.

NUMERICAL SIMULATION

True triaxial compression tests were conducted for different mean stresses (25, 50 and 100 kPa) by controlling the b values from 0 to 1 considering dry granular assemblies under the strain control condition. During the test, the sample height decreased vertically during loading with a very small strain increment of 0.00002% in each time step by adjusting the stresses in other lateral directions in such a way that the given value of b and mean stress were maintained. The parameters considered for the numerical simulations are presented in Table 1. Note that the coefficients of global viscous damping used in the present study (Table 1) have been taken sufficiently small to keep the effect of numerical damping minimum and to obtain more stable solutions during the simulation. The quasi-static state during the numerical simulation was observed to guarantee the accuracy of the simulation.

Table 1. Parameters considered in the present study

Parameters considered in the study	Their Values
Normal contact stiffness (N/m)	1×10^6
Shear contact stiffness (N/m)	1×10^6
Mass density of particle (kg/m^3)	2650
Time step increment (s)	1×10^{-6}
Interparticle friction coefficient	0, 0.50
Damping coefficients	0.05

RESULTS AND DISCUSSIONS

The behavior of the stress ratio, q'/p', with the increase of axial strain , ε_1, for various b values and mean stresses is illustrated in Fig. 1. Here, q' is the equivalent deviatoric stress and defined as $q' = \sqrt{\frac{3}{2}\left(\sigma'_{ij} - p\delta_{ij}\right)\left(\sigma'_{ij} - p\delta_{ij}\right)}$ where p' is the mean effective stress and defined as $p' = \sigma'_{ii}$, and δ_{ij} is the Kronecker parameter. Referring to Fig. 1, it is noted that the development of stress ratio is sturdily dependent on the b values. The peak values of q'/p' gradually deceases with b. This observed behaviors are in agreement with the previous experimental studies (Ergun, 1981; Lade, 2006) and numerical studies (Huang et al., 2014) for different values of b. The effect of intermediate principal stress or in other word, b values for different mean stresses is also illustrated in Fig. 1. The evolution tendency of q'/p' is similar regardless of the mean stress used. Although the tendency is similar, their values are not same and it is obvious in Fig. 1(d). The peak value of q'/p' is significantly smaller for lower values of mean stress. However, the difference of the peak stress ratio is almost same when the vales of mean stress is over 50 kPa. This indicates that the effect of mean stress is significant when the lower mean stress is used.

The evolutions of intermediate principal strain, ε_2 and minor principal strain, ε_3 with the major principal strain component, ε_1 at characteristic b values i.e., b =0 (triaxial compression), b =0.4 (near to plane strain compression, referring to Sazzad and Suzuki, 2013 and Huang et al., 2014) and b =1.0 (triaxial extension) for different mean stresses are depicted in Fig. 2. It is evident that the development of intermediate principal strain and minor principal strain are sturdily dependent on the mean stress used, in particular for lower mean stress. The evolution of intermediate principal strain and minor principal strain are also dependent on the values of b used during the simulation.

The evolution of the dilatancy index defined as $DI = -d\varepsilon_v / d\varepsilon_d$ with ε_d is showed in Fig. 3 for divergent b values and mean stresses. Here, ε_d is defined as $\varepsilon_d = \sqrt{\frac{2}{3}\left(d\varepsilon_{ij} - \frac{d\varepsilon_v \delta_{ij}}{3}\right)\left(d\varepsilon_{ij} - \frac{d\varepsilon_v \delta_{ij}}{3}\right)}$, where $\varepsilon_v = \varepsilon_{ii}$. Note that dilatancy index is a function of mean stress, in particular at lower mean stress.

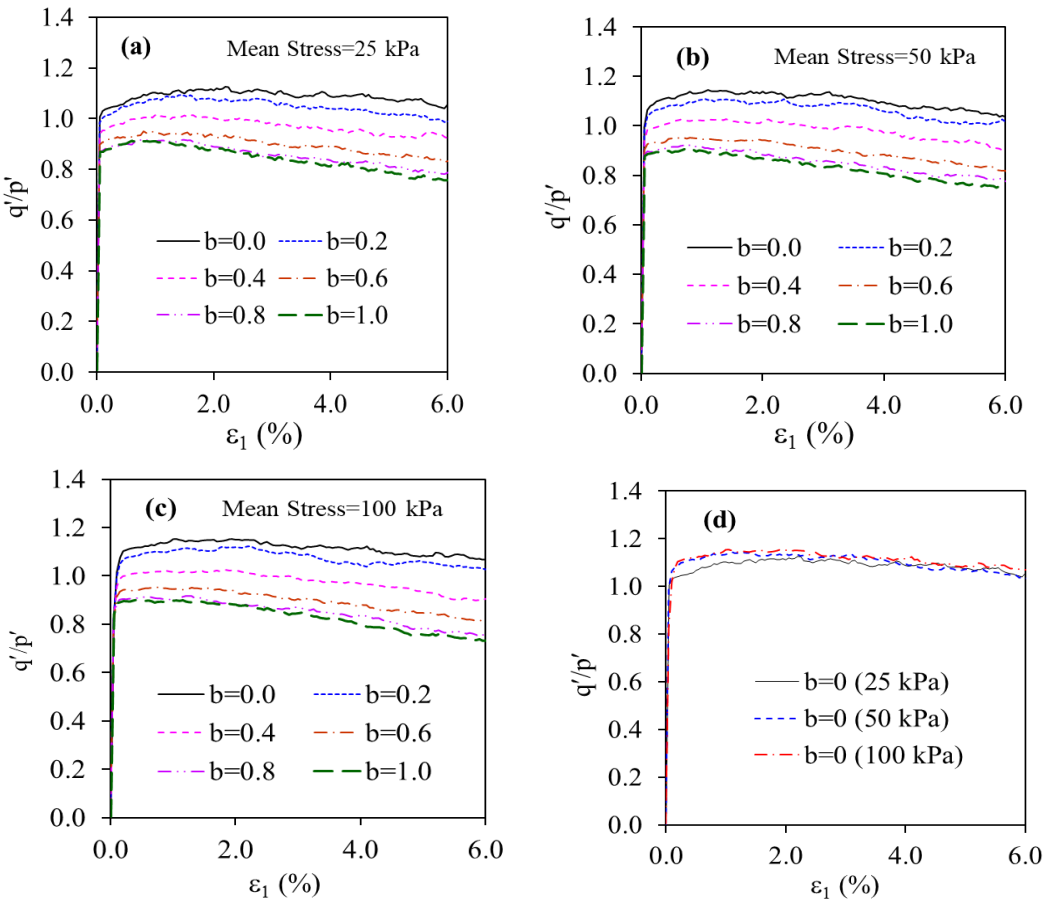

Fig. 1 Evolution of stress ratio with major principal strain for (a) 25 kPa, (b) 50 kPa, (c) 100 kPa at different b values; (d) comparison of stress ratio for different mean stresses

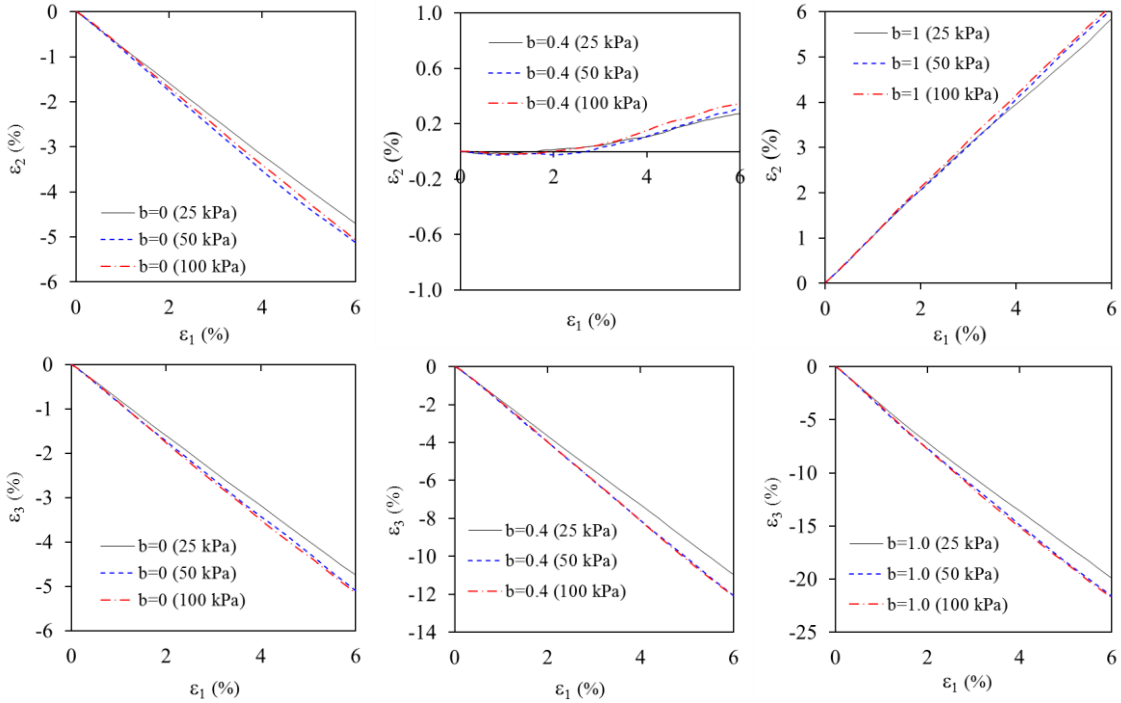

Fig. 2 Evolution of intermediate and minor principal strain components with the major principal strain component for various b values

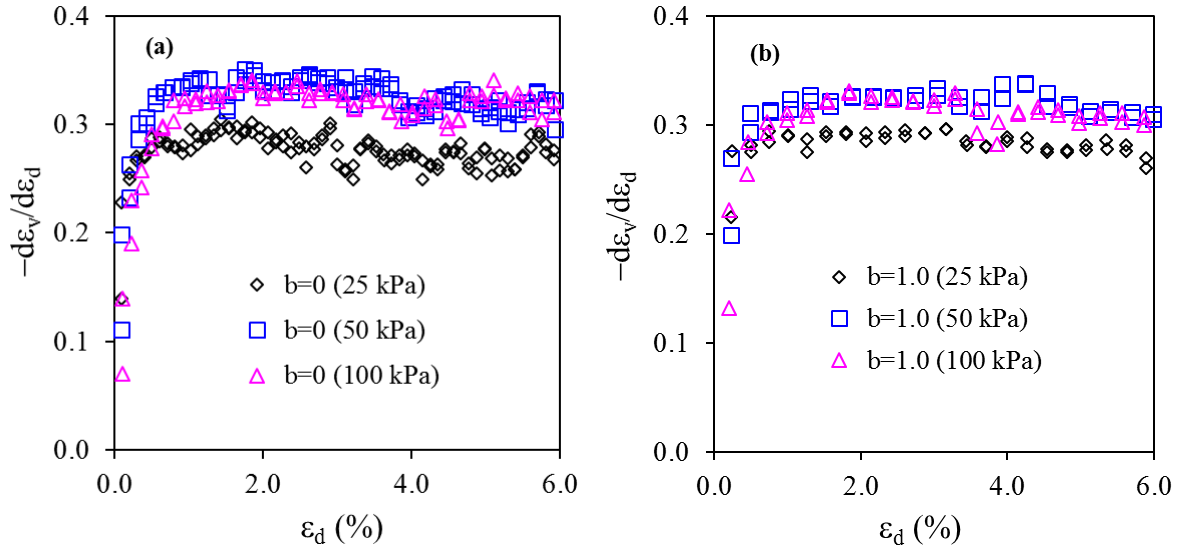

Fig. 3 Evolution of $-d\varepsilon_v/d\varepsilon_d$ with ε_d for different mean stresses and b values

The development of the fabrics can be measured with the help of fabric tensor. The fabric considering all the contacts is quantified using the following tensor (Sazzad et al., 2017):

$$H_{ij} = \frac{1}{N_c}\sum_{\alpha=1}^{N_c} n_i^{\alpha} n_j^{\alpha} \qquad (3)$$

Here, n_i^{α} is the unit contact normal vector of the $\alpha-$th contact and N_c is the number of strong contacts. The evolution of deviatoric fabric, $H_{11}-H_{33}$ considering all contacts involved during the simulation with major principal strain for different mean stresses with b =0 (triaxial compression) and b =1 (triaxial extension) is depicted in Fig. 4. It is noted that the evolution of fabric is mean stress dependent. Moreover, the position of the peak deviatoric fabric is different between b =0 (triaxial compression) and b =1 (triaxial extension). The peak deviatoric fabric yields earlier in case of triaxial extension than triaxial compression while considering all the contacts in quantifying the fabric tensor.

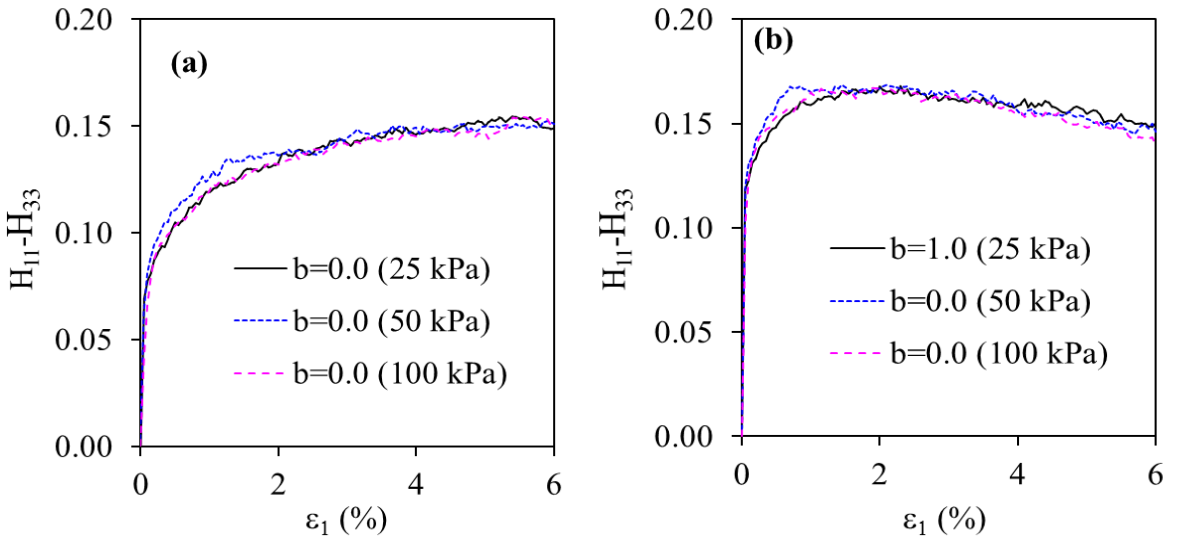

Fig. 4 Evolution of $H_{11}-H_{33}$ with ε_1 for different mean stresses and b values

CONCLUSIONS

The present study depicts the behavior of granular materials considering different mean stresses for general triaxial loading. For this purpose, DEM is applied to capture the discrete behaviors of granulates. A cubic sample consisting of 8000 spheres was prepared and subjected to the variation of intermediate principal stress (i.e., b value). The macro as well as the micro-mechanical responses of the granular system were explored. It is observed that macro-mechanical results are in good agreement with the experimental behaviors for sand. The development of stress as well as strain components are sturdily dependent on the variation of the intermediate principal stress (i.e., b value) and mean stress. The dilatancy index is a function of mean stress, in particular, at lower level of mean stress. The evolution of deviatoric fabric is also mean stress dependent. The maximum deviatoric fabric is peaked earlier in case of triaxial extension than triaxial compression when all contacts are considered in quantifying the fabric tensor.

REFERENCES

Cundall, PA and Strack, ODL. 1979. A discrete numerical model for granular assemblies. *Geotechnique*, 29(1):47-65

Ergun, MU. 1981. Evaluation of three-dimensional shear testing. In: *Proceedings of 10 th International Conference on Soil Mechanics and Foundation Engineering, Stockholm, Sweden*, 1, pp. 593–596

Fukushima, S and Tatsuoka, F. 1984. Strength and deformation characteristics of saturated sand at extremely low pressures. *Soils Found*., 24:30-48

Huang, X, Hanley, KJ, O'Sullivan, C, Kwok, CY and Wadee, MA. 2014. DEM analysis of the influence of the intermediate stress ratio on the critical-state behaviour of granular materials. *Granular Matter*. 16:641-655

Kandasami, RK and Murthy, TG. 2015. Experimental studies on the influence of intermediate principal stress and inclination on the mechanical behaviour of angular sands. *Granular Matter*., 17:217–230

Kuhn MR. 2003 Smooth convex three-dimensional particle for the discrete element method. *J Engrg Mech*, 129:539-547

Kuhn, MR. 2017. Contact transience during slow loading of dense granular materials. *Journal of Engineering Mechanics*, 143 (1):C4015003(9)

Lade, PV. 2006 Assessment of test data for selection of 3-D failure criterion for sand. *Int. J. Numer. Anal. Methods Geomech.*, 30:307 –333

Lam, W-K and Tatsuoka, F. 1988. Effects of initial anisotropic fabrics and σ_2 on strength and deformation characteristics of sand. *Soils Found*., 28:89 –106

Ng, T-T. 2004. Macro- and micro-behaviors of granular materials under different sample preparation methods and stress paths. *Int. J. Solids Struct.*, 41:5871 –5884

Sazzad MM and Suzuki, K. 2010. Micromechanical behavior of granular materials with inherent anisotropy under cyclic loading using 2D DEM. *Granular Matter*, 12:597–605

Sazzad, MM, Suzuki, K and Modaressi-Farahmand-Razavi, A. 2012. Macro-micro responses of granular materials under different b values using DEM. *International Journal of Geomechanics*, 12:220-228

Sazzad MM and Suzuki K. 2013. Density dependent macro-micro behavior of granular materials in general triaxial loading for varying intermediate principal stress using DEM. *Granular Matter* 15:583–593

Sazzad MM. 2014. Micro-scale behavior of granular materials during cyclic loading. *Particuology* 16:132–141

Sazzad, MM and Habib, MA. 2017. Simulation of the behavior of granular materials for varying void ratios using DEM. *International Journal of Advanced Structures and Geotechnical Engineering*, 6(3):96-102.

Sazzad, MM, Poly, SA and Sudipta, NN. 2017. Effect of aspect ratio on the micro-scale responses of granular materials. *International Conference on Mechanical, Industrial and Materials Engineering*, Bangladesh, MS-210:1-6

Sun, D, Huang, W and Yao, Y. 2008. An experimental study of failure and softening in sand under three-dimensional stress condition. *Granular Matter*, 10:187 –195

4th International Conference on Advances in Civil Engineering 2018 (ICACE 2018)
19 –21 December 2018
CUET, Chittagong, Bangladesh
www.cuet.ac.bd

SOIL WASTE REMEDIATION USING VETIVER GRASS

M.S. Islam*, S.M. Shams & F. Sulatna

Department of Civil Engineering, Bangladesh University of Engineering & Technology, Dhaka, Bangladesh.
E-mail:msharifulbd@gmail.com

**Corresponding Author*

ABSTRACT
The objective of the research work was to treat contaminants present in wastewater by applying phytoremediation. Vetiver grass was employed as the phytoremediation plant. Batch experiments were conducted to assess the effectiveness of vetiver grass under controlled environment. Two plastic containers (50 cm × 31 cm × 35 cm) were used as treatment cells. The containers were filled with soil up to a depth of 25 cm and planted with 10 shoots of vetiver grass in two rows. One of the containers was loaded with 30L tap water, while the other was loaded with 30L wastewater collected from Kallyanpur canal. Results from soil and water quality parameter tests reveal that organic matter content of the soil increased from 4.3% to 6.4%, while removal of ammonia and phosphate from wastewater was found to be 96% and 95%, respectively. These results demonstrate that vetiver grass, owing to its unique characteristics like higher biomass, fast growth, strong root system and higher metal tolerance, can play a significant role in the advanced wastewater treatment.
Keywords: Phytoremediation; soil properties; metal tolerances; vetiver grass.

INTRODUCTION

The environment is influenced by human works worldwide. The rate of these consequences is high at present. The domestic and industrial waste discharge is rapidly growing in developing countries due to many reasons including growth of people, urbanization and economic development. Many areas of the world remain polluted with no remediation because it is too costly to treat them with available technologies, which threatens the quality of soils. Additionally, there is scarcity of investment capacity for the establishment and maintenance of sufficient treatment facilities.

Vetiver grass (*Vetiveria zizaniodes* L.) is type of grass that is popularly known as *Binna ghash* in Bangladesh. The suitable temperature for the existence of this grass range from 0 to 50°C. It grows on soil with high acidity from 3.0 to 10.5 at pH scale (Islam et al, 2010). The tensile strength of its roots are 85.10 ± 31.20 MPa, with a root diameter of 0.66 ± 0.32mm. Vetiver hedges are known to survive for more than 100 years (Islam, 2013). As its roots grow downward, vetiver is commonly used for erosion control and to stabilize the soil. It is also used as a good source of animal feed and pest control. Its roots are used for oil extraction. It's fibrous property helps it suitable for making ropes.

The utilization of vetiver grass was first initiated by the World Bank for soil and water conservation in the mid of 1980s. (Truong et al, 2010). This application plays an important role in agricultural system and land management. Owing to it's unique characteristics, vetiver grass is now being utilized as a bioengineering technique for steep slope stabilization, wastewater disposal, phyto-remediation of contaminated land and water, and other environmental protection purposes over the last 20 years (Truong, 2000).

Soil wastage can be defined as the presence of toxic chemicals, pollutants or contaminants in enough concentrations adequate to pose risk to plants, wildlife, humans and the soil itself. It is a part of land degradation. Overthrow of waste materials on land or underground can result in pollution of the soil and groundwater, threaten health of people, and cause unfavourable conditions. Garbage contains moist and decomposable food wastes and rubbish comprises mostly dry materials. Harmful and dangerous substances generated as liquids, solids, sludge or gases by various chemical manufacturing companies, petroleum refineries, paper mills, machine shops, automobile repair shops, and many other industries facilities are included in hazardous wastes. Similarly, continuous discharge of untreated wastewaters into the drainage canals and rivers can have serious adverse impacts on the environment and public health and causes pollution of soil and other water bodies.

In Dhaka, there are 19 primary discharge points mainly to the canals and drains, which, instead of refreshing the city environment, have become dumping grounds for wastes and sites of reproduction for mosquitoes. . In addition, the practice of indiscriminate disposal of solid wastes into canals and low-lying areas further deteriorates the quality of soil. Constructed wetland (CW), which utilizes aquatic plants to treat wastes of soil, could be a promising pre-treatment option of urban waste.

For improvement of water and soil, phyto-remedial technology is a worldwide used mechanism. Phyto-stabilization, phyto-extraction, phyto-volatilisation, phyto-degradation, and rhizofiltration are different mechanisms of phytoremediation. Phyto-stabilization is a mechanism which is used to provide vegetation cover for contaminated soils and prevent wind and water erosion. Phyto-extraction is another mechanism where soil and water contaminants are concentrated and accumulated in their tissues by pollutant tolerant plants. Soluble pollutants are transported to the above ground tissues and volatilize it to the atmosphere in the phyto-volatilisation mechanism. Phyto-degradation is another sub-process where plants, associated with aquatic or soil microorganisms, biodegrade organic pollutants (Bedewi, 2010).

Vetiver grass has short rhizomes and a massive, finely structured root system (Janngam et al., 2010). Its' unique deep root system makes this grass drought tolerant and very difficult to dislodge when exposed to a strong water flow. There are previous reports which shows the use of this plant for phytoremediation of heavy metals, phenol, radionuclides and nuclear waste contaminated soil (Truong et al., 2010). Vetiver grass remove the contaminants present in soil by phyto-extraction process which includes the absorption of pollutants by the root, then root to shoot transfer of the pollutants and at last the pollutants are stored by the plant.

The aim of this research is to observe the growth of the vetiver grass in contaminated soil. Healthy growth of the vetiver grass demonstrates the possibility in treating waste contamination of soil. This paper also represents the effectiveness of plant in removing target contaminants (e.g., ammonia, phosphate, organic matter) from polluted soil and water. Cleaning up the environment is an important focus of this research work.

METHODOLOGY

The experimental set-up for the hydroponic vetiver treatment of the pollutants of wastewater was situated at the roof top of the Civil Engineering Building of BUET premise from March 2017 to August 2017. The plantation process was conducted on 13th March, 2017. The temperature was 26 degree celsius and humidity was 64%. There was enough sunlight. The vetiver grass plant samples were uplifted from the nursery located at the JIDPUS Building, ECE Campus of BUET.

The grass samples were separated into two tillers per clump. Then soil was mixed with stone chips with a proportion of 4:1. After layout of the experimental site, ten shoots were placed at an interval of 9 cm between the columns of the plants and of 13 cm between two rows when the ground was moist [Fig. 1(a)]. The vetiver grasses were planted in two plastic containers with a dimension of 50×31×35 cm (length ×width ×height). A 35 cm long pipe of 2.5 cm dia was connected between the bucket and the vetiver container.

Two types of water were used for conducting experiment. Tap water was available at the location as there was an overhead water tank on the roof top of the Civil Engineering Building of BUET. The tap water was applied to one bucket with the help of a long pipe [Fig. 2]. The bucket was loaded with 30 litre normal water. Wastewater was collected from Kallyanpur canal of Dhaka and another 30 litre bucket was loaded at the time of plantation. There was a gate valve to control the flow rate. As the pipe was at 5% slope with the container where vetiver grass were planted, gradual flow of water to the container was ensured. Both types of water flow at a rate of 2 ml/sec through the pipe. After two months, again 30 litre normal water and wastewater were applied. Growth of vetiver grass was observed regularly. There was heavy rainfall after one month of plantation which increases the growth of the vetiver.

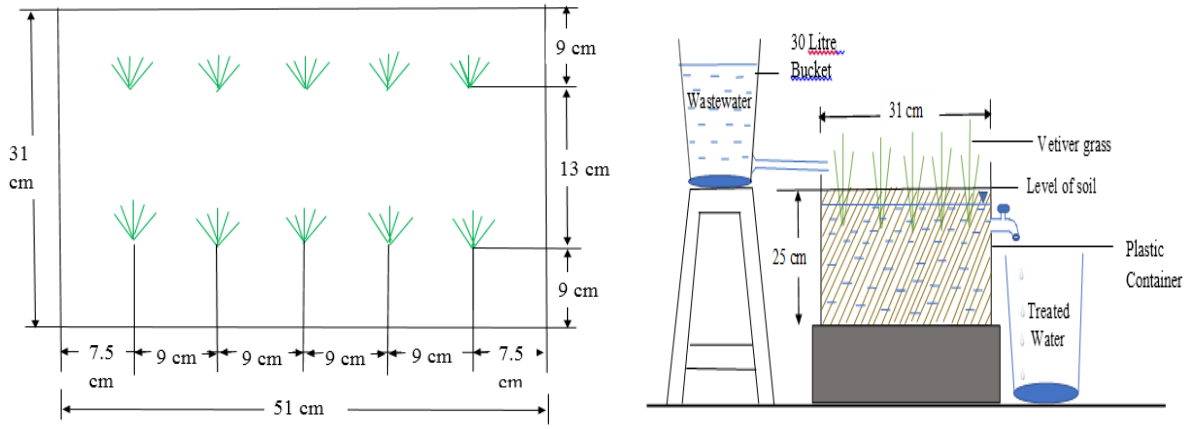

(a) ***(b)***

Figure 1. (a)Details of the plantation, (b) Schematic diagram of waste treatment by vetiver grass

(a) ***(b)***

Figure 2. Full experimental set up for (a) normal water and (b) wastewater

The collected soil sample seems to be clay in naked eye and was blackish in color. It is very important to investigate the basic properties of the soil sample. A soil can commonly be characterized by its grain size, specific gravity and index properties. Before conducting treatment procedure, these basic characteristics of the untreated soil sample were explored at geotechnical engineering laboratory. The specific gravity test of the soil sample was performed according to ASTM D854-14. The Atterberg limits are a basic measure of the critical water contents of a fine-grained soil, its shrinkage limit, plastic and liquid limit. According to ASTM D-4318, Atterberg Limit Test was conducted by using Cassagrande apparatus. Standard test methods for particle size distribution were done according to ASTM D422.

RESULTS AND DISCUSSIONS

Properties of Soil

The specific gravity of the soil is 2.55. It was below the normal range (2.65-2.75) due to presence of some organic content. Liquid limit, plastic limit and shrinkage limit of the collected soil sample are 40%, 22 and 26%, respectively. Plasticity index and flow index are 18 and 16. The co- efficient of uniformity (C_u), the co- efficient of curvature (C_z) and the fineness modulus (F.M.) was found respectively 2.24, 0.62 and 2.93.Grain size distribution curve[Fig. 4] expresses that the soil sample is well graded. All the soil tests were done according to ASTM standard methods.

The organic content test was conducted at an interval of two months and it was found that the content was increased from 4.3% to 6.4%. Increase in organic content indicates that the soil and vetiver grass absorbed the contaminants of the wastewater.

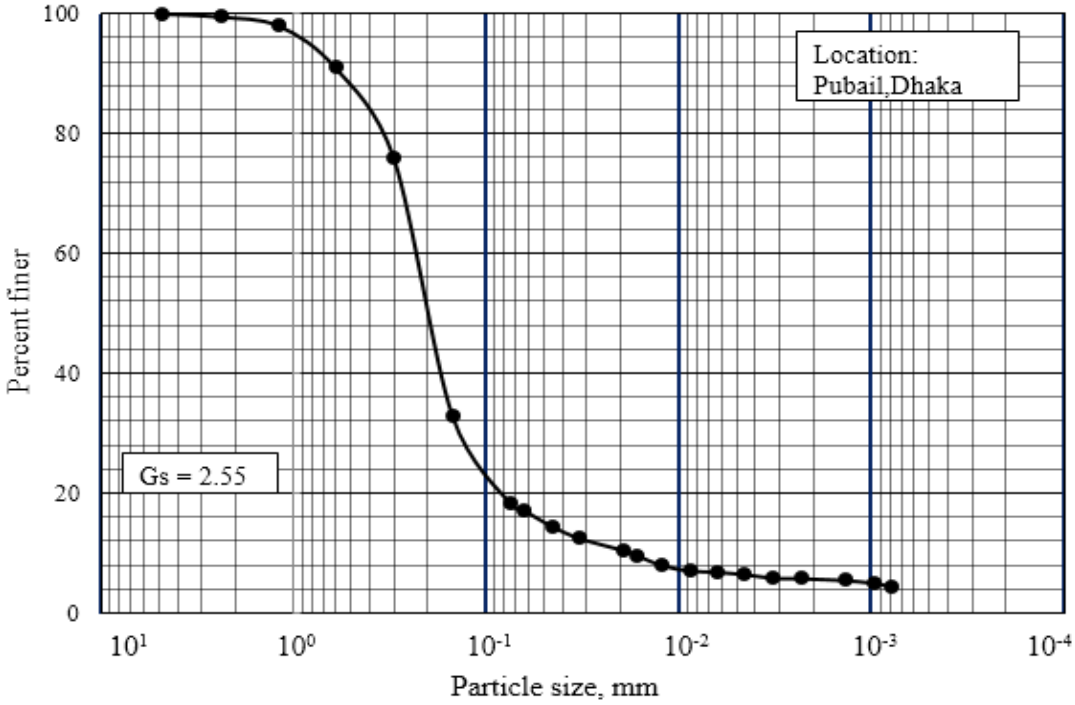

Figure 3. Grain size distribution curve of the soil sample

Classification of Soil

As liquid limit of the soil sample is 40%, plasticity index is 18, the collected soil sample was classified as CL according to USCS classification from the plasticity chart.

Growth of Vetiver Shoots

Growth of the shoots of vetiver grass was observed and it was determined that maximum 8 shoots grew in two months after plantation in wastewater, while 7 shoots grew in normal water. The growth was more in wastewater due to presence of organic matter. The area coverage was approximately 3340 square cm as one shoot goes to adjacent shoot's area when it is grown in height. So the area is huge. The area coverage is approximately same for both types of water. Height of the grass is measured 49 cm in wastewater which is 2 cm longer than the normal water. Height measurement is done after plantation of three months.

Parameters of Water

Table 1 shows the potentiality of vetiver grass in removal of contaminants in percentage form. From this table, it is observed that there was high percentage removal of ammonia (96%), nitrite (68%) and phosphate (95%). On the other hand, nitrate (60%) and COD (54%) were generated.

Table 1. Quality parameters of wastewater and treated water

Water Quality Parameters	Raw Wastewater (mg/L)	Treated Water (mg/L)	Percentage Removal	Percentage Generated
NH3	26.0	1.00	96	—
NO_2	1.0	0.33	68	—
NO_3	1.1	2.70	—	60
PO_4	16.2	0.75	95	—
COD	81.0	176.0	—	54
pH	7.6	7.8	—	—

Generally organic nitrogen is converted to NH_4-N (ammonification process) which may then be nitrified to NO_3-N in nitrification process in the presence of oxygen supply. NO_3-N scatters to anaerobic zone and undergoes de-nitrification process resulting in N_2 and N_2O released to the atmosphere (Gray et al., 2000). NH_4-N is lost to the atmosphere by volatilization process when pH value is higher than 7. The tests revealed that the pH value is always higher than 7, so ammonia removal took place as a percentage of 96 % which is very effective. The amount of ammonia was found about 1 mg /L in treated water. Surely this is above both Bangladesh standard (0.5 mg/L) and WHO guideline value (1.5 mgL/). So, it is helpful to remove (at least lower) the ammonia concentration. The result of the test was satisfactory regarding this. Degradation of Nitrite in treated water was not high but the amount was lowered than raw wastewater. The percentage of nitrite removal is 68% which is gives fairly result.

The statistics data revealed that the phosphate removal is 95% which shows an integrated result. The average value of Phosphate ($PO_4\ as\ P$) concentration is 0.75 mg /L which is within the range of 6 mg/L according to ECR'97. Generally, phosphorus in wastewater may be removed through sedimentation, adsorption and precipitation.

The test results further show that the pH value ranges between 7 and 8 for both types of soil mixed water, and is within the standard range of water set by ECR'97 which is 6.5 to 8.5.

Chemical Oxygen Demand (COD) is the total measurement of all chemicals in the water that can be oxidized. The lab test results indicate that there is an increase of COD value which is unsatisfactory. Organic compounds might have been added externally due to root decomposition, leaf decomposition and plant depth.

A research work was done by Boonsong and Chansiri in Chulalongkorn University, Thailand in 2003. The experiments were carried out under well-ventilated temporary greenhouse at Chulalongkorn University campus. Twelve plastic containers of 0.85 ×1.55 × 0.50 m each (width × length × height) were set up together with the inlet pipe and valve connected to the water storage tank. The wastewater was used for 3, 5 and 7 days' detention time. Laboratory tests of the removal of BOD, phosphate and ammonia were conducted for determining the removal efficiencies of the vetiver grass. Two different domestic wastewater strengths, i.e. HCW: high concentration wastewater and LCW: low concentration wastewaters were continuously distributed to each group. The removal efficiencies for ammonia were ranging from 58% to 62% and phosphate removal was 23% to 35%. But in our study, removal of ammonia and phosphate was found 96% and 95%, respectively.

CONCLUSIONS

In this study, an attempt was made to evaluate the physico-chemical parameters of domestic waste quality before application of vetiver grass and the possibility of vetiver grass in treating contaminants using phyto-remedial technique. Based on the results reported and discussed in the preceding section, the following conclusions are drawn:

(1) Vetiver grass, growing under hydroponic with no supporting medium, can remove pollutants from domestic wastewater. Phyto-extraction mechanism of phytoremediation process worked in this research work.
(2) Growth of the shoots of vetiver grass was observed and it was determined that the area coverage of the shoots of the grass was huge. This growth was very well for both area coverage and height.
(3) The potential of vetiver grass after three weeks hydroponic treatment was found to be efficient for the removal of total nitrogen, and total phosphorous from domestic wastewater. Percentage of removal of ammonia and phosphate was found 96 % and 95%, respectively which is more than expectation.

From above discussions, it can be concluded that the vetiver grass is effective for removal of waste from soil and water.

ACKNOWLEDGMENTS

The authors acknowledge the infrastructural and financial support received from Civil Engineering Department of Bangladesh University of Engineering and Technology (BUET), Dhaka, to conduct the research work.

REFERENCES

ASTM 1989. Annual Book of ASTM Standards, Vol. 04.08, Soil and Rock; Building stones; Geotextiles.

Bedewi, A. 2010. *The Potential of Vetiver grass for Wastewater Treatment.* M.Sc. Engineering Thesis, Department of Soil and Water Conservation Engineering, Haramaya University, Ethiopia.

Environment Conservation Rules (ECR) 1997, Ministry of Environment and Forest, Government of the People's Republic of Bangladesh.

Gersberg, RM; Elkins, BV; Lyon, SR and Goldman, CR. 1986. Role of Aquatic Plants in Wastewater Treatment by Artificial Wetlands. *Journal of Water Resources*, 20(3):363-368.

Islam, MS and Arifuzzaman. 2010. Performance of vetiver grass in protecting embankments in Bangladesh coast against cyclonic tidal surge. 5th National Conference and Expo on Coastal and Estuarine Habitat Restoration, Texas, USA.

Islam, M. S; Shahin HM and Shahriar BAM. 2010. Study on growth of vetiver grass in tropical region for slope protection. *International Journal of GEOMATE*, 5(2):729-734.

Janngam, J; Anurakpongsatorn, P; Satapanajaru, T and Techapinyawat, S. 2010. Phytoremediation: Vetiver Grass in Remediation of Soil Contaminated with Trichloroethylene. *Science Jornal,* 1(2):52-57.

Kramer, U. 2005. Phyto-remediation: Novel Approaches to Cleaning up Polluted Soils. *Journal of National Center for Biotechnology Information,* 16(2):133-141.

Mini, M; Claramma, R; Mathukutty, S and Sandra, M. 2016. Effectiveness of Vetiver System for the Treatment of Wastewater from an Institutional Kitchen. *Journal of Procedia Technology,* 24:203 – 209.

Shams, SM. 2017. *Waste Remediation in Soil Using Vetiver Grass*. B. Sc. Engineering Thesis, Department of Civil Engineering, Bangladesh University of Engineering and Technology, Dhaka, Bangladesh.

Shu, W. and Xia, H. 2003. Integrated Vetiver Technique for Remediation of Heavy Metal Contamination. Available at: https://pdfs.semanticscholar.org/c138/c8d1a23baf046b585044b057e6444e9829bd.pdf [Accessed 2 September 2018].

Summerfelt, ST; Adler, PR; Glenn, DM and Kretschmann 1999. Aquaculture Sludge Removal and Stabilization within Created Wetlands. *Journal of Aquacultural Engineering*, 19(2):81–92.

Truong PTV; Foong, YK; Guthrie, M and Hung, YT. 2010 Phytoremediation of Heavy Metal Contaminated Soils and Water Using Vetiver Grass, *Journal of Biotechnical Engineering*, 11:233-275.

4th International Conference on Advances in Civil Engineering 2018 (ICACE 2018)
19 –21 December 2018
CUET, Chittagong, Bangladesh
www.cuet.ac.bd

AN EXPERIMENTAL AND NUMERICAL ANALYSIS OF IN-SITU EFFECT OF CEMENT HYDRATION AND PULL OUT CAPACITY OF GROUTED SOIL NAILING

A. Ghosh*, S. Chakraborty & A. Juneja

Department of Civil Engineering, IIT Bombay, Mumbai, Maharashtra, India.
E-mail: avishekg90@gmail.com

**Corresponding Author*

ABSTRACT
Soil nailing technique is used as a retaining method for soil excavation and slope stabilization. The effectiveness technique depends on various parameters such as pullout resistance of the nail, the spacing between the nails and the degree of saturation of the soil. Among these parameters, the pullout resistance of soil nail is a paramount criterion for design purpose. In the present study, a number of model 1g model tests have been carried out on cement grouted nails, inserted into the silty soil, to determine the variation of pullout resistance with curing period of the cement grout. Pullout tests have been performed for a curing period of 7, 14 and 21 days. Variation of the moisture content of soil along the length of the nail has been inquired after each pullout test. The reduction in moisture content is the sign of hydration effect by cement grout throughout the process. In the numerical analysis of PLAXIS 2D, the reason behind the reduction in pull-out strength has been investigated and from these analyses presented that, interface between grouted nail along with soil should be maintained and superintended properly if the grouted nail has done at optimum moisture content of soil. A relationship has been developed between moisture content and $R_{interface}$.

Keywords: moisture content; pullout resistance; soil nailing; $R_{interface}$

INTRODUCTION

Soil nailing technique has been widely used for highway and pavement excavations, rapid constructions, widening the purpose road under existing bridge ends, revision flexibility in the construction process and repair, reconstruction of the existing soil nailing structure, (Hong et al. 2003). It is a cost-effective method. Grouted soil nail is a modified soil nailing technique to enhance the existing soil condition.

The determination of pull out force is an important parameter for designing purpose of soil nailing earthwork. When sliding occurs of huge soil mas due to the natural or manmade cause, a critical slip surface will develop to pull-out of grouted soil nail situated in the stabilizing zone by that soil mass, (Akis 2009). When soil masses try to detach from grouted soil nailed system with induces outward shear stress along the nail, pull out reinforcements occur due to skin friction stresses on the grouted soil nails, (Schlosser 1982).

The pullout capacity of grouted nail depends upon many parameters. In this study, the effect of moisture content of soil on the pullout capacity of grouted soil nail had been performed. Typical test outputs indicate that due to the infiltration effect of cement grouting in the surrounding soil, creates an interlocking relationship between the soil nail which increases bond resistance between soil and nail, (Cheng Yu et al. 2013). Though during the process, due to the hydration effect of cement hardening the moisture content to the surrounding soil decreases. Aytekin and Nas (1998) stated that hydrated cement fetches up to 20% of its own weight of water from the surrounding soil. Cheng Yu et al. (2013) stated

that the moisture content of soil samples decreases closer to grouted body soil compares to the distant soil sample. The moisture content ratio varies from 0.15 to slightly less than 1 to the surrounding soil of grouted material, where different laboratory pull out test had been conducted by the different researcher, (Zhou 2008, Chu 2003, Chai and Hayashi 2005). So change in the moisture content in the soil will ultimately affect the final strength of the soil. As a result, an extensive experimental work was carried out to determine the effect of hydration of the cement grout on the pullout capacity.
However, in most of the case, horizontal pull out tests have been carried out to determine the effect of moisture content reduction on pullout capacity of grouted soil nail. It has been observed that the pull out capacity increases as the moisture content reduces.
Although Franzen,(2001) proposed that, in case of the limitation of inserting horizontal nail in the site, vertical nail pull out capacity can be an alternative one to predict the pull out capacity. Albeit the cement hydration effect on the vertical pull out capacity hasn't been determined yet.
The primary objective of performing the numerical analysis in PLAXIS 2D is to check how well the experimental results agreed with the theory along with assessing and predicting the pull out strength of grouted soil nail. Though in this method the soil nail interaction can't be clearly identified (Rawat and Gupta 2016)

1

METHODOLOGY

Experimental Setup:

According to IS (IS 2720(IV)), the soil was fine grain soil. The soil property is given in Table 1

Table 1. Characteristics of tested soils

Parameters	Powai Soil
Moisture content(OMC)	18%
Degree of saturation[1]	90.47%
Liquid limit	50.2%
Plastic limit	33.4%
Shrinkage limit	15.5%
Cohesion (kN/m^2)	22
Angle of internal friction(Φ)	27^0
Sand	44%
Silt	38%
Clay	18%

[1]Degree of saturation at OMC.

Tank dimension was 690*340*555 mm3. The nail head was firmly connected to a load cell 50 kN. On each layer of 120 mm, height was filled up 0.55 kN of soil and compacted thoroughly. The soil was being compacted using a hammer of 0.025 kN and tamped for 30 times for each layer [Figure 1].
To minimize the influence of the front wall, the front wall was lubricated by glycerin, (Palmeira, E.M & Milligan 1989).

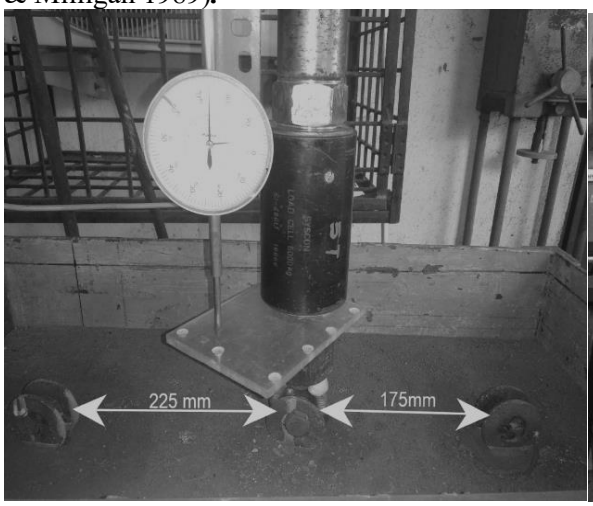

Figure 1. Nail Setup

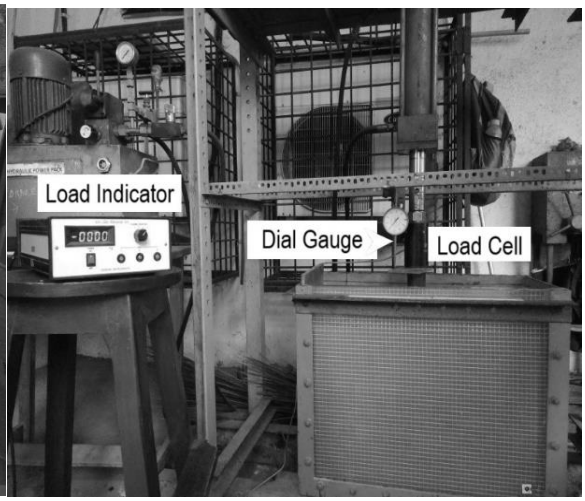

Figure 2. Complete setup

Numerical Analysis:

The diameter of numerical modeling is taken as 0.345 m*0.55 m, as this model is taken as axisymmetric.[Figure 3]. The model is taken as axisymmetric, because in plane strain the length of excavation should be significantly larger than the width of the excavation (Tjie-liong 2016).

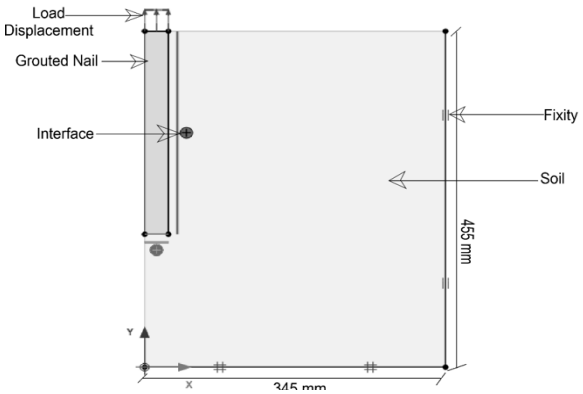

Figure 3. Soil nail model

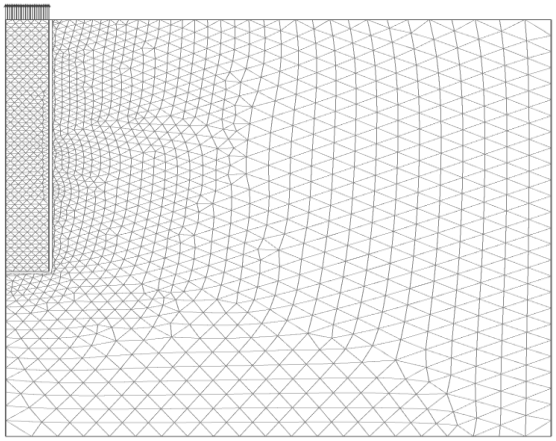

Figure 4. Mesh generation

In case of determining the global factor of safety coarse mesh analysis has been used, (Singh and Babu 2010, Rawat and Gupta 2016). In this analysis for better output, vicinity of the grouted nail surface very fine mesh has been used [Figure 4].

In soil modeling, Mohr-Coulomb model is taken for analysis purpose. According to Rawat (2016) in finite element analysis (FEM), the stress-strain relationship is one of the most important parameters and this parameter creates a perfect elastic-plastic behavior of the material.

Shivakumar and Babu (2010) stated that, depending upon the numerical simulation it's quite essential to consider the bending and axial stiffness of soil nail and considering the parameter plate element is the most suitable system to predict the actual behaviour of soil nail, Table 2.

Table 2:Nail and grouting parameters

Parameters	Value
Height of the tank	0.45m
Nailing	Grouted
Material Model	Elastic
Elastic modulus of reinforcement, E_n	200 GPa
Elastic modulus of grout, E_g	22.0 GPa
Length of nail, L	0.28 m
Diameter of the nail	0.016 m

RESULTS AND DISCUSSION

Experimental:

The change of moisture content due to cement grouting the soil from the surrounding grouting and at a radial distance of 45 mm, 60 mm and 90 mm from the center of grouted nail[Figure 5]

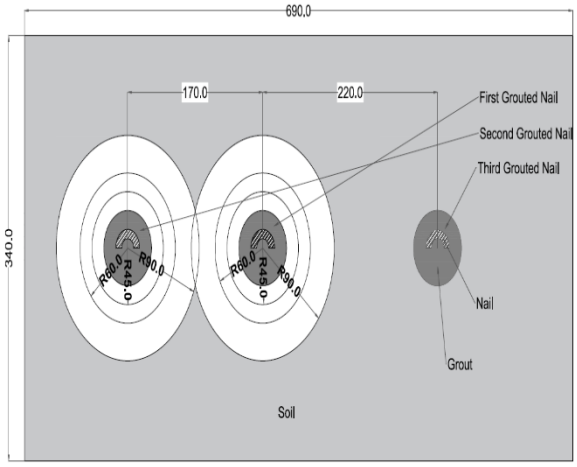

Figure 5..Moisture content measurement zone (top view) (All dims. are in mm)

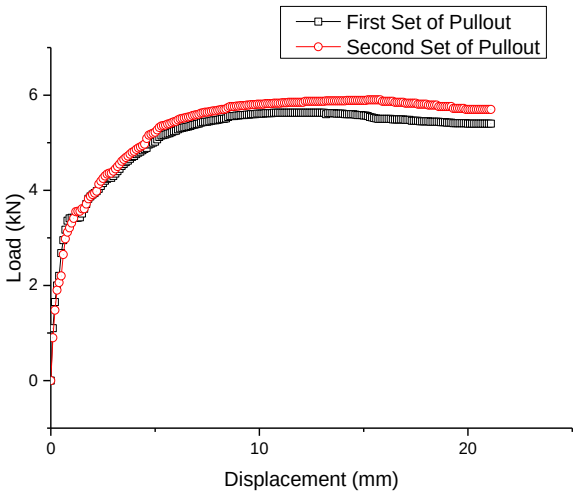

Figure 6. Load vs. Displacement after 7 days

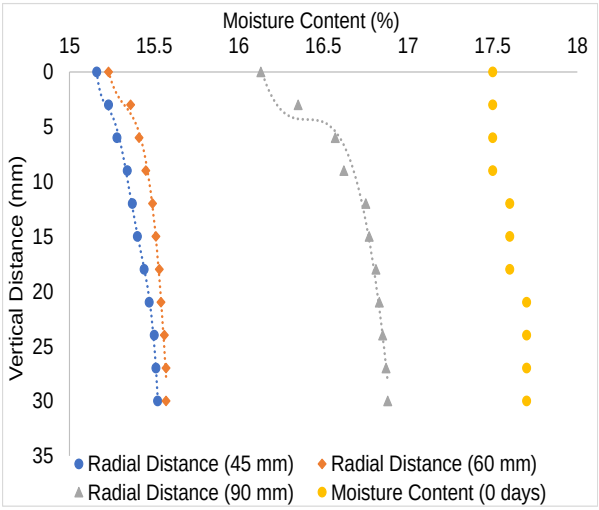

Figure 7. Moisture content in between first and second nail (After 7 days)

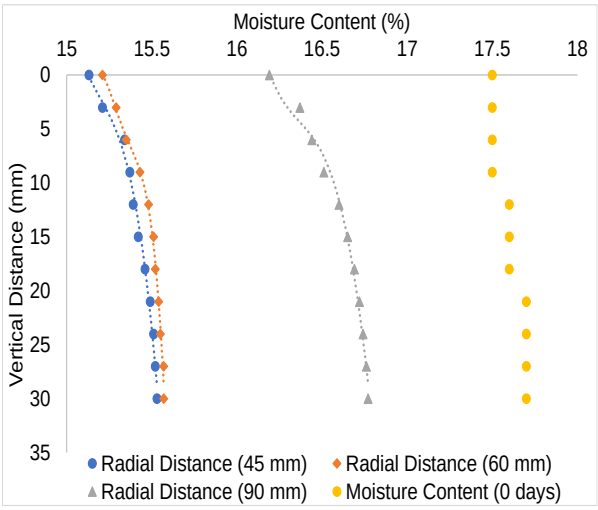

Figure 8. Moisture content in between second and third nail (After 7 days)

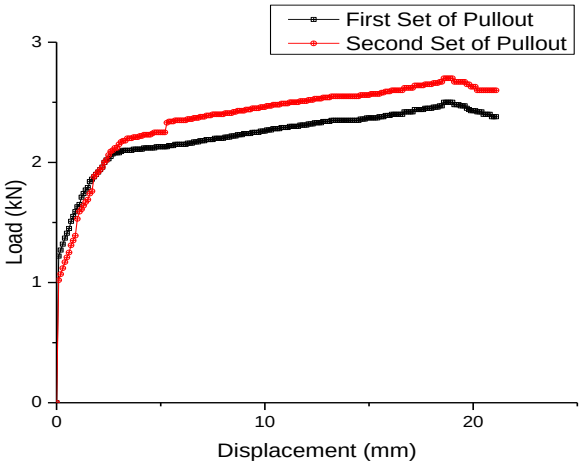

Figure 9. Pullout force vs. Displacement after 14 days

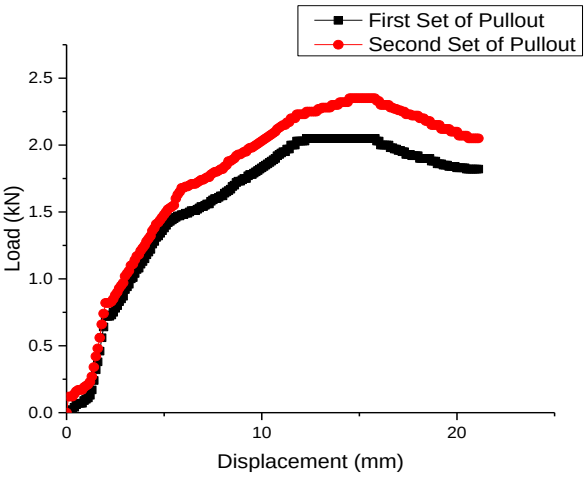

Figure 5. Pullout force vs. Displacement after 21 days

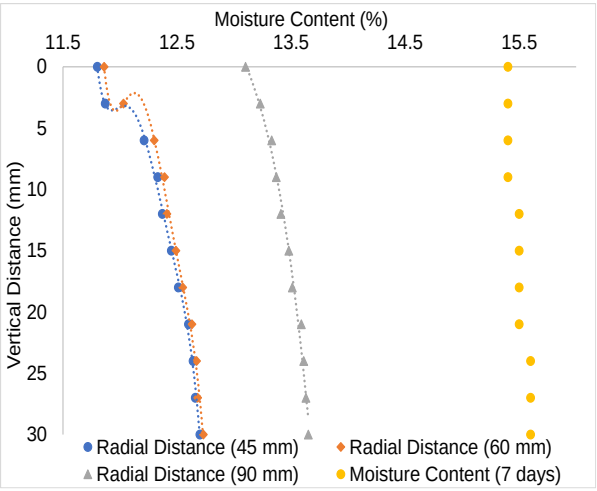

Figure 11.Moisture content in between second and first nail (After 14 days)

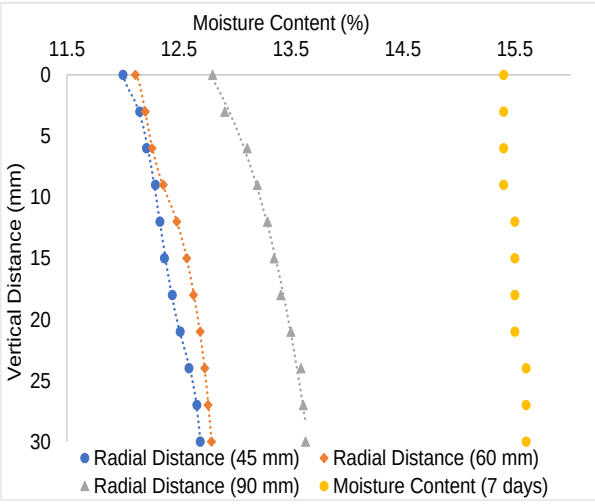

Figure 12. Moisture content in between second and third nail (After 14 days)

After 14 days the data indicates that the moisture content at 45 mm which is around the 2nd grouted nail is around 12.5 %. But in the case of 90 mm distance from the 2nd nail which is in between second and 1st soil nail zone the moisture content is around 14% [Figure 11].

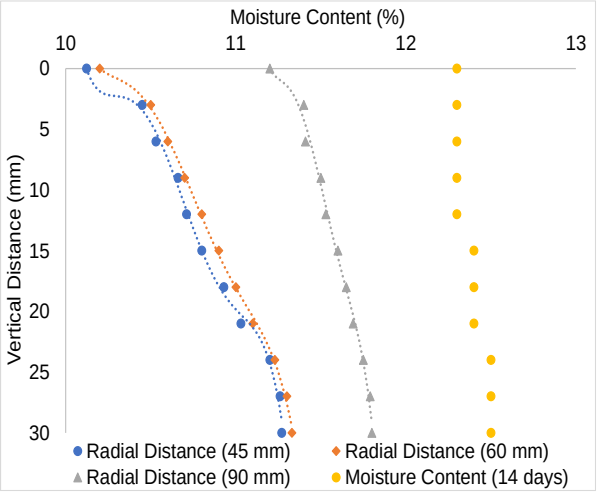

Figure 13. Moisture content in between third and second nail (After 21 days)

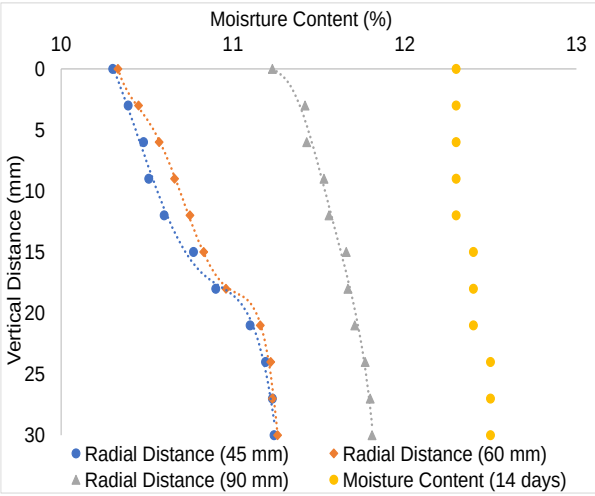

Figure 14. Moisture content in between second and first nail (After 21 days)

The data indicate that the moisture content at 45 mm which was around the 3rd pulled out soil nail was around 10.65%[Figure 13] whereas at 90 mm distance it was around 12% [Figure 14].

Numerical Results:

From numerical experiment, it had been shown that when the grouted nail had displaced about 0.03 m difference was 17.5% between the experimental. After 14 days and 21 days the variance is 6% and 13% [Figure 15].

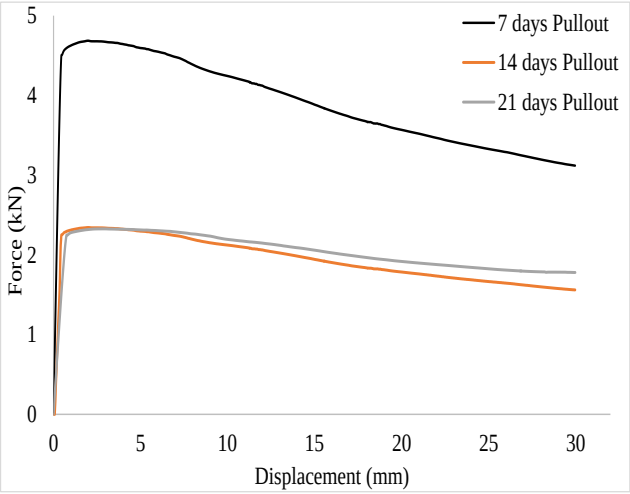

Figure 15. Pull out strength of grouted nail

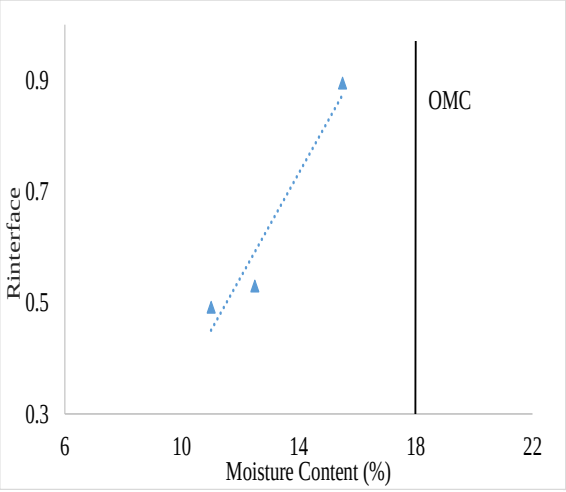

Figure 16. $R_{interface}$ vs. Moisture content

CONCLUSION

Due to the hydration effect or by the development of heat transfer of cement grouting there's always a probability of higher or lower strength of pull out as crack generates throughout the soil mass. This may be due to the creation of a gap between the grouted nail and soil interface with a reduction in moisture content. Heat hydration does not have any sort of binding or strength gaining property but it definitely causes evaporation of free water in capillary pores of soil and thus increases drying shrinkage As the moisture content reduces, the volume of soil shrinks. Shrinkage limit of the soil is 15% and the optimum moisture content (OMC) is 18%. Therefore, the volume of the soil shrinks as the moisture content reduced from the OMC. Subsequently, the contact between the soil and the nail reduces and it is the cause for the reduction in the pull-out strength. As the moisture content goes less than the shrinkage limit (after 14 and 21 days of curing), the volume shrinkage becomes less. That is why the variation in pull-out strength after 14 days is minimal. Therefore it can be concluded that the pull out strength after 14 days should be considered for the design purpose.

In the staged construction of numerical analysis, it had been found that the pull out strength reduced as the interface value between soil and grouted nail reduced. The $R_{interface}$ value reduced to 0.9 to 0.49 from 7 to 21 days later. The pull out strength reduced to 4.7kN to 2.33 kN/rad after 21 days. The $R_{interface}$ values provided in the numerical analysis shows inverse behaviour with direct shear interface friction test value.

Though in this experiment the pull out had done only in the vertical direction which is may be considered in case of pile foundation when due to hydration effect of cement the skin friction failure can occur to pile with soil interface and drag down movement will create an uneven settlement of structure.

REFERENCES

Journal Article

Aytekin, M., and Nas, E. 1998. Soil Stabilization with Lime and Cement, *Technical Journal of Turkish Chamber of Civil Engineers*, 9(1): 471–477.

ASTM D5321/D5321M. 2014. Standard Test Method for Determining the Shear Strength of Soil-Geosynthetic and Geosynthetic-Geosynthetic Interfaces by Direct Shear.*American, Society for Testing and Materials International*, (17): 1–11

Chai, X. J., and Hayashi, S. 2005. Effect of Constrained Dilatancy on Pull-Out Resistance of Nails in Sandy Clay, *Proceedings of the Institution of Civil Engineers-Ground Improvement*, 9(3): 127–135.

Cheng Yu, H., Jian-hua, Y. I. N., and Hua-fu, P. E. I. 2013. Comparative Study on Pullout Behaviour of Pressure Grouted Soil Nails from Field and Laboratory Tests, *Journal of Central South University*, 13(20): 2285–2292

Franzén, G. 2001. Prediction of Pullout Capacity of Soil Nails, *International Society for Soil Mechanics and Geotechnical Engineering*, 3: 1743–1747

Hossain, M., and Yin, J. 2014. Dilatancy and Strength of an Unsaturated Soil-Cement Interface in Direct Shear Tests, *International Journal of Geomechanics*, 15(5): 1–10
Hong, Y. S., Wu, C. S., and Yang, S. H. 2003. Pullout Resistance of Single and Double Nails in a Model Sandbox, *Canadian Geotechnical Journal*, 40(5): 1039–1047
IS 2720(IV). 1985. *Grain Size Analysis*.
Palmeira, E.M & Milligan, G. W. . (1989). "Scale and Other Factors Affecting the Results of Pull-Out Tests Of Grids Buried In Sand." ICE, 3, 511–524.
Potyondy, J. G. 1961. Skin Friction between Various Soils and Construction Materials, *Geotechnique*, 11(4): 339–353
Pradhan, B., Tham, L. G., Yue, Z. Q., Junaideen, S. M., and Lee, C. F. 2006. Soil–Nail Pullout Interaction in Loose Fill Materials, *International Journal of Geomechanics*, 6(4): 238–247
Rawat, S., and Gupta, A. K. (2016). "Analysis of a Nailed Soil Slope Using Limit Equilibrium and Finite Element Methods." *International Journal of Geosynthetics and Ground Engineering*, 2(4), 34.
Schlosser, F. 1982. Behaviour and Design of Soil Nailing, Proc. of Int. Symposium., Asia Institute of Technology, Bangkok, Thailand, 399–419.
Singh, V. P., and Babu, G. L. S. (2010). "2D Numerical Simulations of Soil Nail Walls." *Geotechnical and Geological Engineering*, 28(4), 299–309.
Tjie-liong, G. (2016). "Common Mistakes on the Applicatoin of Plaxis 2D." *International Journal of Applied Engineering Research*, 9(21), 8291–8311.
Yin, J., and Zhou, W. 2009. Influence of Grouting Pressure and Overburden Stress on the Interface Resistance of a Soil Nail, *Journal of Geotechnical and Geoenvironmental Engineering*, 135(9): 1198–1208

Thesis

Akis, E. (2009). "The Effect of Group Behavior on the Pull-Out Capacity of Soil Nails in High Plastic Clay." Doctor of Philosophy, Middle East Technical University, Turkey.
Chu, L. 2003. *Study on the Interface Shear Strength of Soil Nailing in Completely Decomposed Granite Soil*, Master of Philosophy, The Hong Kong Polytechnic University, Hong Kong.
Morris, J. D. 1999. *Physical and Numerical Modelling of Grouted Nails in Clay.* Magdalen College, Doctor of Philosophy, University of Oxford.
Zhou, W.-H. 2008. *Experimental and Theoretical Study on pullout resistance of grouted soil nails*, Doctor of Philosophy, The Hong Kong Polytechnic University, Hong Kong.

4thInternationalConference on Advances in Civil Engineering 2018 (ICACE 2018)
19 –21 December 2018
CUET, Chittagong, Bangladesh
www.cuet.ac.bd

ESTIMATION OF PILE BEARING CAPACITY USING DIFFERENT METHODS

T. Islam[1] & M. S. Islam[2*]

Department of Civil Engineering, Bangladesh University of Engineering and Technology, Dhaka, Bangladesh.
E-mail:ti.cebuet187@yahoo.com
**Corresponding Author*

ABSTRACT
Piles are vertical structural elements which can be driven, bored or drilled. For determining the allowable and ultimate load carrying capacity of pile, a number of arbitrary or empirical methods are used. The paper focuses on determining the pile bearing capacity using α – method, β – method and SPT method specified in BNBC 2015. Spreadsheets for estimating pile capacity from basic parameters using BNBC 2015 formulas are developed. The proportion of load bearing capacity generated by either end bearing or skin friction depends on the sub-soil conditions and pile type. In this paper, the capacities from pile load test, α – method, β – method and SPT method are compared. It is found that allowable capacity calculated from β - method is more acceptable as it varied with pile load bearing capacity than that of SPT method and α – method. But the SPT method is used for all types of soils and also cost-effective, so this method can be used for pile capacity determination if pile load test is not possible.

Keywords: α – method; β – method; BNBC; load test; pile capacity; SPT method

INTRODUCTION

The columnar elements in a foundation and part of structures are called piles which have the function of transferring load from the superstructure through weak compressible strata and water, onto stiffer or more compact and less compressible soils or onto rock (Tomlinson, 1994). The entire area of soil supporting the foundation is exposed, inspected and sampled to ensure that its bearing characteristics conform to those deduced from the results of exploratory boreholes and soil tests. While materials for piles can be precisely specified, and their fabrication and installation can be controlled to conform to strict specifications and code of practice requirements, the calculation of their load-carrying capacity is a complex matter which at the present time is based partly on theoretical concepts derived from the sciences of soil and rock mechanics, but mainly on empirical methods based on experience.

Piles may be loaded axially or transversely. Different methods to calculate pile load capacity has been developed. Early discussions of consequences of the residual load were presented by Terzaghi (1942), Hunter and Davisson (1969), Meyerhof (1976), Fuller (1983), Briaud (1984), and others (Fellenius, 2002). Pile load carrying capacity depends on various factors, including pile characteristics such as pile length, cross-section, and shape; soil configuration and short and long-term soil properties; and pile installation method (Wrana, 2015). Some widely used and recent methods specified in BNBC 2015 for pile design are: α – method used to calculate the short-term load capacity (total stress) of piles in cohesive soils; β – method used to calculate the long-term load capacity (effective stress) of piles in both cohesive and cohesionless soils and direct measurements of residual load by Standard Penetration Test (SPT).In most cases, these component resistance forces are estimated using soil parameters from laboratory tests (Yasin et al, 2009). The objectives of the study of estimating pile load capacity are to review the applicability of the BNBC 2015 specified equations and formulas for estimating pile

capacity, also to determine the load capacity of piles from load test and to compare with the capacity estimated using BNBC equations.

METHODOLOGY

In the first approach, ultimate load bearing capacity from the three methods of BNBC are determined and compared with load test data are shown in graphs and tables. In the second approach, comparison with ultimate pile capacity by BNBC formula and extrapolated load-settlement curves are exhibited. Every related data like soil property, dry density (γ_d), moisture content (ω), undrained shear strength (c_u), SPT value and discussions on soil stratification and soil profiles were collected (Rahaman, 2008).

Location

The piles under this study were installed at the campus of the Independent University of Bangladesh (IUB) located at Basundhara, Dhaka. The whole area was divided into five zones according to the test piles for comparing the load test data with the ultimate load bearing capacity followed by different methods (Islam, 2017). The divisions according to our calculation are shown in Table 1.

Table 1 Distributed zones under IUB area and piles under zones

Zones	Test Piles under zones	Boreholes under zones
1	TPA 1	BH-5, BH-6, BH-7, BH-8, BH-13, BH-28, BH-30, BH-32, BH-36
2	TPA 2	BH-9, BH-10, BH-11, BH-16, BH-26, BH-27, BH-29, BH-31, BH-33, BH-34, BH-35
3	TPB 1	BH-23, BH-24, BH-25, BH-39
4	TPB 2	BH-1, BH-2, BH-3, BH-4, BH-15, BH-19, BH-38
5	TPC 1	BH-17, BH-18, BH-21, BH-20, BH-22, BH-37

Sub-Soil Characteristics

The soil profile of the whole project area was determined by conducting SPT. By sub-soil investigation and test data, it was possible to get a total idea about soil layers of the project area. The borehole location is in Basundhara, Dhaka. In this region, the soil is known as "Dhaka Clay Residuum" which consist medium stiff to stiff clay layer underlain by dense sand layer. The top soil contains soft to firm clayey silt layer, where the bottom layer is medium stiff to very stiff clayey silt in maximum case. In a few boreholes, a layer of fine sandy silt and decomposed wood are found. The SPT value for top soft soil ranged within 1-11, and for bottom stiff soil, the SPT value varied from 12-50. The range of liquid limit of the soil was 37-70 and plasticity index varied within 8-47 (Islam, 2017). So, according to the Unified Soil Classification System (USCS), it can be classified that almost all soil samples fall within CL and CH group.

Parameters for Estimation of Pile Bearing Capacity

Load test was possible conducting on three test piles. The details of the test piles are given in Table 2.

Table 2 Details of test piles

Zone No.	Pile No.	Diameter (mm)	Length (m)
2	TPA-2	750	30
3	TPB-1	600	30
5	TPC-1	500	30

Determination of Static Bearing Capacity of Pile

The skin friction, $Q_s = A_s f_s$, end bearing $Q_b = A_b f_b$ and ultimate bearing capacity $Q_u = Q_s + Q_b$ are calculated. The methods by which pile loads are calculated in this paper are described below (BNBC, 2015).

(1) α-Method:

In this method, unit skin friction resistance on the pile f_s is expressed as the adhesion between pile and soil, c_a. Skin frictional resistance on unit surface area of pile, $f_s = c_a = \alpha c_u$, where, c_u = undrained cohesion or undrained strength (s_u) of soil, α = a factor called adhesion factor.

As such, skin friction is calculated from equation (4).

$$Q_s = \alpha c_u A_s \quad (1)$$

here, α = 1 for clays with $c_u \leq 25$ kN/m^2, α = 0.5 for clays with $c_u \geq 70$ kN/m^2, α = 1- [(c_u-25)/70] for clays with 25 kN/m$^2 \leq c_u \leq 70$ kN/m^{2}and A_s = skin friction area (perimeter area) of the pile = Perimeter × Length

The end bearing is expressed as equation (2).

$$Q_b = (c_u)_b (N_c)_b A_b \quad (2)$$

where bearing capacity factor, $N_c = 6[1 + 0.2(\frac{L}{D_b})] \leq 9$

here, D_b = the diameter of the pile at base, L = the total length of pile, A_b = end bearing area of the pile = Cross-sectional area of pile tip (bottom). The end bearing resistance on unit tip area of pile, $f_b = (c_u)_b (N_c)_b$ should not exceed 4.0 MPa.

(2) β-Method:

The skin friction coefficient, $f_s = K\sigma_z^{'} \tan\phi' = \beta\sigma_z^{'}$

where $\beta = K \tan\phi' = K_o \tan\phi' = (1 - \sin\phi')\sqrt{OCR}$, here, ϕ' = the effective angle of internal friction of soil, OCR = Over Consolidation ratio. For normally consolidated clay, β varies from 0.25 to 0.29, correction factor of β for very long pile = $\log(\frac{180}{L}) \geq 0.5$

The end bearing capacity is determined using equation (3).

$$Q_b = (\sigma_v^{'})_b (N_q)_b A_b \quad (3)$$

where N_q is a bearing capacity factor that depends on the angle of friction ϕ' of the soil at the base of the pile.

(3) Axial capacity of bored piles using SPT Method:

For cohesive soil,

$$f_s = 1.2\overline{N}_{60} \leq 70kPa \text{ (in kPa)} \quad (4)$$

$$f_b = 25N_{60} \leq 4000\,kPa \text{ (in kPa)} \quad (5)$$

where $\overline{N}_{60}$ is the average N-value (SPT value) over the pie shaft length and N_{60} is the N-value (SPT value) in the vicinity of pile tip.

For sand,

$$f_s = 1.0\overline{N}_{60} \leq 60kPa \text{ (inkPa)} \quad (6)$$

$$f_b = 15N_{60}(\frac{L}{D}) \leq 100\,N_{60} and \leq 4000\,kPa \quad (7)$$

For non-plastic silt,

$$f_s = 0.9\overline{N}_{60} \leq 60kPa \text{ (inkPa)} \quad (8)$$

$$f_b = 10N_{60}(\frac{L}{D}) \leq 100\,N_{60} and \leq 4000\,kPa \quad (9)$$

Maintained loading static axial compression test was carried out on the test piles following the standard procedure outlined in ASTM D1143-81 (1989). All the load tests were conducted with application of load equal to two times the allowable, load where the loads were applied in eight increments (Islam, 2017).

Pile Capacity Determination from Load Test

Bearing capacity of piles was estimated according to some of the recommendations proposed by various researchers to obtain the ultimate or failure load from the load-settlement curve. They are:

(a) According to De Beer (1968), the load-settlement curve is plotted in log-log plot and the point of intersection of the two straight lines thus obtained is the failure load.
(b) Mazurkiewicz (1972) assumed that the load-settlement curve is parabolic after an initial straight portion and the ultimate load can be obtained by geometric construction by drawing sets of equidistant settlement lines to intersect load-settlement curve and then drawing vertical lines from the intersections to intersect the load axis. From the points of intersections of the vertical lines with the load axis, a set of 45˚ lines are drawn to intersect the next vertical lines. The line joining the intersection points cuts the load axis at the ultimate load.
(c) Van Weele (1957) suggested that at higher loads, the load-settlement curve tends to be a straight line. A straight line is drawn from the origin and parallel to the straight portion of the curve, separates the total load into skin friction and point bearing at every stage. The former becomes constant after a certain stage and gives the ultimate frictional resistance. In this study, the frictional resistance has been determined from extrapolated load-settlement curves following this method. End bearing calculated as 9c (where c is cohesion) along with this frictional resistance gives the total ultimate pile capacity.

RESULTS AND DISCUSSIONS

The bearing capacities calculated by three methods described in BNBC 2015 and from load-settlement curves are shown to establish the best method among all, comparisons are presented.

Estimation of Pile Capacity by BNBC Methods

The sample calculations by the three methods according to BNBC 2015 of test piles corresponding to respective boreholes are determined by developing a spreadsheet inputting the parameters of piles (Islam, 2017). The ultimate load bearing capacities obtained by BNBC methods are listed in Table 3.

Table 3 Ultimate Load Bearing Capacity of Pile by Static Methods of BNBC

Pile No.	Pile Diameter (mm)	Static Bearing Capacity from BNBC (Tons)		
		α	β	SPT
TPA-2	750	78.9	205.5	133.1
TPB-1	600	58.1	137.8	100.6
TPC-1	500	45.6	106.2	58.3

Determination of Pile Capacity from Load-Settlement Curves

Load settlement curves obtained from load test data are drawn to determine the ultimate load bearing capacity. The different methods to calculate load bearing capacity and included calculation procedures are described in details (Islam, 2017). A sample graph of TPA-2 plotted according to Indian Standard Criteria is shown in Fig. 1. The field test data are taken from previous research (Rahaman, 2008).

Comparison among Ultimate Bearing Capacities from Pile Load Test and BNBC Methods

The ultimate bearing capacities determined by all methods corresponding to the test piles with different diameters are summarized in Table 4. Fig. 2 represents the comparisons of ultimate bearing capacities determined by all methods.

Table 4 Ultimate Load Bearing Capacity of Pile by Static Methods of BNBC and Load Test Data

Pile No.	Pile Diameter (mm)	Static Bearing Capacity from BNBC (Tons)			Bearing Capacity from Extrapolated Load Settlement Curves (Tons)			
		α	β	SPT	De-Beer (1972)	Mazurkiewicz (1957)	Van Weele (1973)	Indian Standard Criteria
TPA-2	750	78.9	205.5	133.1	390.0	435.0	442.0	380.0
TPB-1	600	58.1	137.8	100.6	280.0	335.0	318.0	280.0
TPC-1	500	45.6	106.2	58.3	245.0	280.0	271.0	250.0

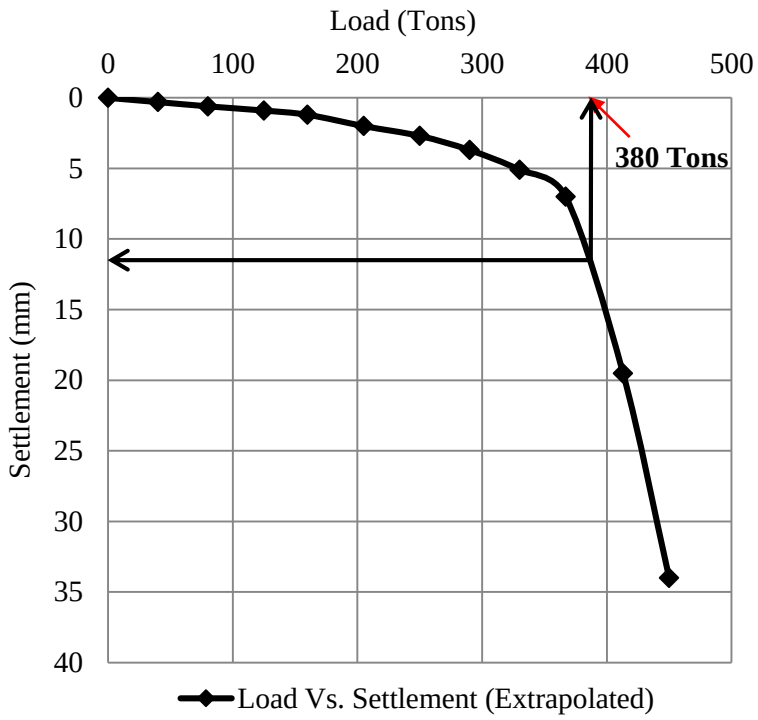

Fig. 1 Pile capacity by Indian Standard Criteria from extrapolated load settlement curve (TPA-2)

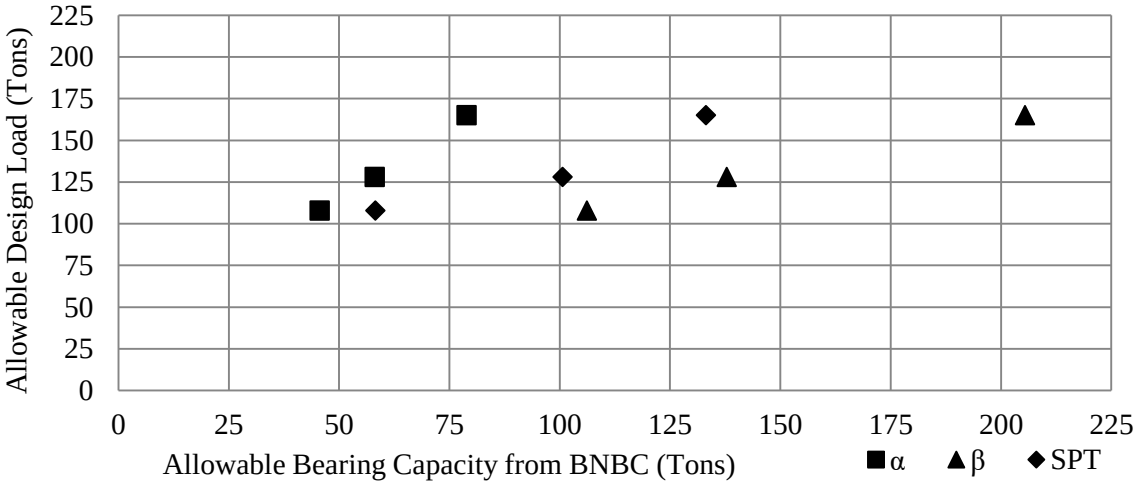

Fig. 2 Graphical representation of ultimate bearing capacities determined by all methods

Comparison among Allowable Bearing Capacities from Pile Load Test and BNBC Methods

The allowable load bearing capacity was determined from load test data by extrapolated load-settlement curves. To compare with the allowable bearing capacities of the test piles, the methods specified in BNBC 2015, a factor of safety of 2.5 is used. Table 5 outlines the comparison between the allowable bearing capacities determined by load test data and by static methods of BNBC.

Table 5 Allowable Load Bearing Capacity of Pile by Static Methods of BNBC and Load Test Data

Pile No.	Pile Diameter (mm)	Allowable Bearing Capacity from BNBC (Tons)			Allowable Design Load (Ton)
		α	β	SPT	
TPA-2	750	31.6	82.2	53.2	165
TPB-1	600	23.2	55.1	40.2	128
TPC-1	500	18.2	42.5	23.3	108

CONCLUSIONS

The purpose of this paper is to establish the applicability of the methods prescribed in BNBC 2015. The main findings of the paper are:

(1) A factor of 3.7 can be multiplied with the allowable capacity calculated from the SPT method to adjust with the allowable pile load test capacity.
(2) The allowable load bearing capacity from β – method is to be multiplied with a factor of 2.3 to get the allowable load bearing capacity from pile load test.
(3) By α – method, pile capacity determined by all criteria and formulas from BNBC is much lower than the capacity found from pile load test. The allowable bearing capacity of the pile determined from the equations of α – method is to be multiplied by a factor of 5.6.

It can be said from all discussions that the capacity of the pile load tests, in general, showed a reasonably good agreement with the calculated ultimate bearing capacity by theoretical equations of BNBC, especially by β – method and SPT method. Along with, β – method is based on both short and long-term loading, which depends on the angle of internal friction, φ. This method is not applicable where $\varphi = 0^o$, in case of pure clay. α – method is related to short-term loading that means undrained shear strength, c_u; so in sandy soil, this method is not applicable as $c_u = 0$. So, SPT method is recommended to determine the actual capacity of a pile following BNBC as it is used for all types of soils, in clay and sand or non-plastic silt, and shows feasible results.

ACKNOWLEDGMENTS

The authors acknowledge the infrastructural support received from Bangladesh University of Engineering and Technology (BUET), Dhaka, Bangladesh for carrying out the research work.

REFERENCES

Bangladesh National Building Code (BNBC). Final Draft 2015.Vol. 2. Chapter 3:6-177 to 6-181; 6-188 to 6-189; 6-207 to 6-208; 6-763 to 6-765. (Accessible in 10-09-2016, http://www.ovice.or.kr/filebank/construction/OVIC16032003/OVIC16032003.pdf)

Davisson, MT. 1973. High Capacity Piles. Innovations in Foundation Construction, Soil Mechanics Division. Illinois, Secretariat, ASCE, Chicago. USA: 81-112.

Fellenius, BH. 2002. Determining the True Distributions of Load in Instrumented Piles. ASCE International Deep Foundation Congress "Down to Earth Technology". Orlando, Florida.

Islam, T. 2017. Estimation of Pile Capacity Using Different Methods Specified by BNBC 2015.BSc. Thesis, Department of Civil Engineering, Bangladesh University of Engineering and Technology, Dhaka-1000.

Mazurkiewicz, BK. 1972. Test Loading of Piles According to Polish Regulations. Preliminary Report No. 35, Comission on Pile Research, Royal Swedish Academy of Engineering Services, Stockholm.

Meyerhof, GG. and Murdock, LJ. 1953. An Investigation of the Bearing Capacity of Some Bored and Driven Piles in London Clay.*Geotechnique*.3: 267.

Rahaman, MS. 2008. *Axial Load Capacity of Cast-in-situ Bored Piles in Stiff Dhaka Clay*. *MSc.* Thesis.Department of Civil Engineering of Bangladesh University of Engineering and Technology (BUET), Dhaka-1000, Bangladesh.

Terzaghi, K. 1943. *The Theoretical Soil Mechanics*. John Wiley & Sons, New York: Victor F. B. de Mello.

Tomlinson, MJ. 1994. *Pile Design and construction practice*. Fourth edition: 1-2, 99-100, 373.

Van Weele AF. 1988. *Cast-in-situ piles – Installation methods, soil disturbance and resulting pile behavior, Deep Foundations on Bored and Auger Piles*. Balkema, Rotterdam: 219-228.

Wrana, B. 2015. Pile load capacity-calculation methods. Civil Engineering Department, Institute of Structures Mechanics, Soil-Structure-Interaction Branch, Cracow University of Technology, Poland.

Yasin, SJM.; Alam, MJ.; Islam, MS. and Siddique, A. 2009. Static load capacity of RCC piles in soft clay – a case study. *Proceedings of the 17th International Conference on Soil Mechanics and Geotechnical Engineering*: 1325-1328.

4th International Conference on Advances in Civil Engineering 2018 (ICACE 2018)
19 –21 December 2018
CUET, Chittagong, Bangladesh
www.cuet.ac.bd

IMPROVEMENT OF SOFT SOIL BY PHYSICAL AND CHEMICAL INTERACTION

[1]Md. Salman Rahman, [2]Sultan Mohammad Farooq &[2*]Md. Aftabur Rahman

[1]Former undergraduate student, Department of Civil Engineering, Chittagong University of Engineering & Technology, Chittagong-4349, Bangladesh
[2]Faculty, Department of Civil Engineering, Chittagong University of Engineering & Technology, Chittagong-4349, Bangladesh
[*]Corresponding author: maftabur@cuet.ac.bd

ABSTRACT

Geo-Jute play a vital role as they improve the bearing capacity of the soft soil. Jute plants are grown most part in Bangladesh. Geo-Jute is our local material and easily available. Using various by-product of industry in soil improvement has not only economic benefit but also having some environmental and social benefit. Steel industry produces GGBFS in large scale. In order to improve the properties of soft soil, a study of a newly proposed mixture of Geo-Jute and Ground granulated blast furnac slag described and reported in the paper. To investigate and understand the effect of the mixture of Geo-Jute and Ground granulated blast furnac slag on engineering properties of soft soil, an optimum percentage of GGBFS was determined based on the density of soil. Soil specimen was collected from Firingi bazar (Inorganic clay) area of Chattogram city. Soil specimens were prepared and tested with different percentage of Geo-jute ((i.e. 1%, 2%, 3%, 4%, 5% by weight of the parent soil) with the Optimum percentage of GGBFS at the curing periods of 0, 7, 14 and 28 days. Physical properties of soil samples had performed to classify the soil. Unconfined compression test, Direct shear test and Compaction were performed on samples to understand the effect of these mixes on their engineering properties. It had been found that, the optimum amount of GGBFS varied from 20-30% and the optimum amount of Geo-Jute varied from 3-4% depending on the type of soil. The values of angle of internal friction increase very slowly for the soil specimen. The compressive strength of treated soil increases 0 to 50% of untreated soil with an increase of curing period with varying amount of Geo-jute and optimum slag for the soil specimen. The angle of internal friction for treated soil specimen increases from 2 to 15 %. After the total investigation and analyzing the whole work following conclusion can be drawn that Geo-jute in addition to slag is very much economical for stabilization of soft soil.

Keywords: Soil improvement, Geo-jute, GGBFS, Physical and chemical interaction

INTRODUCTION

Day by day because of the fast industrialisation and urbanization in the Asian country, the provision of excellent bearing soil is rare. Most of the realm of urban town in Asian country principally built up with structure, the land available currently having soft soil with low bearing capacity. thus it's necessary to carry out more and more civil engineering construction over soft soil, which results in institution and development

of varied ground improvement techniques like soil improvement and reinforcement (Cai, Shi, Ng, & Tang, 2006).

There is numerous ground improvement technique accessible but for a developing country like Bangladesh because of lack of resources and with increasing price of technique and materials have influenced the engineers to seek out some new alternatives. Besides soft soil treatment typically performed by combination soft soils with cement, lime, GGBFS, Geo-fibre or numerous pozzolanic material. (Ngoc, Turner, Huang, & Kelly, 2016).

Geo-Jute could be a native material of Asian country and it's simply out there thus it is used in problematic soil improvement considering economy, environmental and social advantages. varied literature says that Geo-Jute is eco-friendly and environmental property material. (Khan & Binoy, 2012).

According to National Slag Association (NSA) GGBFS is an environmental sustainable element and has no threat to human health thus it takes into account as nonhazardous element(Slags, 1980). In per annum great quantity of is burden uselessly this can consume giant areas and loss of time and cash for handling this once disposal.

The mechanics of the improvement of soil is physical or chemical in nature (Nicholson, 2015). The strength behaviour of soil was related to curing period, higher strength was notified at higher curing days (Higgins, 2005). The main objective of this paper introduces thereby the usefulness and suitableness of environmentally friendly admixture like Geo-Jute and GGBFS as the ground improvement for up the pertinent engineering properties of a soft soil, e.g. Unconfined compressive strength, cohesion, and angle of internal friction considering the economic condition and property.

METHODOLOGY

Materials

The soil sample was collected from Fringi Bazar area of Chattogram city of Bangladesh at a depth of 6ft from the mean ground level.

Geo-Jute is collected from the native market of Chattogram and also the GGBFS is provided by Royal cement limited, Chattogram, Bangladesh.

Experimental Program

At the specific start of the examination according to requisition the index properties of the soft soil e.g. specific gravity (ASTM, 2000), particle size distribution (ASTM D422, 2007), consistency limit(ASTM D4318, ASTM D 4318-10, & D4318-05, 2005), USC classification were determined in the laboratory according to the test indicated in the section. The unconfined compressive strength and angle of internal friction of the specimen were determined by unconfined compression test and direct shear test followed by ASTM D 2166 (ASTM D 2166, 2000) and ASTM D 3080 (Method, n.d.) respectively. This unconfined compressive strength test was performed on specimens at a strain rate of 2.4mm/min. The direct shear test was carried out at the strain rate of 1mm/min under the normal load of 6.5 kg, 13 kg and 26 kg.

Table

Table No 1: Index Properties

Serial Number	Index Properties		Values
1	Specific Gravity		2.45
2		Liquid Limit	37.5

	Consistency limit	(%)	
		Plastic Limit (%)	16.49
		Plasticity Index (%)	21.01
3	USC Classification		CL (Inorganic clays of low to medium Plasticity)
4	Compaction Study	Optimum Moisture Content (%)	19.2
		Maximum Dry Density (kN/m3)	15.8

Table No 2: Engineering Properties

Serial Number	Properties	Soil specimen
1	Cohesion (KPa)	171.5
2	The angle of internal friction (degree)	25^0

Table No. 3

Maximum dry density and optimum moisture content tested at different GGBFS content

Mix Type	**Maximum Dry Density (kN\m3)**	**Optimum Moisture Content (%)**
Only Soil	15.8	19.2
Soil +10%Slag	15.85	19.1
Soil +15%Slag	15.87	19.5
Soil +20%Slag	16.1	20
Soil +25%Slag	16.6	19.5
Soil +30%Slag	16.3	19.9
Soil +35%Slag	16.15	20

Table No. 4

Summary of unconfined compressive strength of soil specimen

Mix type	**Unconfined Compressive Strength(MPa)**			
	0 Days	**7 Days**	**14 Days**	**28 Days**
Only Soil	0.343	0.367	0.414	0.413

Soil + Optimum Slag(25%)+0% Geo-Jute	0.384	0.428	0.443	0.495
Soil + Optimum Slag(25%)+1% Geo-Jute	0.410	0.567	0.632	0.661
Soil + Optimum Slag(25%)+2% Geo-Jute	0.447	0.602	0.653	0.678
Soil + Optimum Slag(25%)+3% Geo-Jute	0.735	0.756	0.761	0.771
Soil + Optimum Slag(25%)+4% Geo-Jute	0.738	0.857	0.861	0.884
Soil + Optimum Slag(25%)+5% Geo-Jute	0.395	0.429	0.452	0.503

Table No. 5

Summary of Angle of Internal Friction (Degree) of the soil specimen

Mix type	**Angle Of Internal Friction (Degree)**			
	0 Days	**7 Days**	**14 Days**	**28 Days**
Only Soil	25	26	26	26.65
Soil + Optimum Slag(25%)+0% Geo-Jute	27	27.51	29.44	30
Soil + Optimum Slag(25%)+1% Geo-Jute	29	33	33.55	34
Soil + Optimum Slag(25%)+2% Geo-Jute	30.25	33.5	32.5	34.2
Soil + Optimum Slag(25%)+3% Geo-Jute	31	34	33.22	34.96
Soil + Optimum Slag(25%)+4% Geo-Jute	28.36	30.53	29.6	29.22
Soil + Optimum Slag(25%)+5% Geo-Jute	27.92	26.87	28	28.6

Figure

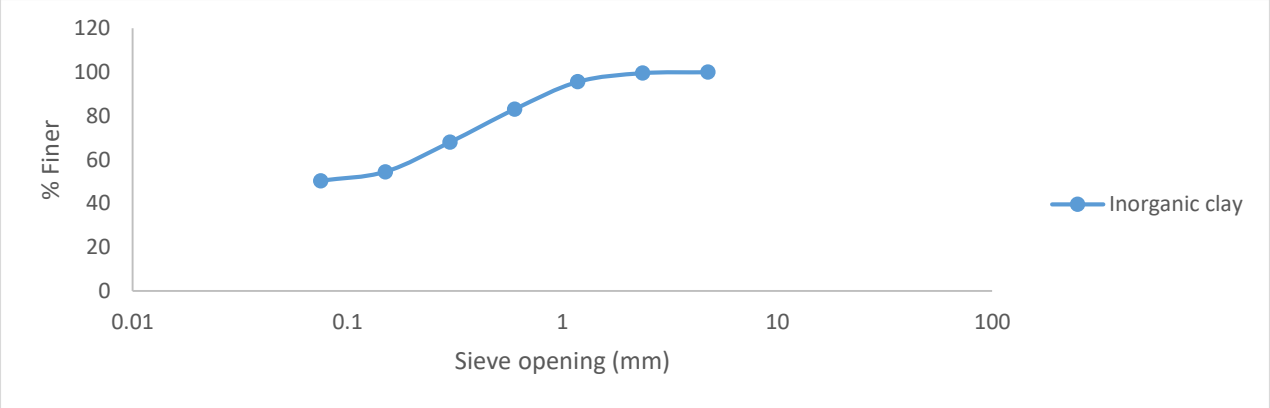

Fig.1. Gradation study of two different types of clay

RESULT AND DISCUSSIONS

Variation of maximum density of the specimen

The values of maximum density and optimum moisture content of the specimen at different GGBFS content was listed in table 4. From Fig. 1 it is observed that the maximum density of soil increases with the GGBFS content up to 25% after that it decreases. So the optimum GGBFS content for the soil is 25%.

Variation of unconfined compressive strength

The values of unconfined compressive strength soil specimen are listed in Table 4. It is observed that the unconfined compressive strength of the soil specimen increasing with the optimum amount of slag (25%) with an increase of Geo-Jute content up to 4%. After that, the compressive strength decreases with increasing Geo-Jute content. The immediate unconfined compressive strength of untreated Soil specimen is 0.343 MPa on the other hand maximum unconfined compressive strength of treated Soil specimen at 28 days of curing is 0.884 MPa.

Variation of angle of internal friction

The values of angle of internal friction increase very slowly for the soil specimen. Angle of internal friction increases with the with increase with Geo-Jute content up to 3%. After that, the angle of internal friction decreases with increasing geo- jute content. The immediate angle of internal friction of untreated Soil specimen is 25^0 whereas for treated soil the corresponding value is 34.96^0 at 28 days of curing

CONCLUSIONS

Both Geo-jute and GGBFS have some influence on the unconfined compressive strength, angle of internal friction and also failure pattern of soft soil. It has been shown that addition of Geo-jute along with GGBFS brings out large-scale change on the properties of soft soil which improve the soil strength. The soil improvement depends on various factor such as Geo-jute amount, GGBFS content, duration of curing. As the curing period increases the rate of improvement of soft soil also increases. The unconfined compressive strength and angle of internal friction increases with a certain amount of Geo-jute and GGBFS content after that it decreases. The optimum gain in strength appears to be with about 3 to 4 % Geo-Jute with 20-30% of slag. The maximum unconfined compressive strength for treated soil specimen with optimum slag (25%) in addition to optimum slag (4%) is 0.884 MPa at 28 days of curing whereas the immediate unconfined compressive strength of the corresponding untreated soil is 0.343 MPa. The increases are more than 100%. The rate of increases of MDD and OMC with varying amount of slag is not significant MDD of untreated

soil specimen is 15.8 kN\m^3 whereas the MDD of treated soil is 16.6 kN\m3 for 25% of slag. The with optimum slag (25%) in addition to optimum slag (3%) is 34.96^0 at 28 days of curing whereas the immediate angle of internal friction of the corresponding untreated soil is 25^0. The increases are about 40%. Geo-jute improves the properties of soft soil by jute fibre reinforcement technique and GGBFS contribute to improvement by chemical stabilization. It will possible to apply the combination of Geo-jute with GGBFS to improve the properties of the soft soil of foundation, subgrade soil or slope. After the total investigation and analyzing the total work, following conclusion can be drawn that Geo-Jute in addition to slag is very much economical for stabilization of soft soil.

REFERENCES

ASTM. (2000). D854 - Standard Test Methods for Specific Gravity of Soil Solids by Water Pycnometer. *Astm D854*, *2458000*(C), 1–7. https://doi.org/10.1520/D0854-10.2

ASTM D422. (2007). Standard Test Method for Particle-Size Analysis of Soils. *Astm*, *D422-63*(Reapproved), 1–8. https://doi.org/West Conshohocken, PA.

ASTM D4318, ASTM D 4318-10, & D4318-05, A. (2005). Standard Test Methods for Liquid Limit, Plastic Limit, and Plasticity Index of Soils. *Report*, *04*(March 2010), 1–14. https://doi.org/10.1520/D4318-10.

Cai, Y., Shi, B., Ng, C. W. W., & Tang, C. sheng. (2006). Effect of polypropylene fibre and lime admixture on engineering properties of clayey soil. *Engineering Geology*, *87*(3–4), 230–240. https://doi.org/10.1016/j.enggeo.2006.07.007

Higgins, D. (2005). Soil stabilisation with ground granulated blastfurnace slag. *UK Cementitious Slag Makers Association (CSMA)*, (September), 1–15. Retrieved from http://www.ukcsma.co.uk/files/csma_report_on_soil_stabilisation.pdf

Khan, A. J., & Binoy, T. H. (2012). Top Soil Erosion Control Using Geo-Jute.

Method, S. T. (n.d.). Standard Test Method for Direct Shear Test of Soils Under Consolidated Drained, *04*, 1–7.

Ngoc, P. Van, Turner, B., Huang, J., & Kelly, R. (2016). Experimental Study on the Durability of Soil-Cement Columns in Coastal Areas, (June), 3–7.

Nicholson, P. G. (2015). Admixture Soil Improvement. *Soil Improvement and Ground Modification Methods*, 231–288. https://doi.org/10.1016/B978-0-12-408076-8.00011-X

Pycnometer, W., & Com-, U. (2000). Standard Test Method for Unconfined Compressive Strength of Cohesive Soil 1. *Current*, *04*.

Slags, S. (1980). NATIONAL SLAG ASSOCIATION IRON and STEEL SLAGS -.

4th International Conference on Advances in Civil Engineering 2018 (ICACE 2018)
19 –21 December 2018
CUET, Chittagong, Bangladesh
www.cuet.ac.bd

BEHAVIOR OF VERTICAL STRIP ANCHOR EMBEDDED IN PURELY FRICTIONAL SOIL UNDER COMBINED LOADING

R. Rahman, M. S. Islam, S. K. Debnath& M.Rokonuzzaman*

Department of Civil Engineering, Khulna University of Engineering & Technology, Khulna,
Bangladesh.
E-mail:rokon@ce.kuet.ac.bd
**Corresponding Author*

ABSTRACT

This paper focuses on the behaviour of vertical strip anchor in frictional soil under vertical, horizontal and moment loading. 2D finite-element models incorporating a Mohr-Coulomb elastoplastic material model were validated against existing upper bound and lower bound solution for the evaluation of failure envelope in all planes at different friction angles. According to the numerical results, it is found that there is significant effect of eccentricity on resultant pullout capacity factors and the failure envelopes are independent of friction angle.

Keywords: FEM analysis; inclined and eccentric loading; combined loading; Interaction diagram.

INTRODUCTION

Plate anchors cannot be used as a permanent solution due to the uncertainties arisen in predicting anchor performances (Yang et al., 2010). Plate anchors are used widely in transmission tower, sheet piles, retaining wall, underwater structures and mooring system for floating structure (Hanna et al., 2014; Merifield and Smith, 2010; Sutherland et al., 1983). Because the available design approach is reasonable for the normal loading (in-plane) conditions. But the anchor can be subjected to the horizontal and overturning moment (out-of-plane line) loadings due to the movement of wind, wave, and many other environmental loadings. These out-of-plane loads can significantly reduce the pullout capacity of the anchor embedded in a particular location and for a particular soil. The majority of the earlier studies either experimental or numerical have focused on the anchor uplift capacity in-plane loading condition (Rowe, 1978; Merifield et al., 2003; Song and Hu, 2005; Song et al., 2008; Wang et al., 2010). Literature reveals that limited studies have performed under combined loading in clay soil (Neill et al., 2003; Yang et al., 2010; Elkhatib, 2006; Wu et al., 2017) and neither of these studies have focused on frictional soil. For this reason, this study focuses on the behaviour of anchor under various loading condition such as inclined loading, eccentric loading and combined loading.

In this study, a two-dimensional finite element analysis (2D-FE) is carried out to investigate the pullout capacity of a strip vertical plate anchor in sand under different loading conditions. Different probe tests are conducted to determine the failure envelope in vertical horizontal plane (V:H, where V>0, H>0 and M=0), vertical moment plane (V:M, where V>0, M>0 and H=0) and horizontal moment plane (H:M, where H>0, M>0 and V=0). The effects of the friction angle, inclination and eccentricity on the pullout capacity factor are also investigated.

METHODOLOGY

2D finite element analysis is conducted through a commercial software ABAQUS to understand the behavior of vertical anchor under combined loading condition (V, H, M). A strip plate anchor of width B =0.5m is embedded at a depth of 0.5m from the existing ground surface. To determine the pullout capacity of the embedded anchor, conventional small strain analysis is carried out. The contact is assumed to be rough between the anchor and the soil.

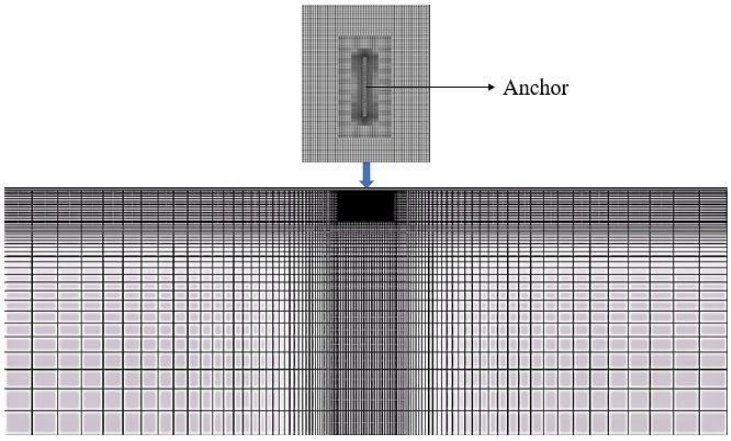

Figure 1: Finite element model used for numerical analysis

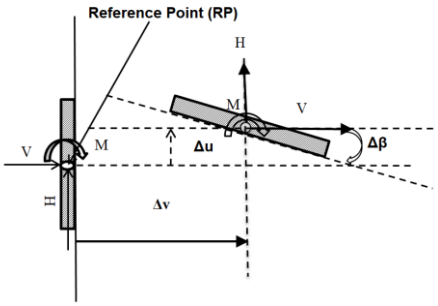

Figure 2: Sign convention adopted

An elastic-perfectly plastic associative Mohr-Coulomb material model is used for purely frictional soil with modulus of elasticity, E= 30 MPa; Poisson's ratio= 0.33. In order to avoid numerical difficulties a minimum cohesion $c/\gamma B=0.25$ is chosen for all analysis (Zhu and Michalowski, 2005; Shafiqul Islam et al., 2017). The anchor is modelled as rigid body with thickness, t= L/20= 0.025 m, young's modulus 10^7 times that of soil and Poisson's ratio 0.15. The soil domain is extended to 25B in horizontal and 10B in vertical directions, respectively. The analysis was based on 8-noded quadrilateral elements of type CPE8R with reduced integration as shown in Fig. 1. The base of the mesh is fixed in both horizontal and vertical coordinate directions. In order to obtain more accurate results, elements are kept very small (L/60) near the plate, increasing gradually in size and moving away from the plate (Nouri et al., 2017). The displacement-based analyses are performed to determine the collapse load of the anchor. All results are presented here as non-dimensional forms.

The centroid of anchor represents the reference point (RP) for application of combined load components V, H and M as shown in Fig. 2. The anchor displacements Δv (vertical), Δu (horizontal) and $\Delta\beta$ (moment) are also illustrated in Fig. 2. This study obeys a right-handed rule and clockwise positive convention proposed by Butterfield et al., (1997).

RESULTS AND DISCUSSIONS

Uplift capacities of vertical strip anchor in current FEM study is compared with various experimental and numerical data available in literature shown in Fig. 3. Results from the present FE study matches well with the upper bound (UB) and lower bound (LB) solution of (Merifield and Sloan, 2006). The result obtained by surcharge method (Neely et al., 1973) for friction angle 40° is seemed conservative as comparison to other studies. The capacity of rectangular (L/B=10) vertical anchor is also recorded by Akinmusuru, (1978). These differences may be due to the uncertainty of soil roughness, soil dilatation angle and complex nature of vertical anchor. Additionally, as model tests are typically conducted at lower stress levels, where Mohr's failure envelope is curved, and difficulties arises in selecting correct friction angles for comparison.

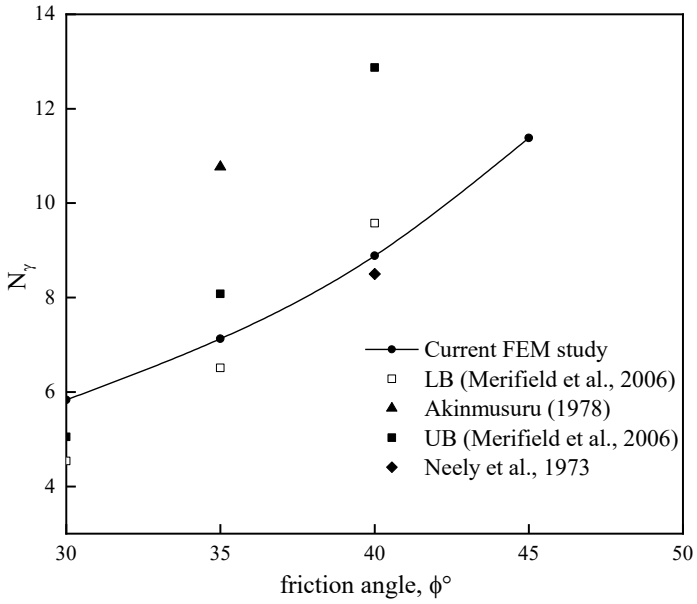

Figure 3: Pullout capacity factor N_γ from finite element method analyses (FEM) compared with other studies.

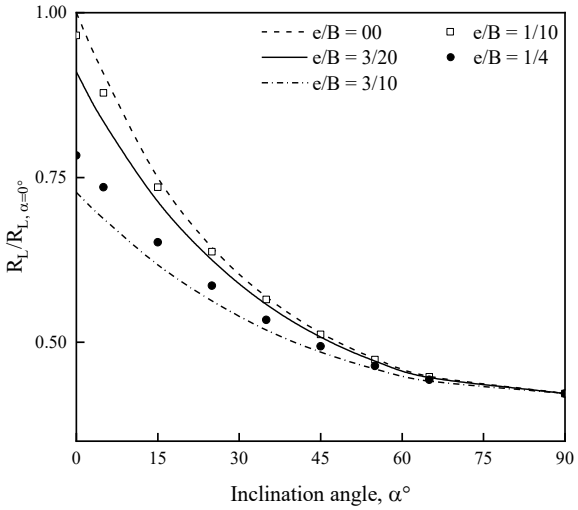

Figure (a)

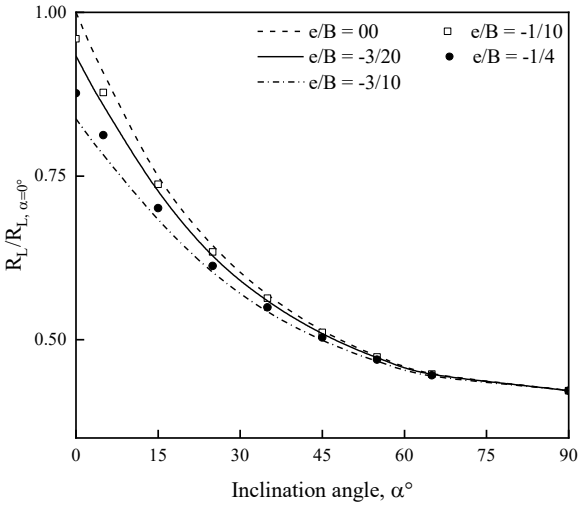

Figure (b)

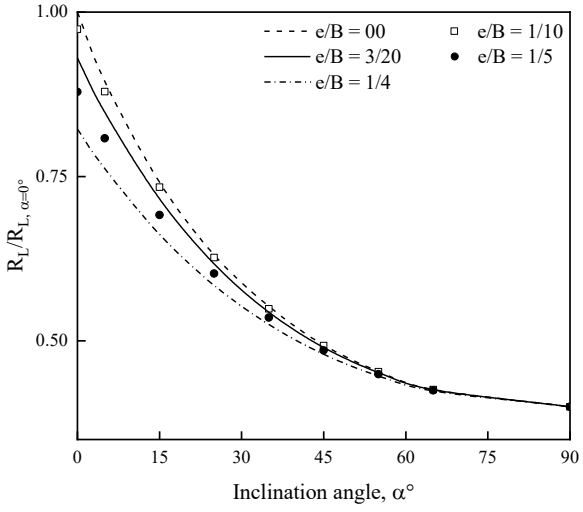

Figure (c)

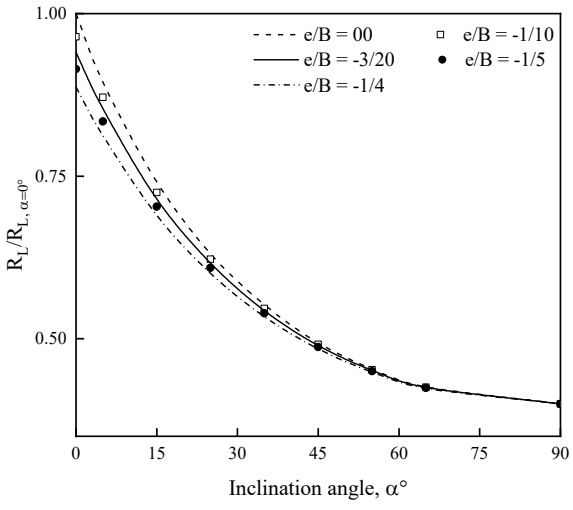

Figure (d)

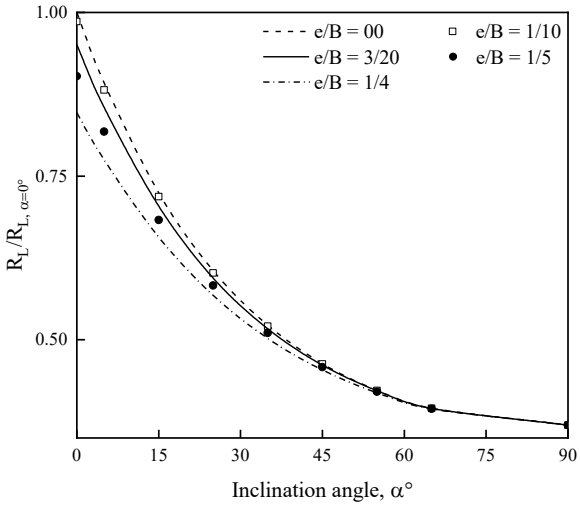

Figure (e)

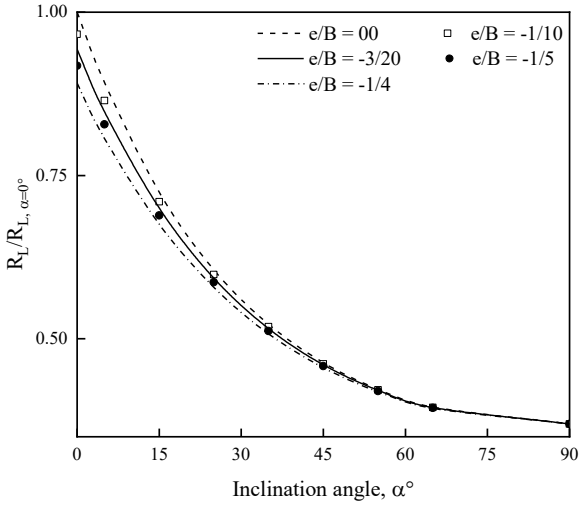

Figure (f)

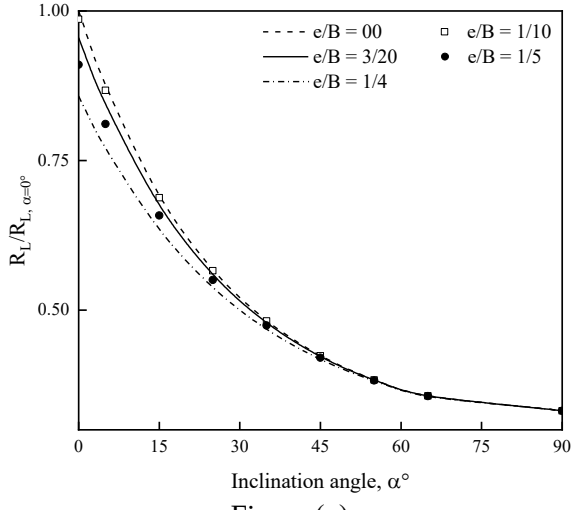

Figure (g)

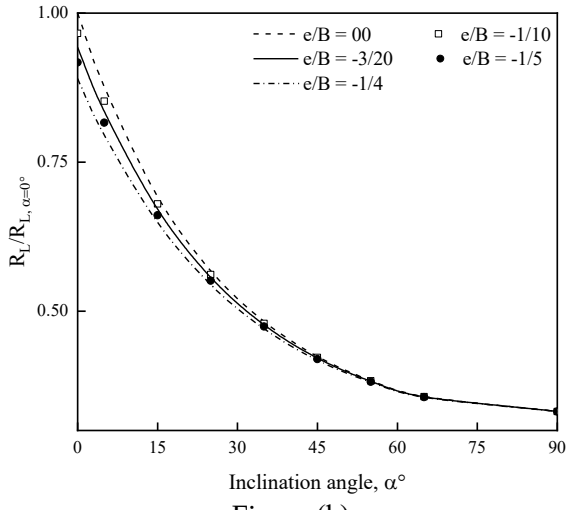

Figure (h)

Figure 4: Ratio $R_L/R_{L,\alpha=0°}$ as a function of inclination angle α, internal friction angle of soil ϕ and load eccentricity e. (a) ϕ= 30° with +e; (b) ϕ= 30° with -e; (c) ϕ= 35° with +e; (d) ϕ= 35° with -e; (e) ϕ= 40° with +e; (f) ϕ= 40° with -e; (g) ϕ= 45° with +e; (h) ϕ= 45° with -e.

The ratio of collapse pullout load R_L from the analyses with different combinations of eccentricity (e) and inclination angle (α) over the corresponding value ($R_{L,\alpha=0°}$) for a centrally loaded anchor (i.e., e=0 and α=0) is represented in Fig. 4. In this study, friction angles (ϕ) varies from 30° to 45° at an interval of 5° and inclination angle varies from 0° to 90°.The capacity drops significantly with the decrease of friction of friction angle. The load factor curves seemed to be linear when α= ϕ. The anchor exhibits opposite behaviour with the decrease of inclination angle and the capacity drops exponentially. For the increase of eccentricity, the load factor curves seemed to be steeper. -e has less impact over load factor then +e.

The interaction diagram describes some behaviour of a group of objects in a single use case. In this diagram, one combination of V, H and M loads initiating anchor to failure either by rotating and/or translating the anchor till a constant load state is reached in that direction. For example, in V-H plane the anchor is pushed in vertical direction into the soil until the vertical load plateaus reached is followed by translating in the horizontal direction. A variety of vertical and horizontal displacement and rotational combinations are required to define a complete failure envelope in different plane. 9 probe tests are conducted to define failure envelope in V-H (i.e. Δv/Δu=0.3 to 128) & H-M plane (i.e. Δv/Δu=0.3 to 128) and 18 probe tests were conducted in V-M plane (i.e. Δv/Δu=0.3 to 128). The failure

load in each probe test is plotted to get the interaction diagram. Normal, shear and rotational capacities are made dimensionless by diving then with their respective ultimate capacity. Fig. 5 & Fig. 6 represents the failure envelope in V-H and V-M plane for all friction angles.

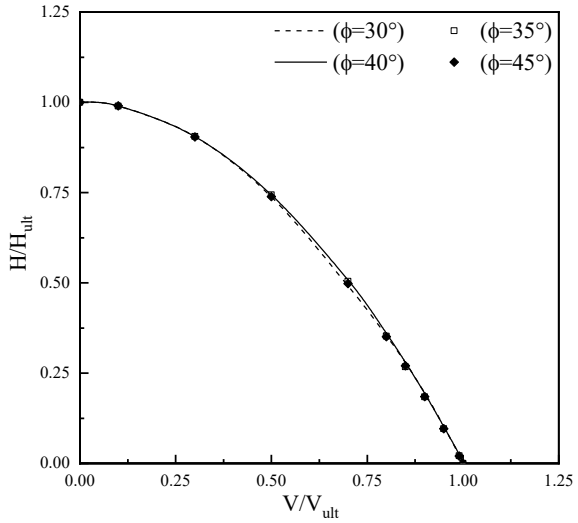

Figure 5: Failure Envelope at V-H plane (M=0)

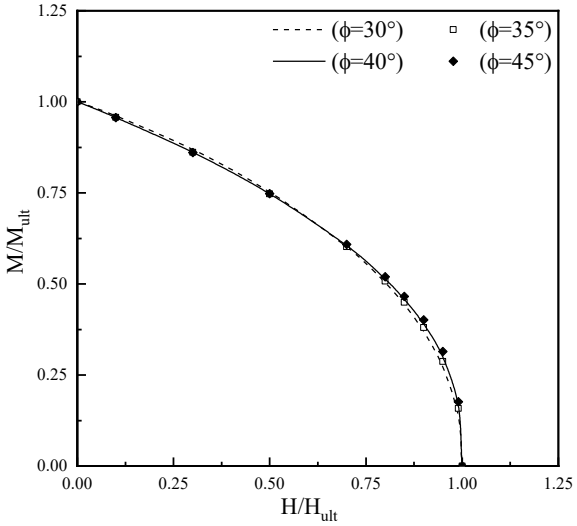

Figure 6: Failure Envelope at H-M plane (V=0)

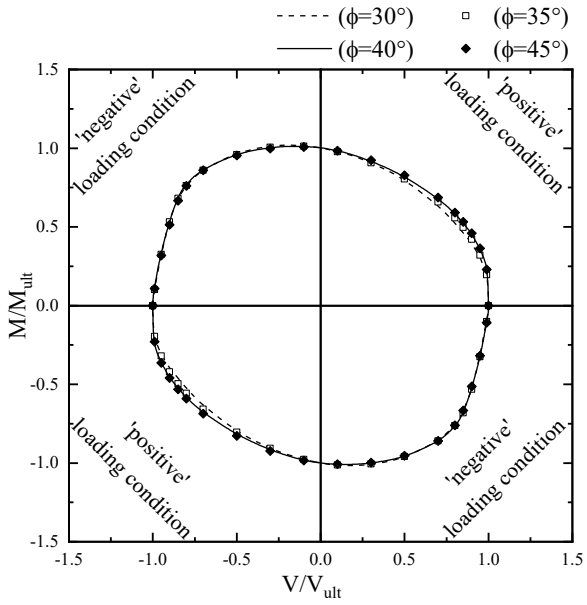

Figure 7: Failure Envelope at V-M plane (H=0)

The diagram is found symmetrical for both negative and positive loading combinations. Furthermore, the diagram coincides each other for all friction angles in both planes. So, it is clear that the effect of friction angle on interaction diagram is negligible. In the V-M plane, the failure envelope is found asymmetrical and the effect of friction angle is also negligible shown in Fig. 7. The moment capacity M drops with the increase of vertical load. A noticeable finding is that, the maximum moment is found $1.014M_{ult}$ at vertical load $V= -0.10V_{ult}$ instead of V=0. Whereas maximum horizontal capacity for V-H plane is reached when vertical load is zero and vice versa.

CONCLUSIONS

A detailed FEM analyses have carried out to determine the behavior of strip vertical anchor in the sand. Based on the study following conclusions can be drawn:

1. The effect of load inclination angle and eccentricity on resultant pullout capacity is significant. The capacity reduces in nonlinear manner with the increase of eccentricity and inclination angle. The effect of eccentricity isn't similar in direction (+e & -e).
2. The failure envelope is found symmetrical for both V-H and H-M plane and asymmetrical in V-M plane. Also, the failure envelope in dimensionless form is independent of friction angle in all three planes.

REFERENCES

Akinmusuru, J. O. (1978) *Horizontally loaded vertical plate anchors in sand*. Journal of the Geotechnical Engineering Division; 104(2); 283-286.

Butterfield, R., Houlsby, G. T. and Gottardi, G. (1997) 'Standardized sign conventions and notation for generally loaded foundations', *Géotechnique*, 47(5), pp. 1051–1054. doi: 10.1680/geot.1997.47.5.1051.

Elkhatib, S. (2006) *The behaviour of drag-in plate anchors in soft cohesive soils*. (Ph.D. thesis), University of Western Australia, Australia.

Hanna, A., Foriero, A. and Ayadat, T. (2014) 'Pullout Capacity of Inclined Shallow Single Anchor Plate in Sand', *Indian Geotechnical Journal*, 45(1), pp. 110–120. doi: 10.1007/s40098-014-0113-7.

Merifield, R. S., Lyamin, A. V., Sloan, S. W. & Yu, H. S. (2003) 'Three-Dimensional Lower Bound Solutions for Stability of Plate Anchors in Clay', *Journal of Geotechnical and Geoenvironmental Engineering*, 129(3), pp. 243–253. doi: 10.1061/(ASCE)1090-0241(2003)129:3(243).

Merifield, R. S. and Sloan, S. W. (2006) 'The ultimate pullout capacity of anchors in frictional soils', *Canadian Geotechnical Journal*, 43(8), pp. 852–868. doi: 10.1139/T06-052.

Merifield, R. S. and Smith, C. C. (2010) 'Computers and Geotechnics The ultimate uplift capacity of multi-plate strip anchors in undrained clay', *Computers and Geotechnics*. Elsevier Ltd, 37(4), pp. 504–514. doi: 10.1016/j.compgeo.2010.02.004.

Neely, W. J., Stuart, J. G. and Graham, J. (1973) 'Failure Loads of Vertical Anchor Plates in Sand', *Journal of Soil Mechanics and Foundations Division, ASCE*, 99(9), pp. 669–685.

Neill, M. P. O., Bransby, M. F. and Randolph, M. F. (2003) 'Drag anchor fluke – soil interaction in clays', 94, pp. 78–94. doi: 10.1139/T02-096.

Nouri, H., Biscontin, G. & and Aubeny, C. P. (2017) 'Numerical prediction of undrained response of plate anchors under combined translation and torsion', *Computers and Geotechnics*. Elsevier Ltd, 81, pp. 39–48. doi: 10.1016/j.compgeo.2016.07.008.

Rowe, R. K. (1978) *Soil structure interaction analysis and its application to the prediction of anchor plate behaviour, (Doctoral dissertation)*.

Shafiqul Islam, M. Rokonuzzaman, M. and Sakai, T. (2017) 'Shape Effect of Square and Circular Footing under Vertical Loading: Experimental and Numerical Studies', *International Journal of Geomechanics*, 17(9), p. 06017014.

Song, Z., Hu, Y., & Randolph, M. F. (2008) 'Numerical Simulation of Vertical Pullout of Plate Anchors in Clay', *Journal of Geotechnical and Geoenvironmental Engineering*, 134(6), pp. 866–875. doi: 10.1061/(ASCE)1090-0241(2008)134:6(866).

Song, Z. and Hu, Y. (2005) 'Vertical pullout behaviour of plate anchors in uniform clay', in. Perth, Western Australia: Taylor & Francis.

Sutherland, H. B., Finlay, T. W. and Fadl, M. O. (1983) 'Uplift capacity of embedded anchors in sand', in *Int Conf Behav Offshore Struct*, pp. 451–463.

Wang, D., Hu, Y., & and Randolph, M. F. (2010) 'Three-Dimensional Large Deformation Finite-Element Analysis of Plate Anchors in Uniform Clay', *Journal of Geotechnical and Geoenvironmental Engineering*, 136(2), pp. 355–365. doi: 10.1061/(ASCE)GT.1943-5606.0000210.

Wu, X., Chow, Y. K. and Leung, C. F. (2017) 'Behavior of drag anchor under uni-directional loading and combined loading - ScienceDirect', *Ocean Engineering*, 129, pp. 149–159.

Yang, M., Murff, J. D. and Aubeny, C. P. (2010) 'Undrained Capacity of Plate Anchors under General Loading', (October), pp. 1383–1393.

Zhu, M. and Michalowski, R. L. (2005) 'Shape factors for limit loads on square and rectangular footings', *Journal of geotechnical and Geoenvironmental Engineering*, 131(2), pp. 223–231.

EFFECT OF LOAD INCLINATION AND ECCENTRICITY ON PULLOUT CAPACITY OF HORIZONTAL ANCHOR IN SAND

S. K. Debnath, M. S. Islam, R. Rahman & M.Rokonuzzaman*

Department of Civil Engineering, Khulna University of Engineering &Technology, Khulna Bangladesh.
E-mail:rokon@ce.kuet.ac.bd

**Corresponding Author*

ABSTRACT

This paper focuses on the pullout capacity of horizontal anchor which is embedded in pure frictional soil under inclined and eccentric loadings. In this study, a 2D finite-element model incorporating a Mohr-Coulomb elasto-plastic material model were validated against existing upper bound and lower bound solution in order to determine the effect of inclination and eccentricity on pullout capacity. The both horizontal and vertical pullout capacity factors are expressed as a function of pure vertical, horizontal, inclination angle and eccentricity.

Keywords: numerical analyis; shallow anchor; bearing capacity; inlination factor

INTRODUCTION

Anchor is an attractive and economic solution of foundational systems in offshore engineering. Severalengineering efforts are conducted from the pastto determine theultimate pullout capaacity of anchor. Therefore, many investigations werecarried outto focused the pullout capacity(Rowe & Davis 1982;Murray & Geddes 1987;Qiao & Ou, 2012;Hanna et al., 2007;Hataf et al., 2010). The previous study proposed rapture of shallow anchor and showed that the ultimate capacity of shallow anchor increase nonlinearly with the shape of coefficient(White et al., 2008).Besides the breakout factor have also been investigated using more conventional displacement finite element method(Das et al., 1985;Merifield& Sloan, 2006).To present validation of a simple limit equilibrium solution for uplift resistance of plate anchor vertical pullout capacity is investigated by(Jin &Yao, 2016).However, the anchor plate may be subjected to combined vertical, horizontal and momentloading.In order to recognize the behavior anchor plate under combined loading andanalyze the failure pattern, it is essential to recognize the anchor behavior under combinedvertical, horizontal and moment loading or combination of all three.But the limited studies has been established to analyze the acting factor for inclined and eccentric load of horizontal shallow anchor embedded in cohesionless soil instead of footing (Meyerhof 1953;Das & Seeley, 1975).

In this paper two-dimensional finite element analysis (2D-FE) is carried out to investigate the behavior of horizontal shallow anchor in sand under different loading condition and also reveals about the variations of uplift capacity for eccentric loading condition.

METHODOLOGY

The two dimensional finite element analysis (FEM) is carried out using **the software ABAQUS.** The soil is considered linear elastic-perfectly plastic materials and the friction angle varies 30°**to** 45°. An elastic associative Mohr-colomb material model is used for purely frictional soil with minimum cohesion c=2kpa to avoid numerical difficulties. The modulus of elasticity of soil E= 30Mpa and anchor elasticity is 10^7

times of soil (Andersen et al., 2003)to ensure to behave as rigid body and poison ratio of soils and anchors are 0.33 and 0.17.The soil and anchor is modelled in such a way that there is no interface element at the contact plane. So, any slippage between the soil nad anchor are occured within the soil.The analysis elements are based on 8-noded quadrilateral elements of type CPE8R with reduced integration. Part by part meshing is applied to accuracy and anchor neighboring elements differ very small to gradually large in size with move away from anchor.

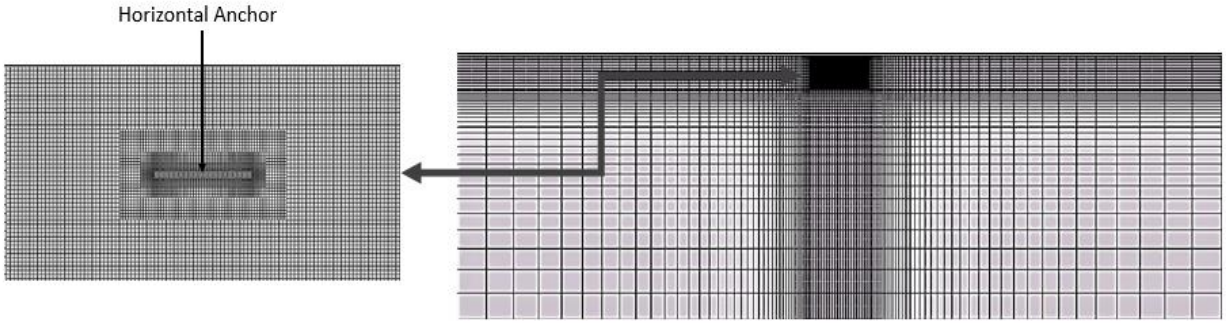

Figure 1: Finite element model used for numerical analysis

The bearing capacity is obtained from numerical analysis value establishing failure envelope graph. The purre vertical and horizontal pullout capacity is obtained to apply H and V direction at cetroid of R.P (Figure2). Furtheremore, in order to determine theinclined load capacity the load is appliedat an angle of α (5°-65°; interval of 5°) with vertical axis. The same procedure is applied in order to determine the combined effect of eccentricityand load inclination on pullout capacity of anchor(see Figure 3).

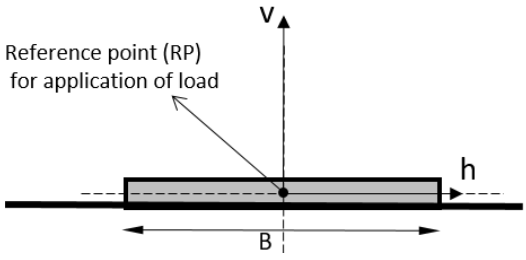

Figure 2: Anchor loading condition (α = 0;e =0)

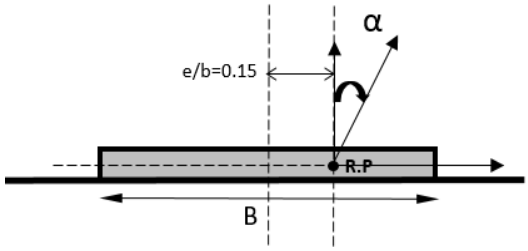

Figure 3: Anchor loading condition (α > 0; e > 0)

RESULT AND DISCUSSION

Uplift capacities of horizontal shallow anchor in current FEM study is compared with various experimental and numerical data(Koutsabeloulis and Griffiths 1989) available in literature (Figure4).Pullout capacities are found to increase linearly with the increase of friction angle which is also similar in all other studies. Results from the present FE estimates slightly higher value than the upper bound (UB) of Merifield et al. (2006). The result obtained by (Dickin 1988) for friction angle 43.8° is seemed conservative as comparison to other studies. These differences may be due to the uncertainty of soil roughness , soil dilatation angle. Additionally, as model tests are typically conducted at lower stress levels, where Mohr's failure envelope is curved, and difficulties arises in selecting correct friction angles for comparison.

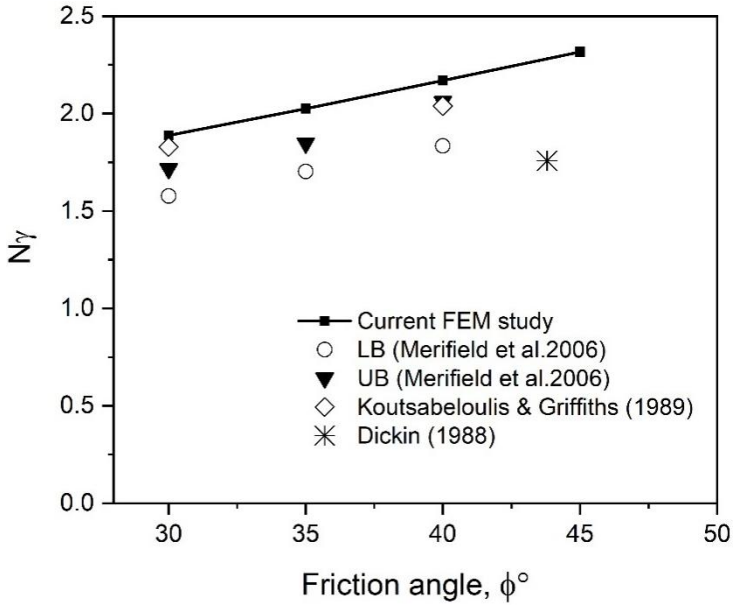

Figure 4: Uplift force capacity factor Nγ from finite element method analyses (FEM) compared with that from limit analysis and the method of characteristics: Nγ vs soil friction angle ϕ.

Table 1 shows the pure horizontal and vertical the pullout capacity factor N_γ of centrally loaded anchor.This factor is computedby the equation $N\gamma = \frac{P}{B\gamma H}$ where P considered as limit pulloutload and B & H width of anchor and hieght of embedment.

Table 1: Bearing capacity factor Nγ from finite element method analyses (FEM)

Friction Angle	$N_\gamma(V_{L,\ e=0,\ \alpha=0})$	$N_\gamma(H_{L,\ e=0,\ \alpha=0})$
30°	1.89	2.69
35°	2.03	3.24
40°	2.17	3.91
45°	2.32	4.78

Figure 5 shows the variation of both horizontal and vertical pullout capacity factor for different friction angle. The pullout capacity factor is obtained by dividing each pullout load with the pure capacities as shown in table 1.

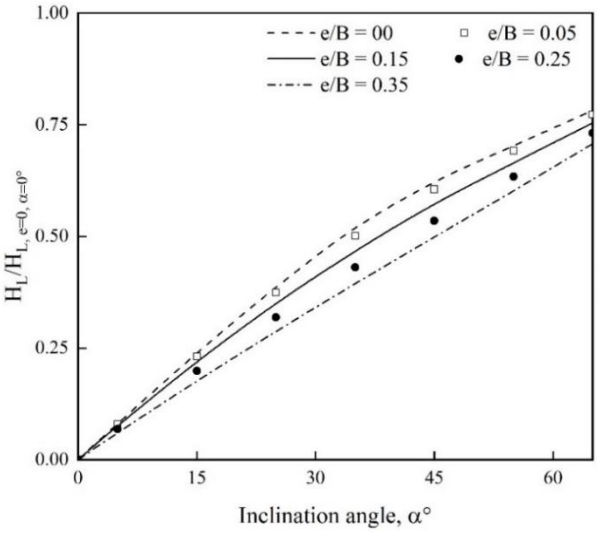

Fig. (a)

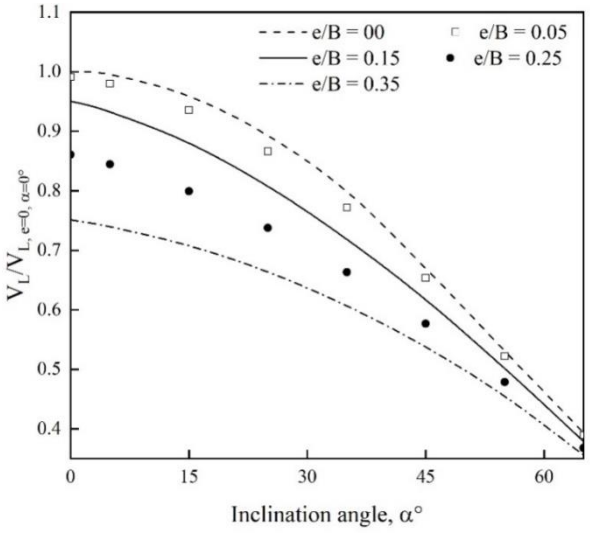

Fig. (b)

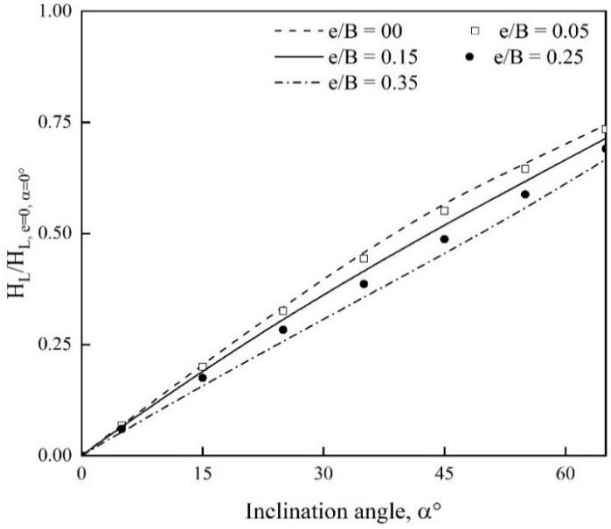

Fig. (c)

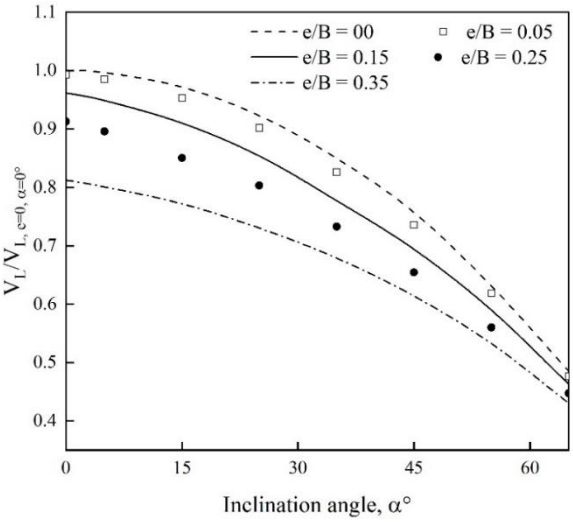

Fig. (d)

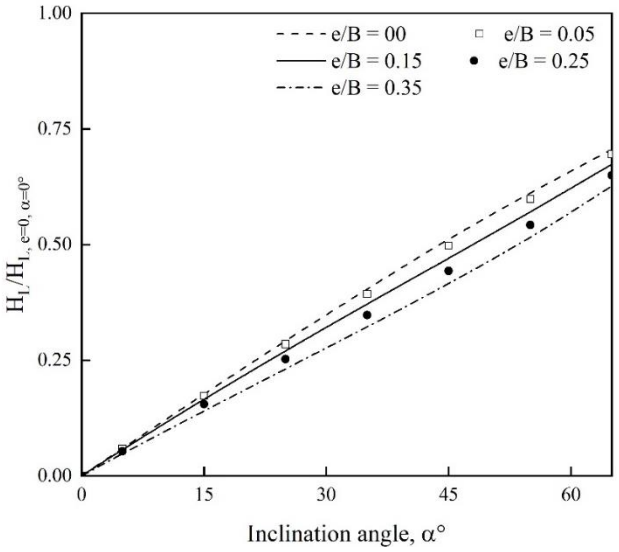

Fig. (e)

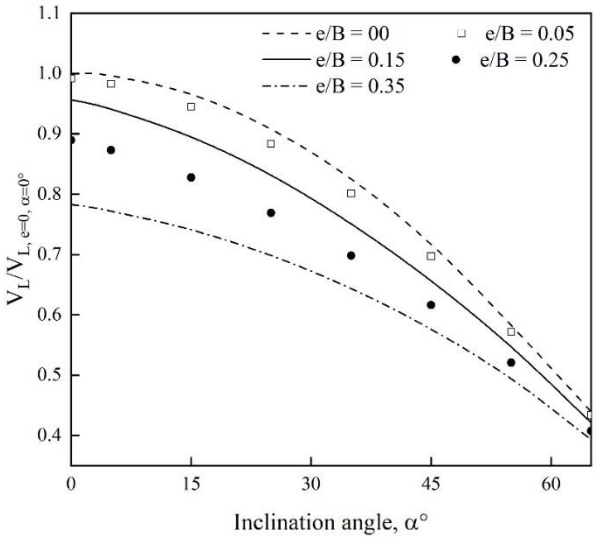

Fig: (f)

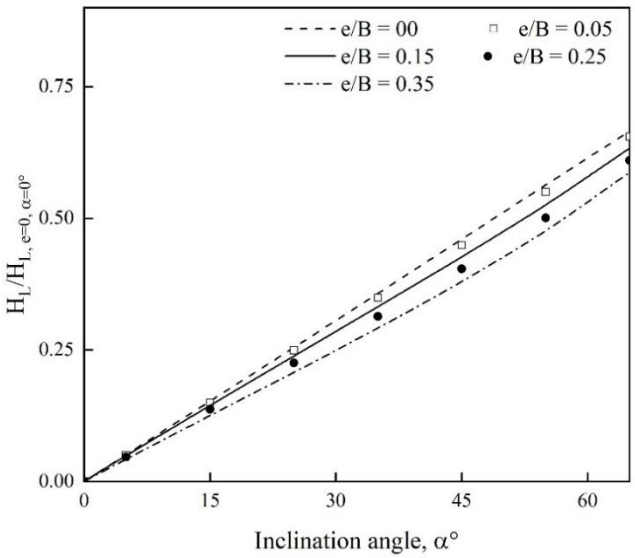

Fig. (g)

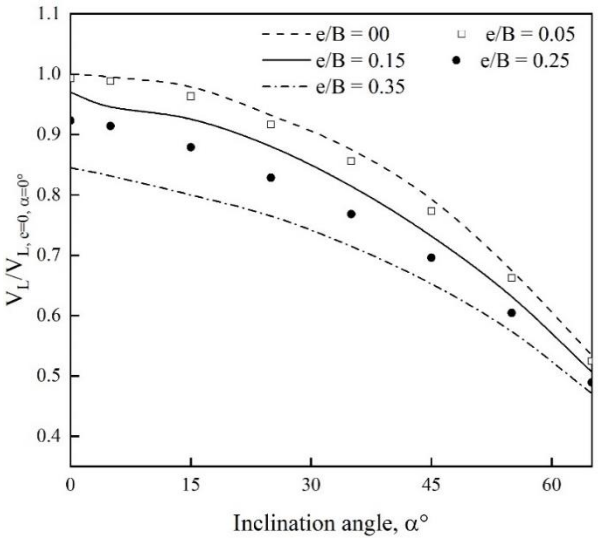

Fig. (h)

Figure 5: Ratio $H_L/H_{L,\ e=0,\ \alpha=0}$ and $V_L/V_{L,\ e=0,\ \alpha=0}$ as a function of inclination angle α, internal friction angle of soil ϕ and load eccentricity e. (a) ϕ= 30° with horizontal; (b) ϕ= 30° with vertical; (c) ϕ= 35° with horizontal; (d) ϕ= 35° with vertical; (e) ϕ= 40° with horizontal; (f) ϕ= 40° with vertical; (g) ϕ= 45° with horizontal; (h) ϕ= 45° with vertical.

For horizontal pullout capacity, graphical result shows that the ratio of H_L and $H_{L,\ e=0,\ \alpha=0}$ increase linearly for all frictional angle. That's why we can say that the pullout capacity is proportionally increased by increasing the inclined angle.It is also evident that, the effect of eccentricity on horizontal pullout capacity factor issmall as comparison to the vertical pullout capacity factor.This effect is countered too much in loading position between e/b=0.25 to e/b=0.35 for each friction angle. It is also found that horizontal pullout capacity is higher than the vertical load capacity for all friction angles.

CONCLUSIONS:

The finite element method is used to study the collapse of shallow anchor subjected to inclined and eccentric loading resting on purely frictional soils.The following conclusions can be drawn from the results presented in this paper.

1. The inclination angle and eccentricity have a significant effect on the pullout capacity of horizontal shallow anchor in sand. The vertical pullout capacity factor decreases in nonlinear manner and horizontal pullout capacity factor increases almost linearly with the inclination angle.
2. The horizontal pullout capacity is higher than the vertical pullout capacity at all embedment friction angles.The vertical and horizontal pullout capacity factor reduces with the increase of e/b ratios.

REFERENCE

AndersenH., K., Murff, J. D., and Randolph, M. F. (2003). "Deepwater anchor design practice-vertically loaded drag anchors." *Phase II Report to API/Deepstar, Norwegian Geotechnical Institute, Norway, Offshore Technology Research Center, USA and Centre for Offshore Foundation Systems, Australia*.

Das, B. M., Moreno, R., and Dallo, K. (1985). "Ultimate pullout capacity of shallow vertical anchors in clay." *Soils and Foundations*, 25(2), 148–152.

Das, B. M., and Seeley, G. R. (1975). "INCLINED LOAD RESISTANCE OF ANCHORS IN SAND." *Journal of Geotechnical and Geoenvironmental Engineering*, 101(GT9).

Dickin, E. A. (1988). "Uplift behavior of horizontal anchor plates in sand." *Journal of geotechnical engineering*, 114(11).

Hanna, A., Ayadat, T., and Sabry, M. (2007). "Pullout resistance of single vertical shallow helical and plate anchors in sand." *Geotechnical and Geological Engineering*, 25(5), 559–573.

Hataf, N., Boushehrian, A. H., and Ghahramani, A. (2010). "Experimental and numerical behavior of shallow foundations on sand reinforced with geogrid and grid anchor under cyclic loading." *Scientia Iranica*, 17(Compendex), 1–10.

Jin-Feng, Z., and Ming-Yao, X. (2016). "Uplift capacity of shallow anchors based on the generalized nonlinear failure criterion." *Mathematical Problems in Engineering*, 2016.

Koutsabeloulis, N. C., and Griffiths, D. V. (1989). "Numerical modelling of the trap door problem." *Geotechnique*, 39(1), 77–89.

Merifield, R. S., and Sloan, S. W. (2006). "The ultimate pullout capacity of anchors in frictional soils." *Canadian Geotechnical Journal*, 43(8), 852–868.

Meyerhof, G. T. (1953). "The bearing capacity of foundations under eccentric and inclined loads." *In Proceedings, 34th International Conference on Soil Mechanics and Foundation Engineering*, Zürich, Switzerland, 440–445.

Murray, E. J., and Geddes, J. D. (1987). "Uplift of anchor plates in sand." *Journal of Geotechnical Engineering*, 113(3), 202–215.

Qiao, D., and Ou, J. (2012). "Numerical analysis on ultimate pullout bearing capacity of drag embedment anchor based on elastic-plastic FEM." *Electronic Journal of Geotechnical Engineering*, 17 A, 65–78.

Rowe, R. K., and Davis, E. H. (1982). "The behaviour of anchor plates in sand." *Géotechnique*, 32(1), 25–41.

White, D. J., Cheuk, C. Y., and Bolton, M. D. (2008). "The uplift resistance of pipes and plate anchors buried in sand." *Géotechnique*, 58(10), 771–779.